NATO Science for Peace and Security Series - C:
Environmental Security

Recent Advances in Adsorption Processes for Environmental Protection and Security

Edited by
José Paulo Mota
Svetlana Lyubchik

Springer

NATO OTAN

This publication is supported by:

The NATO Science for Peace and Security Programme

Recent Advances in Adsorption Processes for Environmental Protection and Security

NATO Science for Peace and Security Series

This Series presents the results of scientific meetings supported under the NATO Programme: Science for Peace and Security (SPS).

The NATO SPS Programme supports meetings in the following Key Priority areas: (1) Defence Against Terrorism; (2) Countering other Threats to Security and (3) NATO, Partner and Mediterranean Dialogue Country Priorities. The types of meeting supported are generally "Advanced Study Institutes" and "Advanced Research Workshops". The NATO SPS Series collects together the results of these meetings. The meetings are co-organized by scientists from NATO countries and scientists from NATO's "Partner" or "Mediterranean Dialogue" countries. The observations and recommendations made at the meetings, as well as the contents of the volumes in the Series, reflect those of participants and contributors only; they should not necessarily be regarded as reflecting NATO views or policy.

Advanced Study Institutes (ASI) are high-level tutorial courses intended to convey the latest developments in a subject to an advanced-level audience

Advanced Research Workshops (ARW) are expert meetings where an intense but informal exchange of views at the frontiers of a subject aims at identifying directions for future action

Following a transformation of the programme in 2006 the Series has been re-named and re-organised. Recent volumes on topics not related to security, which result from meetings supported under the programme earlier, may be found in the NATO Science Series.

The Series is published by IOS Press, Amsterdam, and Springer, Dordrecht, in conjunction with the NATO Public Diplomacy Division.

Sub-Series

A.	Chemistry and Biology	Springer
B.	Physics and Biophysics	Springer
C.	Environmental Security	Springer
D.	Information and Communication Security	IOS Press
E.	Human and Societal Dynamics	IOS Press

http://www.nato.int/science
http://www.springer.com
http://www.iospress.nl

Series C: Environmental Security

Recent Advances in Adsorption Processes for Environmental Protection and Security

Edited by

José Paulo Mota
Universidade Nova de Lisboa
Caparica, Portugal

and

Svetlana Lyubchik
National Academy of Science of Ukraine
Donetsk, Ukraine

Springer

Published in cooperation with NATO Public Diplomacy Division

Proceedings of the NATO Advanced Research Workshop on
Recent Advances in Adsorption Processes for Environmental Protection and Security
Kyiv, Ukraine
9–12 September 2006

A C.I.P. Catalogue record for this book is available from the Library of Congress.

ISBN 978-1-4020-6804-1 (PB)
ISBN 978-1-4020-6803-4 (HB)
ISBN 978-1-4020-6805-8 (e-book)

Published by Springer,
P.O. Box 17, 3300 AA Dordrecht, The Netherlands.

www.springer.com

Printed on acid-free paper

ORGANIZATION

Workshop Committee

José Paulo Mota (Universidade Nova de Lisboa, Portugal)
Svetlana Lyubchik (Institute of Physical Organic and Coal Chemistry, Ukraine)

Sándor Bárány (University of Miskolc, Hungary)
François Beguin (CNRS-University, France)
Eiliv Steinnes (Norwegian University of Science and Technology, Norway)
Isabel Fonseca (Universidade Nova de Lisboa, Portugal)

Advisory Committee

Sándor Bárány (University of Miskolc, Hungary)
François Beguin (CNRS-University, France)
Tatiana Burdejnaya (Institute of Physical Organic and Coal Chemistry, Ukraine)
Isabel Fonseca (Universidade Nova de Lisboa, Portugal)
Peter Lodewyckx (Royal Military Academy, Belgium)
Francisco Rodriguez-Reinoso (Universidad de Alicante, Spain)
Eiliv Steinnes (Norwegian University of Science and Technology, Norway)
Fritz Stoeckli (Université de Neuchâtel, Switzerland)

Local Organizing Committee

João Fraga
Anna Kladova
Olena Lygina
Natalie Lygina
Andriy Lyubchik
Sergiy Lyubchik
Yury Neylo
Patrícia Oliveira
Tatiana Shendrik
Liliya Tikhonova

PREFACE

The NATO Advanced Research Workshop on *Recent Advances in Adsorption Processes for Environmental Protection and Security* was held during, September 9–12, 2006, at Hotel Salyut, Kiev, Ukraine. There were 45 participants from 12 NATO countries, 8 Eligible Partner and Mediterranean dialog home and one key speaker from Switzerland. We hope that everyone went home with excellent memories and new ideas to enhance environmental protection and security through adsorption science and technology.

The purpose of the Workshop was to bring together researchers and engineers working in adsorption-related fields, to share knowledge on the latest advances on adsorption processes for environmental security and protection, as well as to cross-link and disseminate to the scientific community the main results and achievements of recent NATO SfP projects on environmental security and protection.

Topics covered by the Workshop include recent theoretical and experimental developments on environmental adsorption, adsorption processes, as well as synthesis and tailoring of novel adsorbents, including the assessment of materials and processes.

The invited lectures provided a comprehensive report on adsorption and colloids, carbon materials and adsorbents for various industrial applications, and ecological safety and antiterrorism. Because rapidly developing areas in nanotechnology for fine chemistry, air quality, and environmental protection, are based on the synthesis and modification of the adsorbents, special attention was given to synthesis and chemical tailoring of porous materials to achieve desired properties as adsorbents and separation media.

We hope that the Workshop helped to intensify the cooperation between scientists from NATO countries, USA, Central Europe and FSU countries, and to shorten the gap between Partner/Mediterranean Dialogue countries and NATO countries with respect to environmental protection and security standards. Finally, we also hope that the Workshop opened a forum for discussion on possibilities for further improvements and areas still lacking critical knowledge and expertise.

We would like to express our gratitude to the members of the local organizing committee for all their hard work to make this Workshop a success. The Workshop would not have been possible without the generous financial support from the NATO Science for Peace and Security Programme.

José Paulo Mota
Svetlana Lyubchik

CONTENTS

LIST OF PARTICIPANTS

Andriy Lyubchik Donetsk National University, Department of Chemistry, Donetsk, Ukraine

Angel Linares-Solano Department of Inorganic Chemistry, University of Alicante, Alicante, Spain

Anna Kladova Chemistry Department, Faculty of Sciences and Technology, Universidade Nova de Lisboa, Caparica, Portugal

Boris Voevoda Donetsk National Technical University, Department of Geology, Donetsk, Ukraine

Christina Hakopian Yerevan State University, International Scientific Research Center of Water, Climatic and Recreational Resources, Yerevan, Armenia

Dilek Gulbayir Yildiz Technical University, Chemical Engineering Department, Davutpasa Campus, Esenler, Istanbul, Turkey

Dmitriy Shvets Institute for Sorption and Endoecology, NAS of Ukraine, Kiev, Ukraine

Eiliv Steinnes Department of Chemistry, Norwegian University of Science and Technology, Trondheim, Norway

Elena Lygina Donetsk State University of Economics and Trade, Department of Chemistry, Donetsk, Ukraine

Encarnacion Raymundo-Pinero Research Center on Divided Matter, Orléans University, Orlans, France

Eugene Katz Ben-Gurion University of the Negev, Department of Solar Energy and Environmental Physics, Israel

Fabian Suarez Garcia Department of Inorganic Chemistry, University of Alicante, Alicante, Spain

Francisco Rodriguez-Reinoso Department of Inorganic Chemistry, University of Alicante, Alicante, Spain

François Beguin Research Center on Divided Matter, Orlans University, Orlans, France

Fritz Stoeckli IMT-Chimie des Surfaces, University of Neuchâtel, Neuchâtel, Switzerland

Georgios Gallios Aristotle University of Thessaloniki, Chemical Technology Division, School of Chemistry, Thessaloniki, Greece

Ilknur Kucuk Yildiz Technical University, Chemical Engineering Department, Davutpasa Campus, Esenler, Istanbul, Turkey

Janos Lakatos University of Miskolc, Department of Chemistry, Miskolc-Egyetemvaros, Hungary

Jelena Chirkova Latvian State Institute of Wood Chemistry, Riga, Latvia

José Paulo Mota Chemistry Department, Faculty of Sciences and Technology, Universidade Nova de Lisboa, Caparica, Portugal

Juriy Hradil Institute of Macromolecular Chemistry AS CR, Prague, Czech Republic

K. Mark Thomas University of Newcastle upon Tyne, School of Natural Sciences, Newcastle upon Tyne, UK

Kristina László Department of Physical Chemistry, Budapest University of Technology and Economics, Budapest, Hungary

Marco Linders TNO Defense, Security and Safety, Rijswijk, The Netherlands

Marina Sosina Institute for Sorption and Endoecology, NAS of Ukraine, Kiev, Ukraine

Massoud Rostam-Abadi Illinois State Geological Survey, University of Illinois, Champaign, Illinois, USA

Miguel Loureiro LSRE/DEQ, Faculty of Engineering, University of Porto, Porto, Portugal

Miroslava Vaclavikova Institude of Geotechnics of the Slovak Academy of Sciences, Kosice, Slovac Republic

Nataliya Mishchuk Institute of Colloid and Water Chemistry, Vernadskogo, Kiev, Ukraine

Nazim Narsullayev Baku State University, Department of Physics, Baku, Azerbaijan

Nik Kanellopoulos NCSR "Demokritos", Institute of Physical Chemistry, Agia Paraskevi Attikis, Greece

Nikolai Kartel Institute of Sorption and Problems of Endoecology, NAS of Ukraine, Kiev, Ukraine

Nina Tchanishvili The Eliava Institute of Bacteriophage, Microbiology and Virology, Tbilisi, Georgia

Patrícia Oliveira Chemistry Department, Faculty of Sciences and Technology, Universidade Nova de Lisboa, Caparica, Portugal

Peter Lodewyckx Royal Military Academy, Belgium

Sandor Barany University of Miskolc, Department of Chemistry, Miskolc-Egyetemvaros, Hungary

Sergei Lyubchik Donetsk National University, Department of Chemistry, Donetsk, Ukraine

Sergey Mikhalovsky University of Brighton, Brighton, UK

Svetlana Lyubchik Institute of Physical Organic and Coal Chemistry, National Academy of Science of Ukraine, Donetsk, Ukraine

Tata Burburatshvili The Eliava Institute of Bacteriophage, Microbiology and Virology, Tbilisi, Georgia

Tatiana Shendrik Institute of Physical-Organic and Coal Chemistry, Department of Coal Chemistry, Donetsk, Ukraine

Tatjana Dizbite Latvian State Institute of Wood Chemistry, Riga, Latvia

Teresa Centeno Instituto Nacional del Carbón-CSIC, Oviedo, Spain

Valentin Tertykh Institute of Surface Chemistry of Academy of Sciences of Ukraine, Kiev, Ukraine

Valentin Tret'yakov Lomonosov Moscov State Academy of the Fine Chemical Technology, Moscow, Russia

EXTENSION OF DUBININ'S THEORY TO ADSORPTION FROM FROM AQUEOUS SOLUTIONS

FRITZ STOECKLI*
IMT-Chimie des Surfaces, Université de Neuchâtel. Rue Emile Argand 11, CH-2009 Neuchâtel, Switzerland

DASHA M. NEVSKAIA, EVA CASTILLEJOS-LOPEZ
Departamento de Quimica Inorganica, Facultad de Ciencias UNED, Paseo Senda del Rey 9, 28040 Madrid, Spain

TERESA A. CENTENO
Instituto Nacional del Carbón-CSIC. Apartado 73, 33080 Oviedo, Spain

Abstract. Adsorption of sparingly soluble organics from aqueous solutions, by activated carbons, can be described within the framework of Dubinin's theory by using a modified Dubinin–Radushkevich–Kaganer (DRK) equ-equation, where relative pressures are replaced by relative concentrations. With respect to the descriptions based on the Langmuir model and similar expressions, this approach has the advantage that it allows predictions on the basis of simple physico-chemical properties of the solid and of the adsorbate. Preliminary experiments indicate that in the case of dilute binary mixtures, the model of independent coadsorption, based on the DRK equation, applies. However, more experimental evidence is needed to confirm this potentially very useful approach in filtration technology.

Keywords: Dubinin's theory; adsorption; aqueous solutions; binary mixtures

1. Introduction

The removal of sparingly soluble organics from aqueous solutions is a relatively important topic, in particular for the purification of drinking

* To whom correspondence should be addressed. Institut de Microtechnique-LCPS, rue Emile Argand 11, CH-2009 Neuchâtel, Switzerland; E-mail: fritz.stoeckli@unine.ch

J.P. Mota and S. Lyubchik (eds.), Recent Advances in Adsorption Processes for Environmental Protection and Security, 1–8.

water by activated carbon. So far, a variety of theoretical models have been proposed, which can reproduce accurately the experimental data.[1,2]

However, a major shortcoming in the use of Langmuir- or Freundlich-based approaches is the fact that predictions are difficult, and even impossible in many cases, due to the complexity of the parameters used in these expressions. It is therefore necessary to find alternative descriptions, which provide a tool for quantitative or at least semi-quantitative predictions in filtration technology.

Active carbons are very efficient adsorbents and the adsorption of vapours is well described by Dubinin's theory,[3,4] which uses relatively simple parameters and allows predictions over relatively wide pressure and temperature ranges. As shown in detail elsewhere,[5–7] for relative concentrations $c_{eq}/c_s < 0.01–0.05$ (submonolayer conditions) adsorption of sparingly soluble species such as phenol and its derivatives can be described by the modified Dubinin–Radushkevich–Kaganer (DRK) equation.

$$N_a(T;p) = N_{am} exp[-(A/E_s)^n] \quad (1)$$

where

$$A = RTln(c_s/c_{eq}) \text{ and } n \sim 2–4 \quad (2)$$

In the case of sparingly soluble species, N_{am} corresponds to the monolayer capacity of the walls of the micropores and not to the filling of these pores, as opposed to adsorption from the vapour phase. This means that the sorptive capacity of a microporous carbon is often smaller in the case of adsorption from dilute aqueous solutions, than from the vapour phase. This point is clearly illustrated by the adsorption of phenol from both phases.[8]

It appears that the principle of temperature invariance observed by Dubinin for micropore filling also applies here, as parameters n and E_s are practically constant over a range of 20°–30°.

One can also introduce specific scaling factors (surface affinity coefficients β_s) for E_s, to correlate the adsorption of different species relative to a reference solute (benzene or phenol). These properties are reflected in the logarithmic plot (Figure 1) for the adsorption of various phenolic compounds from aqueous solutions, at different temperatures and on three different activated carbons, with n = 4. As shown in the case of the DRK equation[9] (adsorption of vapours by non-porous solids), exponent n is related to the heterogeneity of the surface and it appears that for certain systems n = 3 (or even 2) also provides a good fit.

As observed for adsorption from the vapour phase, the characteristic adsorption energy E_s, depends on both the adsorbent and the adsorbate. It appears that in the case of aqueous solutions of phenol,[5–7] E_s is practically equal to the characteristic energy of adsorption of benzene vapours E_o,

which is a reference in adsorption by microporous carbons.[3] For other species (i) removed from aqueous solutions, one finds specific scaling factors β_s relative to phenol and defined by

$$E_s(i) = \beta_s E_s(phenol) \quad (3)$$

Typical values are shown in Table 1, with the values observed for adsorption from the vapour phase or calculated as described elsewhere.

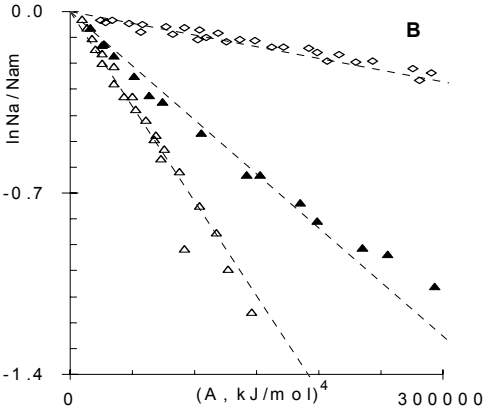

Figure 1. Logarithmic plot of Eq. (2) for the adsorption of various organics from aqueous solutions onto activated carbons: ◊ carbon CP (phenol, 4-cresol, 3-chlorophenol, 3-aminophenol, 4-nitrophenol); ▲ carbon PC (phenol, *m*-chlorophenol); Δ carbon AC (phenol, aniline).

TABLE 1. Typical affinity coefficients β_s (average values) for the adsorption of sparingly soluble organics from aqueous carbons onto activated carbons. For comparison purposes, the affinity coefficients for adsorption from the vapour phase[9,10] are also given (in the case of compounds with low vapour pressures, β is estimated[10] from parachors or molar volumes).

Compound	βs = Es/Eo	β (vapour phase)	βs/β
Phenol	1.03	1.09	0.95
3-chlorophenol	1.02	1.24	0.82
4-nitrophenol	0.90	1.20	0.75
Aniline	0.80	1.05	0.74
Benzene	0.54	1.00	0.54
Benzoic acid	0.80	1.04	0.77
Caffeine	1.28	1.85	0.69

These results show that predictions can be made for the removal of sparingly soluble organics by activated carbons at $c_{eq}/c_s < 0.05$, on the basis of relatively simple physico-chemical and structural properties. The latter are the characteristic energy E_o of the carbon, which varies typically between 30 kJ/mol (micropore width around 0.5 nm) and 16–17 kJ/mol

(supermicropores of ~2 nm) and the surface area of the micropore walls S_{mi}. This area can be assessed by different techniques, but in view of the good correlation observed with the adsorption of phenol from aqueous solutions based either on the solution isotherm or immersion calorimetry, the latter technique is now used to determine surface areas (see the contribution of Centeno and Stoeckli in this volume). For example, on the basis of a molecular surface area of 45×10^{-20} m^2 (molecule lying flat on the carbon surface), the specific enthalpy h_i(phenol) = –(0.109 ± 0.03) J/m^2. Moreover, and in spite of the fact that phenol is excluded from the oxygen-containing surface sites, it appears that, due to a compensation effect, the enthalpy of immersion $\Delta_i H$(J/g) of a carbon into an aqueous solution of phenol (usually 0.4 M) leads to a good approximation of the total surface area by[6]

$$S_{tot}\ (m^2/g) = \Delta_i H(phenol\ 0.4\ M)/h_i \qquad (4)$$

This area corresponds to S_{mi} and the external surface S_e area found in larger pores and on the outside. Experiments with graphitized carbon blacks suggest a similar relation for caffeine solutions with –(0.112 ± 0.015 J/m^2), but in view of the structure of this molecule, the technique is limited to micropores larger than 0.55–0.6 nm.

In the low concentration range, Eq. (1) corresponds to adsorption on the micropore walls, where the adsorption energy is higher than on the external surface area. Typically, E_o is around 11 kJ/mol for non-porous carbons, and the adsorption of phenol from an aqueous solution onto graphitized carbon black N234-G leads to E_s(phenol) = 13 kJ/mol. This experiment confirms that adsorption on the open surface, also limited to a monolayer, becomes effective only at relatively high relative concentrations. In Figure 1, this corresponds to an additional section, not shown, at the upper end of the graph (c_{eq}/c_s > 0.05–0.1). On the other hand, in calorimetric experiments, the concentration is high enough (0.4 M) to form a monolayer on S_{tot}.

2. Binary Adsorption from Aqueous Solutions

Following the success obtained with the adsorption of single species, it is tempting to extend the Dubinin-based approach to binary and, hopefully, to multiple adsorption. The advantage is obvious, as it should allow predictions for the simultaneous removal of organics from water on the basis of simple parameters and over a range of temperatures. Obviously, within the framework of the modified DRK theory, the situation should correspond to the submonolayer region and describe the final stages of purification of water.

A convenient working hypothesis is the model of independent coadsorption, which assumes that each species is adsorbed according to its DRK

equation (1), but only on the surface area left free by the other component. In the case of binary adsorption, this corresponds to the set of coupled equations

$$N_{aA} = [N_{amA} - N_{aB}\,(N_{amA} / N_{amB})]\,\exp\{-[RT\ln(c_s / c_{eq})_A / E_{sA}]^n\} \quad (5)$$

$$N_{aB} = [N_{amB} - N_{aA}(N_{amB} / N_{amA})]\,\exp\{-[RT\ln(c_s / c_{eq})_B / E_{sB}]^n\} \quad (6)$$

The subsidiary condition, leading to the pre-exponential terms, is

$$S_{mi} = N_{amA}.A_{mA}.N_{Av} = N_{amB}.A_{mB}.N_{Av} \quad (7)$$

where A_{mA} and A_{mB} are the molecular surface areas of species A and B and N_{Av} is Avogadro's number.

In the case of a single species, exponent n = 4 often provides a good fit.[5–7] However, it is not a prerequisite, as n probably reflects the heterogeneity of the surface. As discussed elsewhere,[9] this is clearly the case with the original DRK equation, where the fixed value n = 2 is responsible for the discrepancy often observed between the monolayer capacities N_{am}(DRK) and N_{am}(BET). Exponent n may therefore vary from carbon to carbon and it is possible to obtain a better overall fit with n = 3 or even 2.

The set of Eqs. (5) and (6) is potentially interesting, provided that two requirements are fulfilled:

1. The principle of temperature invariance of E_s and n applies, which allows predictions over a range of concentrations and temperatures
2. The parameters E_{sA} and E_{sB} should be the same as those obtained for the adsorption of the individual species.

At this stage, the analysis of the phenol + aniline mixture in water, adsorbed by activated carbon AC at 298 K[1] and 313 K (new data) provides a first and interesting illustration of the potentiality of the present approach.

The analysis of the nitrogen adsorption isotherm at 77 K, using the Dubinin–Radushkevich equation, leads to a micropore volume W_o = 0.418 cm^3/g, and a characteristic energy E_o = 23.0 kJ/mol. With the help of the correlations[3,4]

$$L_o(nm) = 10.8/(E_o - 11.4\ kJ/mol) \quad (8)$$

$$S_{mi}(m^2/g) = 2500\,W_o(cm^3/g)/L_o(nm) \quad (9)$$

one obtains respectively L_o = 0.93 nm and S_{mi} = 898 m^2/g.

The adsorption isotherms of the single species at 298 and 313 K provide the best fits for Eq. (1) with n = 3, rather than n = 4, where a slight upward curvature is observed in the logarithmic plots. This leads to the values of N_{am} and E_s given in Table 2. They correspond to the domain of relative concentrations c_{eq}/c_s between 5×10^{-5} and 0.01.

TABLE 2. Parameters of Eq. (1) with n = 3 for the single adsorption from unbuffered aqueous solutions by carbon AC (E_o = 23.0 kJ/mol and S_{mi} = 898 m^2/g) at 298 and 313 K.

Adsorbate (single)	Phenol	Aniline
E_s(298 K) (kJ/mol)	22.9 ± 0.4	17.9 ± 0.4
E_s(313 K) (kJ/mol)	23.7 ± 0.5	18.0 ± 0.5
N_{am} (298 K) (mmol/g)	3.16 ± 0.07	3.14 ± 0.07
N_{am} (313 K) (mmol/g)	3.12 ± 0.07	3.00 ± 0.07
S_{mi} (average) (m^2/g)	848 ± 20	–

This data is coherent and suggests average surface affinity coefficients β_s(phenol) = 1.01 ± 0.04 and β_s(aniline) = 0.78 ± 0.04, in agreement with other determinations.[7] Moreover, the molecular surface area of 45×10^{-20} m^2 obtained for phenol adsorbed on graphitized carbon blacks, leads to a micropore surface area of 848 m^2/g, which is in reasonable agreement with the value derived from Eq. (9). The difference may be ascribed to the presence of surface oxygen, on which water is preferentially adsorbed in unbuffered solutions. The data also suggests that the molecular surface area of aniline is close to the value observed for phenol, as expected.

The analysis of the data for binary adsorption based on Eqs. (5) and (6) using again n = 3 and the values for N_{am}(phenol) and N_{am}(aniline) of Table 2, leads to the best fit values of E_s given in Table 3.

TABLE 3. Values of E_s(phenol) and E_s(aniline) for binary adsorption at 298 and 313 K.

Adsorbate (in the mixture)	Phenol	Aniline
E_s(298 K) (kJ/mol)	22.5 ± 0.5	18.1 ± 0.5
E_s(313 K) (kJ/mol)	22.3 ± 0.5	18.1 ± 0.5

These values are in good agreement with those obtained for the single adsorption (Table 2) and suggest that for the present binary system the adsorption equilibrium between 298 and 313 K could have been predicted with a reasonable accuracy by using the structural parameters of the carbon (E_o = 23.0 kJ/mol and S_{mi} = 898 m^2/g), with the affinity coefficients β_s of Table 1 and the saturation concentrations of phenol and aniline found in standard tables. The correlation between the experimental and amounts adsorbed in the submonolayer region and the values calculated using the best fits for E_s and N_{am} is shown in Figure 2. The data corresponds to

adsorption in the submonolayer region, with N_a(phenol) + N_a(aniline) below 2–2.5 mmol/g.

Obviously, the uncertainty on β_s introduces a corresponding uncertainty in the amounts adsorbed. However, the approach outline here and based on the extended DRK equation provides a good estimate, as opposed to the Langmuir-based models, where the parameters cannot be determined "a priori" or extrapolated to other temperatures.

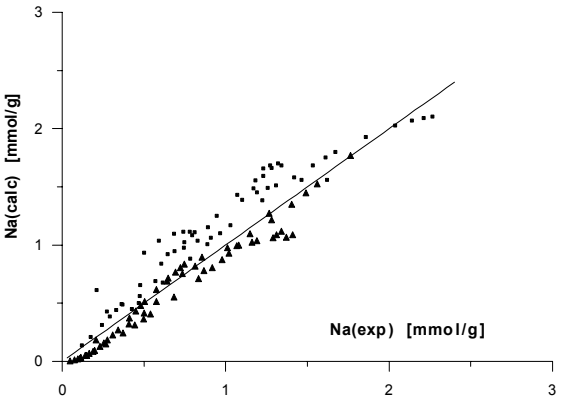

Figure 2. Correlation between the calculated and experimental amounts of phenol (■) and aniline (▲) adsorbed from binary mixtures in water, by active carbon AC, at 298 and 313 K.

3. Conclusions

The present study shows that Dubinin's theory can be extended to the adsorption, by activated carbons, of sparingly soluble organics from aqueous solutions. The basic equation is a modified Dubinin–Raduskkevich–Kaganer equation, where relative pressures are replaced by relative concentrations and the exponent n around 3–4. The principle of temperature invariance of parameters E_s and n has been established for single adsorption of a variety of organics and predictions can be made for a range of concentrations and temperatures.

Preliminary studies on binary systems in water, for example, phenol + aniline adsorbed by a typical industrial active carbon, suggest a similar pattern in the submonolayer region. In this case, the model of independent coadsorption can be applied and, with a good approximation, the individual isotherms are those obtained for single adsorption. This extension must be confirmed by a systematic study of more systems and special attention should be given to the value of exponent n, probably on the basis of a refined analysis of the carbon itself.

The approach outlined here is of great relevance to filtration technology, where semi-quantitative and quantitative predictions can be made on the basis of relatively simple physico-chemical properties of the adsorbates and the structural parameters of the carbon.

References

1. D.M. Nevskaia, E. Castillejos-López, A. Guerrero-Ruiz, and V. Muñoz, Effect of the Surface chemistry of carbon materials on the adsorption of phenol-aniline mixtures from water, *Carbon* 42(3), 653–665 (2004).
2. R. Leyva-Ramos, J. Zoto-Zuñiga, J. Mendoza Barron, and R.M. Guerro Coronado, Adsorption of phenol from aqueous solutions onto activated carbon. Effect of solvent, temperature and particle size, *Adsorpt. Sci. Technol.* 17(7), 533–543 (1999).
3. F. Stoeckli, in: *Porosity in Carbons*, edited by J. Patrick (E. Arnold, London, 1995), pp. 67–97.
4. F. Stoeckli and T.A. Centeno, On the determination of surface areas in activated carbons, *Carbon* 43(6), 1184–1190 (2005).
5. F. Stoeckli, M.V. López-Ramón, and C. Moreno-Castilla, Adsorption of phenolic compounds from aqueous solutions, by activated carbons, described by the Dubinin-Astakhov equation, *Langmuir* 17(11), 3301–3306 (2000).
6. E. Fernández, D. Hugi-Cleary, M.V. López-Ramón, and F. Stoeckli, Adsorption of phenol from dilute and concentrated aqueous solutions by activated carbons, *Langmuir* 19(23), 9719–9723 (2003).
7. D. Hugi-Cleary, A. Slasli, and F. Stoeckli, *Helv. Chim. Acta* 88, 470–477 (2005).
8. F. Stoeckli and D. Hugi-Cleary, *Russ. Chem. Int. Ed.* 50(11), 2060–2063 (2001).
9. D. Hugi-Cleary, S. Wermeille, and F. Stoeckli, *Chimia* 57(10), 611–615 (2003).
10. G.O. Wood, Affinity coefficients of the Polanyi/Dubinin adsorption isotherm equations, Carbon 39(3), 343–356 (2001).

APPLICATIONS OF IMMERSION CALORIMETRY IN DUBININ'S THEORY AND IN ELECTROCHEMISTRY

TERESA A. CENTENO*
Instituto Nacional del Carbón-CSIC. Apartado 73, 33080 Oviedo, Spain
FRITZ STOECKLI
IMT-Chimie des Surfaces, Université de Neuchâtel. Rue Emile Argand 11, CH-2009 Neuchâtel, Switzerland

Abstract. This study shows that immersion calorimetry is a useful technique which simplifies considerably the analysis of porosity and chemical nature of activated carbons.

The characterization of activated carbons in the general theoretical framework of Dubinin's theory with its extensions to calorimetry and adsorption from solutions allows the identification of some key parameters for the performance of these materials in electrochemical capacitors.

Keywords: activated carbon; immersion calorimetry; porosity; electrochemical capacitor

1. Introduction

Activated carbons can be characterized within the framework of Dubinin's theory. The basic relation is the Dubinin–Radushkevitch (DR) equation[1]

$$W = W_o \exp\left[-\left(\frac{A}{\beta \mathrm{E_o}}\right)^2\right] \quad (1)$$

where W represents the volume adsorbed at temperature T and relative pressure p/p_s, W_o is the limiting volume adsorbed in the micropores and

*To whom correspondence should be addressed. E-mail: teresa@incar.csic.es

J.P. Mota and S. Lyubchik (eds.), Recent Advances in Adsorption Processes for Environmental Protection and Security, 9–18.

$A = RT\ln(p_s/p)$; β and E_o are specific parameters depending on the adsorptive and on the adsorbent. W_o and E_o are usually obtained from the adsorption of small molecular probe (typically CO_2, CH_2Cl_2, and C_6H_6) with critical dimensions around 0.33–0.40 nm, and unhindered by constrictions in the structure.

In view of its thermodynamic basis, the DR equation can easily be used in the context of immersion calorimetry.[1,2] Starting from the definition of the isosteric heat of adsorption of a vapour q^{st} (>0)

$$[\,\partial ln(p)/\partial T\,]_{Na} = q^{st}/RT^2 \tag{2}$$

The inversed DR equation leads to q^{st} as a decreasing function of the micropore filling

$$q^{st}(T;\theta) = \beta E_o\{\,[ln(1/\theta)]^{1/2} + (\alpha T/2)[\,ln(1/\theta)]^{-1/2}\,]\} + \Delta H_{vap} \tag{3}$$

where α is the thermal expansion coefficient of the adsorbate. On the other hand, the net heat of adsorption defined as

$$q^{net}(T;\theta) = q^{st} - \Delta H_{vap} \tag{4}$$

is related to the enthalpy of immersion of the solid into the corresponding liquid by

$$-\Delta_i H(T) = \int q^{net}\, d\theta + h_{LV} S_{LV} \tag{5}$$

Taking into account that there is practically no liquid–vapour interface in micropores, it follows that

$$-\Delta_i H_{mi}\left(Jg^{-1}\right) = \int q^{net}\, d\theta = \frac{\beta\, W_o E_o \sqrt{\pi}\left(1+\alpha T\right)}{2V_m} \tag{6}$$

Since active carbons often present an external (non-microporous) surface area, S_e, the experimental enthalpy of immersion will include an extra contribution, corresponding to the wetting of this surface and

$$-\Delta_i H\left(Jg^{-1}\right) = \frac{\beta\, W_o E_o \sqrt{\pi}\left(1+\alpha T\right)}{2V_m} - h_i S_e \tag{7}$$

It appears, as a thermodynamic consequence of Dubinin's theory, that the enthalpy of immersion of a microporous carbon into organic liquids is

related to the parameters of the adsorption isotherm (W_o, E_o and S_e). This formal link between both approaches leads to a detailed picture of the porous structure and of the chemical nature of activated carbons.

The experimental set-up required for immersion calorimetry is relatively simple.[1] The sample is outgassed at 10^{-5} Torr and around 523 K in a glass bulb with a brittle end. The bulb is sealed, introduced into a cell containing around 5 cm^3 of the wetting liquid and placed inside the calorimeter. Once thermal equilibrium is achieved, the brittle end of the bulb is gently broken and the liquid wets the sample. The corresponding heat evolution through 180 thermocouples is monitored as a function of time and the integration of this signal leads, with the help of an electrical calibration, to the enthalpy of immersion $\Delta_i H$. A typical experiment lasts approximately 30–45 min, which allows an important gain in time, if compared with classical adsorption experiments.

2. Application of Immersion Calorimetry for Structural and Chemical Characterization of Activated Carbons

2.1. STRUCTURAL ASPECTS OF IMMERSION CALORIMETRY

2.1.1. *Calorimetric studies of selective adsorption from aqueous solutions: determination of specific surface areas*

This section shows how the enthalpy of immersion of carbons into aqueous solution of caffeine (0.1 M) or phenol (0.4 M) becomes another source of information for the determination of specific surface area of carbons.[1,3–6]

Some years ago, a calorimetric approach[3] showed that the enthalpy of immersion of carbon blacks into aqueous solutions of caffeine is a linear function of the mass of carbon. The comparison of $\Delta_i H$ (J g^{-1}) with the S_{BET} (m^2 g^{-1}) of the materials led to an average specific enthalpy h_i of $-(0.112 \pm 0.015)$ J m^{-2}. This correlation, confirmed by the corresponding adsorption isotherm from the solution, implies that adsorption is limited to a single layer. This is also true for microporous carbons, where no volume filling process takes place, as opposed to adsorption from the vapour phase. It follows that for both porous and non-porous carbons the total surface area can be determined with a good accuracy from the enthalpy of immersion into an aqueous solution of caffeine with the help of the simple relation[1,3]

$$S_{total}\left(m^2\,g^{-1}\right) = \frac{\Delta_i H_{\,caffeine}\,(J g^{-1})}{0.112\ (J m^{-2})} \tag{8}$$

Since the caffeine molecule cannot penetrate into micropores of less than approximately 0.6 nm, this procedure provides an estimate of the total surface area in carbons with pores wider than 0.6–0.7 nm.[1,3,4]

Subsequently, this technique has been used successfully with diluted aqueous solutions of phenol (0.4 M) and the study of carbon blacks and active carbons[5,6] suggested a process similar to that observed for caffeine. Phenol appears to form a monolayer, which provides information on the surface area of pores above approximately 0.45 nm. In this case, the specific enthalpies h_i corresponded to $-(0.109 \pm 0.003)$ J m^{-2} and

$$S_{total}\left(m^2\,g^{-1}\right) = \frac{\Delta_i H_{\ phenol}\,(J g^{-1})}{0.109\,(J m^{-2})} \tag{9}$$

It should be pointed out that the enthalpy of immersion into aqueous solution of phenol is affected by the surface acidity of the carbon since water is adsorbed preferentially by the oxygen-containing surface groups.[5,6] The reduction in specific surface area has been estimated to be around 70 m^2 per mmol of surface oxygen, but due to a compensation effect, Eq. (9) still provides a good assessment of S_{total} in the case of oxidized carbons.

On the other hand, it appears that the enthalpies of immersion of the microporous carbons into concentrated solutions are generally larger than observed for the dilute solution. This increase confirms that the adsorption of phenol from concentrated aqueous solutions corresponds to a process of micropore filling and that it is not limited to the coating of the micropore walls, as observed for dilute solutions.[6]

2.1.2. *The assessment of micropore size distribution of carbons*

Equation (7) can be used to evaluate, on the basis of the experimental enthalpies of immersion, the volumes $W(L_c)$ filled by a molecular probe of critical dimension L_c,[1]

$$W(L_c) = -\frac{\left[\Delta_i H - h_i S_e\right] 2 V_m}{\beta E_o \sqrt{\pi}\left(1+\alpha T\right)} \tag{10}$$

E_o is the characteristic energy obtained from the reference isotherm of a small adsorbate (CH_2Cl_2, C_6H_6, CO_2, etc.) and L_c is the smallest micropore width accessible to the molecules of the liquid.

The use of a series of liquids of known molecular dimensions (i.e. dichloromethane [0.33 nm], benzene [0.41 nm], cyclohexane [0.54 nm], carbon tetrachloride [0.63 nm], cyclododeca-1,5,9-triene [0.76 nm], tri-2,4-xylyl phosphate [1.5 nm]) leads to the micropore size distribution.[1,7–9]

However, this technique reflects the true pore size distribution only as long as the entry into wider pores is not limited by constrictions smaller

than their actual size. If such "gate" effects are present, one obtains an apparent pore size distribution.[8,9] The difference between the apparent and the real pore size distributions can been illustrated if one uses the approach based on the modelling of CO_2 adsorption, a molecule which is small enough to bypass gate effects.[9] The two techniques are therefore complementary and provide a refined picture of the porous structure.

2.2. CHEMICAL ASPECTS OF IMMERSION CALORIMETRY

2.2.1. *Detection of surface oxygen from immersion into water*

As opposed to organic liquids and vapours, where the volume filling of micropores and adsorption on the external surface area S_e are the fundamental processes, water interacts strongly with functional groups of carbon surface. An interesting consequence is the possibility to estimate the number of surface groups from the experimental enthalpies of immersion of active carbons into water and into benzene at 293 K and taking into account the chemistry of the surface through an excess enthalpy of immersion, $\Delta_i H(H_2O)_{excess}$. As reported earlier,[10,11] water interacts in a similar fashion with surface functionalities containing mainly oxygen (–12.1 J $mmol^{-1}$) and with basic groups (–10.3 J $mmol^{-1}$). The latter are characterized by their equivalents of HCl and it appears that most of them do not contain oxygen. An overall assessment for a large variety of activated carbons led to[10]

$$\Delta_i H\,(H_2O)\,(J\,g^{-1}) = 0.210\,\Delta_i H\,(C_6H_6) - 9.9\,(J\,mmol^{-1})\,[O + HCl] \quad (11)$$

with average specific interactions around –(9.9 ± 0.7) J $mmol^{-1}$ of oxygen or HCl mequivalents of basic sites. As the concentration of the basic sites of typical carbons is not high, the bulk of the specific interactions is related to oxygen atoms.

2.2.2. *Determination of acidic and basic groups on carbon surface*

The correlation between the net enthalpy of neutralization into 2N aqueous solution of NaOH

$$\Delta_i H(NaOH)_{net} = \Delta_i H(NaOH) - \Delta_i H(H_2O) \quad (12)$$

and the number of equivalents of acid obtained from direct titration leads to a net enthalpy of neutralization of –(41.1 ± 1.8) kJ eq^{-1} for acidic sites. A similar approach for the net enthalpy of neutralization into 2N HCl

$$\Delta_i H(HCl)_{net} = \Delta_i H(HCl) - \Delta_i H(H_2O) \quad (13)$$

leads to a neutralization energy of –(52.3 ± 2.0) kJ eq^{-1} for basic sites.[12]

Further calorimetric experiments with 1N aqueous solutions of $NaHCO_3$ allow a clear distinction between carboxylic sites the other acidic sites. Selective neutralization of carboxylic groups reported a value of –(39.7 ± 1.7) kJ eq^{-1} which is close to the result obtained with NaOH for the bulk of the acidic groups.[12]

3. Application of Immersion Calorimetry to the Characterization of Carbons Used in Electric Double Layer Capacitors

Electrochemical capacitors have generated wide interest in recent years for high power applications where high efficiency and long cycle life are required. At the present, most commercial devices correspond to those referred to as electrical double layer capacitors (EDLCs) which perform by an electrostatic attraction between electric charges accumulated on the electrode surface and ions of opposite charge in the electrolyte side.[13]

Activated carbons are widely used as electrodes in EDLCs systems, as far as their high surface areas provide large interfaces for the formation of the electric double layer.[14] The reliable characterization of activated carbons in the general theoretical framework of Dubinin's theory, with its extensions to calorimetry and adsorption from solutions, leads to the identification of key parameters for high performance in electrochemical capacitors.[15–17] In this context, the determination of the real surface of the carbons is of prime importance and immersion calorimetry plays a major role, as illustrated below. Useful information can only be gained from several independent techniques, including the technique based on aqueous phenol solutions (see Section 2.1). As discussed in detail elsewhere, S_{BET}, is often too large[18] and leads to erroneous surface related properties.[15,17] As a consequence, it is difficult to establish reliable correlations.

In the case of 2M H_2SO_4 aqueous electrolyte, the study of a large variety of activated carbons showed that the specific capacitance at low current density (1 mA cm^{-2}), C_o, depends on standard contributions from the total surface area and from the surface groups which desorb as CO in Thermally Programmed Desorption (TPD)[15]:

$$C_o[H_2SO_4]\,(F\,g^{-1}) = 0.081\,(F\,m^{-2})\,S_{tot} + 63\,(F\,mmol^{-1})[CO](mmol\,g^{-1}) \quad (14)$$

This approach reflects the important role played by both the surface area S_{tot} and its chemical nature in the overall capacitance of activated carbons. It also establishes the origin of a pseudocapacitive process (via redox reactions involving CO-desorbing groups) which should be added to the purely EDLC mechanism. Furthermore, this approach explains the important scatter for the values of surface-related capacitance in (F m^{-2})

quoted in the literature with no clear linear correlation between the specific capacitance and the specific surface area of activated carbons.

On the other hand, surface oxide related pseudocapacitance contributions in the aprotic electrolyte 1M $(C_2H_5)_4NBF_4$ in acetonitrile are much weaker (9 F $mmol^{-1}$ of CO generated in TPD, for the best performing carbons) than in the H_2SO_4 electrolyte (63 F $mmol^{-1}$ of CO).[16] As illustrated by Figure 1, the specific capacitance at low current density, C_o, increases linearly with the total specific surface area, following the approximate correlation

$$C_o[(C_2H_5)_4NBF_4]\ (Fg^{-1}) = 0.09\ (Fm^{-2})\ S_{tot}\ (m^2g^{-1}) \qquad (15)$$

The deviation observed for some carbons is attributed to exclusion effects in the aprotic electrolyte. The fact that these materials display average micropore sizes or "gate" effects around 0.5–0.6 nm[16] limits the internal surface area accessible to ions $(C_2H_5)_4N^+$ with critical dimension around 0.69 nm.

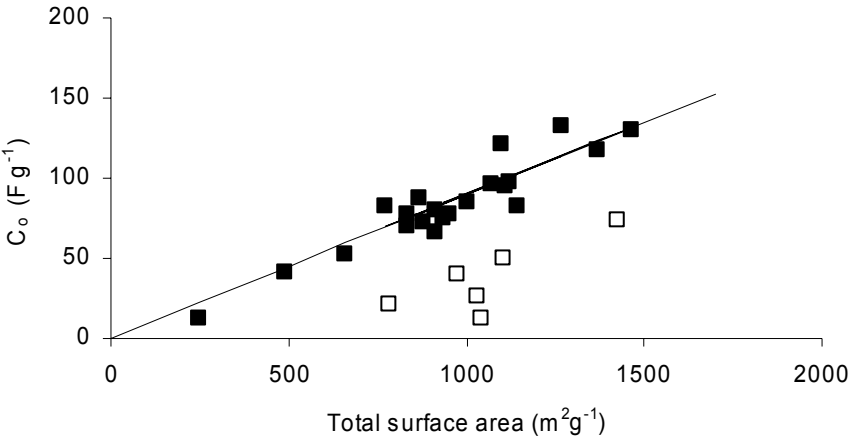

Figure 1. Variation of the specific capacitance (1 mA cm^{-2}) of activated carbons with the total surface area in 1M $(C_2H_5)_4NBF_4$/acetonitrile. The deviation for some carbons (□) reflects exclusion effects in the aprotic electrolyte.

Finally, the present work confirms the possibilities of immersion calorimetry used alone for the prediction of the specific capacitance at low current density of unknown activated carbons in the aprotic electrolyte 1M $(C_2H_5)_4NBF_4$ in CH_3CN (Figure 2). As far as the specific capacitance and the enthalpy of immersion into benzene, $-\Delta_iH[C_6H_6]$, are surface-related properties of the materials, one obtains a relatively good correlation between both parameters

$$C_o[(C_2H_5)_4NBF_4]\ (Fg^{-1}) = -0.57\ (F\ J^{-1})\ \Delta_i H[C_6H_6]\ (J\ g^{-1}) \quad (16)$$

As suggested by recent calorimetric tests,[17] the micropore system of typical activated carbons where the average micropore size is above 0.8 nm displays a similar accessibility to $(C_2H_5)_4NBF_4$/acetonitrile and to benzene. The deviations observed in Figure 2 (□) confirm the limited accessibility of the aprotic electrolyte into micropores of less than 0.7 nm.

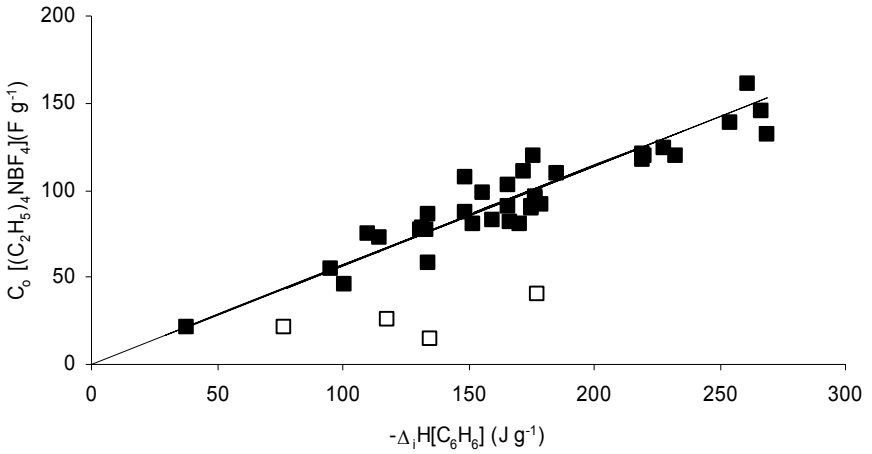

Figure 2. Correlation between the specific capacitance (1 mA cm^{-2}) of different activated carbons in the aprotic electrolyte, C_o $[(C_2H_5)_4NBF_4]$, and the enthalpy of immersion of carbons into benzene, $-\Delta_iH(C_6H_6)$. (□) Carbons with micropore widths below 0.7 nm.

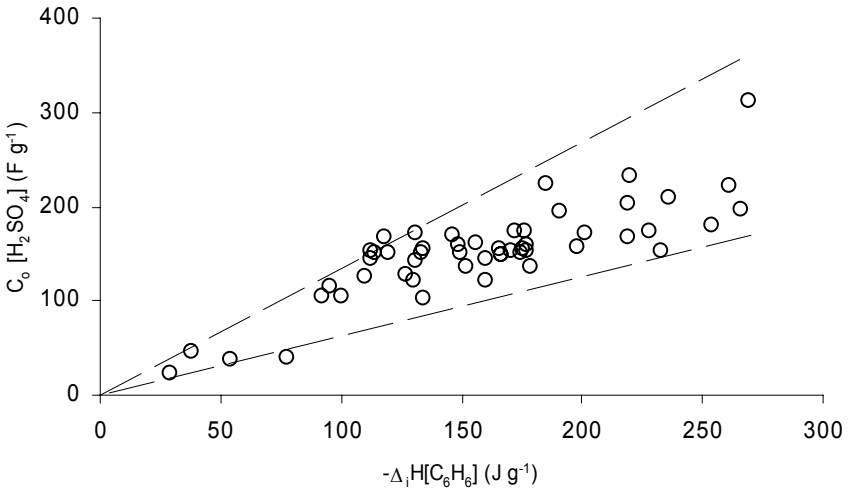

Figure 3. Evolution of the specific capacitance (1 mA cm^{-2}) of different activated carbons in H_2SO_4 aqueous electrolyte, C_o $[H_2SO_4]$, and the enthalpy of immersion of carbons into benzene, $-\Delta_iH(C_6H_6)$.

On the other hand, Figure 3 shows the limitations of this technique to assess, with a good accuracy, the suitability of a carbon to be used in H_2SO_4 aqueous capacitors. It is not surprising, in view of the significant influence of the CO-generating surface groups on the capacitance in H_2SO_4 aqueous medium (see Eq. (14)) whereas the enthalpy of immersion into a non-specific liquid such as benzene does not depend on the presence of oxygen.

4. Conclusions

Immersion calorimetry provides complementary information to the adsorption isotherms and simplifies considerably the assessment of porosity and chemical nature of activated carbons.

The assessment of activated carbons in the framework of Dubinin's theory with its extensions to calorimetry and adsorption from solutions led to the identification of key parameters for the performance of these materials in electrochemical capacitors. For 2M H_2SO_4 aqueous electrolyte, the limiting capacitance of activated carbons at low current densities depends essentially on the total surface area and on the surface groups which generate CO in TPD. In the case of the aprotic electrolyte 1M $(C_2H_5)_4NBF_4$ in acetonitrile, the specific capacitance increases linearly with the total specific surface area, the contribution from surface oxygen groups being less significant.

Micropore widths or "gate" effects of less than 0.7 nm notably reduce the internal surface area accessible to ions $(C_2H_5)_4N^+$ of the aprotic electrolyte, as opposed to the SO_4^{2-} ion of the aqueous medium.

This work confirms the possibilities of immersion calorimetry used alone for the prediction of the specific capacitance of carbons in 1M $(C_2H_5)_4NBF_4$ in CH_3CN, but it also shows the limitations of this technique to assess, with a good accuracy, the suitability of a carbon to be used as electrodes in H_2SO_4 aqueous capacitors.

References

1. F. Stoeckli, in: *Porosity in Carbons*, edited by J. Patrick (E. Arnold, London, 1995), pp. 67–97.
2. H.F. Stoeckli and F. Kraehenbuehl, The enthalpies of immersion of active carbons, in relation to the Dubinin theory for the volume filling of micropores, *Carbon* 19(5), 353–356 (1981).
3. L. Ballerini, D. Huguenin, P. Rebstein and F. Stoeckli, Determination of the total surface area in carbonaceous adsorbents by the selective adsorption of caffeine from water, *J. Chim. Phys.* 87, 1709–1714 (1990).

4. F. Stoeckli, T.A. Centeno, J.B. Donnet, N. Pusset and E. Papirer, Characterization of industrial activated carbons by adsorption and immersion techniques and by STM, *Fuel* 74(11), 1582–1588 (1995).
5. F. Stoeckli, M.V. López-Ramón and C. Moreno-Castilla, Adsorption of phenolic compounds from aqueous solutions, by activated carbons, described by the Dubinin-Astakhov equation, *Langmuir* 17(11), 3301–3306 (2000).
6. E. Fernández, D. Hugi-Cleary, M.V. López-Ramón and F. Stoeckli, Adsorption of phenol from dilute and concentrated aqueous solutions by activated carbons, *Langmuir* 19(23), 9719–9723 (2003).
7. T.A. Centeno and F. Stoeckli, The oxidation of an asturian bituminous coal in air and its influence on subsequent activation by steam, *Carbon* 33(5), 581–586 (1995).
8. F. Stoeckli and T.A. Centeno, On the characterization of microporous carbons by immersion calorimetry alone, *Carbon* 35(8), 1097–1100 (1997).
9. F. Stoeckli, A. Slasli, D. Hugi-Cleary and A. Guillot, The characterization of microporosity in carbons with molecular sieve effects, *Micropor. Mesopor. Mat.* 51, 197–202 (2002).
10. F. Stoeckli and A. Lavanchy, The adsorption of water by active carbons, *Carbon* 38(3), 475–494 (2000).
11. M.V. López-Ramón, F. Stoeckli, C. Moreno-Castilla and F. Carrasco-Marín, Specific and non-specific interactions of water molecules with carbon surfaces from immersion calorimetry, *Carbon* 38(6), 825–829 (2000).
12. M.V. López-Ramón, F. Stoeckli, C. Moreno-Castilla and F. Carrasco-Marín, On the characterization of acidic and basic surface sites on carbons by various techniques, *Carbon* 37(8), 1215–1221 (1999).
13. R. Kötz and M. Carlen M, Principles and applications of electrochemical capacitors, *Electrochim Acta* 45(15–16), 2483–2498 (2000).
14. A.G. Pandolfo and A.F. Hollenkamp, Carbon properties and their role in supercapacitors, *J. Power Sources* 157(1), 11–27 (2006).
15. T.A. Centeno and F. Stoeckli, The role of textural characteristics and oxygen-containing surface groups in the supercapacitor performances of activated carbons, *Electrochim. Acta* 52(2), 560–566 (2006).
16. T.A. Centeno, M. Hahn, J.A. Fernández, R. Kötz and F. Stoeckli, Correlation between capacitances of porous carbons in acidic and aprotic EDLC electrolytes, *Electrochem. Comm.* 9, 1242–1246 (2007).
17. T. A. Centeno and F. Stoeckli, in: *Recent Advances in Supercapacitors*, edited by V. Gupta (Transworld Research Network, Kerala, 2006), pp. 57–77.
18. F. Stoeckli and T.A. Centeno, On the determination of surface areas in activated carbons, *Carbon* 43(6), 1184–1190 (2005).

ADSORPTION ON ACTIVATED CARBON: ONE UNDERLYING MECHANISM?

PETER LODEWYCKX*
Department of Chemistry, Royal Military Academy, Renaissancelaan 30, B-1000 Brussels, Belgium

Abstract. This paper deals with the differences and similarities that are observed for isotherms of different adsorbates on activated carbon. In stead of the commonly used classification of isotherms in six "basic shapes", a more general approach is suggested. Each isotherm can be subdivided in different, distinct, parts, each of which is the result of a different adsorption mechanism. The relative importance of these parts, even the fact if they exist or not, depends on a number of parameters. The most important are the pore size distribution (PSD) and active surface groups of the adsorbent, the strength of the adsorbate–adsorbent interactions and the temperature at which the isotherm is measured. As all these parameters are either constant (e.g. PSD) or can be estimated (e.g. interaction energies) it is possible to calculate a complete isotherm for one adsorbate on the basis of that of another one. But in order to achieve this, one must fully comprehend the meaning of each and every part of the isotherm: isotherm equations must reflect the physical processes involved rather than just fit the (complete) isotherm.

Keywords: adsorption; activated carbon; mathematical modelling

1. Introduction

Activated carbons are widely used, and the number of possible applications is still growing. In many, if not all, of these applications adsorption comes into play. Therefore, most researchers are used to characterize their activated

*To whom correspondence should be addressed. E-mail: Peter.Lodewyckx@rma.ac.be

J.P. Mota and S. Lyubchik (eds.), Recent Advances in Adsorption Processes for Environmental Protection and Security, 19–28.

carbons by some kind of gas phase adsorption measurements, leading to adsorption isotherms. These isotherms contain a wealth of information about the carbon but, sadly, there remains a lot of uncertainty about their exact interpretation. Not only do the applied models differ from the ones used for other adsorbents (e.g. zeolites), but in many cases different models are used for different adsorbates. This is the direct result of (apparent) dissimilarities between the isotherms. In this work we will try to demonstrate that there is one underlying setcvcx of adsorption mechanisms that is applicable to all adsorbates (perhaps even to all adsorbents), the differences in the shape of the isotherms being only the result of interaction energy levels between the activated carbon and the vapour.

2. Type I Isotherms

2.1. GENERAL

According to the BDDT-classification isotherms can be subdivided into six major categories.[1] Only four of them will be treated. Type III is in fact identical to the first part of type V, and type VI is a step-wise isotherm that is very seldom seen in real adsorption measurements on activated carbon. The type I isotherm is the typical shape attributed to adsorption into micropores. However, it can also be found in other adsorption processes: the first part of both type II and type IV isotherms is clearly of this same shape. This is also valid for the very first part of the type V isotherm: if ones carefully studies the isotherm under $p/p_o = 0.2$ it becomes apparent that the very start of the convex type V isotherm is in fact concave towards the relative pressure axis (see Sections 2.3 and 5.1).

2.2. MICROPORE FILLING

The typical knee of the "real" type I isotherm is attributed to micropore filling. This can be described by a number of equations, the most commonly used being the Dubinin–Radushkevich or DR equation[1] (Eq. (1)) that gives the amount adsorbed W_e as a function of partial pressure p/p_o or concentration c/c_S. The parameters depending on the adsorbent–adsorbate combinations are the micropore volume of the adsorbent W_o, the liquid density of the adsorbate d_L, the scaling factor β (dependent on the energy of interaction) and B, related to the interaction energy and proportional to the mean micropore half-width.

$$W_e = W_o d_L \exp\left[\frac{-BT^2}{\beta^2}\log^2\left(\frac{c_s}{c}\right)\right] \tag{1}$$

It has been observed that in some cases, where there is clearly volume filling of micropores, the DR equation does not provide a good fit. In these cases one should use the Dubinin–Astakhov (DA) equation in which the factor 2 is replaced by a factor n.

2.3. NON-MICROPORE FILLING: THE WATER ISOTHERM

The start of the water adsorption isotherms on activated carbons seems to be of type I. It has also been demonstrated that it can be fitted with a DR or DA equation.[2] However, it is clear this first part is not related to micropore filling as this phenomenon does not start before $p/p_o \approx 0.3$ (see Section 5.2). Hence fitting by DR or DA is just a mathematical tool but has no physical meaning. It is generally agreed upon[3] that water adsorption on activated carbon starts with specific adsorption on active surface sites. These sites contain mostly oxygen (and sometimes nitrogen) and can be of an acidic or basic nature. Then water–water interactions (hydrogen bonding) promote the formation of water clusters around these active sites. Subsequently, these clusters are adsorbed in the micropore volume (see Section 5.2). Therefore, this part of the water isotherm can be considered as an adsorption on a non-porous surface with active sites, thus being described by a Langmuir type equation[1]:

$$n = \frac{n_m . b . (p/p_o)}{[1 + b . (p/p_o)]} \tag{2}$$

In which n represents the amount adsorbed, n_m the monolayer, b is related to the interaction energy and p_o/p is the partial water vapour pressure. Equation 2 gives a very good fit of the experimental isotherms for a wide variety of activated carbons. An example can be found in Figure 1.

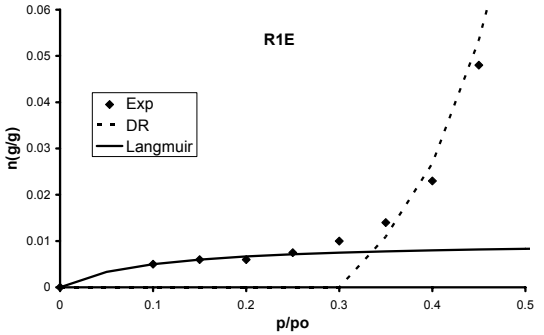

Figure 1. Langmuir fit of the initial part of the water isotherm.

The fitted parameters differ from one activated carbon to another. But there is a clear positive correlation between n_m and the number of oxygenated surface sites. The coefficient b is very small, in the order of magnitude of 5. This is rather surprising, b being a measure for the interaction energy. Therefore it seems logical to assume that b is not only related to the specific interaction between water and the active sites, but also comprises the mutual bridging between water molecules leading to the formation of water clusters. As these clusters will be formed around the initially (specifically) adsorbed water molecules, the number of clusters will still be related to the number of active sites. Therefore, n_m is still related to the number of active sites, even though the value of b is the result of two separate mechanisms.

2.4. NON-MICROPORE FILLING: TYPE II ISOTHERMS

The initial part of a type II isotherm, typical for adsorption onto non-porous surfaces, also has the characteristic type I form. It is clear that in this case it does not represent micropore filling, but only the formation of a monolayer on the surface of the adsorbent. How this monolayer is exactly forming on an activated carbon is, however, not really understood. It is clear it is not an instant coverage of the total surface. Most likely, as it is the case for water vapour adsorption, it will start at those spots that present the highest interaction energy with the adsorbate, i.e. oxygen surface groups. Then adsorption will spread out to form a monolayer. Even though it is clear that in some places multilayer adsorption will precede complete surface coverage by a monolayer (see also Section 3).

2.5. NON-MICROPORE FILLING: N_2 AND ARGON ISOTHERMS

There has been much debate about the thermodynamic inconsistency of the DR equation as for $p/p_o \rightarrow 0$ it does not reduce to Henry's law.

On the other hand there is the strange behaviour of nitrogen when measuring adsorption isotherms at 77 K: the very first part of the isotherm does not obey the DR equation. This is commonly ascribed to activated diffusion at the pore entrances.[4] At the very low temperature of 77 K the nitrogen molecules are believed to lack the necessary energy to overcome the potential of entering pores with diameter only slightly bigger than these molecules. So these points are considered to be "false". When waiting a long time (up to one day) per point one can clearly see the experimental isotherm approaching the DR curve, but without reaching it. The experimental points are giving a good, continuous, curve but with uptakes still smaller than predicted by DR or DA equations.

A third reflection can be made regarding adsorbent–adsorbate interactions. It is clear that not every location on the carbon surface will have the same interaction potential with the nitrogen molecules. It is reasonable to suggest that heteroatoms and other disturbances to the carbon surface will have a higher affinity towards nitrogen atoms.

Taking all this into account it seems likely that not only water molecules exhibit a specific interaction with the carbon surface at (very) low partial pressures but also other compounds such as nitrogen. To test this hypothesis the first "false" points were fitted with a Langmuir-type equation, Eq. (2).[5] After a slight modification a very good fit was achieved with Eq. (3):

$$n = \frac{n_m . b . (p/p_o - x_o)}{[1 + b . (p/p_o - x_o)]} \tag{3}$$

In this equation all parameters have the same meaning as in Eq. (2). The supplementary parameter, x_o, is a very small correction accounting for the offset of the apparatus: i.e. the lowest measurable data point. Figure 2 shows the fitting with the DR equation and Eq. (3):

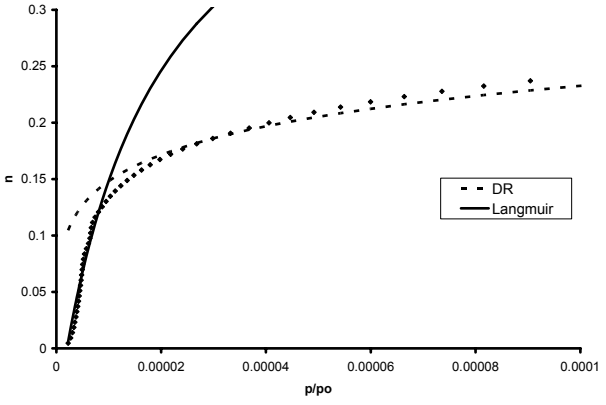

Figure 2. DR and Langmuir fitting of low pressure part of the N_2 isotherm (77 K) of Norit R1Extra.

Clearly, the DR equation gives an adequate fit of the experimental data points for values of $p/p_o > 2.10^{-5}$. For lower values, the Langmuir equation, Eq. (3), gives a very good fit. There is also an interesting direct relation between n_m and the DR micropore volume W_o. This is not surprising as the higher the micropore volume (which accounts for the majority of the adsorption surface on activated carbons), the higher the amount of "active surface sites". The values of b are much higher (20.000–50.000) than in

the case of water adsorption, indicating a pure specific interaction between the surface and the N_2-molecules.

It is also interesting to notice that the same fitting could be achieved for Ar isotherms on a zeolite, indicating a more general principle.

2.6. GENERALIZED INTERPRETATION OF TYPE I

From Section 2.5 it is clear that the typical "shoulder" of the type I isotherm is not always to be associated with micropore filling. It can also be the result of specific interactions: between surface groups and adsorbate molecules (H_2O, N_2, chemisorption), between adsorbate molecules (H_2O cluster formation) or between adsorbate molecules and the carbon surface (monolayer formation on non-porous carbons). In general, a type I isotherm, or a part of an isotherm with a type I shape, can be related to strong adsorbate–adsorbent interactions. The exact nature of these interactions depends on many different parameters such as pore size distribution, surface complexes, the nature of the adsorbate, and isotherm temperature.

3. Type II Isotherms

The type II isotherm, the straight line with a rather small but positive slope is normally associated with multilayer coverage of a non-porous surface. In the case of activated carbon non-porous is not the right word. It would be better to call it non-reinforced adsorption. It is the basic BET-type adsorption: the formation of a monolayer on the surface of the adsorbent due to adsorbate–adsorbent interaction, followed by multi-layer adsorption due to adsorbate–adsorbate and adsorbate–adsorbent interactions. In terms of PSD this phenomenon can be found in the meso- and macropores and on the external surface of the carbon. That is, everywhere where there is no enhanced adsorption due to specific interactions or overlapping potentials.

4. Type IV Isotherms

The type IV isotherm is associated with capillary condensation in mesopores. This accounts for the hysteresis loop. The models that are normally used all depend on the Kelvin equation, Eq. (4)[1]:

$$\ln\left(\frac{p}{p_o}\right) = -\frac{2\gamma V_L}{RT}\left(\frac{1}{r_m}\right) \tag{4}$$

Where p/p_o is the relative pressure of the adsorbate (–), γ the surface tension of the liquid adsorptive (N/m), V_L the molar volume of the liquid adsorptive (m^3/mol), R the universal gas constant (N m/mol K), T the temperature of the isotherm (K) and r_m the radius of the "cone" that is filled in a pore at pressure p (assuming a contact angle $\theta = 0°$). Even though this equation presents several disadvantages, it is straightforward and its use does not involve any heavy mathematics.

Normally there are two "modifications" to the Kelvin equation. The first one is to take into account the thickness of the adsorbed layer on the pore wall (adsorbed before the actual capillary condensation started and necessary to initiate this process), i.e. a type IV isotherm can not exist without a type II.

A second phenomenon is the difference between adsorption and desorption: the radius r_m given by Eq. (4) is only equal to the core radius in the case of desorption. For cylindrical pores open at both ends r_m equals twice the core radius and, consequently, r_m is two times the pore diameter r_p. It is very difficult to estimate the percentage of (meso-)pores open at both ends. But as the hysteresis loop in the mesopore region of the isotherms is usually quite marked for activated carbons, it is not uncommon to use a value of 100%. This means that the value of $2/r_m$ of Eq (4) can be replaced by $1/r_p$ when examining the adsorption branch of the isotherm and neglecting the thickness of the adsorbed surface layer.[8]

5. Type III and V Isotherms

5.1. FIRST PART

The water isotherms on activated carbons are usually of type V. They present three distinct regions. In the first one, typically between $p/p_o = 0$ and ≈ 0.4 there is very little uptake. In the second one ($p/p_o \approx 0.4$ to ≈ 0.6) there is a steep rise that accounts for about 80% of the total water uptake. In the last region there is a more gradual uptake reaching its maximum at $p/p_o \approx 1$.

The first part of the water isotherm has already been treated in Section 2.3. Historically, water isotherms have been fitted customarily by the Dubinin–Serpinsky[1] or DS equation, which, in its most simple form reduces to Eq. (5):

$$n = \frac{n_m . b . (p/p_o)}{[1 - b . (p/p_o)]} \tag{5}$$

The analogy with Eq. (2), the Langmuir equation, is striking. The only difference being the sign minus in stead of plus in the denominator. This was clearly put in to fit the convex shape of the type V isotherm. However, as demonstrated in Section 2.3, this does not explain the type I knee at the start. In addition, the convex shape of the DS equation could explain the steep rise in the second part of the water isotherm. But, as explained in Section 5.2, this rise is linked to the volume filling of micropores and has no direct link with the specific water–surface interactions described by Eq. (5). For these reasons the use of the DS equation for describing water vapour isotherms on activated carbon should be discontinued. It is an unambiguous example of one single equation trying to describe two distinct physico-chemical phenomena.

5.2. SECOND PART

The second part of the water isotherm, the steep rise, has, in the past, been erroneously ascribed to capillary condensation. Actually, it is none other than the equivalent of the type I steep rise found at the start of isotherms of N_2 or organic vapours: the volume filling of the micropore volume. The fact it is shifted to much higher values of p/p_o and it is not quite as steep as the type I can be fully explained by the weak interaction between carbon and water vapour.

This can be illustrated by the use of the Dubinin–Radushkevich equation. If the rise around $p/p_o = 0.4$ is really the filling of the micropores, one should be able to fit this part of the isotherm with the DR equation. The parameter β, as a measure for the interaction energy between the adsorbent and the adsorbate, should be (much) lower that, for example, nitrogen or

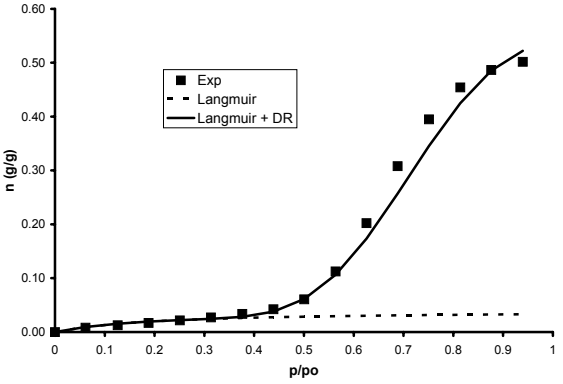

Figure 3. Fitting the second part of the water isotherm on NC100 with a combination of Langmuir and DR equations.

organic vapours. In Figure 3 an isotherm taken from literature[6,7] has been fitted with a combination of the Langmuir equation (see Section 5.1) and the DR equation taking a β value[8] of 0.06. The micropore volume W_o and the parameter B were taken to be identical with the values derived from the nitrogen isotherm as they are essentially linked to the pore size distribution of the carbon. It is clear that in the region of interest ($p/p_o < 0.7$) the combination of Langmuir and DR gives a good prediction. Especially because only the constants n_m and b of the Langmuir equation were used as fitting parameters.

5.3. THIRD PART

In the third part of the water isotherm, typically from p/p_o = 0.6–0.7 onwards, the DR equation usually underestimates the experimental data points. This is in agreement with the isotherms of other adsorbates, such as nitrogen, where for higher values of p/p_o the amount adsorbed according to the DR equation (volume filling of micropores) has to be supplemented by a contribution of the capillary condensation in the mesopores. This can be done by using the Kelvin equation (see Section 4).

Again it is possible to construct the water isotherm solely on the basis of the knowledge of the mesopore size distribution, e.g. from the nitrogen isotherm. As the volume of the pores of a certain radius r_p is known, the corresponding filling pressure can be derived from Eq. (4), substituting $2/r_m$ by $1/r_p$ (see Section 4). This gives, for each discrete value of p/p_o, the extra amount of water adsorbed by the mesopore system.[9]

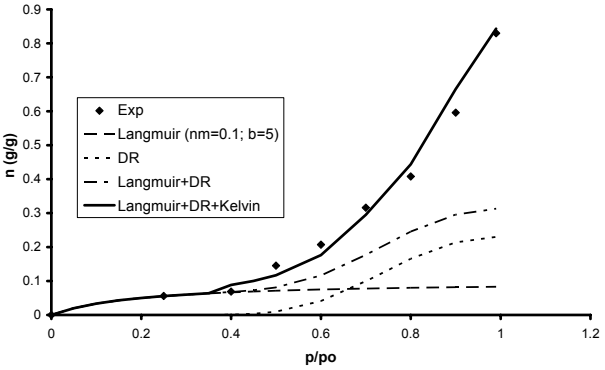

Figure 4. Combining Langmuir, DR and Kelvin equations to reconstruct the water isotherm on Norit C Granular (high amount of surface oxygen groups and large mesopore volume).

Not surprisingly, the modified Eq. (4) yields a contribution from capillary condensation for values of $p/p_o > \approx 0.6$. This theory has been tested on different activated carbons, both on highly microporous ones (i.e. with small amounts of mesopores) and carbons presenting a predominantly mesoporous structure. In both cases the water adsorption fitting was more than reasonable. This is illustrated in Figure 4.

6. Conclusion: a Generalized Model for Gas Phase Adsorption Isotherms

Equations describing an isotherm on activated carbon should be more than just a fitting of the isotherm graph. They should reflect the actual physico-chemical interactions occurring in the adsorption process. In almost all cases, there is not just one type of interaction but different ones, each representing a different part of the isotherm. Hence it is impossible to describe adsorption isotherms on activated carbon by one single equation. Adsorption on activated carbon can involve specific interactions, mono- and multilayer adsorption on "open" surfaces, micropore filling, capillary condensation and adsorbate clustering. Whether each of these processes occur, and when (i.e. for what value of p_o/p), depends on the adsorbate and on the type of carbon. Finally, it seems logical that the same reasoning would stand for other adsorbents such as zeolites.

References

1. Gregg, S.J. and Sing, K.S.W., Adsorption, Surface Area and Porosity. London: Academic Press, 1982
2. Slasli, A.M., Jorge, M., Stoeckli, F. and Seaton, N.A., Water adsorption by activated carbons in relation to their microporous structure, *Carbon*, 41, 479–486 (2003)
3. Brennan, J.K., Bandosz, T.J., Thomson, K.T. and Gubbins K.E., Water in porous carbons, *Colloid Surface A*, 187–188, 539–568 (2001)
4. Byrne, J.F. and Marsh, H., in Porosity in Carbons (J.W. Patrick ed.). London: Edward Arnold, 1995, 35
5. Lodewyckx, P. and Verhoeven, L., The applicability of the Dubinin-Radushkevich equation to the very low pressure region of isotherms of various microporous solids, *Stud. Surf. Sci. Catal.*, 144, 731–735 (2002)
6. Neitsch, M., Heschel, W. and Suckow, M., Water vapor adsorption by activated carbon: a modification to the isotherm model of Do and Do, *Carbon* 39(9), 1437–1438 (2001)
7. Neitsch, M., private communication.
8. Lodewyckx, P. and Vansant, E.F., Water isotherms of activated carbons with small amounts of surface oxygen, *Carbon*, 37, 1647–1649 (1999)
9. Lodewyckx, P., Van Rompaey, D., Verhoeven, L. and Vansant, E.F., Water isotherms of activated carbons with small amounts of surface oxygen: fitting the mesopore region, *Carbon*, 39, 309–310 (2001)

ADSORPTION OF ORGANIC VAPOUR POLLUTANTS ON ACTIVATED CARBON

A.J. FLETCHER,* M.J. KENNEDY, X.B. ZHAO, J.G. BELL, K.M. THOMAS*

Northern Carbon Research Laboratories, Bedson Building, Newcastle University, NE1 7RU, UK

Abstract. Emissions of organic vapor pollutants, arising mainly from anthropogenic sources have major environmental impact and the low emission levels required by increasingly stringent legislation are difficult to achieve. Adsorption on activated carbon can be used as a final stage for removal of very low concentrations of volatile organic pollutants present in air and gas streams. Isotherms and adsorption kinetics for a range of carbons with different porous structures and volatile organic compounds (VOCs) with a range of properties provide an improved understanding of the relationship between pore structure, adsorptive properties and adsorption characteristics. Competitive adsorption of other species present in gas flows, in particular water vapor, reduces adsorption capacity and kinetics. Laboratory measurements, which simulate process conditions, for example, very low vapor pressure, high temperature and competitive adsorption; provide an insight into the mechanisms associated with adsorption processes allowing process optimization.

Keywords: adsorption; volatile organic compounds; activated carbon; competitive adsorption

1. Introduction

Volatile organic compounds (VOCs) present a major environmental problem because of their toxicity and chemical reactions in the troposphere leading

*To whom correspondence should be addressed. E-mail: a.j.fletcher@ncl.ac.uk; mark.thomas@ncl.ac.uk

J.P. Mota and S. Lyubchik (eds.), Recent Advances in Adsorption Processes for Environmental Protection and Security, 29–54.

to ozone formation. Emissions of VOCs from anthropogenic sources for 1989 amounted to 23.8 million tonnes; in the UK alone and emissions were 80 times greater than natural sources. A study of hydrocarbons in Leeds city centre, identified the major sources as petrol and diesel emissions.[1] Several hundred different hydrocarbons have been identified in urban areas[2,3] and these species represent one of the most important classes of trace atmospheric constituents. Many VOCs degrade in the troposphere to produce a variety of secondary pollutants that may be harmful to human health as well as the environment.[4–7] Some VOCs are known to be carcinogenic,[8] or react in the atmosphere to form mutagenic or carcinogenic species. Relatively unreactive species may diffuse in the troposphere and form a uniform global distribution. Legislation to limit and ultimately reduce amounts of VOCs entering the atmosphere from chemical processes has been introduced in recent years making improved abatement methods necessary as part of the global strategy to reduce air pollution and tropospheric ozone.

Removal of the final traces of VOCs from process streams is inherently difficult because of the low concentrations. This can be achieved by adsorption on activated carbon. However, competitive adsorption, due to the presence of other species, such as water vapor, is a major problem. In this paper we investigate the factors which control the adsorption of VOCs on activated carbons and optimization of the adsorbent for specific applications covering a wide range of conditions.

2. Environmental Impact and Legislation

In 1979, EU member states signed the first international treaty targeting reductions in transboundary air pollution, called the UN Economic Commission for Europe Convention on Long Range Transboundary Air Pollution, which came into force in 1983, representing the initial European step towards effective reduction of emissions contributions from energy usage, industry, transportation, etc. Adoption of the ruling produced abatement strategies and development of emissions monitoring from each member state progressing towards proposed emission targets. The original targets were sulfur dioxide, non-methane volatile organic compounds and nitrogen oxides, while amendments in 1998–1999 saw this extended to include heavy metals and persistent organic compounds, including dioxins, and ammonia.[9] Directive 1999/13/EC applies to all member states, covering emissions of organic solvents from stationary commercial and industrial sources, including the replacement of species that are deemed to have a serious impact on human health, i.e. mutagens, carcinogens, etc.[10] VOC emissions released into the atmosphere contribute to the formation of tropospheric ozone, which can be harmful to human health, vegetation, forests and crops. Emissions of benzene and butadiene are already limited,

by governmental legislation, in most countries. However, they are not alone as potential carcinogens. Guidelines for limitation do not include synergistic effects, which are probably important in mixtures of VOCs.

3. Adsorption of Organic Pollutants from the Gas Phase

Sorption Studies on Porous Materials. Porous carbon adsorbents have extensive pore volumes, often greater than 0.4 $cm^3\ g^{-1}$, large apparent surface areas of 2,000–3,000 $m^2\ g^{-1}$, wide pore size distributions and mainly hydrophobic graphene layer surfaces with a variety of surface functional groups. Hence, activated carbons are widely used for removal of very low (ppm) concentrations of environmentally unfriendly VOCs from process and air streams.[11] The most important characteristics for porous adsorbents are amount adsorbed and rate of adsorption under specified conditions. Adsorbents with a wide range of pore size distributions and surface functional groups can be prepared. Many adsorption isotherms have been recorded for porous materials; however, very little work has been conducted on related dynamics due to experimental difficulties. Recent work has developed methods for the measurement of adsorption kinetics. Studies conducted within NCRL have focused on removal of VOCs in gas phase process effluent streams and air including emissions from coke ovens, hydrocarbon emissions from fuels, and removal of dioxins in flue gases. The Henry's law constant, which describes the adsorbate–adsorbent interaction at low pressure, is particularly important compared with standard adsorption parameters such as surface area, micropore volume or total pore volume. Molecular transport mechanisms controlling rates of diffusion and adsorption processes are crucial to understanding interactions in adsorption systems, especially the increased complexity of competitive adsorption systems. Hence, it is important to determine structural properties such as pore size distribution, and functional group concentrations; thermodynamic properties of adsorption systems including isosteric heats, and virial parameters; and kinetic parameters, which provide information on adsorption rates and activation energies of mechanisms involved.

The surface area of an activated carbon is predominantly composed of internal surface, and activated carbons owe their adsorptive properties to this and their pore size distribution, with external surface area and functional groups usually playing a comparatively minor role.[12] Oxygen-based functional groups on the edge of graphene layer surfaces may have a marked effect on adsorption.[13–15] Surface groups are extremely important in the adsorption of water vapor, acting as primary adsorption centers. An imperfect graphene layer structure, such as those found in activated carbons, has incompletely saturated valences and unpaired electrons that may also influence molecular adsorption, particularly for polar or polarizable

species.[16] Total pore volume is independent of adsorbate if the amount adsorbed is expressed as a liquid volume according to Gurvitsch's rule.[17] Water is an exception to this rule since the hydrogen-bonded structure of water adsorbed in hydrophobic carbon micropores has a lower density than water. This phenomenon has been observed in adsorption studies.[18–22] Size exclusion effects may also influence the measurement of apparent total pore volume in the case with carbon molecular sieves (CMS) used for air separation, where the selective porosity excludes larger adsorptives from the majority of the porous structure.[23]

Adsorption isotherms are conventionally expressed as amount adsorbed (mmol g^{-1}) versus relative pressure (p/p^0), for comparison purposes. Isotherms provide significant information about the adsorbate–adsorbent interactions, including assessment of surface chemistry and porous structure including estimates of surface area, pore volume and pore size distribution. All adsorption isotherms should fit one, or a combination of two or more, of the six recognized types classified by Brunauer, Deming, Deming and Teller.[24,25] Figure 1 shows the six possible shapes, and information relating to each class.

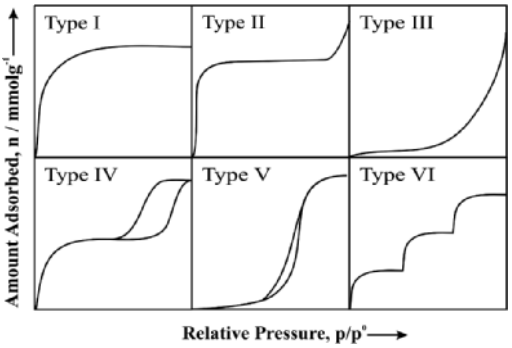

Figure 1. Schematic representation of adsorption isotherm classification[24]: Type I – Typical of predominantly microporous adsorbents, as majority of pore filling occurs at $p/p^0 < 0.1$. Adsorption is usually complete at $p/p^0 \sim 0.5$. Type II – Typifies physical adsorption of gases by non-porous solids; monolayer coverage followed by multilayering at high p/p^0. Type III – The isotherm is convex to the p/p^0 axis; characteristic of weak adsorbate–adsorbent interactions[26] leading to low uptake at low p/p^0. At high p/p^0, adsorbed molecules act as primary adsorption sites increasing adsorbate–adsorbate interactions and increasing uptake at higher p/p^0. Type IV – This isotherm commonly has a hysteresis loop associated with mesoporosity and associated capillary condensation[27]; the shape of the hysteresis loop is unique to each system. Type V – The isotherm is convex to p/p^0 axis and, similar to Type III, characteristic of weak adsorbate–adsorbent interactions,[26] indicative of microporous/mesoporous solids. Type VI – This isotherm is observed when complete monolayers form before progression to subsequent layers. This arises from adsorption on extremely homogeneous, non-porous surfaces where monolayer capacity corresponds to step height.[28]

Adsorption Dynamics. In addition to thermodynamic information obtained from isotherms, the kinetics for equilibration of each isotherm point allow study of the variation of kinetic parameters with surface coverage. Figure 2 shows the relationship between the isotherm and kinetic profiles for corresponding pressure increments and the rapid change in pressure for the pressure increment and the corresponding adsorption response.

Normalized kinetic profiles can be described using a series of nested models based on a double stretched exponential (DSE) model which describes a two process mechanism (Eq. (1)).

$$M_t / M_e = A_1(1 - e^{-(k_1 t)^{\beta_1}}) + (1 - A_1)(1 - e^{-(k_2 t)^{\beta_2}}) \quad (1)$$

where M_t is uptake at time t, M_e is equilibrium uptake, k_1 and k_2 are rate constants, β_1 and β_2 are exponents and A_1 and $1 - A_1$ are fractional contributions for process mechanisms corresponding to k_1 and k_2, respectively. The double exponential (DE) model is a nested model of the DSE model with $\beta_1 = \beta_2 = 1$ (Eq. (2)).

$$M_t / M_e = A_1(1 - e^{-k_1 t}) + (1 - A_1)(1 - e^{-k_2 t}) \quad (2)$$

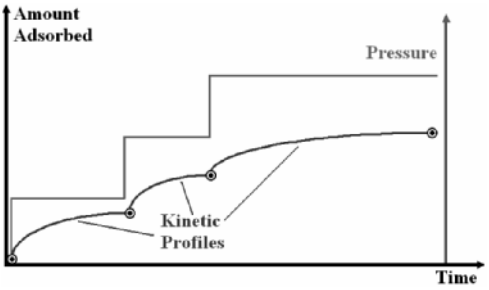

Figure 2. Schematic diagram of measurement techniques for kinetic parameters.

Diffusion of methanol and ethanol into $Ni_2(4,4'bipyridine)_3.(NO_3)_4$ porous materials followed the DE model. Since there are equal numbers of pore cavities and windows in these materials, as shown from crystallographic studies, diffusion through them have equal contributions ($A_1 = 0.5$). The slower kinetic process for diffusion through the windows have high activation energies, while the faster process with low activation energy involved diffusion along the pore cavities.[29,30] The stretched exponential (SE) model is a nested model of the DSE model where $A_1 = 1$, i.e. $k_1 = k_2 = k$ and $\beta_1 = \beta_2 = \beta$, described by Eq. (3).

$$M_t / M_e = 1 - e^{-(kt)^{\beta}} \quad (3)$$

Derivation of the SE model for different physical mechanisms has an underlying common mathematical structure, which is one-dimensional with a distribution of relaxation times when β = 0.5, and three-dimensional with a single relaxation time when β = 1. The SE model was observed in quantum molecular sieving of H_2 and D_2 on a carbon molecular sieve (CMS T3A) at 77 K and a porous carbon.[31] The Linear Driving Force (LDF) model is a special case of the SE model when β = 1, described by Eq. (4).

$$M_t / M_e = 1 - e^{-kt} \tag{4}$$

A plot of $\ln(1 - M_t/M_e)$ versus time is linear with a gradient equal to the rate constant (k). The LDF model is observed for adsorption of gases such as oxygen, nitrogen, carbon dioxide, and noble gases on carbon molecular sieves and vapors on activated carbons.[23,32–38] The change from LDF to SE represents a change from a single relaxation time to a distribution of relaxation times.

Criteria for acceptable fits of experimental data to a kinetic model were 99% of residuals within ±0.02 for the model with the least numbers of variables. Comparison of the models is difficult due to the different number of variables. Similarities between the shapes of DE and SE curves produce additional difficulties in distinguishing between models. The most appropriate model was selected on the basis of lowest number of variables consistent with the adsorption mechanism, which fitted the experimental data.

4. Experimental

Static Adsorption Systems. Kinetic measurements were performed using a Hiden Isochema Intelligent Gravimetric Analyzer (IGA); an ultrahigh vacuum system that allows isotherms and corresponding kinetics to be determined, for set pressure steps.[39] Balance and pressure control systems were fully thermostated to 0.2 K to eliminate the influence of changes in the external environment. The micro-balance had 1 μg long-term stability with weighing resolution of 0.2 μg. The sample (100 ± 1 mg) was outgassed to constant weight, at $<10^{-6}$ Pa, at an appropriate temperature. The liquid used to generate the vapor was degassed fully by repeated evacuation and vapor equilibration cycles of the liquid supply side of the vapor reservoir. VOCs typically have vapor pressures, at 293 K, in the range 0.13–101.3 kPa, or corresponding volatility under particular conditions of use.[10] The degas procedure is particularly critical for measurements of VOCs with very low vapor pressures. The gas/vapor pressure was gradually increased, over ~30 s to prevent microbalance disruption, until the desired value was achieved. Pressure control was via two transducers with ranges 0–0.2 and 0–10 kPa

(±0.02% for each range). Set pressure was maintained by active computer control of the inlet/outlet valves. Mass uptake was measured as a function of time and the approach to equilibrium monitored in real time with a computer algorithm. After equilibrium was established, the gas/vapor pressure was increased to the next set pressure value and the subsequent uptake measured until equilibrium was re-established (see Figure 2). Mass increase due to adsorption for each step was used to calculate kinetic parameters for adsorption, using an appropriate kinetic model. Errors in calculated rate constants were typically < ±2%. Sample temperature was monitored throughout and variation was minimal (< ±0.05 K). Isotherms were carried out in steps of relative pressure, corresponding to steps in surface coverage. Saturated vapor pressures were calculated using the Antoine equation (Eq. (5)),[40] where p^0 is the saturated vapor pressure, T is the temperature (°C) and A, B and C are constants defined by the adsorbate.

Flowing Adsorption Systems. The IGA can also be used in flow control mode, including four component streams. Figure 3 shows the additional mixing stage required to produce multi-component gas/vapor mixtures for adsorption, fed into the base of the reaction chamber, near the sample bucket, producing a continuous flow over the sample. The vapor generator unit was isothermal to prevent condensation of vapor species, allowing accurate mixing of gas/vapor species. The heating element, for a fast response furnace (≤50 K min^{-1}), and mass spectrometry sampling line were in close proximity to the sample allowing direct determination of evolved species. Particular issues in the design of a competitive adsorption instrument are the effects of helium carrier gas on adsorption of single components, accurate mixing of vapor streams under precise temperature/pressure, mass

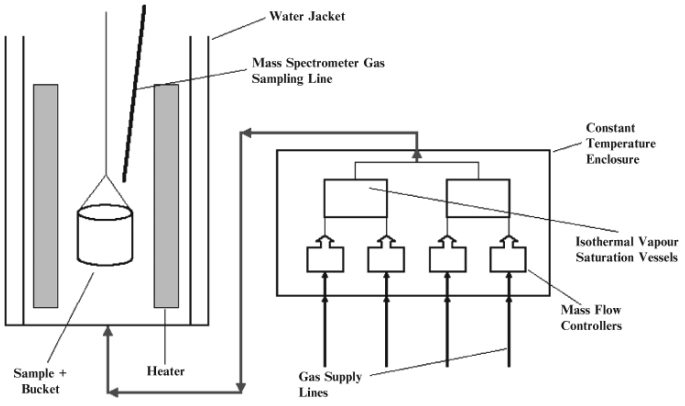

Figure 3. A schematic diagram of the IGA competitive adsorption instrument.

spectrometer response to avoid signal saturation, repeatability of the gravimetric system in response to flow of multi-component vapor streams, direct measurement of gas phase compositions during adsorption and determination of amounts of adsorbed species using TPD.

5. Effect of Porous Structure and Surface Chemistry on Adsorption

Adsorption characteristics are influenced by porous structure characteristics, including pore size distribution, pore shape and pore volume, as well as surface chemistry. It is possible to use specific adsorbates with a range of shapes and sizes as molecular probes of the porosity present in an adsorbent structure, including the elucidation of transport mechanisms and pore geometry. The minimum molecular dimension needs to be considered for slit shaped pores, whereas for spherical pores two molecular dimensions are important.[41] Hence, the minimum dimensions of a microporous structure may be determined using a carefully selected series of gases and vapors with varying shapes and sizes.[23,32,33] An example of this is the determination of the size of the selective porosity in CMS materials.[23]

Surface functional groups are generally considered to fall into two main groups: oxygen containing species, e.g. carboxylic, anhydride and phenolic (Figure 4), or nitrogen containing groups, e.g. pyrrolic, pyridinic, quaternary and nitrogen oxides (Figure 5). Unpaired sigma electron and in-plane sigma electron pair sites also exist in carbons (see Figure 4).[42] The functional groups may have a variety of interactions, e.g. electrostatic, hydrogen bonding, and van der Waals with given adsorbates.

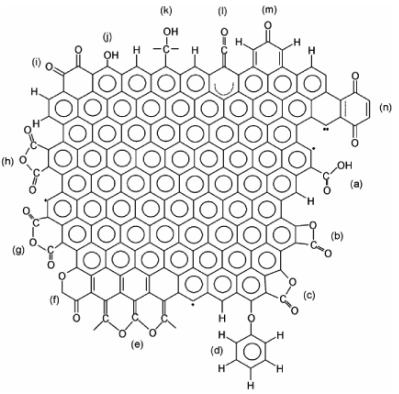

Figure 4. Possible oxygen functional groups on carbon surfaces: (a) carboxylic groups; (b) lactone (four-membered ring); (c) lactone (five-membered ring); (d) ether bridge; (e) cyclic ethers; (f) pyrone; (g) cyclic anhydride (six-membered ring); (h) cyclic anhydride (five-membered ring); (i) quinone; (j) phenol; (k) alcohol; (l) ketene; (m) carbonyl; (n) *p*-quinone.[42,43]

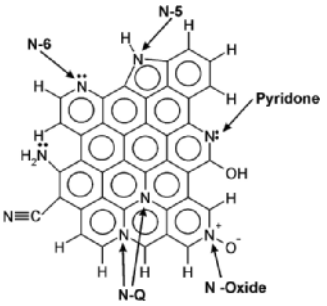

Figure 5. Representation of nitrogen functionalities in carbon. N-6: pyridinic; N-5: pyrrolic; pyridones[44]; N-Q: nitrogen substituted for carbon in aromatic graphene structure, resembling quaternary nitrogen in NH_4^+ ions[45,46]; nitrogen oxide[47–50]; and $–NH_2$ and –CN groups.[45,46]

Hydrophobic/Hydrophilic Surface Interactions. The effect of adsorbate/adsorbent interactions was investigated using a series of adsorptives varying from hydrophilic to hydrophobic (water, straight chain aliphatic alcohols and long chain *n*-alkanes). Figure 6 shows isotherms obtained for an increasingly hydrophobic series of adsorbates. It is evident that isotherm shape changes according to interactions within the system. Water gives a classic Type III isotherm, through Type II character for the alcohols and finally Type I/Type II isotherms are obtained for the aliphatics.[38] Carbon BAX950 has a low concentration of surface oxygen functional groups and the water vapor adsorption isotherm has a small uptake at low relative pressures due to weak adsorbate–adsorbent interactions.[36–38] The shape of the isotherms for the alcohol series shows increasing uptake at low relative pressure and Type I character increased as chain length and hydrophobicity increased. The *n*-alkanes show high uptake at low relative pressure with a small increase in the mid-range pressure, leading to pore filling.[38] Recent work shows that oxidation of activated carbon increases surface hydrophilic character, and an associated increase in low pressure adsorption of water vapor[51] but a reduction for benzene.

Adsorption Dynamics. Associated dynamics for these adsorption isotherms can be determined using the methods outlined previously. However, it is essential that adsorption isotherms agree over an adequate temperature range, in order for steps to be considered comparable on a constant surface coverage basis to allow comparison of rates obtained at different temperatures. Figure 7 shows adsorption isotherms obtained for methanol and ethanol adsorption on BAX950 over the temperature interval 288–313 K.[38] The isotherms obtained for ethanol show a greater uptake at lower relative

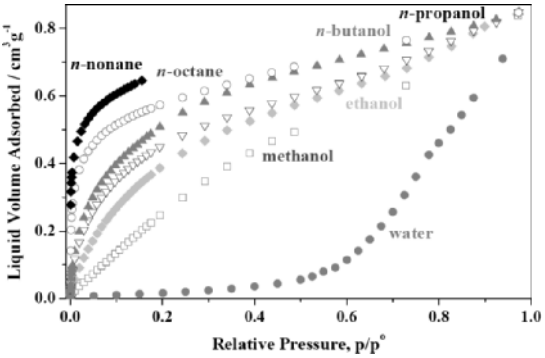

Figure 6. Adsorption isotherms for a range of hydrophobic/hydrophilic adsorptives on BAX950 at 303K.[38]

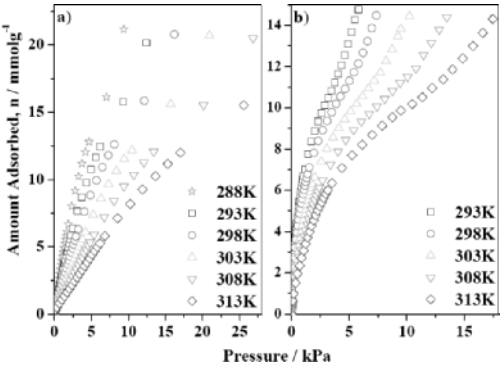

Figure 7. Adsorption of (a) methanol and (b) ethanol on BAX950 (288–313 K).[38]

pressure, compared to methanol, which is consistent with the greater hydrophobic character of the former due to the longer chain length.

Adsorption kinetics for these isotherms can be determined using the models discussed previously, using normalized data for each pressure increment expressed as M_t/M_e versus time. Figure 8 shows fits of the SE kinetic model to the experimental data for water and benzene adsorption on BAX950. Residuals of the fit demonstrate the accuracy of the kinetic modeling, with all residuals within ±0.02. The models can also be used to determine kinetics of desorption. Figure 9 shows SE fits obtained for desorption of water and methanol from BAX950.

The graphs demonstrate kinetic analysis and modeling of a series of kinetic profiles obtained for a complete isotherm. The kinetic parameters change with adsorption mechanism with surface coverage. The trend of

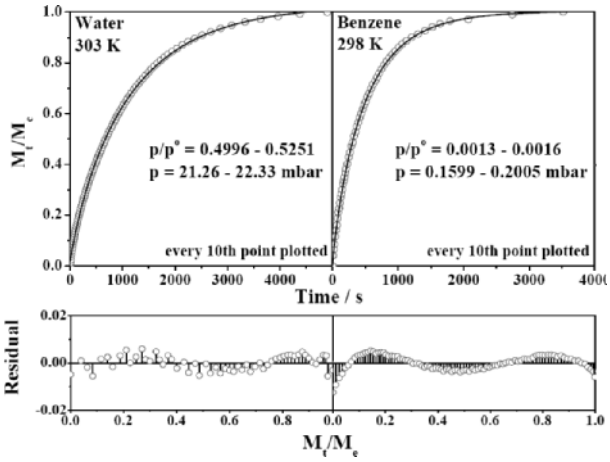

Figure 8. Adsorption profiles for water and benzene vapors on BAX950 and the corresponding fits of the SE kinetic model.[52]

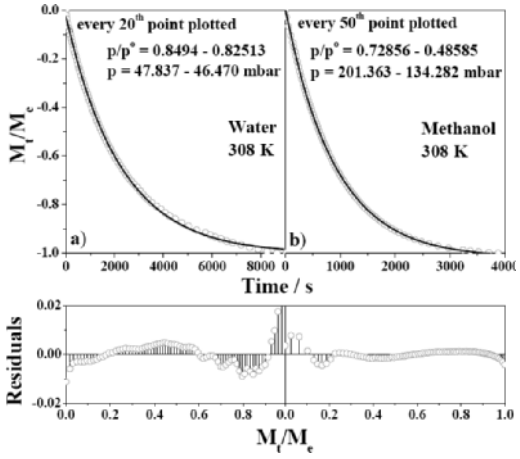

Figure 9. Desorption profiles for water and methanol vapors from BAX950 and the corresponding fits of the SE kinetic model.[52]

adsorption kinetic rates obtained for the series of adsorption isotherms shown in Figure 6 are shown in Figure 10. The rate constants obtained for water vapor decrease with increasing uptake whereas the opposite trend is observed for adsorption of *n*-alkanes. Alcohols show intermediate behavior and change progressively with increasing hydrophobic/hydrophilic character. The trend of decreasing rate constant with increasing water vapor pressure has been observed previously.[19,21,37,38,52,53] This is ascribed to decreasing

adsorbate–adsorbent interactions and increasing importance of the associative mechanism involving adsorbate–adsorbate interactions with increasing extent of adsorption.[37,38]

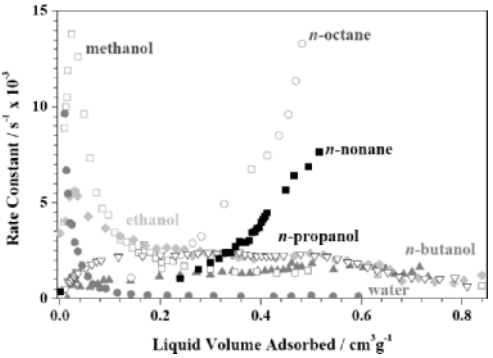

Figure 10. Adsorption kinetics for adsorptives with varying hydrophobic/hydrophilic character on BAX950 at 303K.[38]

Compensation Effect. Measuring isotherms on a fixed relative pressure basis, results in corresponding steps of surface coverage, allowing the kinetic data obtained to be used in the determination of activation energies associated with the adsorption mechanisms of the system using the Arrhenius equation. Correlations are often observed between activation energy (E_a) and associated ln(A) where A, is the pre-exponential factor for different members of a series of related reactions. This is referred to as a compensation effect (CE). Arrhenius graphs for a family of reactions are often straight lines of varying gradient, which intersect at one point, the *isokinetic point*. The effect has been observed for a wide variety of systems but there is no generally accepted theoretical explanation for the CE.[54] It has been attributed to experimental error,[55] or to a mathematical consequence of the rate constant exponent in the Arrhenius equation.[56–58] However, the additional condition for the CE of non-zero isokinetic rates was used.[59,60] A series of ln(k) against 1/T plots, for a family of processes, will give one of two results (Figure 11). A true CE yields a linear correlation between ln(A) and E_a; and graphs of ln(k) vs 1/T have a point of concurrence, the *isokinetic point*. When graphs of ln(A) and E_a show linearity, but do not exhibit a point of concurrence, the CE is not valid. The *isokinetic point* is observed at T_{iso} where $m = 1/RT_{iso}$, and m is the gradient of the graph in Eq. (6). Hence all ln(k) values must be equal at T_{iso}.

$$\ln(k) = E_a(m - 1/RT) + const. \tag{6}$$

Measurements over relatively large temperature ranges and minimization of sources of error are essential to confirm a compensation effect. Suàrez et al.[61] suggested that caution be exercised if the range in activation energy is small. Although the experimental temperature range must be wide, it appears to have little effect, at least in catalysis, with respect to its position relative to the isokinetic point. Isokinetic temperatures above and below the temperature range used have been observed.[38,62] Kinetic analysis for the series of adsorbates shown in Figure 6, using the Arrhenius equation produced activation energies and pre-exponential factors for the adsorption mechanisms involved. Figure 12 shows the correlation obtained between ln(A) and E_a for 16 different adsorption systems. It is clear that, although each individual system exhibits a unique gradient and changes in slope within its own dataset, there is an overall trend. The volume of data exhibiting positive CE confirms the presence of an effect. The correlation is ascribed to build-up of material at adsorption barriers, i.e. larger barriers produce greater amounts of adsorbate at the barrier and slow the rate of diffusion.[38]

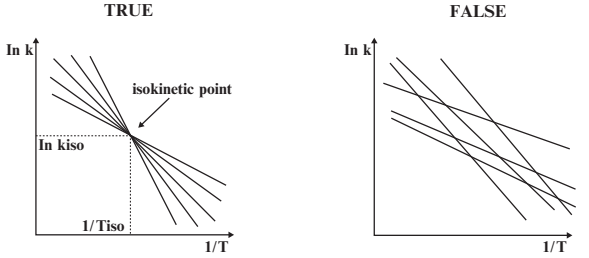

Figure 11. Examples of true and false compensation graphs.

6. Competitive Adsorption

High concentrations of environmentally unfriendly species can be removed from process streams by various treatment techniques such as condensation, but these methods cannot be used with very low concentrations, which are found in the final cleanup stage.[1] Adsorption methods can be used for the removal of trace quantities of pollutants. Previous studies have focused on adsorption of single components. However, to simulate a real application scenario, it is necessary to consider mixed component streams, introducing the complication of competitive or co-adsorption. Very few experimental studies have been carried out and, as a result, very little information is available on competitive adsorption.

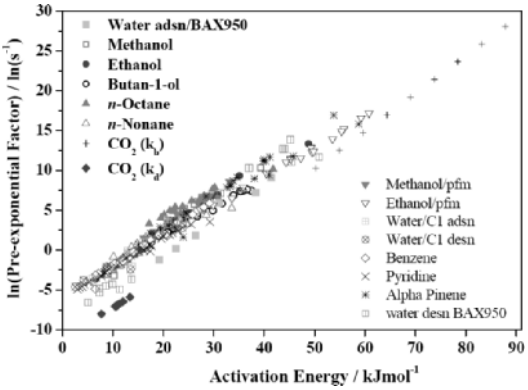

Figure 12. Compensation effect for adsorption/desorption kinetics on activated carbons.[38]

In the adsorption of VOC species from ambient air, there is competitive adsorption with nitrogen, oxygen, and water vapor. The presence of water vapor is a very specific major problem, varying with weather conditions and can produce degradation in the breakthrough times of other species.[63,64] Hence, carbon bed performance, for emissions abatement from process streams is influenced by multicomponent adsorption. Primary adsorption sites for organic species in activated carbons are hydrophobic graphene basal plane layers. Hydrophilic species are adsorbed initially on functional groups.[19,20,37,65,66] Clusters of water molecules develop around functional groups with increasing relative pressure.[66] The isolated clusters of water molecules are potential barriers to diffusion of organic species.[37] At higher p/p^0 bridging occurs between clusters or a continuous surface film is formed depending on the surface functional group distribution.[66] Pore volume filling occurs at high relative pressure but the density of adsorbed water is usually lower than that of the liquid.[19,20,37,65] This is ascribed to the inability of adsorbed water to form a full three dimensional structure in micro-porosity.[19,20,37,65] Competitive adsorption is difficult to study because of problems associated with quantifying the uptakes and adsorption dynamics of various adsorbed species in multicomponent adsorption systems. Amounts adsorbed may be calculated indirectly from a complete set of adsorption isotherms for the total adsorption of the multicomponent system, using various models based on thermodynamic principles, or determined by direct measurement of the amounts of each component adsorbed.[67] In the case of the latter, there is only limited experimental information available in the literature.[68–73]

Adsorption equilibrium theories for multicomponent systems have been developed based on extended Langmuir,[74] ideal adsorption solution,[75–80] and

real adsorption solution[75,81–83] theories, but their predictive value is limited because it is not possible to select a priori the most suitable model without extensive experimental measurements to validate the model for a particular system.[67] The experimental data required to establish and validate a model are extensive and time-consuming to obtain. Single component isotherms can be measured by volumetric or gravimetric methods for pure species with the latter providing a direct measurement of the amount adsorbed.[84] Gravimetric studies of adsorption of mixed flow systems have been conducted.[21] Volumetric, gravimetric, and chromatographic methods have been used to study multicomponent isotherms, whereas breakthrough curves and flow desorption have been used, combined with direct determination of amounts adsorbed by gas analysis to give multicomponent isotherms.[67] Secondary, competing species can reduce adsorption capacity for an adsorbate by occupying specific sites. Competitive effects will also be evident in kinetic parameters. The effects of competitive adsorption are due to occupation of surface sites, interactions between adsorbed species and the influence of additional species on surface and gas phase diffusion. Variations in the kinetic parameters have been observed in binary systems even if one of the species is not adsorbed to any significant extent.[35]

Separating Thermodynamic and Kinetic Effects in Flowing Systems. In order to separate the effects on thermodynamic and kinetic parameters, it is necessary to consider the relevant data separately. Isotherms and isosteric heats of adsorption can provide a representative view of the thermodynamic properties of an adsorption system. Figure 13 shows isotherms obtained for the adsorption of pure vapors (water and *n*-octane) compared with adsorption of the same vapors in flowing helium streams. These experiments allow the effect of an essentially non-adsorbing, secondary species, helium, to be investigated.

Kinetic Parameters. It is evident that the systems are not affected thermodynamically as there is no significant difference in the adsorption isotherms obtained. However, analysis of the corresponding kinetic profiles using the LDF model shows that there is a dramatic difference in the effect of helium on the adsorption of water compared with *n*-octane (Figure 14). Adsorption of water as a simple component is much slower than the adsorption of pure *n*-octane and the introduction of helium has a greater effect on the species which has faster adsorption kinetics. In contrast, the trend for water vapor adsorption, which is significantly slower than *n*-octane adsorption, is virtually unchanged with the reduction in mean free path.

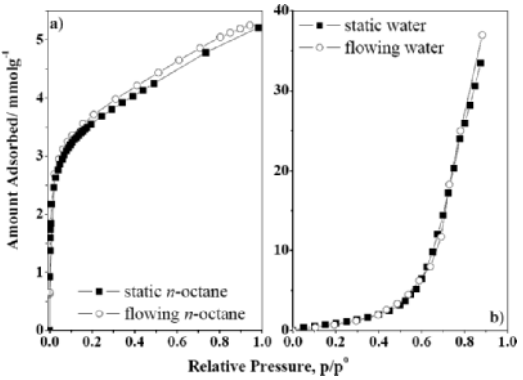

Figure 13. Static vapor and vapor/helium isotherms obtained for adsorption of (a) water and (b) *n*-octane on BAX950.[35]

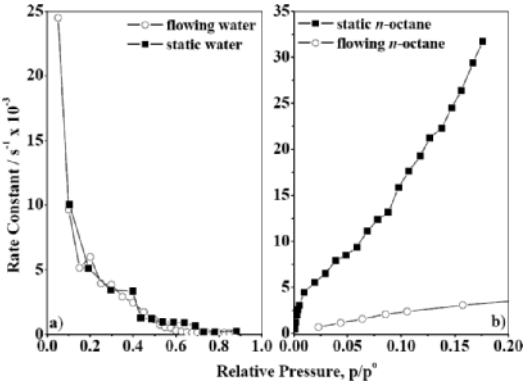

Figure 14. Kinetics under static and flowing vapor conditions for adsorption of (a) water and (b) *n*-octane on BAX950.[35]

Mass Spectrometric Resolution of Competitive Adsorption. In order to analyze and interpret the relative concentrations of each component adsorbed in a multi-component system, it is necessary to calibrate the partial pressure of vapor in the system (μPa) with flow rate (cm^3 min^{-1}). Figure 15 shows the correlation of partial pressure with flow rate. It is evident that there is good agreement between the two parameters and that the flow rate can be used as an accurate measure of the partial pressure in the system.

One method of determining the effect of a competing species is perturbation, where a single component is adsorbed and allowed to equilibrate before the introduction of a second adsorbate. Figure 16 shows a sequential adsorption profile, where water has been adsorbed at a flow rate corresponding to a partial pressure of $p/p^0 = 0.6$ and equilibration established. After equilibrium the $p/p^0 = 0.6$ flow of water vapor in helium is maintained

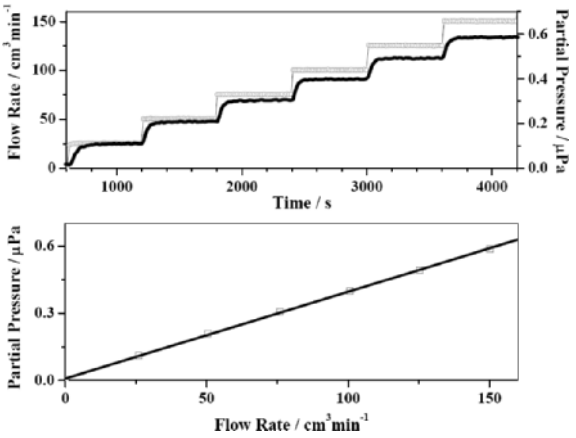

Figure 15. Mass spectrometric calibration of vapor flow in IGA flowing adsorption assembly.[35]

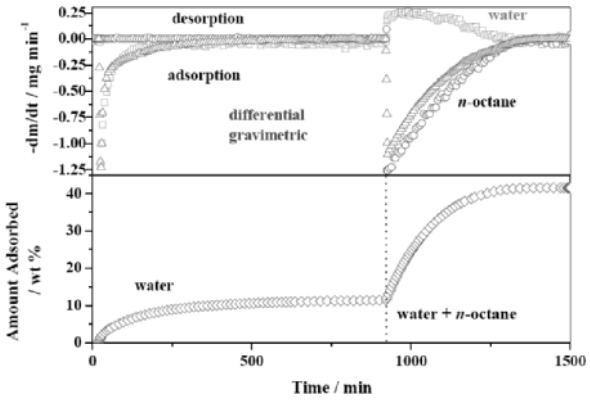

Figure 16. Sequential adsorption of: (1) water vapor, $p/p^0 = 0.6$; (2) *n*-octane, $p/p^0 = 0.1$ + water, $p/p^0 = 0.6$ vapor on BAX950.[35]

and a second flow corresponding to $p/p^0 = 0.1$ of *n*-octane in helium is added. It is evident that some water is displaced by *n*-octane before re-equilibration of the system with an associated increase in mass.[35]

Figure 17 shows a similar profile to that in Figure 16 but, in this case, the primary stream is $p/p^0 = 0.1$ of *n*-octane in helium and the secondary flow corresponds to $p/p^0 = 0.6$ of water in helium. This graph again exhibits displacement of the primary species for the secondary and relaxation back to equilibrium.[35] Understanding the mechanisms involved in the displacement of one species by another can assist in the interpretation of adsorption profiles for simultaneous adsorption. Figure 18 shows the simultaneous adsorption of water ($p/p^0 = 0.6$) and *n*-octane ($p/p^0 = 0.1$) in helium on

activated carbon BAX950. The adsorption of water occurs quickly but there is displacement of water with increasing *n*-octane uptake, which is slower as a result of the presence of a second adsorbate.[35] It is interesting to note that the final uptakes for both "combined" profiles are not significantly different (~42 mmol g^{-1}) irrespective of order of adsorbate loading.

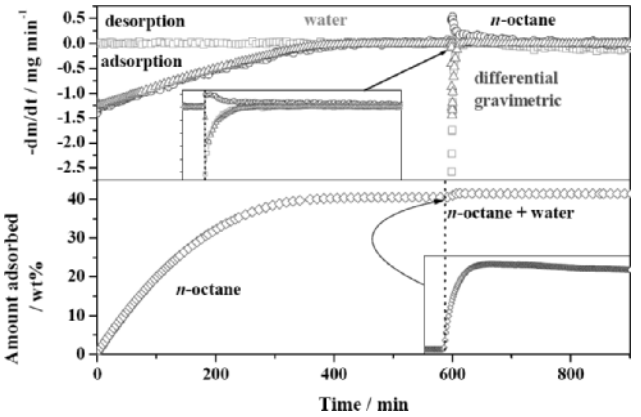

Figure 17. Sequential adsorption: (1) *n*-octane vapor, $p/p^0 = 0.1$ in helium, (2) water, $p/p^0 = 0.6$ + *n*-octane vapor, $p/p^0 = 0.1$ in helium on BAX950.[35]

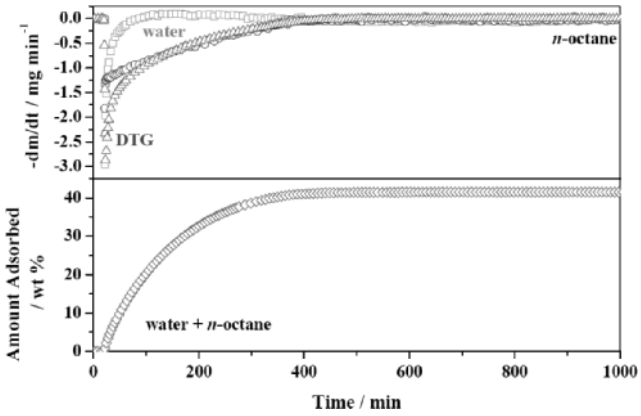

Figure 18. Simultaneous adsorption: water ($p/p^0 = 0.6$) and *n*-octane ($p/p^0 = 0.1$) vapors in helium on BAX950 at 294K.[35]

Figure 19 shows the mass spectrometric profiles obtained for the temperature programmed desorption of water and *n*-octane from activated carbon BAX950. It is evident that the differential thermal gravimetric profile (DTG) and the mass spectrometric profiles obtained for the two components are consistent. A small amount of water, by mass, is adsorbed

on the carbon compared with *n*-octane for relative pressures, p/p^0 H_2O = 0.8 and p/p^0 C_8H_{18} = 0.1. The study was extended to competitive adsorption of a low relative pressure of *n*-butane (p/p^0 = 0.023) and water at various relative pressures. The trend of mass uptake with increasing water content of the vapor flow, in a constant relative pressure (0.023) of *n*-butane is shown in the comparison of temperature programmed desorption profiles with increasing relative pressure (see Figure 20).

Figure 21 shows the adsorption of water vapor in the presence of *n*-butane (p/p^0 = 0.023). It is evident that water vapor adsorption increases with increasing relative pressure similar to the pure vapor, but at greatly

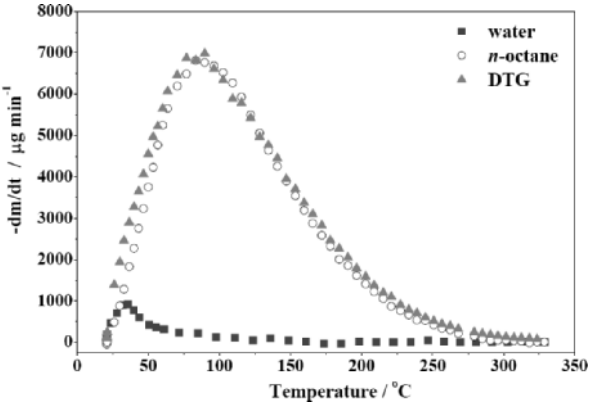

Figure 19. Mass spectrometric and DTG graphs for temperature programmed desorption of water (p/p^0 = 0.8) and *n*-octane vapors (p/p^0 = 0.1) from BAX950.[35]

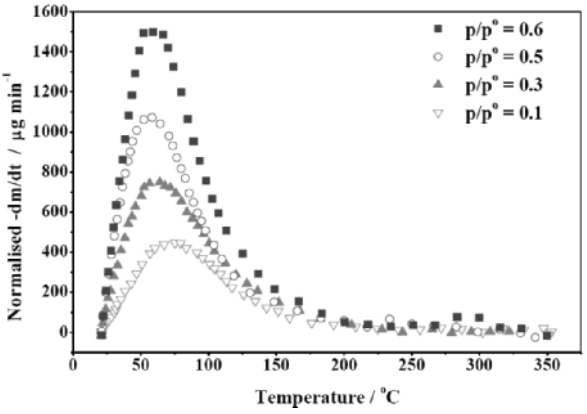

Figure 20. Temperature programmed desorption of water from BAX950 following equilibration with *n*-butane (p/p^0 = 0.023) and water vapor at various p/p^0.[35]

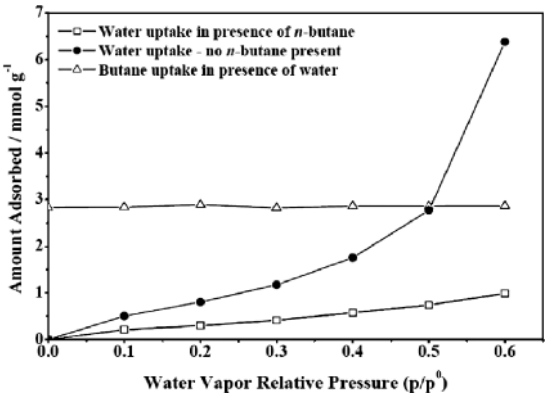

Figure 21. Adsorption isotherms for (–●–) pure water vapor and (–□–) water vapor + *n*-butane ($p/p_0 = 0.023$) on BAX950.[35]

reduced values. The associative adsorption mechanism of water vapor adsorption is apparent in the rapid increase in water vapor adsorption for $p/p^0 > 0.5$. These results demonstrate the detrimental effect of secondary species on adsorption capacity.

Competitive Adsorption between Organic Vapors. Previous studies of low concentration benzene and toluene adsorption showed that both porosity and surface chemistry of activated carbons play important roles,[85,86] but information regarding mixed systems has not been available. A recent study investigated the adsorption behavior of a VOC mixture (benzene–toluene) on activated carbon, in relation to the performance of chemically activated carbons, carbons physically activated with steam and commercial samples. The results showed that chemically activated carbons performed better than the other samples, with higher adsorption capacities, breakthrough times and separation times. Porosity is a key factor and activated carbons with higher volumes of micropores exhibited higher adsorption capacities and breakthrough times. The composition of the mixture in the adsorbed phase was found to be very similar for all samples. Enhanced adsorption potential in micropores gives an adsorbed phase composition, similar in composition to the liquid phase equilibrium in the absence of activated carbons at much lower temperatures. Ideal Adsorbed Solution Theory (IAST) was applied to equilibrium data for single benzene and toluene adsorption isotherms to predict binary equilibrium. The study showed good agreement between experimental and predicted values for low-concentration benzene–toluene adsorption.[87]

7. Removal of Dioxin Simulants

Recent years have seen an increase in public and scientific concerns over the potential risks of the adverse health effects of the primary pollutants emitted from municipal waste combustors (MWC): polychlorinated dibenzo-*p*-dioxins (PCDD) and dibenzofurans (PCDF).[88–97] These are among the most toxic species released from combustion processes, present in concentration in the range from <1.0 to >20,000 ng/m^3 and were first discovered in the stack gas of municipal waste incinerators in 1977. Since then a considerable amount of research has been devoted to identifying PCDD/PCDF emission sources and understanding formation mechanisms, as well as improving the control methods.[98,99]

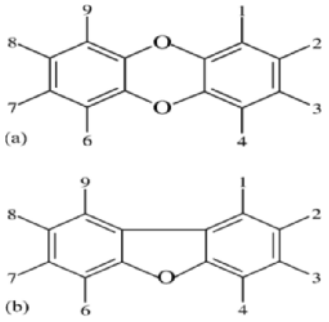

Figure 22. Generic structures of (a) dibenzo-*para*-dioxin and (b) dibenzofurans.[89]

Each compound comprises two benzene rings interconnected by oxygen atoms. In the case of PCDDs, the benzene rings are joined by two oxygen bridges forming a six-membered ring and in the case of the PCDFs, the benzene rings are connected by one carbon bond and one oxygen bridge to form a five-membered ring (Figure 22).[89] The numbers 1–9 shown in Figure 22 are the possible positions for chlorine atoms. The toxicity of the dioxins varies with the number of chlorine atoms. The monochlorodioxins are less toxic, while dioxins with more than one chlorine atoms are highly toxic. There are 75 possible PCDDs and 135 possible PCDFs, each differing in the number and position of the chlorine atoms.[100] The chlorine atoms in positions 2, 3, 7 and 8 are of particular environmental concern, especially the tetrachloro-CDD congener, which is the most toxic of these compounds. Their presence in the environment poses a potential health hazard to humans and other organisms because of their lipophilicity, low-volatility, and resistance to degradation.[89] As the design, management and control of waste incinerators has evolved in recent years, so the PCDD/PCDF content in ash has decreased and modern well-operated plants are net destroyers of

PCDD/PCDFs, with lower concentrations in the stack, wastewater and solid residues than is in the feedstock.[99,101]

Current technology for removal of PCDD/PCDFs from flue gases uses activated carbon injection, in the temperature range 423–473 K, and fabric filtration. However, the optimum properties for the activated carbon and most cost effect carbon for use in these abatement processes are not known with any degree of certainty. Experimentally, it is necessary to study simulants of dioxin species since PCDD/PCDF are very highly toxic. Hence, recent work [102,103] has focused on the adsorption of chlorobenzene and related chloroaromatic species, as model compounds under conditions that simulate those in flue gas treatment systems because of their similar structural characteristics and comparatively low toxicity.

Adsorption of Dioxin Simulants. The techniques discussed have been applied to the industrially relevant area of flue gas emission abatement. In order to simulate conditions in such systems, it is necessary to perform adsorption measurements at high temperatures (~473 K). Adsorption measurements have been demonstrated for temperatures up to 573 K and pressure increments greater than 0.004 mbar, due to resolution of the pressure transducers. Isotherms have been obtained for adsorption of chlorinated aromatics on activated carbon over a large temperature range (293–453 K) and a range of adsorbents (Figure 23).[103,104]

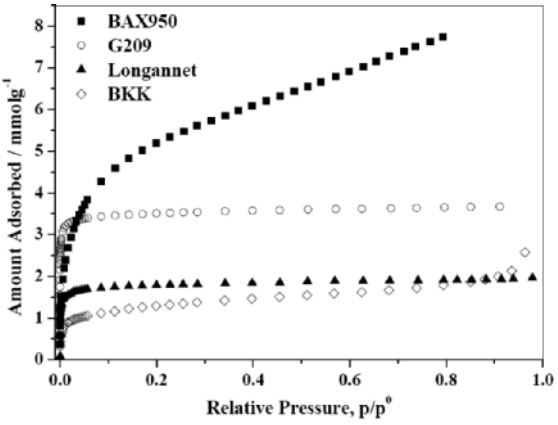

Figure 23. Comparison of chlorobenzene adsorption on BAX950, G209, LG and BKK at 313 K.

The amount adsorbed decreases with increasing temperature at constant pressure for physical adsorption. Adsorption of chlorinated aromatics at low relative pressures and high temperatures is technically very demanding. Variations in surface chemistry and porous structure can greatly affect uptake

at low pressure, which has major implications for adsorbent selection in associated applications. It is possible that the complex mixtures involved may cause competitive or co-adsorption at the low concentrations of target species, introducing additional problems: lower sensitivity, reduced temperature control, etc.

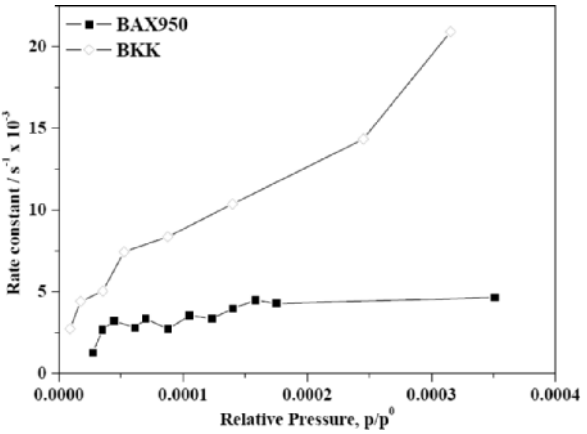

Figure 24. Comparison of LDF rate constants for 2-chloroanisole on BAX950 and BKK at 453K.[103]

Adsorption Dynamics. Adsorption kinetics can be modeled using Linear Driving Force (LDF), Stretched Exponential (SE) or Double Exponential (DE) kinetic models as discussed previously. The LDF Rate constants for adsorption of 2-choloranisole on two activated carbons are shown in Figure 24 and, although there is negligible difference in adsorption uptake at $p/p^0 < 0.01$, the variation in rate constant is significant, with BKK adsorbing 2-chloroanisole at a much faster rate than BAX950. This is a major consideration in adsorbent selection in conjunction with overall cost.

8. Conclusions

Activated carbons are excellent adsorbents for removing very low concentrations of volatile organic vapor pollutants. Comparisons of porous materials based on standard measurements, such as nitrogen adsorption, provide only limited information and may be misleading. Adsorption isotherms and kinetics for specific organic vapor pollutants are important for assessing the suitability of activated carbons for given applications. Laboratory measurements should be carried out under conditions that simulate process conditions, for example, in the case of dioxin removal from flue gases, these are very low vapor partial pressures and high temperatures. Multi-component streams

are a very complex scenario but binary systems can be studied by micro-gravimetry combined with dynamic sampling mass spectrometry. Results have shown that competitive adsorption is a major issue since it slows the adsorption kinetics and species may be displaced from the surface, increasing the complexity of associated studies.

References

1. Hassoun, S., Pilling, M. J., Bartle, K. D. *J. Environ. Monitor.* 1999, *1*, 453.
2. Appel, B. R., et al. *Environ. Sci. Technol.* 1979, *13*, 98.
3. Louw, C. W., Richards, J. F., Faure, P. K. *Atmos. Environ.* 1977, *11*, 703.
4. Finlay-Pitts, B. J., Pitts, J. N. *Atmospheric Chemistry: Fundamentals and Experimental Techniques*, Wiley, New York, 1986.
5. Jenkin, M. E., Saunders, S. M., Pilling, M. J. *Atmos. Environ.* 1997, *31*, 81.
6. Leighton, P. A. *Photochemistry of Air Pollution*, Academic Press, New York, 1961.
7. Wayne, R. P. *Chemistry of Atmospheres*, Clarendon, Oxford, 1991.
8. Strauss, W., Mainwaring, S. J. *Air Pollution*, Edward Arnold, London, 1984.
9. Eggleston, S., et al. Emission of Atmospheric Pollutants in Europe 1980–1996, European Topic Centre.
10. Council Directive 1999/13/EC of 11 March 1999 on the limitation of emissions of volatile organic compounds due to the use of organic solvents in certain activities and installations. *Official Journal of the European Communities*, 1999, 42, 1.
11. Hester, R., Harrison, R. (eds), *Volatile Organic Compounds in the Atmosphere*, The Royal Society of Chemistry, Cambridge, 1995.
12. Cheremisinoff, P. N. (eds), Ellerbusch, F. *Carbon Adsorption Handbook*, Ann Arbor, Science Publishers, Michigan, 1978.
13. Cookson, J. J. J. In *Carbon Adsorption Handbook*, Cherimisinoff, P. N., Ellerbusch, F. (eds), Ann Arbor, Science Publishers, Michigan, 1978.
14. Faust, S. D., Aly, O. M. In *Chemistry of Water Treatment*, Butterworth and Company, Woburn, MA, 1983.
15. Mattson, J. S., et al. *J. Colloid Interface Sci.* 1969, *31*, 116.
16. Bansal, R. C., Donnet, D. B., Stoeckli, F. *Active Carbon*, Marcel Dekker, New York, 1988.
17. Gurvitsch, L. *J. Phys. Chem. Soc. Russ.* 1915, *47*, 805.
18. Arnell, J. C., McDermott, H. L. *Can. J. Chem.* 1952, *30*, 177.
19. Foley, N. J., et al. *Langmuir* 1997, *13*, 2083.
20. Freeman, J. J., et al. *Carbon* 1993, *31*, 865.
21. O'koye, I. P., Benham, M., Thomas, K. M. *Langmuir* 1997, *13*, 4054.
22. Rodriguez-Reinoso, F. *Carbon* 1998, *36*, 159.
23. Reid, C. R., Thomas, K. M. *J. Phys. Chem. B* 2001, *105*, 10619.
24. Brunauer, S., et al. *J. Am. Chem. Soc.* 1940, *62*, 1723.
25. IUPAC. *Carbon* 1985, *23*, 601.
26. Kiselev, A. V. *J. Colloid Interface Sci.* 1968, *28*, 430.
27. Sing, K. S. W., et al. *Pure Appl. Chem.* 1985, *57*, 603.
28. Halsey, G. D. *J. Chem. Phys.* 1948, *16*, 931.
29. Fletcher, A. J., et al. *J. Am. Chem. Soc.* 2001, *123*, 10001.

30. Fletcher, A. J., et al. *J. Am. Chem. Soc.* 2004, *126*, 9750.
31. Zhao, X., et al. *J. Phys. Chem. B* 2006, *110*, 9947.
32. Reid, C. R., O'koye, I. P., Thomas, K. M. *Langmuir* 1998, *14*, 2415.
33. Reid, C. R., Thomas, K. M. *Langmuir* 1999, *15*, 3206.
34. Chagger, H. K., et al. *Carbon* 1995, *33*, 1405.
35. Fletcher, A. J., Benham, M. J., Thomas, K. M. *J. Phys. Chem. B* 2002, *106*, 7474.
36. Fletcher, A. J., Thomas, K. M. *Langmuir* 1999, *15*, 6908.
37. Harding, A. W., et al. *Langmuir* 1998, *14*, 3858.
38. Fletcher, A. J., Thomas, K. M. *Langmuir* 2000, *16*, 6253.
39. Benham, M. J., Ross, D. K. *Z. Phys. Chem. Neue Folge* 1989, *163*, 25.
40. Dean, J. A. *Lange's Handbook of Chemistry*, 15th ed., McGraw-Hill, New York, 1999.
41. Webster, C. E., Drago, R. S., Zerner, M. C. *J. Am. Chem. Soc.* 1998, *120*, 5509.
42. Radovic, L. R., Moreno-Castilla, C., Rivera-Utrilla, J. Carbon Materials as Adsorbents in Aqueous Solutions. In *Chemistry and Physics of Carbon*, Radovic, L. R. (ed.) Marcel Dekker, New York, 2001, Vol. 27, p. 227.
43. Xiao, B. Characterisation of functionalised nanoporous carbon materials and adsorption of aqueous metal ions. Ph.D., University of Newcastle upon Tyne, 2004.
44. Zhu, Q., Money, S. L., Russel, A. E., Thomas, K. M. *Langmuir* 1997, *13*, 2149.
45. Grant, K. A., Zhu, Q., Thomas, K. M. *Carbon* 1994, *32*, 883.
46. Pels, J. R., et al. *Carbon* 1995, *33*, 1641.
47. Stohr, B., Boehm, H. P., Schlogl, R. *Carbon* 1991, *29*, 707.
48. Jia, Y. F., Thomas, K. M. *Langmuir* 2000, *16*, 1114.
49. Jia, Y. F., Xiao, B., Thomas, K. M. *Langmuir* 2002, *18*, 470.
50. Xiao, B., Boudou, J. P., Thomas, K. M. *Langmuir* 2005, *21*, 3400.
51. Fletcher, A. J., Uygur, Y., Thomas, K. M. *J. Phys. Chem. C* 2007, *111* (accepted for publication).
52. Fletcher, A. J., Yuzak, Y., Thomas, K. M. *Carbon* 2006, *44*, 989.
53. Fletcher, A. J., Thomas, K. M. *J Phys. Chem. C* 2007, *111*(5), 2107.
54. Somorjai, G. A. *Introduction to Surface Chemistry and Catalysis*, Wiley, New York, 1994.
55. Krug, R. R. *Ind. Eng. Chem. Fund.* 1980, *19*, 50.
56. Sestak, J. Thermal Analysis (6th ICTA), 1980, Stuttgart.
57. Sestak, J. *Thermophysical Properties of Solids*, Elsevier, Amsterdam, 1984.
58. Sestak, J. *J. Thermal Anal.* 1987, *32*, 325.
59. Agrawal, R. K. *J. Thermal Anal.* 1986, *31*, 73.
60. Agrawal, R. K. *J. Thermal Anal.* 1989, *35*, 909.
61. Suàrez, M. P., Palermo, A., Aldao, C. M. *J. Thermal Anal.* 1994, *41*, 807.
62. Sinfelt, J. H. *Catal. Rev.* 1969, *3*, 175.
63. Nelson, G. O., Correia, A. N., Harder, C. A. *Am. Ind. Hyg. Assoc. J.* 1976, *37*, 280.
64. Okazaki, M., Tamon, H., Toei, J. *J. Chem. Eng. Jpn.* 1978, *11*, 209.
65. McDermot, H. L., Arnell, A. C. *J. Phys. Chem.* 1954, *58*, 492.
66. Muller, E. A., Rull, L. F., Rega, L. F., Gubbins, K. E. *J. Phys. Chem.* 1996, *100*, 1189.
67. Malara, C., et al. *Separ. Technol.* 1994, 413.
68. Bering, B. P., Serpinskii, V. V. *Z. Fiz. Khim. SSSR* 1952, *26*, 253.
69. Bering, B. P., Serpinskii, V. V. *Dokl. Akad. Nauk. SSSR*+ 1953, *90*, 811.
70. Dubinin, M. M., Zaverina, E. D. *Z. Fiz. Khim. SSSR* 1949, *23*, 469.
71. Finger, G., Noack, U., Buelow, M. *Z. Phys. Chem. (Leipzig)* 1983, *264*, 170.
72. Keller, J. U., Standt, R., Tomalla, M. *Ber. Bunsen-Ges. Phys. Chem.* 1992, *96*, 28.
73. Sarraf, R., et al. *Langmuir* 1997, *13*, 1274.
74. Markham, E. D., Benton, A. F. *J. Am. Chem. Soc.* 1931, *53*, 497.

75. Le Van, M. D., Vermeulen, T. *J. Phys. Chem. B* 1981, *85*, 3247.
76. O'Brien, J. A., Myers, A. L. *J. Chem. Soc. Farad. Trans.* 1984, *80*, 1467.
77. O'Brien, J. A., Myers, A. L. *Ind. Chem. Eng. Res.* 1988, *27*, 2085.
78. Richter, E., Schutz, W., Myers, A. L. *Chem. Eng. Sci.* 1989, *44*, 1609.
79. Sircar, S., Myers, A. L. *Chem. Eng. Sci.* 1973, *28*, 489.
80. Van Ness, H. C. *Ind. Eng. Chem. Fundam.* 1969, *8*, 464.
81. Chen, Y. D., Ritter, J. A., Yang, R. T. *Chem. Eng. Sci.* 1990, *45*, 2877.
82. Dunne, J., Myers, A. L. *Chem. Eng. Sci.* 1994, *49*, 2941.
83. Karavias, F., Myers, A. L. *Chem. Eng. Sci.* 1992, *47*, 1441.
84. Rouquerol, F., Rouquerol, J., Sing, K. S. W. *Adsorption by Powders and Porous Solids*, Academic Press, London, 1999.
85. Foster, K. L., et al. *Chem. Mater.* 1992, *4*, 1068.
86. Ruhl, M. J. *Chem. Eng. Prog.* 1993, *89*, 37.
87. Lillo-Rodenas, M. A., et al. *Carbon* 2006, *44*, 1455.
88. Mandal, P. K. *J. Comp. Physiol. B* 2005, *175*, 221.
89. McKay, G. *Chem. Eng. J.* 2002, *86*, 343.
90. Matzing, H., et al. *Chemosphere* 2001, *42*, 803.
91. Bertazzi, P. A., et al. *Am. J. Epidemiol.* 2001, *153*, 1031.
92. Fell, H. J., Tuczek, M. *Chemosphere* 1998, *37*, 2327.
93. Buekens, A., et al. *Environ. Eng. Sci.* 1998, *15*, 29.
94. Harrison, R. O., Carlson, R. E. *Chemosphere* 1997, *34*, 915.
95. Bertazzi, P. A., et al. *Epidemiology* 1997, *8*, 646.
96. Tejima, H., et al. *Chemosphere* 1996, *32*, 169.
97. Landi, M. T., et al. *Lancet* 1997, *349*, 1811.
98. Dyke, P., Coleman, P., James, R. *Chemosphere* 1997, *34*, 1191.
99. Kilgroe, J. D. *J. Hazard. Mater.* 1996, *47*, 163.
100. Khazipov, V. A., et al. *Khim. Tverd. Top.* 1995, *4*, 67.
101. Yasuda, K., Takahashi, M. *J. Air Waste Manage.* 1998, *48*, 441.
102. Zhao, X., Thomas, K. M. Models for the adsorption of dioxins and furans on activated carbons: adsorption of chlorinated aromatic species, Carbon'03 An International Conference on Carbon, 2003, Oviedo, Spain, Paper 9.4.
103. Zhao, X. B. Adsorption of pollutants and hydrogen storage on nanoporous materials, University of Newcastle upon Tyne, 2006.
104. Zhao, X. B., Bell, J., Fletcher, A. J., Thomas, K. M. Models for the adsorption of dioxins and furans on activated carbons: adsorption of chlorinated aromatic species, The International Carbon Conference, 2006, Aberdeen, Paper 6A3.

ADSORPTION BEHAVIOUR OF LIGNOSULPHONATES ON THE INTERFACES WATER–INORGANIC/ORGANIC SOLIDS, USED FOR PAPER PRODUCTION

GALINA TELYSHEVA,* TATIANA DIZHBITE,
ANNA ANDERSONE, ALEKSANDRS VOLPERTS
Latvian State Institute of Wood Chemistry, 27 Dzerbenes Street, Riga, LV-1006, Latvia

Abstract. The regularities of adsorption of lignosulphonates from water solutions onto cellulose, kaolin, TiO_2 and $CaCO_3$ was studied and the high values of the non-electrical portion of free energy of adsorption were shown, which provide effective adsorption of polymer on the surfaces charged similarly with lignosulphonates. Modification of lignosulphonates with siliconorganic oligomers increased significantly their affinity to cellulose and kaolin due to changing hydrophobicity and introducing of new active centers in the lignosulphonates macromolecules. Comparative study of compatibility of lignosulphonates and modified lignosulphonates with polyacrylamide was carried out.

Keywords: lignosulphonates; adsorption; cellulose; kaolin; modification; siliconorganic oligomers; compatibility with polyacrylamide

1. Introduction

The work was carried out in order to continue our study[1] aimed at the development of interface additives on the basis of lignin, which is produced as a multi-tonnage waste under various processings of plant raw materials. During cellulose manufacture by sulphite pulping, lignin component of plant tissue is transformed and water-soluble sulphonated lignin, so-called

*To whom correspondence should be addressed. E-mail: ligno@edi.lv

J.P. Mota and S. Lyubchik (eds.), Recent Advances in Adsorption Processes for Environmental Protection and Security, 55–64.

lignosulphonates (LS) passes into cooking solution. Non-controlled discharging of LS into aquatic system creates serious environmental problems. Due to surface active properties, the LS-based products have wide application as dispersants, stabilizers, adhesives, etc.[2–4] However, only 5% from total LS production are used as commercial products, the rest has not found yet other application besides burning.[5] LS macromolecule is negatively charged, carries sulphonate, phenolic, aliphatic hydroxyl and carboxyl functional groups (Figure 1) and shows polyelectrolyte behaviour.[6]

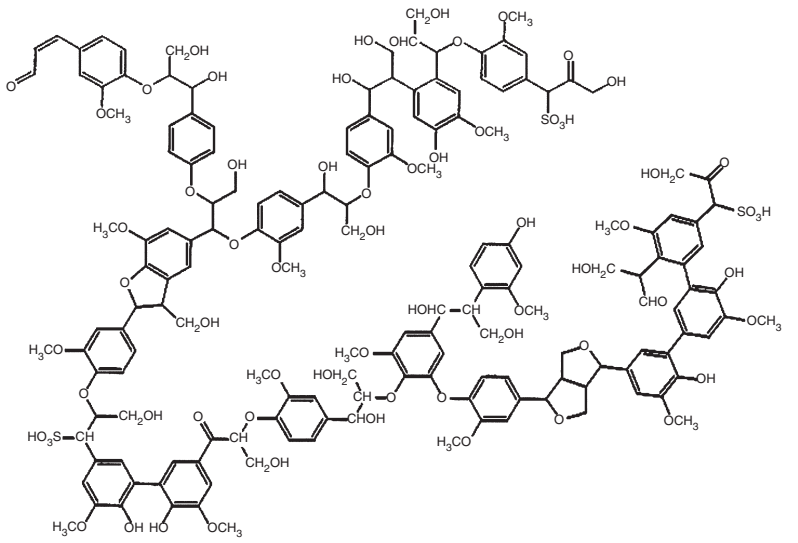

Figure 1. Schematic presentation of lignosulphonate molecule chemical structure [6].

In the last decades lignins, in particular in mixtures with conventional adhesives and flocculants and complexes with cationic polymers are considered as special additives for improvement of operating characteristics of paper and cardboard.[7–9] In order to enhance the paper strength, polyelectrolyte complexes of cationic and anionic naturally originated and synthetic polymers are proposed, e.g. carboxymethyl cellulose combined with cationic polyamideamine epichlorohydrin condensate provided a significant increase in strength of the paper, compared to sheets prepared with only the cationic condensate.[10] Building of polyelectrolyte multilayers on the fibre surface, when consecutive layers of cationic and anionic polymers are deposited on cellulosic fibres is a developing trend.[11] The use of sulphonated kraft lignin/PEO complexes as a dual retention system for newsprint and groundwood stocks was suggested in,[12] where it was showed that the complexes improved fines retention without decreasing pulp brightness.

The present work is focused on the main features of LS adsorption onto various solid components of paper composite materials (cellulose, kaolin, calcium carbonate, titanium dioxide) and is aimed at purposeful alteration of the LS efficiency as auxiliary substances by modification with silicon-organic oligomers[1] and blending with polymeric flocculants.

2. Experimental

A commercial sodium LS purified by ultrafiltration from Borregaard Lignotech as well as the products of their modification with sodium diethylalumoethylsiloxanolate (Si-LS) by the method described elsewhere[1] were used in the work as adsorptives. Purified LS had M_w = 42,800 (HPLC) and contained less than 1% of carbohydrates, sulphonate groups 1.23 mequivalents/g, phenolic groups 1.06 mequivalents/g (conductometry titration).

Synthetic flocculant polyacrylamide (PAA) with M_W 6,000,000 was purchased from Sigma.

Bleached sulphate cellulose from coniferous wood (α-cellulose content 98%), kaolin, titanium dioxide (rutile) and calcium carbonate were applied as adsorbents.

The BET specific surface areas of adsorbents were determined by the method of nitrogen adsorption–desorpion (Sorptometer KELVIN 1042 from COSTECH Microanalytical OU).

LS adsorption measurements were performed by a batch equilibrium method in suspensions of 10 g of an adsorbent in 100 ml of water, previously thermostated at 20 ± 1°C. The suspensions were kept in closed polyethylene flasks to avoid water loss by evaporation. Two milliliters of LS solution (at concentrations which did not exceed LS water solubility value) were added with a micropipette. The suspensions (pH of the suspensions was 7 ± 0.1) were then kept for 24 h at 20 ± 1°C under inert atmosphere with agitation to obtain stationary conditions.[1]

At the end of agitation time, the suspensions were centrifuged 5 min at 3,000 rpm at the same temperature as the sorption experiments were carried out. The supernatant solution and calibration standards filtered through a 0.45 μm filter mounted on a dispensable syringe were analyzed by UV spectroscopy (Perkin Elmer, mod. Lambda 25) at λ = 280 nm. The adsorption isotherms were obtained by plotting amount of LS adsorbed per mass of adsorbent (A) against equilibrium LS concentration in solution (C_{eq}). The average results from three different adsorption experiments were taken for experimental adsorption isotherms plotting.

Microstructure of LS adsorption layer was characterized by a spin probe method[13] using 4-benzoyloxi-2,2,6,6-tetramethylpiperidine-1-oxyl (further named "the probe"). When the probe was to be coadsorbed with LS, the probe, dissolved in methanol (a concentration of 10^{-4} mol L^{-1}), was added to an adsorbent and methanol was removed by evaporation. LS aqueous solutions were added next, the mixtures were equilibrated for 24 h at 20 ± 1°C. Then the adsorbent particles were collected on a Bichner funnel, rinsed with water, and dried in air overnight. EPR spectra of adsorbents with the adsorbed spin probe were recorded at 20 ± 1°C on a Bruker EMX 6/1 X-band spectrometer using the following instrumental parameters: scan width, 125 G, time constant, 0.25 s, scan time, 4 min, modulation amplitude, 0.33 G, microwave power, 10 mW, modulation frequency, 100 Hz. The rotational correlation time (τ_c) of the probe was calculated from its EPR spectrum using equations derived from the theory of Kivelson.[14]

LS/Si-LS compatibility with a polymeric flocculant was studied using DSC (differential scanning calorimetry). The blends of LS and Si-LS with PAA were prepared by solution-casting method from the 1% polymers water solutions and dried at the room temperature. The films obtained exhibited an uniform and homogenous appearance. All films obtained from casting were ground to the fine powder using a ball mill and tempered at room conditions. All tests were done in the presence of residual water since without its softening effect it was not possible to observe any glass transition points for the mixtures. The water content in all samples has been around 10%. The samples (approximately 40 mg) were placed into the hermetically closed high pressure crucibles and tested using computer controlled METTLER TOLEDO DSC system in the stream of nitrogen from –10 to 200°C at the rate of 10°C/min. From the thermograms the *Tg* midpoints were calculated using METTLER TOLEDO software. An excellent reproducibility of results was obtained: for 10 parallel samples a deviation was about of 0.5°C.

3. Results and Discussion

The characteristics of adsorbents surface detected are given in the Table 1.

TABLE 1. Characteristics of adsorbents surfaces.

Sorbent	Specific surface area (m^2/g)	Zeta potential (mV)
Cellulose	2.0	–25
Kaolin	15.1	–30
Calcium carbonate	7.1	–16
Titanium dioxide	9.2	+67

The solids used in the present work as adsorbents, excluding TiO_2, have the surface charge of the same sign as LS polyanions. Therefore, it could be waited that electrostatic interactions between the negative charges of the sulphonic, carboxylic and phenolic groups of the macromolecule and the positively charges at the surface of the adsorbent will be the driving force of adsorption for TiO_2 only. In this case, the regularities of LS adsorption can be described in accordance with Fleer and Scheutjens theory[15] as polyelectrolyte adsorption on a charged surface. The maximum on the experimental curve of the relationship "LS adsorption on TiO_2 plateau value – solution pH" was observed at pH 4–5, that corresponded to the effective pK for lignosulphonic acids. The shape of the experimental relationship corresponded to the theoretical one calculated according the self consistent field (SCF) model[15] for polyelectrolyte adsorption on an oppositely charged surface. The amount of LS adsorbed is larger at the low values of pH than at high pH due to a decrease of intersegmental repulsion. The presence of a maximum can be explained by the fact, that LS macroions with non-zero degree of dissociation, thus having some charge, more effectively compete with counterions to compensate the positive charge on the TiO_2 surface. At these values of pH electrostatic forces between adsorbate and adsorbent are higher than intersegmental repulsion.

The adsorption isotherms obtained for LS and Si-LS adsorption on all solids investigated are shown in the Figure 2a and b, respectively. It has been shown[7] by the authors of the present paper that the adsorption isotherms of LS on the interfaces are described satisfactory by the Aranovich model of polylayer adsorption[16]:

$$A = \frac{A_m \cdot C \cdot N_\infty / N_\infty^* \left(1 - Z/Z_0 \cdot N_\infty / N_\infty^*\right)^{1/2}}{\left(1 + C \cdot N_\infty / N_\infty^*\right)\left(1 + C \cdot N_\infty / N_\infty^*\right)^{1/2}}$$

where A – current adsorption value; A_m – adsorption plateau value; N_∞ – current equilibrium adsorptive concentration in the solution; $N_\infty^* = N_\infty$ for the saturated solution; C – energetic constant of adsorption equilibrium.

The good fit of the Aranovich model of polylayer adsorption not only for LS but also for Si-LS experimental isotherms was observed (Figure 3).

On the basis of the experimental adsorption isotherms the value of differential adsorption heat at infinitesimal coverage, Δq_A, can be calculated by application of the Aranovich adsorption model:

$$\Delta q_A = \Delta q_W + kT\left(\ln C - \ln N_\infty^*\right)$$

where Δq_W is the heat of wetting of the adsorbent.

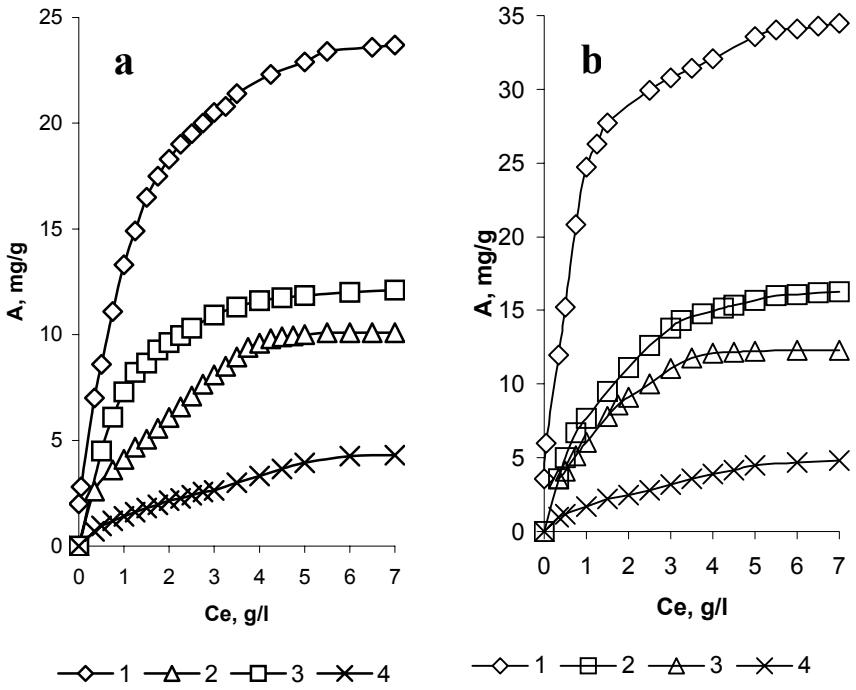

Figure 2. Experimental isotherms of LS (a) and Si-LS (b) adsorption on cellulose (1), titanium dioxide (2), kaolin (3) and calcium carbonate (4).

The physical meaning of the parameter Δq_A is the energy of bonding of adsorbate molecules with adsorbent surface.

In accordance with characteristics shown in the Table 2, the solids studied can be classified according to their affinity towards lignosulphonates, in decreasing order: ***Cellulose > TiO_2 ≅ Kaolin > $CaCO_3$***

TABLE 2. Characteristics of LS and Si-LS adsorption on solids.

Adsorptive	Adsorbent	A_m (mg/g)	Δq_A (kJ/mol)
LS	Cellulose	25.1	46.1
	Kaolin	14.0	32.9
	TiO_2	10.3	25.4
	$CaCO_3$	5.0	n.d.
Si-LS	Cellulose	36.6	51.2
	Kaolin	18.0	34.3
	TiO_2	12.4	33.2
	$CaCO_3$	6.3	n.d.

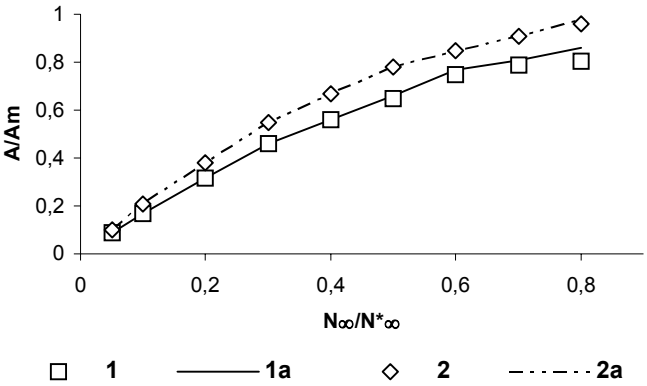

Figure 3. Example of the fit of the Aranovich model to the experimental adsorption data: 1, 2 – experimental data for LS and Si-LS adsorption, respectively, on kaolin; 1a, 2a – model fits.

The data obtained show that LS adsorbs efficiently on the kaolin surface. At the pH 7 the kaolin surface charge density is about 6 μKl/cm^2 and specific adsorption of LS reaches up to 14 mg/g (about 1 mg/m^2), which is a typical value for the adsorption of polyelectrolyte on the oppositely charged surface. This proves that in the LS-kaolin system non-electrical contributions to the free energy of adsorption are significant. Based on the literature data, hydrophobic interaction could contribute significantly in the adsorption interaction on the kaolin surface. The comparison of adsorption characteristics of LS and Si-LS (Table 2) with their hydrophobicity (values of the Gibbs free energy of polymer macromolecules transfer from aqueous in ethyl acetate phase, $-\Delta G^{o}_{aq \rightarrow oil}$, were 3.93 and 2.00 kJ/mol for LS and Si-LS, respectively) confirmed this suggestion.

The LS adsorption isotherm on cellulose indicates their high affinity (Figure 2a). It also shows larger values of LS adsorption within the whole concentration region under investigation, in comparison with those obtained for inorganic solids. Cellulosic fibres are negatively charged in aqueous suspensions, mainly due to the dissociation of carboxylic groups. Therefore, the two most important long-range surface forces in fibre–lignin systems should be van der Waals' attraction and electrostatic repulsion. The adsorption of LS by cellulose can be caused by such phenomena as physical adsorption due to van der Waals' forces or hydrophobic interactions and formation of acceptor–-donor complexes between lignin and cellulose.

The co-adsorbed spin-probe method used in the present work allowed to show that at low levels of the sorbent surfaces coverage ($\theta \leq 0.2$) two-component EPR spectra were observed. The outer peaks in these spectra, representing the probe with correlation time of rotational movement, $\tau_c \approx 10^{-6} - 10^{-8}$ s, was attributed to a flat immobilized position of the probe

surrounded by the polymer molecules. Growth of adsorbed LS amount resulted in the increase in the intensity of inner peaks characteristic for the probe having rotational movements with small correlation time, $\tau_c < 10^{-9}$ s. For samples prepared by sorption from LS solutions with a concentration value, corresponded to the adsorption plateau, one-component spectra with $\tau_c = 2 \times 10^{-11}$ s were observed, which are characteristic for relatively free movement of the spin probe among tails and loops of adsorbed LS molecules in the first layer (shell). Total combination of EPR spectroscopy data obtained indicates a gradual decrease of the fraction of adsorbed polymer segments laying flat on the surface of adsorbent and an increase in the amount of oriented into the solution loops and tails forming pseudo-liquid microphase at the adsorbent surface. These observations are in good compliance with the results obtained recently in computational investigations of the cellulose–lignin assembly.[17] Due to a significant contribution of H-bonding interactions, in the first shell, lignin at its low concentration adsorbs flat on the surface in order to maximize the interactions with cellulose. However, such type of orientation of lignin aromatic rings becomes rapidly less apparent for units located at greater distance from the interface.

A significant increase in the adsorption value and energy of adsorption interaction as the result of LS modification by the siliconorganic oligomers (Figure 2a and b, Table 2) indicates the possibility to regulate the adsorption behaviour of LS. The presence of the Al^{3+} in the siliconorganic block permits the Si-LS molecules approaching closer to the negatively charged adsorbent surface than in the case of non-modified LS.

Besides cellulose and the above mentioned inorganic solids used as filler for production of different kinds of paper, the organic polymer flocculants are widely applied in papermaking. Therefore, interaction of LS/Si-LS with polymeric flocculants is a matter of high importance.

The results from the DSC testing of the LS and Si-LS blends with PAA flocculant show (Table 3) that non-modified LS has a partial miscibility with PAA, which reveals in two sets of glass transition points (*Tg*): one for PAA rich and other for LS rich blends. Modification with siliconorganic oligomers leads to compatibility of the Si-LS and PAA in the whole range of their ratio, that was exhibited in single *Tg* and almost perfect correlation with the Fox equation.[18] The forming one phase structure was characterized by a synergistic flocculation effect.

As the result of enhanced adsorption of Si-LS on the surface of the cellulose and inorganic fillers, its addition into paper composition improves uniformity of distribution of fillers and fine cellulose fibers leading to higher mechanical strength of paper as well as increases fine fibers retention diminishing their coming into environment.

TABLE 3. DSC data from testing of LS-PAA and Si-LS-PAA blends.

Composition	Proportion of the first component (%)	Proportion of the second component (%)	Tg_1 (°C)	Tg_2 (°C)	*Tg* calculated according the Fox equation[18] (°C)
PAA and LS	0	100	n.o.*	79.1	
PAA and LS	10	90	63.4	77.6	73.2
PAA and LS	20	80	62.0	76.0	69.0
PAA and LS	33	66	39.7	62.4	61.2
PAA and LS	50	50	41.7	62.2	55.0
PAA and LS	75	25	41.2	61.1	47.7
PAA and LS	100	0	42.1	n.o.*	42.1
PAA and Si-LS	0	100	71.2	n.o.*	71.2
PAA and Si-LS	10	90	66.5	n.o.*	67.0
PAA and Si-LS	20	80	63.4	n.o.*	63.8
PAA and Si-LS	33	66	57.1	n.o.*	57.9
PAA and Si-LS	50	50	49.8	n.o.*	52.9
PAA and Si-LS	75	25	47.9	n.o.*	46.9
PAA and Si-LS	100	0	42.1	n.o.*	42.1

*Not observed

4. Conclusions

The adsorption of the LS at the water–solid interface is characterized by high values of the non-electrical portion of the free energy of adsorption, which provide effective adsorption on the surfaces charged similarly to LS. Balance of the LS adsorption forces can be regulated by modification with silicon containing organic oligomers enhancing polymer hydrophobicity. Modification of LS with silicon oligomers changes hydrophilic properties and introduces new active centers in the LS molecules, which results in the increased interaction with the synthetic flocculant PAA. The developed dual retention system Si-LS–PAA reveals high flocculation effect towards organic and inorganic components of paper compositions and could be recommended as a special additive for operating characteristics improvement of non-bleached paper and cardboard.

Acknowledgements

The financial supports from the 6th European FP (Contract IRRISEASOIL) and the Latvian Budget (Grants 1564 and National Programme 1-23/65 and Collaboration Programme “Integrated Utilization of Renewable Raw Materials”) are gratefully acknowledged.

References

1. G. Telysheva, T. Dizhbite, E. Paegle, A. Volperts, A. Shapatin and I. Demidov, Surface-active properties of hydrophobized derivatives of lignosulphonates: effect of structure of organosilicon modifier, *J. Appl. Pol. Sci.* 82, 1013–1020 (2001).
2. V. Hornof and R. Hombek, Surface-active agents based on propoxylated lignosulfonate, *J. Appl. Pol. Sci.* 41, 2391–2398 (1990).
3. F. Perche, Y.F. Houst, P. Bowen, and H. Hofmann, in: *Supplementary Papers, 7th CANMET/ACI International Conference on Superplasticizers and Other Chemical Admixtures in Concrete*, V.M. Malhotra, ed. (American Concrete Institute, Detroit, 2003), pp. 1–15.
4. M. Zhou, X. Qiu, D. Yang, and H. Lou, Properties of different molecular weight sodium lignosulphonate fractions as dispersants of coal-water slurry, *J. Dispers. Sci. Technol.* 27(6) 851–856 (2006).
5. J. Plank, Applications of biopolymers and other biotechnological products in building materials, *Appl. Microbiol. Biotechnol*. 66(1), 1–9 (2004).
6. F. Perche, Thèse no 3041 (École Polytechnique Fédérale de Lausanne, Lausanne, EPFL, 2004).
7. N. Afanasev, G. Telysheva, N. Makarevitch, Surface activity and mechanism of lignosulphonates adsoption layers formation, *Khymya Drevesiny* 1990(1), 20–26 (1990).
8. N. Maximova, M. Osterberg, K. Koljonen, and P. Stenius, Lignin adsorption on cellulose fibre surfaces: effect on surface chemistry, surface morphology and paper strength, *Cellulose* 8(2), 113–125 (2001).
9. G.E. Fredheim and B.E. Christensen, Polyelectrolyte complexes: interactions between lignosulfonate and chitosan, *Biomacromol*. 4, 232–239 (2003).
10. L. Gärlund, L. Wågberg, and R. Gernandt, Polyelectrolyte complex for surface modification of wood fibres. II. Influence of complexes on wet and dry strength of paper. *Colloids Surf. A* 218, 137–149 (2003).
11. L. Wågberg, S. Forsberg, A. Johansson, and P. Juntti, Engineering of fibre surface properties by application of the polyelectrolyte multiplayer concept. Part 1: modification of paper strength. *Pulp Pap. Sci. J.* 28(7), 222–227, (2002).
12. R. Pelton, L. Allen, and H. Nugent, Novel dual-polymer retention aids for newsprint and groundwood specialities. *Tappi J.* 64(11), 89–92, (1981).
13. J. Yao and G. Strauss, Adsorption of quaternary ammonium surfactants on poly (tetrafluoroethylene) surfaces, *Langmuir* 7(10), 2353–2357 (1991).
14. C. G. Pitt, J. Wang, S. S. Shab, R. Sik, and C. F. Chignell, ESR spectroscopy as a probe of the morphology of hydrogels and polymer-polymer blends, *Macromolecules* 26(9), 2159–2164 (1993).
15. G. J. Fleer and J. M. H. M. Scheutjens, in: *Coagulation and Flocculation*, B. Bogus, ed. (Springer, Berlin, 1994), 105–183.
16. G.L. Aranovitch, The determination of adsorption heat from adsorption isotherm at infinitively little coverage, *Zhurn Fiz Khim*, 64(1), 161–165 (1990).
17. S. Besombes and K. Mazeau, The cellulose/lignin assembly assessed by molecular modeling. Part 2: seeking for evidence of organization of lignin molecules at the interface with cellulose, *Plant Physiol. Biochem.* 43(2), 277–286 (2005).
18. O.O. Santana, M.L. Maspoch, and A.B. Martinez, Polycarbonate/acrylonitrite-butadiene-styrene blends: miscibility and interfacial adhesion. *Polym. Bullet.* 41,721–728 (1998).

ADSORPTION PROPERTIES OF POLYMER ADSORBENTS

J. HRADIL*
Institute of Macromolecular Chemistry AS CR, Heyrovsky Sq. 2, 162 06 Prague 6 Czech Republic

Abstract. The adsorption properties of the macroporous, hypercrosslinked, and functional polymers were studied. A series of macroporous methacrylate sorbents with different chemical structure and polarity was prepared to examine the effect of polarity and porous structure on the sorption of organic compounds from aqueous solutions.

The sorption of organic compounds by porous copolymers of different porous structure and polarity with laboratory and commercial samples was compared. The sorption capacity of hypercrosslinked copolymers is up to five times higher than that of macroporous samples. The phenols are more strongly sorbed on the methacrylate copolymers bearing ethyleneamine groups than on styrene–divinylbenzene copolymers. The interactions of adsorbates with polymer adsorbent are discussed. The difference between carbonaceous and polymer adsorbents are in variability of composition of later and therefore different mechanism of interactions adsorbate–adsorbent. Polymer adsorbents are superior to the carbonaceous adsorbents in sorption of organic compounds and in simply desorption.

Keywords: polymer adsorbents; macroporous; hypercrosslinked; adsorption; polarity; interaction; organic compounds

1. Introduction

Polymer adsorbents included macroporous and hypercrosslinked copolymers. Polymer adsorbents are synthesized by two methods: (i) suspension polymerization and (ii) by post-crosslinking of polymers. As early as 1963 Millar and coworkers[1] described the preparation of the macroporous

*To whom correspondence should be addressed. E-mail: hradil@imc.cas.cz

J.P. Mota and S. Lyubchik (eds.), Recent Advances in Adsorption Processes for Environmental Protection and Security, 65–74.

styrene–divinylbenzene copolymer and the criterion of macroporosity: uptake of the non-swelling solvent greater than 0.1 mL/g and opalescence of beads. It was supposed that macroporous copolymers crosslinked to a high degree are rigid systems, in which swelling changes, are almost imperceptible. Such copolymers for adsorption applications were produced as marks Amberlite XAD-2 and Amberlite XAD-4. Later also adsorbents based on methacrylate macroporous copolymers for chromatographic applications under a mark Porapak and Chromaton were produced. These adsorbents were prepared by suspension polymerization. Hypercrosslinked polymer adsorbents were obtained by post-crosslinking of linear polystyrene[2] or its macroporous[3] copolymers in the swollen state by Friedel-Crafts reaction. Such adsorbents are produced by Purolite International UK (Hypersol-Macronet, MN-series), Bayer AG Germany (Lewatit VP OC 1163, Lewatit S 7768) Dow Chemical USA (Optipore) and Jiangsu A & G Environmental Technology Co Ltd China (NG-99, NG-100).

The polymer adsorbents found application in gas[4,5] and liquid chromatography, adsorption of organic compounds from gas as so as from water phase. The new application consists in membrane technologies and in storage of gases. Macroporous and hypercrosslinked adsorbents were used as fillers in polymer membranes,[6,7] on which separation of gases and small organic molecules was occurred. Hypercrosslined polymer adsorbents with high values of specific surface area were tested for reversible hydrogen storage.[8] In the past we determine the sorption of organic compounds with macroporous[9, 10] and hypercroslinked[11] polymers.

In this paper we show the presence of polar adsorbate–adsorbent interaction on functionalized polymer adsorbent and increasing effect of nonpolar interaction on macroporous and especially hypercrosslinked adsorbents with high values of specific surface area.

2. Experimental

Macroporous copolymers of styrene, 2,3-epoxypropyl methacrylate with ethylene dimethacrylate or divinylbenzene were obtained by suspension radical polymerization in presence of dodecanole and cyclohexanole as inert solvent at 80°C for 8 h.

Hypercrossliked polymers were obtained by Friedel-Crafts reaction of styrene–divinylbenzene copolymer with chloromethyl methyl ether in 1,2-dichloroethane by catalysis of anhydrous aluminium chloride at 15°C.

The adsorption isotherms of adsorbed organic on polymer adsorbents compounds were determined by batch method.

3. Results and Discussion

Physical adsorption is preferred due to the easy desorption and regeneration of the adsorbent. A common reason of physical adsorption of molecules is the dispersion energy of interaction molecules and atoms which forming the adsorbent surface. The commonly known types of interaction adsorbate–adsorbent are formed also by using polymeric adsorbents, e.g. nonspecific interaction (van der Waals) and specific interactions (Keesom forces – orientation forces, Debye forces – induction forces).[12] Therefore, the hydrophobic adsorbents most effective by sorption of organic compounds from water. But even on the carbonaceous adsorbents the pure physical adsorption did not proceed it is always accompanied with polar interaction.

3.1. ADSORPTION ON MACROPOROUS ADSORBENTS

The sorption properties of polymer adsorbents are determined by their porous structure and polarity, which can be changed, depending on their composition, with the wide range. According to microscopic observation agglomerates of spherical particle of diameter about 6 nm compose the polymer material. The gaps between particles form continuous channels. Two kind of porosity can be observed: micro- and mesoporosity between particles and macroporosity of channels between agglomerates as follows from BET isotherm and mercury porosimetry measurements (Table 1).

TABLE 1. Porous structure of macroporous and hypercrosslinked adsorbents.

Adsorbent	Specific surface area (m^2/g)	Total pore volume (ml/g)	Micropore volume (ml/g)	Porosity (%)	Mean pore radius (nm)
Poly(EDMA)	486	1.64	0.27	64.3	6.7
Amberlite XAD-4	638	1.07	0.30	54.0	2.8
Lewatit EP63	1,250	1.04	0.54	53.3	1.7
Sample 390	941	0.86	0.60	48.6	1.8

Moreover, in the polymer adsorbent pores are not effect of increasing adsorption potential of narrow micropore walls, which is in these adsorbents low (about 0.30 mL/g). The values of specific surface area, are the highest, which were in copolymers prepared by suspension polymerization achieved. The styrene–divinylbenzene show higher values of specific surface area and also the amount of micropores than of methacrylate adsorbents. Therefore also the adsorption of phenol on Amberlite XAD-4 is higher than on Poly(EDMA) (Table 2, Figure 1). The Freundlich equation fits the adsorption of phenol on the adsorbents from aqueous solution tested adsorption systems well.

TABLE 2. Phenol adsorption capacity, enthalpy and diffusion coefficients in macropore and mesopore (D_1) and micropore region (D_2) at 26°C.

Adsorbent	Adsorption capacity (mmol/g)	Energy of adsorption (kcal/mol)	$D_1\ 10^5$ (cm^2/s)	$D_2\ 10^5$ (cm^2/s)
Poly(EDMA)	0.210	6.34	0.094	32.7
Amberlite XAD-4	0.310	11.06	0.273	4.78
Lewatit EP63	1.350	5.30	0.119	7.67
Sample 390	1.480	7.13	0.493	6.94

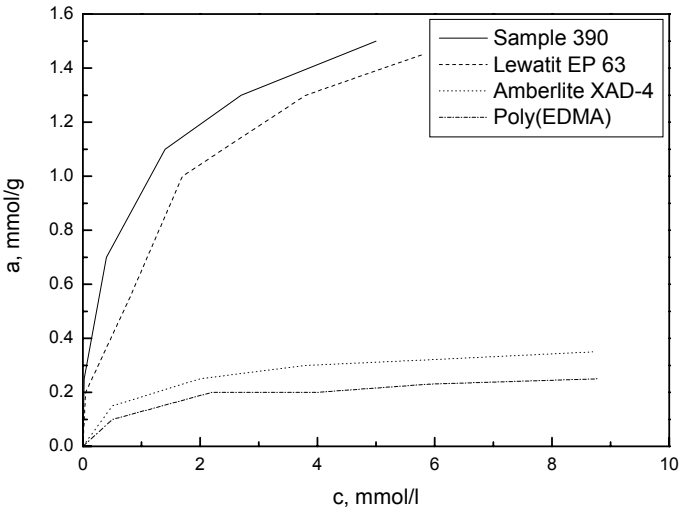

Figure 1. Adsorption of phenol from water solution by macroporous and hypercrosslinked adsorbents.

The sorption of aromatic adsorbates, such as aniline and phenol, on styrene–divinylbenzene and methacrylate copolymers indicates a considerable effect of the porous structure on the sorption. In general, the maximum of adsorbate adsorption increases with the increasing amount of micropores in the polymer. As the lipophilicity of the adsorbate increases, the amount of adsorbate adsorbed from water is also increased:

$$\text{Phenol} < \text{aniline} < \text{benzene} < \text{toluene}$$

The values of diffusion coefficients of phenol in polymeric adsorbents (Table 2) is high and not too far from the diffusion of phenol in water (9.2×10^{-4} cm^2/s). Therefore, the adsorption proceeds rather fast. The diffusion

coefficient of phenol in micropores (D_1) is about of the order of magnitude lower than in mezopores (D_2).

Thanks the lower adsorption energy of polymer adsorbents, due to hindering of the carbon atoms by hydrogen atoms and lower sp^2-interactions, desorption of compounds proceed easier than from active coal. In the consequence the regeneration of polymer adsorbents is more economical in comparison with microporous carbonaceous adsorbents. It is possible to desorb adsorbate by solvent or by water steam distillation.

3.2. ADSORPTION ON HYPERCROSSLINKED COPOLYMERS

The hypercrosslinked polymers represent a second type of adsorption materials in addition to the traditional macroporous copolymers (Table 1). Subjecting gel-type and macroporous styrene–divinylbenzene based copolymers swollen in dichloroethane to a Friedel-Crafts reaction catalyzed by catalyst afforded beads with surface areas more than 1,000 m^2/g as calculated using the BET equation. We described the method of hypercrosslinked copolymer preparation, which consists of using tetrachloromethane,[13] a less carcinogenic reagent, in the Friedel-Crafts-type reaction, leading to sorbents with the same adsorption properties as those using carcinogenic chloromethyl methyl ether. Therefore, in comparison with macroporous copolymers the specific surface is high and the pore volume is low and the mean pore radius is in the microporous region. The adsorption capacities of hypercrosslinked copolymers are as result more than five times higher as of macroporous copolymers. The high adsortion capacities of hypercrosslinked adsorbents may be attributed to the uniform micropore structure and partial polarity on the network of the hypercrosslinked resins, as well as the enhanced [π]–[π] interactions and the better compatibility between the adsorbates and adsorbents. The hypercrosslinked adsorbents showed not only higher adsorption activity (Figure 1), than by macroporous adsorbents, but also faster adsorption kinetics and good thermal and mechanical stability (Table 3). The weight loss at 300°C amounts to only 2 wt.%, and at 400°C it amounts to 6 wt.%.

TABLE 3. Mechanical and thermal properties of copolymers.

Copolymer	Structure	Penetration modulus (MPa)	Maximum depolymerization rate temperature (°C)
Macroporous	GMA-EDMA	61	250
Macroporous	St-DVB	748	350
Hypercrosslinked	St	1,350	470

3.3. ADSORPTION OF ORGANIC COMPOUNDS BY GMA-ST-EDMA ADSORBENTS

With the goal to study the effect of polarity on sorption copolymers 2,3-epoxypropyl methacrylate–styrene crosslinked with ethylene dimethracrylate (40 wt.%) were prepared (Table 4). No substantial changes of specific surface area pore volume and pore radius were observed with changing 2,3-epoxypropyl methacrylate to styrene ratio. Adsorption of phenols, amines and carboxylic acids from water solutions on macroporous GMA-St-EDMA adsorbents (Table 4, Figure 2) indicates a considerable effect of the adsorbate type and polymer composition on adsorption.

TABLE 4. Porous structure of GMA-St-EDMA copolymers.

Copolymer	GMA (wt.%)	St (wt.%)	Specific surface area (m^2/g)	Pore volume (ml/g)	Pore radius (nm)	$-\Delta G_{CH2}$ (kJ/mol)
G-60	60	–	58	1.38	51	1.13
G-55-5	55	5	56	1.37	49	–
G-50-10	50	10	53	1.21	45	1.20
G-30-30	30	30	50	1.24	49	1.30
G-10-50	10	50	50	1.53	61	1.50
S-60	–	60	60	1.62	54	1.69

As follows from the adsorption isotherms the adsorption activity of the polymers is determined primarily by the properties of the adsorbate. The lipophilicity of GMA-St-EDMA terpolymers was characterized by the free energy of sorption of methylene group (ΔG_{CH2}). The ΔG_{CH2} values confirmed the stronger interactions of adsorbates with nonpolar terpolymers. As the styrene content in the adsorbent increased, i.e. as the lipophilicity increased, the amount of adsorbate increased, e.g. in the series:

$$\text{G-60} < \text{G-55-5} < \text{G-50-10} < \text{G-30-30} < \text{G-10-50} < \text{S-60}$$

The determined adsorption isotherms were described by the Aranovich equation for polymolecular adsorption for determination of the parameters of the adsorption equlibria on porous polar and non-polar polymeric adsorbents. The following mechanism can be operative: adsorption of adsorbate molecules on the polymer surface, multilayer adsorption and sorption of organic molecules in the bulk of polymer.

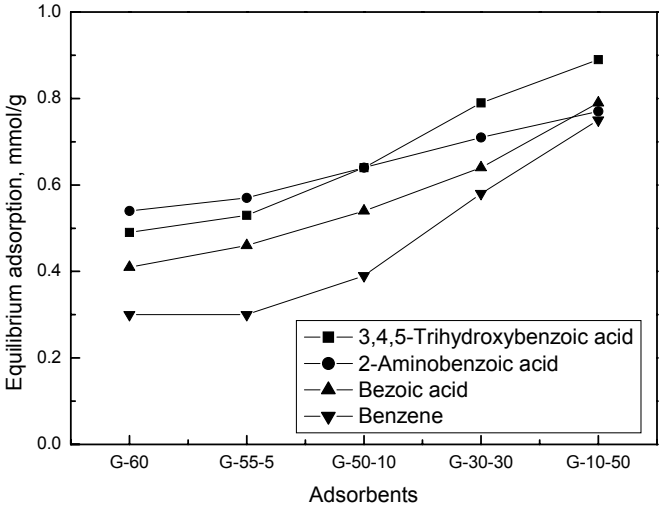

Figure 2. Effect of GMA-St-EDMA adsorbents composition on benzene derivatives adsorption.

3.4. INTERACTION OF ORGANIC COMPOUNDS WITH POLYMER ADSORBENTS BEARING FUNCTIONAL GROUPS

Application of hydrophilic adsorbents with the surface active functional groups, for adsorption is possible only in such cases when the adsorbate organic compounds forming H-bonds or ion–ion bonding of adequate strength with the adsorbent surface. The phenols are more strongly sorbed on the more polar methacrylate copolymers bearing ethyleneamine groups[14,15] (Table 5) than on styrene–divinylbenzene copolymers. The aminated polymers had higher adsorption capacities due to the Lewis acid–base interaction between the phenolic compounds and the tertiary amino groups on the polymer matrix.

TABLE 5. Porous structure of functionalized GMA-EDMA copolymers.

Derivative of GMA-EDMA copolymer	Group content (mmol/g)	Specific surface area (m^2/g)	Pore volume (ml/g)	Pore radius (nm)
Ammonia	1.76	80.6	1.28	31.8
Ethylene diamine	1.90	34.5	1.49	86.4
Diethylene triamine	2.35	67.0	0.90	26.9
Tetraethylene tetramine	2.39	55.0	1.1	40.0

The adsorbate adsorption increased on all adsorbents as follows:

p-Aminophenol <dihydroxybenzene < *p*-cresol < phenol < *p*-chlorophenol < *p*-nitrophenol

The adsorption is positively affected by the presence of ethyleneamine adsorbent functionality. The phenol adsorption decreases in the serie ethylenediamine, diethylenetriamine and triethylenetetramine functionality (Figure 3). The changes in adsorption capacity are assigned to a decrease in the dissociation constant of the adsorbent ethylenediamine groups.

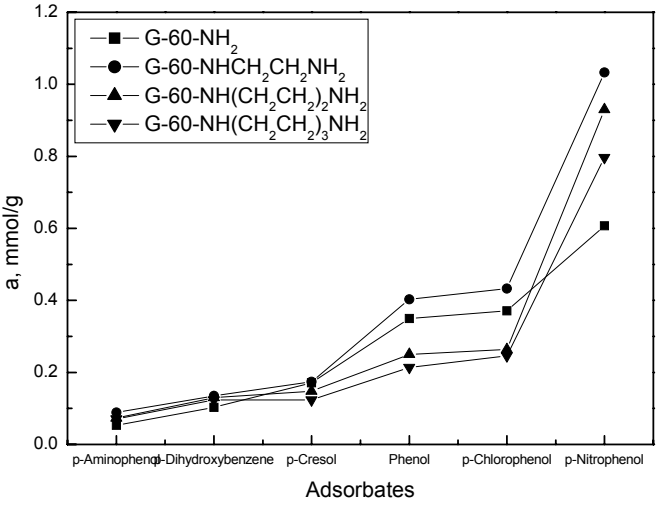

Figure 3. Adsorption of phenols on methacrylate adsorbent containing ethylenediamine groups.

4. Conclusions

The polymer adsorbent under investigation includes the macroporous, hypercrosslinked, and also functional polymers. The sorption of organic compounds by porous copolymers of different porous structure and polarity with laboratory and commercial samples was compared. The sorption capacity of hypercrosslinked copolymers is up to five times higher than that of macroporous samples. The presence of micropores and lipophilicity of adsorbate and adsorbent positively affect adsorption. Interaction by dispersion forces characterised the physical adsorption of adsorbate molecules and adsorbent. Polymer adsorbents are superior to the carbonaceous adsorbents in sorption of organic compounds and simply desorption.

The methacrylate copolymers bearing ethyleneamine groups have higher adsorption capacities due to the Lewis acid–base interaction between the phenolic compounds and the tertiary amino groups on the polymer matrix. The phenols are more strongly sorbed on the more polar methacrylate functional copolymers than on styrene–divinylbenzene copolymers. The adsorbate adsorption increased with the increasing polarity of adsorbate.

Acknowledgements

Financial support of the Grant Agency of the Czech Republic No. 104/03/0680 is gratefully acknowledged.

References

1. J. R. Millar, D. G. Smith, W. E. Marr, T. R. E. J. Kressman, *Chem. Soc.*, 1963, 218.
2. V. A. Davankov, S. V. Rogozhin, M. P. Tsyurupa, Macrocrosslinked polystyrenes, Ger. Pat. 2,045 096 (1971), US Pat. Appl. 3,729 457 (1971), USSR Appl. 1969, Chem. Abstr. 75, 6841v (1971).
3. D. Kraus, G. Popov, G. Schwachula, L. Feistel, R. Hauptmann, Verfahren zur Nachvernetzung von Schwach vernetzten Styrol Polymeren, Ger Pat. (East) 125 824 (1976), Chem. Abstr. 88, 7998g (1978).
4. L. D. Belyakova, N. P. Platonova, T. I. Shevchenko, F. Svec, and J. Hradil, Surface Chemistry of Methacrylate Polymeric Sorbents: Chromatography and Adsorption, *Pure Appl. Chem.*, 61, 1889–1896 (1989).
5. L. D. Belyakova, N. P. Platonova, J. Hradil, V. Marousek, and F. Svec, Adsorption properties of porous methacrylate polymers, *Reactive Polymers, Ion Exchangers, Sorbents*, 9, (1) 128–129 (1988).
6. J. Hradil, V. Krystl, P. Hrabanek, B. Bernauer, and M. Kocirik, Heterogeneous membranes based on polymeric adsorbents for separation of small molecules, *React. Funct. Polym.*, 61, 303–313 (2004).
7. J. Hradil, V. Krystl, P. Hrabanek, B. Bernauer, and M. Kocirik, Heterogeneous membranes filled with hypercrosslinked microparticle adsorbent, *React. Funct. Polym.*, 65, 57–68 (2005).
8. J. German, J. Hradil, J. M. P. Frechet, and J. Svec, High Surface Area Nanoporous Polymers for Reversible Hydrogen Storage, *Chemistry of Materials*, 18, 4430–4435 (2006).
9. V. V. Podlesnyuk, J. Hradil, R. M. Marutovskii, N. A. Klimenko, and L. E. Fridman, Sorption of organic compounds from aqueous solutions by glycidyl methacrylate-styrene-ethylene dimethacrylate terpolymers, *React. Funct. Polym.*, 33, 275–288 (1997).
10. J. Hradil, M. J. B. Benes, and Z. Plichta, Contribution on interaction of phenolic compounds with polymeric adsorbents, *React. Polym.*, 44, 3, 259–272 (2000).
11. V. V. Azanova and J. Hradil, Sorption properties of macroporous and hypercrosslinked copolymers, *React. Funct. Polym.*, 41, 163–175 (1999).

12. J. Hradil, Mechanism of interaction of organic compounds with polymeric adsorbents, in J. Fraissard and C. W. Conner (Eds), Physical Adsorption: Experiment, Theory and Applications, p. 591–597. Kluwer Academic Publishers, 1997.
13. J. Hradil and E. Kralova, Styrene-divinylbenzene copolymers post-crosslinked with tetrachloromethane, *Polymer*, 39, (24) 6041–6048 (1998).
14. J. Hradil, M. Wojaczynska, F. Svec, and B. N. Kolarz, Sorption of phenols on macroporous methacrylate copolymers containing ethyleneamine groups, *React. Polym., Ion Exchangers, Sorbents*, 4, (4). 277–283 (1986).
15. J. Hradil, M. Wojaczynska, F. Svec, and B. N. Kolarz, The sorption of phenols on macroporous methacrylate copolymers containing ethylene amine groups, *React. Polym., Ion Exchangers, Sorbents*, 7, (2–3) 316 (1988).

SAXS CHARACTERIZATION OF SOLID/VAPOR INTERFACES IN POLYMER-BASED MICROPOROUS CARBONS WITH DIFFERENT SURFACE CHEMISTRY

KRISZTINA LÁSZLÓ*
Department of Physical Chemistry and Materials Science, Budapest University of Technology and Economics, H-1521 Budapest, Hungary

ERIK GEISSLER
Laboratoire de Spectrométrie Physique CNRS UMR 5588, Université J. Fourier de Grenoble, BP 87, 38402 St. Martin d'Hères Cedex, France

Abstract. The equilibrium adsorption of non-polar and polar molecules, *n*-hexane and water, in activated carbons, functionalized by oxidation with concentrated nitric acid, is investigated by small angle x-ray scattering (SAXS). As condensed fluid modifies the electronic contrast of the carbon, the resulting changes in the SAXS intensity reveal the way in which the pores are filled. Filling of the pores from the vapour or the liquid phase is found to depend both on the surface treatment and on the nature of the liquid. For *n*-hexane vapour at $p/p_0 \approx 0.4$ the dispersion interaction ensures complete filling of the narrow pores, while larger pores are unpopulated. For water vapour cluster formation and the degree of filling depend on the relative humidity and the extent of surface oxidation. At a given applied relative pressure, the pores are completely filled by *n*-hexane, while, at the same relative pressure, water only partially fills the pores, even in the most oxidized carbon.

Keywords: activated carbon; water vapour; adsorption; contrast variation

*To whom correspondence should be addressed. E-mail: klaszlo@mail.bme.hu

J.P. Mota and S. Lyubchik (eds.), Recent Advances in Adsorption Processes for Environmental Protection and Security, 75–85.

1. Introduction

Carbons with high surface area and tailor-made porosity have been commercially available for several decades. [1–3]. In the 1980s their potential application as catalysts revealed the importance of the surface chemistry. In adsorption processes affinity between the carbon surface and the fluid phase plays a major role, as their interaction, which is generally non-specific, significantly affects the distribution of the adsorbed molecules within the pores.

In this paper we investigate the influence of the chemical character of a set of highly porous carbons on the pore filling behaviour of non-polar and polar adsorbates. The interaction of carbon samples of increasing oxygen content is studied with two different wetting liquids. In the non-polar *n*-hexane the intermolecular interaction is weak. Its attraction to the carbon surface favours significant adsorption already at low relative pressures p/p_0. Under real operating conditions, however, the relative humidity of the environment often sets water in competition with other target molecules for adsorption sites. Water molecules, which interact only weakly with graphitic carbon surfaces, adsorb on the carbon surface by a different mechanism [4, 5]. At low p/p_0 hydrogen bonding among the water molecules in the liquid phase makes the carbon–water interaction even less attractive. Water uptake in the carbon may be enhanced by introducing oxygen functionalities, since surface sites, through a cooperative bonding mechanism, can have the same effect as pre-adsorbed water [6]. The surface functional groups act as nucleation centres that, upon further accretion, ripen into clusters at p/p_0 as low as 0.1 [7]. At very low surface coverage water adsorption is governed both by the surface chemistry and the porosity of the carbons. For higher relative pressures the Dubinin–Astakhov equation yields excellent fits to the isotherm [8]. Water, therefore, on account of its particular relevance in activated carbon–vapour phase interactions, is used in this study as the polar probe.

Pore filling mechanisms with these two liquids is conveniently monitored by small angle x-ray or neutron scattering (SAXS or SANS), as these techniques furnish structural information down to the nanometre scale range. The spatial distances deduced from the SAXS response can be easily translated into the pore size w as $2\pi/q$ through the transfer wave vector q. Such observations yield model-independent information about pore filling by any adsorbed molecule. Since molecules adsorbed inside the pores modify the electronic contrast of their immediate surroundings, the small angle scattering signal of the local carbon matrix is sensitive to the adsorbed layer [9–11]. The present article reports SAXS measurements on microporous activated carbon samples of well characterized surface morphology

and chemistry equilibrated with *n*-hexane and water vapour of different relative pressure.

2. Experimental

To avoid inorganic impurities from the raw materials, microporous-activated carbons were prepared from a polymer precursor and chemically modified by oxidation with nitric acid. Granular activated carbon (APET) was prepared from poly(ethylene terephthalate) (PET) pellets [12]. Steam-activated carbon, obtained at 900°C, was treated for 3 h with room temperature (APETA) and boiling (APETB) concentrated nitric acid to obtain different degrees of surface functionalization. Before use, the samples were thoroughly washed with distilled water until neutral pH was attained. The morphology and surface chemistry of these carbons have been characterized elsewhere [13, 14]. Relevant characteristic data are listed in Table 1.

TABLE 1. Characteristic data derived from the low temperature nitrogen adsorption* and x-ray photoelectron spectroscopy (XPS).

		APETW	APETA	APETB
S_{BET}	m^2/g	1,156	1,114	304
W_0/V_{tot}		0.96	0.96	0.86
w_{DR}	Å	8.4	8.6	11.0
d_{He}	g/cm^3	1.74	1.82	1.50
O/C	Atomic ratio	0.064	0.098	0.27

*S_{BET}: surface areas from BET and Dubinin–Radushkevich (DR) models; V_{tot}, W_0: total and micropore volume, resp.; w_{DR}: average micropore width; d_{He}: true density from helium pycnometry.

The powdered samples, inserted into 1.5 mm diameter glass capillaries, were heated to 110°C for 24 h. The capillaries were equilibrated in air containing water vapour at various degrees of relative humidity (RH) and then sealed. Other samples were exposed either to liquid hexane or to hexane vapour at 40% partial vapour pressure at 20°C for 2 weeks, before sealing.

The SAXS responses were measured on the BM2 beam line at the European Synchrotron Radiation Facility (ESRF), Grenoble, France, in the wave vector range 6×10^{-3} Å^{-1} < q < 6 Å^{-1}, using an indirect illumination CCD detector. Data were corrected for grid distortion, dark current, sample transmission and background scattering. In the wide-angle x-ray scattering region (1 Å^{-1} < q < 6 Å^{-1}) no sign of Bragg scattering peaks was detected, indicating that the carbons are fully amorphous. Intensities were normalized with respect to a standard (lupolen), assuming an effective sample thickness of 1 mm to account for the filling factor of the powder in the capillary

tubes. The SAXS measurements were made at the same temperature as the sample preparation (20°C).

3. Theoretical Background

The distance by which x-rays penetrate into matter depends on their wavelength λ and on the electron density of the atoms in the substance. In porous materials, variations in electron density between solid regions and pores cause the x-rays to scatter in a way that depends on the shape and arrangement of the pores, i.e. on the internal structure of the material. The scattering pattern from a dry porous carbon is governed both by the structure factor describing the spatial distribution of the carbon atoms in the specimen, $S_1(q)$, and the electron density difference between the carbon matrix and the air-filled pores. Thus,

$$I_1(q) = r_0^2 \rho_C^2 \, S_1(q) \tag{1}$$

In Eq. (1), r_0 is the classical radius of the electron (2.82×10^{-13} cm) and $q = (4\pi/\lambda)\sin(\theta/2)$ is the magnitude of the transfer wave vector, θ being the scattering angle. The electron density of the carbon matrix is

$$\rho_C = Z d_{He} N_A / M \tag{2}$$

where Z is the atomic number, M the atomic mass, d_{He} the helium density of the sample and N_A Avogadro's number. The electron density of the air in the pores, much smaller than ρ_C, is neglected in Eq. (1).

If the same sample is impregnated with a liquid that does not completely fill the pore volume, then it contains three components, carbon, liquid and vapour. The scattered intensity is that of a ternary system, namely

$$I_{tern}(q) = r_0^2 \{(\rho_C - \rho_l)^2 \, S_{cl}(q) + \rho_C^2 \, S_{cv}(q) + 2\rho_C(\rho_C - \rho_l) S_{lv}(q)\} \tag{3}$$

where $S_{cl}(q)$ is a *partial structure factor* describing the relative positions of carbon and liquid, $S_{cv}(q)$ that between carbon and vapour phase, while $S_{cv}(q)$ is that between liquid and vapour phase. Since the electron density of the vapour phase is much smaller than that of the liquid it is neglected. As the micropores are small and spatially uncorrelated, the effective liquid–vapour interface is in many cases also small and the third term in Eq. (3) can be overlooked. This is generally true for molecules that wet the carbon surface: at a given relative pressure they condense in the smallest pores, but merely wet the inner surface of larger pores, rather than filling them. This modifies the electron density of the liquid-filled pores, leaving the larger ones unaffected. The first two terms in Eq. (3) can then be replaced by a single pseudo-binary expression of the form

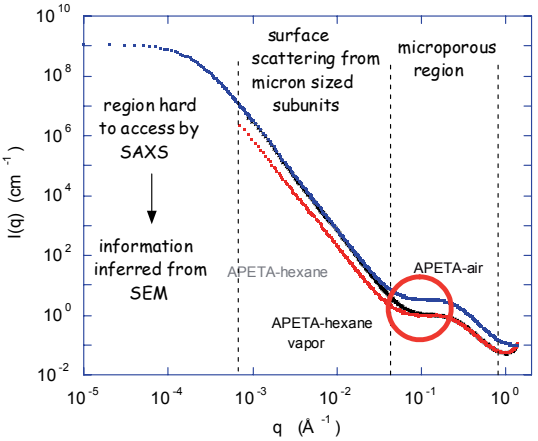

Figure 1. SAXS response from activated carbon APETA in dry air (upper curve) and in liquid hexane (lower curve). The curve for hexane vapour displays the transition from vapour phase at low q to liquid in the microporous region at $q \approx 0.1$ Å^{-1} (circled).

$$I_2(q) = r_0^2\,(\rho_C - \rho_S)^2\,S_2(q), \tag{4}$$

where ρ_S is the effective solvent density. Figure 1 shows the scattering response of an activated carbon in air, in hexane vapour and immersed in liquid hexane. At low q the intensity from the liquid hexane-containing sample is below that in air, owing to the lower contrast ($\rho_C - \rho_S$). At high q, since the hexane molecules cannot penetrate into the smallest spaces, $\rho_S = 0$ and the curves converge.

The degree to which the pores appear to be filled thus depends on the spatial scale of the observation, i.e. it is q-dependent. Equation (4) is an average over the regions in the sample where the fluid is condensed and those where it is still vapour. As $S_1(q)$ and $S_2(q)$ both describe the same total structure factor of the carbon, we set $S_1(q) = S_2(q)$. If the pores were uniformly filled then the two signals $I_1(q)$ and $I_2(q)$ would be everywhere proportional to each other, i.e. ρ_S is independent of q. To account for a non uniform distribution, e.g. molecules condense only in the finest pores while remaining in the vapour state elsewhere, the effective electron density of the fluid is expressed as $\rho_S(q) = p(q)\rho_l$, where ρ_l is the bulk density of the liquid and $p(q)$ is the relative density of the fluid with respect to its bulk value. The filling can then be expressed by the ratio

$$u(q) = I_2(q)/I_1(q) = [\rho_C - p(q)\rho_l]^2/\rho_C^2, \tag{5}$$

$$\text{i.e. } p(q) = \rho_C\,[1 - u(q)^{1/2}]\,/\rho_S \tag{6}$$

In principle, $0 \le p(q) < 1$, but $p(q)$ may be somewhat greater than unity in the case of strong interaction between the surface and the adsorbed layer. Negative values of $p(q)$, however, signify that the system no longer corresponds to the pseudo-binary model of Eqs. (4) and (6) and that the third term in Eq (3) is contributing to the scattering intensity. This happens when the contact area between the condensed solvent and its vapour becomes large, such as when liquid clusters develop.

4. Results and Discussion

Figure 2 shows the values of the relative density function $p(q)$ for *n*-hexane in APETA, calculated with Eq. (6) from the data of Figure 1. On immersion in liquid hexane all the pores fill, including those at low q. The contribution of the latter to the total adsorption is, however, small. (Values of $p(q)$ in excess of unity in the low q region may be an instrumental artefact.) The sharp cut-off at the highest values of q indicates that hexane molecules do not penetrate into spaces smaller than 4.5 Å [15]. At values of q below 1 $Å^{-1}$ the effective density of the hexane in the pores rises quickly to its bulk value. At the relative pressure $p/p_0 = 0.4$, the larger pores ($q < 0.1$ $Å^{-1}$) are less populated and filling drops to zero in the largest cavities. In interpreting Figure 2, however, it should be recalled that larger pores scatter more strongly than smaller pores. The *volume* filling of the pores is thus defined not by $p(q)$ but by $q^2p(q)$. Figure 2 thus implies that the carbon is almost completely saturated with hexane at $p/p_0 = 0.4$.

Water molecules, being smaller than hexane, can penetrate into smaller spaces. Figure 3 shows the density functions $p(q)$ calculated for water vapour at 43% relative humidity in APETA and APETB. In both samples,

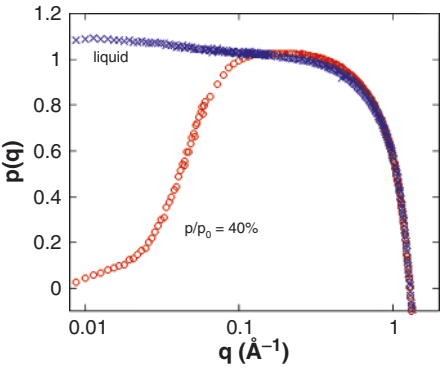

Figure 2. Relative density $p(q)$ in APETA in hexane vapour at $p/p_0 = 0.4$ (O) and in liquid hexane, $p/p_0 = 1$ (×).

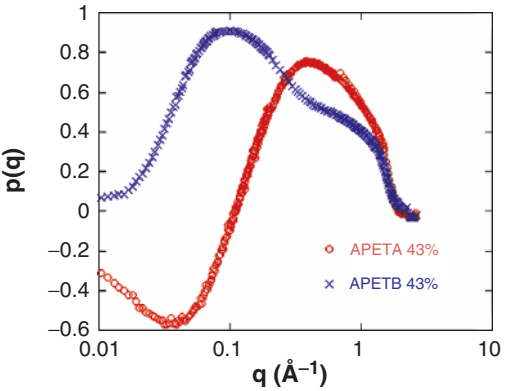

Figure 3. Relative density $p(q)$ in APETA (O) and in APETB (×) with water vapour at $p/p_0 = 0.43$.

$p(q)$ is effectively zero at $q \approx 2.1$ Å^{-1}, corresponding to a limiting size $d = 2\pi/q \approx 3$ Å. This result agrees with the critical size of the water molecule, 2.92 Å [15].

The different SAXS responses of APETA and APETB reflect their different surface treatment. In APETB, $p(q)$ in the nanopore region of the spectrum (0.3 Å$^{-1} \leq q \leq 1.5$ Å^{-1}, i.e. 20 Å $\geq d \geq 4$ Å) rises to only 40–50% of the density of bulk water. In the next larger pore size range ($q \approx 0.1$ Å^{-1}, $d \approx 60$ Å), filling reaches 90%, although these pores, owing the q^2 weighting factor, contribute little to the total amount of adsorbed water. The response of APETA to water vapour is markedly different. At the same relative humidity the sample displays a broad q region of apparently negative values of $p(q)$. As noted earlier, this is the signature of cluster formation. Since the sign of the third term in Eq. (3) is not positive for all q, it cannot be concluded from this figure alone that the filling in the nanoporous region is higher in APETA than in APETB. Figures 2 and 3 illustrate how the adsorption profiles of hexane and water vapour are qualitatively different and that water is highly sensitive to the surface chemistry of the carbon.

The pseudo-binary model, which quantifies the adsorption of wetting fluids, also reveals non uniform adsorption mechanisms, due either to surface chemistry or polarity of the probe molecules. The general case of water vapour equilibrated systems, however, requires independent information, such as water vapour adsorption isotherms, to refine the above results.

Figure 4a and b shows the direct SAXS spectra of APETA for various values of RH. At low RH small amounts of water condense initially in the micropores ($q > 0.2$ Å^{-1}), while cluster formation develops in the more open surfaces. Between 33% and 43% RH the amount of condensed water in the micropores increases significantly, while at low q, cluster formation becomes

more pronounced. A simple estimate of the contribution from the clusters can be made based on a lognormal distribution of cluster sizes. This yields the broad bell-shaped curve on the lower left in Figure 4b. Subtraction of this function, centred at q = 0.036 Å^{-1}, from the experimental spectrum, yields the flat plateau region shown as a dashed line. It can be seen from the figure, however, that the approximation underestimates the broad q-range of

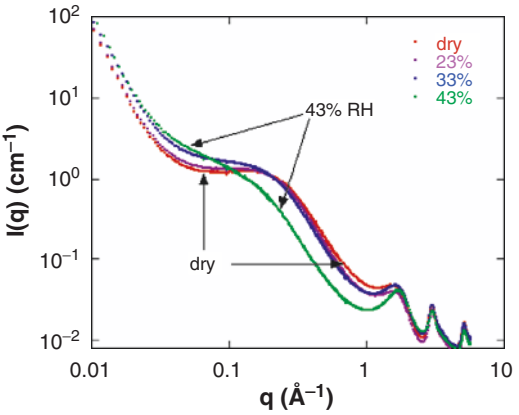

Figure 4a. SAXS response for APETA in the dry state and in water vapour at three degrees of relative humidity. Scattering intensity in excess of that of the dry sample is visible for q < 0.2 Å^{-1} even at RH = 23%.

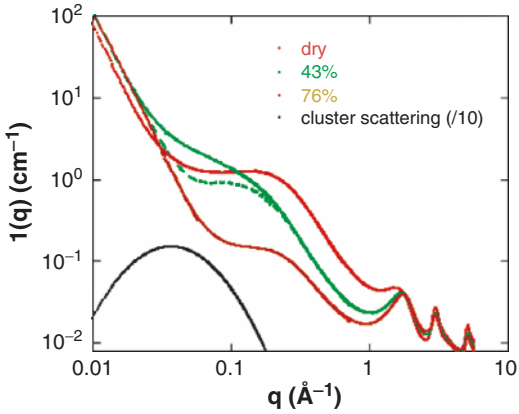

Figure 4b. SAXS from same sample showing in addition spectrum at 76% RH. Bell shaped curve is estimate for the third term in Eq. (3) (based on a lognormal function and divided by 10 for clarity), chosen to yield a plateau in the difference curve at $q \approx 0.1$ Å^{-1}. Dashed curve is the resulting difference between the full 43% curve and the lognormal function.

the scattering from clusters, since the intensity of the water vapour samples exceeds that of the dry carbon at much lower q. The cluster size distribution is therefore much wider than that of a simple lognormal distribution.

For the more oxidized APETB sample the various stages of the SAXS response as a function of RH are shown in Figure 5. Adsorption starts already at the lowest RH in the smallest pores ($q \approx 1$ Å^{-1}), but the corresponding values of $p(q)$ indicate that even at RH = 76% complete filling is not achieved. Occupation of pores in the nanometre size range is limited to less than to ~60%. For both APETA and APETB, access to the pores can be blocked by water clusters developing around functional groups located at the entrance of the pores, thus hindering the passage of further adsorbates.

The SAXS curves of Figure 5 indicate that cluster formation is not dominant in the highly oxidized sample for RH ≤ 0.5. Above this value, however, the intensity of the plateau at $q \approx 0.1$ Å^{-1} starts to increase monotonically. This unexpected finding shows that scattering from clusters becomes stronger at high relative humidity.

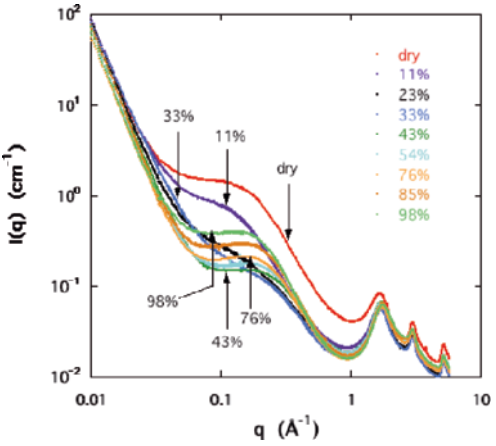

Figure 5. Pore filling sequence in APETB with increasing RH as observed by SAXS.

5. Conclusions

The chemical character of both the adsorbent and the adsorbate influences the wetting mechanism of the adsorbing vapour. The presence of adsorbed molecules changes the intensity of the small angle x-ray scattering (SAXS) response in a way that depends on how the pores are filled. Two carbon samples of different surface polarity were investigated. For the wetting fluid *n*-hexane, the dispersion interaction ensures progressive filling in both

carbons. For water vapour the degree of filling in the smaller pores and the cluster formation in the wider pores depend on the extent of oxidation. In the highly oxidized sample a cooperative mechanism enhances the filling of even larger pores.

The pseudo-binary model employed gives a satisfactory quantitative description at $p/p_0 \approx 0.4$ for both surfaces with hexane, while with water it gives quantitative results only for the highly oxidized sample. In the latter case the contribution of the water–air interfaces, corresponding to the cross term in the full scattering expression, cannot be neglected. Quantitative evaluation of this situation can be obtained only with the help of contrast variation, such as afforded by solvent deuteration in SANS.

In conclusion, firstly, the nature of the wetting liquid and of the surface chemistry is of major importance in the pore filling process. Secondly, competition between the non-polar molecules and water can be significant at high RH values.

Acknowledgements

The ESRF is gratefully acknowledged for access to the French CRG small angle beam line BM2. We express our thanks to G. Bosznai and C. Rochas for their invaluable assistance. This research was supported by the EU – Hungarian Government joint fund (GVOP-3.2.2-2004-07-0006/3.0).

References

1. D. Lozano-Castelló, M. A. Lillo-Ródenas, D. Cazorla-Amorós and A. Linares-Solano, Preparation of activated carbons from Spanish anthracite: I. Activation by KOH, *Carbon* 39(5), 741–749 (2001)
2. M. A. Lillo-Ródenas, D. Lozano-Castelló, D. Cazorla-Amorós and A. Linares-Solano, Preparation of activated carbons from Spanish anthracite: II. Activation by NaOH, *Carbon* 39(5), 751–759 (2001)
3. R. K. Dash, G. Yushin and Y. Gogotsi, Synthesis, structure and porosity analysis of microporous and mesoporous carbon derived from zirconium carbide, *Micropor. Mesopor. Mater.* 86(1–3), 50–57 (2005)
4. M. M. Dubinin, Water-vapor adsorption and microporous structures of carbonaceous adsorbents, *Carbon* 18, 355–364 (1980)
5. D. Mowla, D. D. Do and K. Kaneko, In *Chemistry and Physics of Carbon*, Vol. 28, edited by L. R. Radovic (Marcel Dekker, New York, 2003) pp. 230–262
6. E. A. Muller, L. F. Rull, L. F. Vega LF and K. E. Gubbins, Adsorption of water on activated carbons: a molecular simulation study, *J. Phys. Chem*. 100, 1189–1196 (1996)
7. J. K. Brennan, T. K. Bandosz, K. T. Thomson and K. E. Gubbins, Water in porous carbons, *Colloids Surf. A* 187–188, 539–568 (2001)

8. P. Lodewyckx and E. F. Vansant, Water isotherms of activated carbons with small amounts of surface oxygen, *Carbon* 37, 1647–1649 (1999)
9. E. Hoinkis, Small-angle scattering studies of adsorption and of capillary condensation in porous solids. *Part. Part. Syst. Charact.* 21, 80–100 (2004)
10. J. D. F. Ramsay, Applications of neutron scattering in investigations of adsorption processes in porous materials, *Pure Appl. Chem.* 65(10), 2169–2174 (1993)
11. M. M. Antxustegi, P. J. Hall and J. M. Calo, Development of porosity in Pittsburgh No. 8 coal char as investigated by contrast-matching small-angle neutron scattering and gas adsorption techniques, *Energy Fuels* 12, 542–546 (1998)
12. A. Bóta, K. László, L. G. Nagy and T. A. Copitzky, Comparative study of active carbons from different precursors, *Langmuir* 13, 6502–6509 (1997)
13. K. László, O. Czakkel, K. Josepovits, C. Rochas and E. Geissler, Influence of surface chemistry on the SAXS response of polymer-based activated carbons, *Langmuir* 21, 8443–8451 (2005)
14. K. László, E. Tombácz and K. Josepovits, Effect of activation on the surface chemistry of carbons from polymer precursors, *Carbon* 39(8), 1217–1228 (2001)
15. C. E. Webster, R. S. Drago and M. C. Zerner, Molecular dimensions for adsorptives, *J. Am. Chem. Soc*. 120, 5509–5516 (1998)

CO-ADSORPTION OF CESIUM CHLORIDE MOLECULES AND THULIUM ATOMS ON 2DGF ON Re

N.M. NASRULLAYEV*
Department of Physics, Baku State University,
Z. Khalilov St., 23, AZ-1148 Baku, Azerbaijan

Abstract. Adsorption co-adsorption of Tm atoms and CsCl molecules on two-dimensional graphite film (2DGF) on Re(1010) is investigated using the method of continuous flow. For these purposes, adsorption of CsCl molecules on the surface of 2DGF on Re(1010) is studied separately. It is found that molecules of CsCl on 2DGF are physically adsorbed. At 300 K ≤ T ≤ 750 K the adsorption of molecules leads to creation of salt islands. At 750 K < T < 1,500 K the salt islands do not appear. The exchange reaction, Tm + 3CsCl → TmCl3 + 3Cs, takes place when Tm atoms and CsCl molecules co-adsorb on the surface of 2DGF.

Keywords: co-adsorption; graphite; thulium; cesium chloride molecules

1. Introduction

For explaining the available experimental data on the co-adsorption of alkaline metal atoms and gas molecules on metals, a model for the surface atom–gas complex has been proposed by Bonzel.[1] This model is based on the transition of electrons from the top surface to CO molecule, and it has been introduced to explain the increasing in adsorption energy in Fe + K catalysis.[2,3] The potassium adsorbed on the Pt(111) surface decreases the work function. Due to a local change of the work function[4,5] on alkali adsorption, one can also expect a strong local effect of alkali on the gas chemisorptions.

* To whom correspondence should be addressed. E-mail: nasrullayev_n@hotmail.com

J.P. Mota and S. Lyubchik (eds.), Recent Advances in Adsorption Processes for Environmental Protection and Security, 87–95.

Lamoen[6] has been performed electronic structure calculations of the interaction of the potassium and the oxygen with the graphite (GR), individually and as well co-adsorbate. The authors show that at low coverage the potassium graphite bond is largely ionic and the variation of the K–GR bond energy with the lateral position of the K atom in the graphite unit cell is very small. On the clean surface the O_2–GR interaction is found to be repulsive in accordance with the extremely low sticking coefficient observed for O_2 on clean graphite. When potassium is adsorbed on the graphite surface, O_2 chemisorbs at the potassium-covered surface. The energy barrier towards dissociation of O_2 on the clean graphite surface is estimated to be similar to that of the gas phase O_2. Authors find that for O_2 on K–GR the barrier for dissociation is much smaller than in the gas phase or on the clean graphite surface.

The potential ionisation of thulium atoms is more than the work function of graphite and it can be expected that local change of work function of graphite at adsorption of atoms Tm will be less than the same for K atoms. We are studying the reaction between $CsCl$ molecules with Tm atoms at co-adsorption of these particles on 2DGF on Re with the aim to research the role of potential ionisation of atoms in the interaction on the surface. It is possible to expect, that products of $CsCl + Tm$ reaction will allow defining the valence of Tm in the adsorbed condition. It was informed about the possible change of the valence of atoms of rare earth elements at adsorption on transitive metals.[7]

2. Theory

The method of investigation the catalytic activity of the solid by the dissociation of CsCl molecules[8] offers a number of significant advantages.[9] CsCl is the simplest molecule with one break up channel only. One of the dissociation products, the Cs atom, has a low ionization potential (V_{Cs} = 3.89 eV), and under conditions where V_{Cs} is less than the substrate work function (this requirement is met on the surface of high melting point metals, graphite and many others) each Cs ad atom desorbs from the surface of heated adsorbent as Cs^+ ion (the mechanism of ion formation is surface ionization[10]).

If a beam of CsCl molecules of flow density ν_{CsCl} strikes the surface of the solid the not dissociated molecules with flow density ν'_{CsCl} escape rapidly, then the degree of dissociation $\gamma = (\nu_{CsCl} - \nu'_{CsCl})/\nu_{CsCl}$ will be a measure of the catalytic activity in question. Measuring under conditions of complete ionization ($V_{Cs} \ll \varphi$), the current density of the Cs^+ ions desorbing from the surface one can calculate γ, as $j = e \cdot (\nu_{CsCl} - \nu'_{CsCl}) = e \cdot \nu_{CsCl} \cdot \gamma$.

At adsorption CsCl molecules, on many metal (Ir, W, Mo, Re, Pt, Pd, Rh) surfaces at T > 800 K, $\gamma = 1$. Graphite stands out in its unique catalytic passivity: indeed, one monolayer of graphite on rhenium γ reduces from 1 to 10^{-3}–10^{-6}.[11]

3. Experimental

The experiments were carried out in a UHV metal installation: a magnetic sector mass-spectrometer with a residual pressure $\leq 5 \times 10^{-10}$ Torr was used for surface studies by the methods of TDS, surface ionization and thermo-ionic emission.[12] Flows of Tm atoms and CsCl molecules were supplied to the substrate from a Knudsen cell and could be made to overlap. The ions or electrons emitted from the ribbon's 4 mm long central part were measured by a collector system. Parts of the ions entered the mass analyzer through a slit in the collector and detected at the analyzer exit by means of an ion-electron multiplier.

The used samples were directly heated the polycrystalline rhenium ribbons of $40 \times 1.5 \times 0.02$ mm^3 dimensions, which were textures by passing them trough an AC current. The work function of the ribbon, φ, was (5.15 ± 0.05) eV, which coincides with the value of φ for the (1010) face of the Re.[13]

The Re ribbon was covered by a graphite layer at a substrate temperature of 1,600~1,790 K by admission of benzene vapour at a pressure of 10^{-5} Torr, until the electron emission reached a high and stable value, indicating a work function in the range 4.3~4.4 eV.

The kinetics of the reaction between Z (K, Na, Li) atoms and CsCl molecules with different T, ν_Z and ν_{CsCl} were experimentally investigated via the following two characteristics[14–16]:

1. The efficiency of reaction,

$$\eta(T) = \frac{\nu_{CsCl} - \nu'_{CsCl}}{\nu_{CsCl}} = \frac{\nu'_{Cs^+}(T)}{\nu_{CsCl}}, \quad (1)$$

where ν'_{CsCl} is the density of inverse molecule flow, desorbed from the emitter and uninvolved in the reaction. The difference $\nu_{CsCl} - \nu'_{CsCl}(T)$ is equal to the amount of Cs atoms, separated during the reaction, as the CsCl molecules are not reflected from the 2DGF. These atoms are desorbed as Cs^+ ions by surface ionization on 2DGF in the temperatures higher than the threshold temperatures for the light ionization of Cs on 2DGF.

2. The utilization factor of Tm atoms in reaction, is

$$Q(T) = \frac{\nu'_{Cs^+}(T)}{\nu'_{Tm}}, \tag{2}$$

where $\nu'_{Cs^+}(T)$ is the density of the flow of Cs atoms appearing in the reaction, that desorbed from surface as Cs^+ ions; ν'_{Tm} is the density of flow of Tm atoms to surface.

According to Eqs. (1) and (2), $\eta(T)$ and $Q(T)$ are related by a similar relationship:

$$Q(T) = \frac{\nu'_{CsCl}}{\nu'_{Tm}}\eta(T). \tag{3}$$

The method of steady-state flow provides that the concentration of particles on the surface is constant and is highly sensitive at the transformation of evaporated particles into ions through light surface ionization. In this case every particle evaporated from the surface becomes the ion and this is inaccessible to other forms of ionization. Light surface ionization takes place at evaporation of Cs atoms from the 2DGF on Re.

The atoms emerged from the surface are passive relative to dissociation of CsCl molecules and do not enter chemical reaction with reagents and weakly affect the composition of the reaction products.

4. Experimental Results and Discussion

4.1. FORMATION AND PROPERTIES OF 2DGF ON Re

The formation of 2DGF on Re is done by adsorption of benzene molecules on Re at $T \approx$ 1,600~1,700 K.[17] It is known, that molecules of benzene are adsorbed on (0001)Re with factor of sticking close to unit, and at heating only molecular hydrogen leaves from ad layer benzene, desorption of which is over at $T \leq 800$ K. The breaking of C–C bond on a surface releases atoms of carbon, which diffuse in Re till their concentration in a layer, near the surface will not be made even with maximum permissible. After that, carbon atoms collect on a surface of Re (Figure 1). In the interval $18 \leq t \leq 21$ min the monolayer of graphite is formed on the surface. The layer of graphite is valent-saturated and interferes with the catalytic dissociation molecules of C_6H_6.

Therefore the film ceases to grow on thickness. Work function of 2DGF on Re was determined in several ways: from Richardson's graph, by surface ionization of atoms difficultly ionized on a surface elements (Na, Ba), and also on a full ionic current (Na, K, Ba). It has been established,

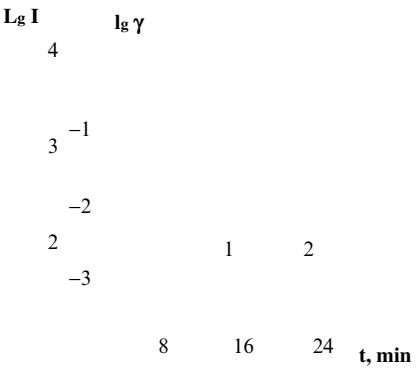

Figure 1. The dependences of thermo electronic current (1) and degree of dissociation γ of CsCl molecules on time, at high temperature adsorption of C_6H_6 molecules.

that the surface of a monolayer of graphite on Re is homogeneous on work function and had $\varphi = (4.45 \pm 0.05)$ eV, that well coincided with work function of the same surfaces.[17,18]

At formation of 2DGF on Re the degree of dissociation of CsCl molecules γ reduces from 1 to 10^{-3}–10^{-6}. On Figure 2 it is shown the characteristic dependence course of change of $\gamma(T)$ for dissociation on pure Re and for dissociation on Re with graphite monolayer.

Apparently from this figure $\gamma \approx 10^{-5}$ over the region 800 K $\leq T \leq$ 1,100 K. At temperature $T \approx 1{,}950$ K graphite collapses and dissociation of CsCl molecules on pure Re, γ increases up to 1 (Figure 2). One monolayer of graphite on Re is sufficient, that the surface becomes catalytic passive for dissociation of CsCl molecules. Tontegode[11] attributes this fact to saturation of valence bond saturation of a graphite layer, which inhibits electron change interaction with adsorbed particles. Because of its valence bonds are saturated, single crystal graphite has a layered structure with van der Waals forces coupling the layers. Valence bond saturation is responsible for specific features in the adsorption and catalytic processes occurring on the graphite layer. Indeed, if the quasilevel of V′ of the valence electron of an ad particle lies below the Fermi level (V′ > φ) then the ad particle maintains electrical neutrality and is coupled to the surface by van der Waals forces only (physisorption). If, however, V′ < φ, then the ad atom is partially charged, and image forces are added to the van der Waals forces. As the ad particles have orbitals that are not used in bonds to the substrate, this may enhance lateral interaction between them resulting in the formation in the ad layer of clusters and islands, with the particles on the graphite layer being in a less perturbed state than those on the metal surface. Finally, the dissociation

catalysis originating from the electron exchange between the adsorbed molecule and the surface will be inhibited.

Indeed, many molecular gases (I_2, Br_2, O_2, CO, H_2O),[19] a number of molecules ($C_6H_3Br_3$, GeJ_2, $FeCl_3$, As_2O_3)[20,21] as well as the Cu and Au atoms on the basal plane of the single crystal graphite[22] and Pt and Ni atoms on the graphite monolayer on Ir and Re[15] undergo only physisorption.

Apparently from Figure 2, on 2DGF on Re the degree of dissociation of CsCl molecules considerably falls, but above zero. We attribute this fact with dissociation on defects of graphite layer.

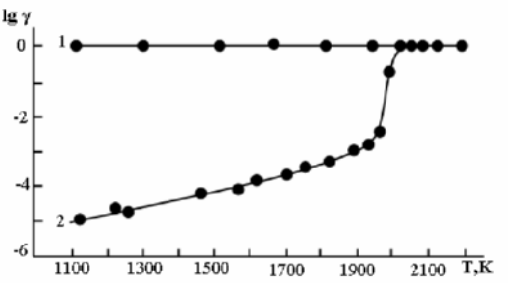

Figure 2. The dissociation of CsCl molecules on (1) Re and (2) Re covered with graphite monolayer.

4.2. ADSORPTION OF CSCL MOLECULES ON 2DGF ON Re(1010)

Previously adsorption of CsCl molecules on 2DGF is investigated separately for investigation of co-adsorption of Tm atoms and CsCl molecules on 2DGF surface on (1010)Re. Experiments have shown, that even at 300 K about one third of incident flow is desorbed with a time constant ~10^{-2} s, which coincides with the time of incident flow. Through the use of the Frenkel formula, $\tau = \tau_0 \exp(E/kT)$, we have estimated the upper limit of the desorption energy for CsCl at the temperature of the adsorbent below 750 K. Assuming $\tau_0 = 10^{-13}$ s, we have obtained $E < 0.65$ eV.

In Figure 3 dependences of desorbing flows, ν_{des}, versus time at opening (1) and closing (2) incident to 2DGF on Re flow, ν_{inc}, of CsCl molecules ($T_{adsorbent}$ = 650 K, $\nu_{inc} = 6.3 \times 10^{12}$ cm^{-2} s^{-1}) are plotted. It is seen that initially ν_{des} increases and quickly becomes equal to ν_{inc}. This means that in ad layer steady-state cover, by N_s molecules ($\nu_{inc} = \nu_{des} = N_s/\tau_{des}$), is established quickly. Time-by-time ν_{des} becomes lower than ν_{inc} and continues to decrease. This means that on the surface the condensation of particles begins, with condensation coefficient $\sigma = (\nu_{inc} - \nu_{des})/\nu_{inc}$.

TD spectra show that adsorption of CsCl molecules on 2DGF leads to island formation at the temperature of the adsorbent below 750 K. At

temperatures of the adsorbent higher than 800 K creation of islands was not observed. It has been found that at wide range of surface concentrations 1×10^{10}–5×10^{15} cm^{-2} of molecules from 2GDF only CsCl molecules are desorbed.

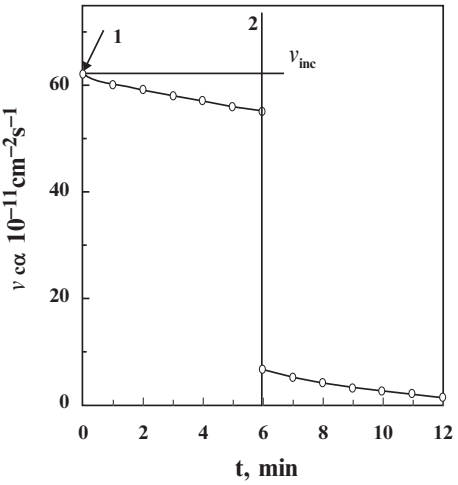

Figure 3. The dependences of desorbing flows ν_{des} versus t at (1) opening and (2) closing incident to 2DGF on Re flow ν_{inc} of CsCl molecules; T_{ads} = 650 K, $\nu_{inc} = 6.2 \times 10^{12}$ cm^{-2} s^{-1}.

4.3. INTERACTION OF CSCL MOLECULES WITH TM ATOMS AT CO-ADSORPTION OF THESE PARTICLES

Experiments were hold at temperatures of substrate T = 840–1,100 K and at density of flows $\nu_{CsCl} = 1 \times 10^{10}$–$6 \times 10^{13}$ cm^{-2} s^{-1} and $\nu_{Tm} = 2 \times 10^{10}$–$3.4 \times 10^{13}$ cm^{-2} s^{-1}. According to these circumstances Tm was on a surface only in the form of chemisorbed atoms and islands did not form. In the Figure 4 it is shown the dependence of Q on T. At 820 K ≤ T ≤ 875 K, Q = 3. This fact indicates to ongoing exchange reaction $Tm + 3CsCl \rightarrow TmCl_3 + 3Cs$. At $T \approx 920$ K, $Q \approx 2$, in this region of temperature from surface mainly $TmCl_2$ desorbs. At $T \geq 970$ K, $Q \leq 1$. This indicates that in the reaction mainly TmCl forms and Tm atoms desorb effectively from the surface. The maximum quantity of the efficiency of reaction was determined as $\eta \approx 0.6$. This quantity is less than obtained for K + CsCl ($\eta = 1$) reaction on such a surface.

Under the conditions of experiments concentration of particles on the surface were so less, that simultaneous meetings of three or four particles were less probably. There for it is assumed that the reaction

goes in three levels: in the first TmCl is got, in the second – $TmCl_2$ and in the third $TmCl_3$.

Thus, it is possible to expect, that on a surface of 2DGF at interaction with CsCl molecules valence of Tm atoms in these reactions is equal to 3.

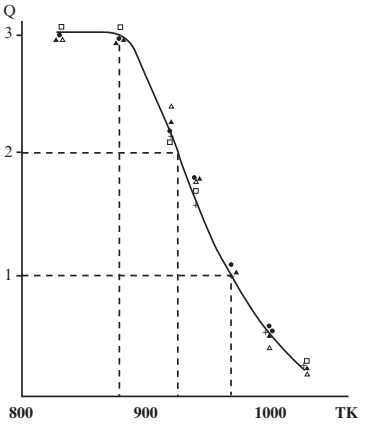

Figure 4. The dependence of $Q = f(T)$ at $\nu_{CsCl} = 6.8 \times 10^{12}$ cm^{-2} s^{-1} and different flows of Tm. $\nu_{Tm} \times 10^{-10}$ (cm^{-2} s^{-1}): **Δ,** 1.8; ▲, 4.9; ●, 10.2; +, 19.5; □, 32.9.

5. Conclusions

It is found that molecules of CsCl on 2DGF are physisorbed. At 300 K ≤ T ≤ 750 K the adsorption of molecules leads to the creation of salt islands. At 750 K < T < 1,500 K the salt islands do not appear. The exchange reaction Tm + 3CsCl → $TmCl_3$ + 3Cs takes place when Tm atoms and CsCl molecules co-adsorb on 2DGF surface.

References

1. (a) Bonzel H.P. Alkali-promoted gas adsorbtion and surface reactions on metals. *J. Vacuum Sci. Technol.* 1984, A2(2), 866–872; (b) Nevskaia, E. Castillejos-López, A. Guerrero-Ruiz and V. Muñoz, Effect of the surface chemistry of carbon materials on the adsorption of phenol-aniline mixtures from water. *Carbon* 2004, 42(3), 653–665.
2. Dry M.E., Shingles T., Boshoff L.J. and Oosthuizen G.J. Heats of chemisorption on promoted iron surfaces and the role of alkali in Fisher-Tropsch synthesis. *J. Catal.* 1969, 15. 190–199.
3. Dry M.E., Shingles T. and Boshoff L.J. Rate of the Fischor-Tropsch reaction over catalysis. *J. Catal.* 1972, 22, 99–104.

4. Kuppers J., Wandelt K. and Ertl G. Influence of local surface structure on the sp photoemission of adsorbed xenon. *Phys. Rev. Lett.* 1979, 43, 923–931.
5. Rotermund H.H. and Jacobi K. Physisorbtion on a low work function metal: arups from xenon on cesium. *Surf. Sci.* 1983, 126, 32–40.
6. Lamoen D. and Persson B.N.J. Adsorption of potassium and oxygen on graphite: A theoretical study. *J. Chem. Phys.* 1998, 108 (8), 3332–3341.
7. Nikulin V.K. and Potechina N.D. Effect of change valent state of atoms of rare earth elements at adsorption on refractory metals. *Fizika Tverdogo Tela* (Physics of Solid State), Russia, 1978, 20, 3354–3357.
8. Zandberg E.Ya. F., Tontegode A.Ya. and Yusufov F.K. Surface ionization of CsCl molecules on Ir(111)-C. *Jurnal Texnicheskoy Fiziki* (Journal of Technical Physics), Russia, 1972, 42, 171–174.
9. Rutkov E.V. and Tontegode A.Ya. A study of the carbon adlayer on iridium. *Surf. Sci.* 1985, 161, 373–389.
10. Zandberg E. Ya. and N.I. Ionov, Poverkhnostnaya Ionizatsia (Surface Ionization) (Nauka, Moscow, 1969).
11. Tontegode A.Ya. Carbon on transition metal surfaces. *Prog. Surf. Sci.* 1991, 38, 201–430.
12. Kholin N.A., Rutkov E.V. and Tontegode A.Ya. The nature of the adsorption bond between graphite islands and iridium surface. *Surf. Sci.* 1984, 139, 155–172.
13. Fomenko, V.S., Emissionnye Svoistva Materialov (Emitting Properties of Materials), *Handbook* (Naukova Dumka, Kiev, 1981).
14. Nasrullayev N.M. Interaction between cesium chloride molecules and metal atoms at coadsorption on the graphite single layer on iridium. *Turkish J. Phys.* 2000, 4, 617–622.
15. Nasrullayev N.M. Adsorption of Pt or Ni on graphite monolayer of rhenium, *Synth. React. Inorg. Metal. Org. Nano-Metal Chem.* 2005, 35, 7.
16. Nasrullyev N.M. and Panahov M.M. Co-adsorption Cesium Chloride Molecules and K, Na, Li Atoms on 2DGF on Re., 24th European Conference on Surface Science (ECOSS 24) Paris, September 3–9, 2006.
17. Gall N.R., Mikhailov S.N., Rutkov E.V. and Tontegode A.Ya. Carbon interaction with the rhenium surface. *Surf. Sci.* 1987, 191, 185–202.
18. Holmlid L. Complex kinetics of desorption and diffusion. Field reversal study of K. Exited- State desorption from graphite layer surfaces. *J. Chem. Phys.* 1998, 102, 10636–10646.
19. Lander J.J. and Morrison J. Low-energy electron diffraction study of graphite. *J. Appl. Phys.* 1964, 35, 3593–3598.
20. Lander J.J. and Morrison J. Ordered Physisorbed layer on graphite. *Surf. Sci.* 1966, 4, 103–107.
21. Morrison J. and Lander J.J. Ordered physisorption of xenon of graphite. *Surf. Sci.* 1966, 5, 163–169.
22. Arthur J.R. and Cho A.Y. Adsorption and desorption kinetics of Cu and Au on (0001) graphite. *Surf. Sci.* 1973, 36, 641–660.

CONTROLLING POROSITY TO IMPROVE ACTIVATED CARBON APPLICATIONS

A. LINARES-SOLANO,* D. LOZANO-CASTELLÓ, M.A. LILLO-RÓDENAS, D. CAZORLA-AMORÓS
Departamento de Química Inorgánica. Universidad de Alicante. Ap. 99, E-03080, Alicante, Spain

Abstract. This chapter presents an overview of preparation and characterization of activated carbons (ACs), activated carbon fibres (ACFs) and activated carbon monoliths (ACMs) to be used in different applications. Examples of the performance of these materials in environmental, energy storage and space applications are presented, remarking the importance of carrying out a suitable porous texture characterization of the materials to understand and optimize their performance in each application. Development of narrow microporosity, which is assessed by CO_2 adsorption at 273 K, has been demonstrated to be necessary for these applications. This type of porosity has been obtained by chemical alkaline hydroxide activation of carbon precursors with careful control and thorough understanding of the variables affecting the carbon activation process.

Keywords: activated carbon; narrow microporosity; VOC adsorption; gas storage; adsorption compressor

1. Introduction

Activated carbons are a group of carbonaceous materials with a very high porosity. Activated carbons are not present in nature. To prepare this type of materials it is necessary the selection of the precursor and the method of

*To whom correspondence should be addressed. E-mail: linares@ua.es

J.P. Mota and S. Lyubchik (eds.), Recent Advances in Adsorption Processes for Environmental Protection and Security, 97–106.

preparation. Several precursors, as wood, coals, pitches, polymers, residues with a high amount in carbon, etc., and also different methods of preparation have been used. These two factors have great importance as they determine the final porous structure of the activated carbon.

The very high porosity existing in activated carbons, together with the fact that they can be prepared with different morphologies (powders, granular, monolithic shape, fibres, cloths, pellets and others), makes them very suitable for adsorption applications both in gas and liquid phase.[1,2] The efficiency of a porous material to be used in an adsorption process depends not only on the surface or the pore volume but also on the size of the porosity and on the surface chemistry of the material. Therefore the characterisation of the activated carbons is crucial for determining if it is suitable or not for a given application.

This chapter presents an overview of preparation and characterization of activated carbons (ACs), activated carbon fibres (ACFs) and activated carbon monoliths (ACMs) to be used in different applications. Examples of the performance of porous carbon materials in environmental, energy storage and space applications are presented, remarking the importance of carrying out a suitable porous texture characterization of the materials to understand and optimize their performance in each application.

2. Porous Carbon Materials Preparation and Characterization

The main stage determining the porous structure is the activation method. The objective during the activation is both to increase the number of pores and to increase the size of the existing ones, so that the activated carbon has a high adsorption capacity. The different activation processes are divided into two different groups: chemical and physical activation.[1] The differences between both are the procedure and the activating agents used.

The preparation of activated carbons by physical activation[3] includes a controlled gasification of the carbonaceous material that has previously been carbonised although, occasionally, the activation of the precursor can be directly done. Thus, the samples are treated to 800–1,000°C with an oxidant gas (usually CO_2 and steam), so that carbon atoms are being removed selectively. Pore size distribution in the activated carbon depends on the precursor, the preparation conditions (mainly temperature, time and gas flow), the activating agent used and the presence of catalysts.

On the other hand, the chemical activation process consists of mixing a carbonaceous precursor with a chemical activating agent, followed by a heat treatment stage, and finally by a washing step to remove the chemical agent and the inorganic reaction products.[1,4] Several activating agents can be used in a chemical activation process, including phosphoric acid, zinc

chloride, and the hydroxides and carbonates of alkaline metals. Our research group has developed a deep research in the potassium and sodium hydroxides activation process,[5–8] obtaining very interesting results and developing high performance materials for different applications, as it will be shown later in this chapter.

For those applications using porous materials where the volume available is a constraint, an essential property is the material density. To minimize the useless voids (interparticle space), where gas adsorption does not take place, while maintaining a high porosity, carbon can be produced as a monolith. These monoliths consist of cylindrically shaped pieces, which pack uniformly, lessening wasted space in the system. Another advantage of producing carbons in an efficient space-filling form is that they are also strong, resist attrition and are easy to handle. Monoliths can be produced using a binder, which helps to keep the carbon particles in a compressed state. Conventional preparation methods[9,10] consist of mixing the activated carbon with a binder, compression and moulding using a hydraulic press and, finally, pyrolysis to improve the binder properties and decrease the weight of binder in the monolith. Our research group has developed activated carbon monoliths (ACMs) with tailored porosity and high density for specific applications, as shown later. The preparation details can be found elsewhere.[10]

As it has been mentioned in the introduction, characterization is an essential step. Since the porosity in activated carbons is responsible for their adsorption properties, the analysis of the different types of pores (size and shape), as well as the pore size distribution, is very important to foresee the behavior of these porous solids in final applications. The complete characterisation of porous carbons is complex due to the heterogeneity in the chemistry and structure of these materials. Thus, the selection of the appropriate method can be difficult and, most of the times, a combination of techniques is used.

Regarding the evaluation of the porosity of activated carbons, physical adsorption of gases is, undoubtedly, the most widely used technique.[11] Due to the considerable sensitivity of nitrogen adsorption isotherms to the pore structure in both microporous and mesoporous regimes and to its relative experimental simplicity, measurements of subcritical nitrogen adsorption at 77 K are the most used. However, the main disadvantage of N_2 adsorption at 77 K is that when it is used for the characterization of microporous solids, diffusional problems of the molecules inside the narrow microporosity (i.e. pore size below 0.7 nm) may occur.[12–15]. Moreover, there is an additional experimental difficulty in the adsorption of subcritical nitrogen because very low relative pressures (10^{-8}–10^{-4}) are needed to extend the range of porosity studied to the narrow microporosity, what requires more sophisticated and expensive adsorption equipments. To overcome these

problems, the use of other adsorptives has been proposed.[12–15] CO_2 adsorption, either at 273 K or 298 K,[12–15] is a useful alternative for the assessment of the narrow microporosity. Though the critical dimension of the CO_2 molecule is similar to that of N_2, the higher temperature of adsorption used for CO_2 results in a larger kinetic energy of the molecules, which are able to enter into the narrow porosity. In this way, CO_2 adsorption has been demonstrated to be an appropriate complementary adsorptive for the analysis of the microporosity.[15] In the following examples, the usefulness of CO_2 adsorption at 273 K to achieve a rather complete characterisation of the porous texture of microporous carbons will be discussed.

3. Examples of Improving Performances of Porous Carbon Materials on Different Applications

3.1. POLLUTION CONTROL

In the last years, great attention has been paid to the removal of volatile organic compounds (VOC) at low concentration, since the presence of these pollutants is detrimental both for human health and environment, even at very low concentrations.[16–19] As an example, the adsorption of benzene, toluene or their mixture at low concentration (200 ppmv for single VOC or 200 ppmv each for the mixture) have been studied at room temperature in a fixed bed reactor coupled to a mass spectrometer.[20–22] Both AC and ACF have been studied and the effect of a thermal treatment to reduce most of the surface oxygen groups has been analysed.

Regarding porosity, not a clear conclusion about its importance on the VOC adsorption capacity at low concentration was found previously in the literature. This is due to the fact that porous texture characterisation of the activated carbons was not complete from the point of view of the narrow microporosity. Figure 1A shows the correlation found by our research group between the volume of narrow micropores (assessed by CO_2 adsorption at 273 K) and the amount of benzene adsorbed, for both the AC[20–22] and ACF. This correlation also exists for toluene. It is also important to underline that the adsorption capacities for benzene (as high as 34 g benzene/100 g AC) and toluene (as high as 64 g toluene/100 g AC) at 200 ppmv achieved by the AC prepared by hydroxide activation are higher than those of commercial samples and higher than those previously reported in the literature.[21]

Surface chemistry has also proved to be crucial for the adsorption capacity. Thus, Figure 1B compares the adsorption capacity of samples thermally treated, with a lower content of surface oxygen groups (including T in their nomenclature), and pristine carbons, showing that the reduction of the oxygen content in the carbons favours the adsorption capacity.[21]

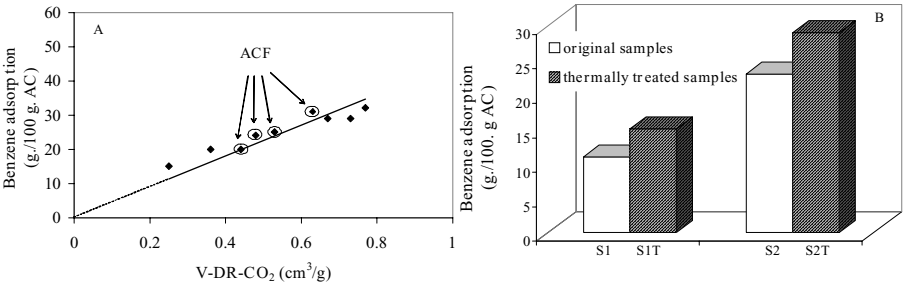

Figure 1. (A) Relationship between the benzene adsorption capacity and the narrow micropore volume for AC and ACF; (B) Comparison between benzene adsorption for pristine and thermally treated samples.

3.2. METHANE AND HYDROGEN STORAGE

At a given pressure, a strong adsorption potential inside the micropores acting on gas molecules significantly increases the density of the adsorbed molecules in relation to the gas-phase density. This phenomenon can be exploited for enhancement of gas storage capacity through adsorption. This has been the main reason for the strong interest in using AC as a medium to reduce the pressure required to store gases such as methane and hydrogen. The search for ACs able to store large amounts of natural gas at a reasonable pressure (3.5–4 MPa), as substitute for natural gas compressed at much higher pressure (e.g. 21 MPa) has been very intense in the last years.[23–26]

In all previous studies[23–26] it has been concluded that, in general, the higher the surface area (or micropore volume), the higher the methane adsorption capacity. In our research group, a systematic study of the performance of KOH-activated carbons in methane storage has been carried out. We concluded that, in addition to surface area and packing density, the micropore size distribution (MPSD) is also important.[26] Thus, Figure 2 contains the methane uptake versus the apparent BET surface area corresponding to a series of KOH-activated carbons. The objective of this correlation was to extend the BET surface area range beyond 2,000 m^2/g. The linear relationship is seen to reach a maximum for AC with a very high surface area. If only the apparent BET surface area or the micropore volume were responsible for the methane uptake, sample 5/1 (see Figure 2) should have a higher methane capacity than sample 3/1; however, the opposite behaviour is observed. These results can be explained analysing the porous texture in more detail. Thus, Table 1 contains the porous texture characterization results and the gravimetric methane adsorption capacities (up to 4 MPa) for the same samples. It can be concluded that the reason for a better

performance of sample 3/1 compared to 5/1, lies in their very different MPSD, as evidenced by the values of $V_{DR\ N2}$–$V_{DR\ CO2}$ (Table 1). Sample 3/1 has a narrower MPSD, which results in a higher methane uptake, consistent with the enhanced adsorption potential argument.[16]

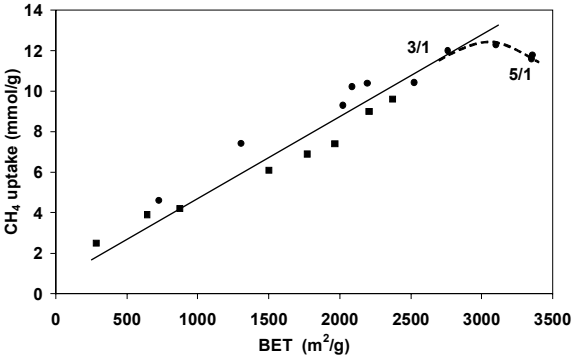

Figure 2. CH_4 uptake at 298 K and 4 MPa in chemically activated carbons versus the BET surface area.

TABLE 1. Porous texture characterisation and gravimetric methane adsorption capacity (up to 4 MPa) for two KOH AC.

Sample	BET (m^2/g)	$V_{DR\ N2}$ (cm^3/g)	$V_{DR\ CO2}$ (cm^3/g)	$V_{DR\ N2}$–$V_{DR\ CO2}$ (cm^3/g)	CH_4 uptake (mmol/g)
3/1	2,758	1.35	0.72	0.63	12
5/1	3,350	1.48	0.67	0.81	11.6

From a practical point of view, to increase the methane adsorption capacity we need to develop not only micropore volume, but also we have to control carefully the micropore size distribution. Thus, samples with high surface areas and very narrow micropore size distribution are required for this application. For this reason, in our studies of methane storage, KOH instead of NaOH was used as the activating agent for the preparation of ACs due to the narrower MPSD that can be obtained by KOH.

In relation to high-pressure storage of H_2 on activated carbons at room temperature, it must be remarked that this requirement is much more difficult than that of methane storage, due to the much lower H_2 uptake (either per unit mass of AC or per unit volume). However, to get the maximum H_2 uptake, the properties of the adsorbent that need to be optimised are very similar to those analysed for methane storage. More details of our results about hydrogen storage in carbon materials are not included here because a specific paper of our research group on this topic is also included in this book.

3.3. SPACE CRIOCOOLERS

The European Space Agency's (ESA) *Darwin Mission* is a future space interferometer dedicated to search for terrestrial planets in orbit around other stars. The interferometric imaging of astrophysical objects will be accomplished via four free-flying telescopes and a central hub. To guarantee proper mechanical stability, any vibration of the optical system (with its integrated 4.5 K cryocoolers) cannot be tolerated. To reach such low temperature, a two-stage vibration-free sorption He/H_2 cooler has to be designed with a suitable AC.[27] In this section, an example corresponding to the development of such an adsorbent is presented.

A sorption cooler has two parts: (i) a *cold stage*; and (ii) a *sorption compressor*. The *cold stage* consists of a counterflow heat exchanger and a Joule-Thomson expansion valve. This cold stage works as a typical refrigerator. The high-pressure gas needed comes from the *sorption compressor*. A *sorption compressor* can be described as a thermodynamic engine that transfers thermal energy to the compressed gas in a system without moving parts. Its operation is based on the principle that large amounts of gas can be adsorbed on certain solids such as highly porous ACs. The amount of gas adsorbed is a function of temperature and pressure. If a pressure container is filled with an adsorbent and gas is adsorbed at low temperature and pressure, then high pressure can be produced inside the closed vessel by an increase in the adsorbent temperature. Subsequently, a controlled gas flow out of the vessel can be maintained at high pressure by a further increase in temperature until most of the gas is desorbed.

ACs are obviously very interesting candidates for this application. They have to satisfy three essential requirements: (i) a large adsorption capacity per mass of adsorbent; (ii) a minimum void volume; and (iii) very good mechanical properties.

In order to optimise AC properties for this application, studies with samples prepared from different raw materials and using different activation processes have been carried out. To predict their adsorption performance, helium adsorption isotherms at different temperatures and pressures have been obtained. Figure 3 shows these isotherms corresponding to an AC prepared by anthracite activation. According to the conditions needed in the compressor stage, we are interested in obtaining a material with a maximum helium adsorption capacity at 2 bar and 50 K (adsorption stage) and a minimum adsorption capacity at 13 bar and 120 K (desorption stage). The best adsorption capacity has been obtained with an activated carbon monolith with relatively high development of porosity and, most importantly, with high narrow micropore volume assessed by CO_2 adsorption at 273 K. This material also presents quite high density (0.7 g/cm^3). A very high activation degree of the material is not desired because the density of the

material becomes low. In addition this activated carbon monolith presents a low pressure drop and a low thermal expansion, it has very good mechanical properties and it is easy to machine, which makes this material promising for adsorption compressor applications.

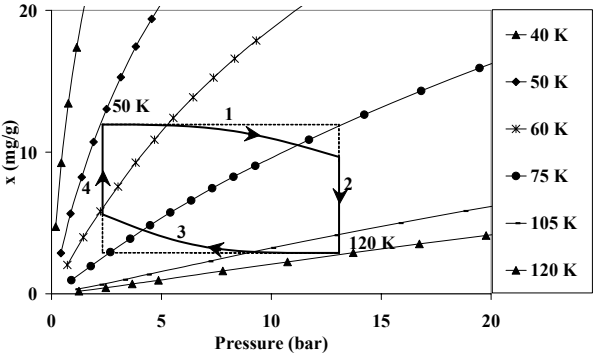

Figure 3. Helium adsorption isotherms at different temperatures corresponding to an activated carbon prepared by KOH activation of an anthracite. The numbers 1–4 correspond to each step of a complete cycle of a cell.

4. Conclusions

An overview of preparation methods of activated carbons (ACs), activated carbon fibres (ACFs) and activated carbon monoliths (ACMs) has been presented. It has been remarked that the analysis of the different types of pores (size and shape), as well as the pore size distribution, is very important to foresee the behavior of porous solids in final applications. Examples of the performance of porous carbon materials in environmental (VOC abatement), energy storage (CH_4 and H_2) and space (adsorption compressors) applications, have been included. For these applications, the importance of developing materials with a high volume of narrow microporosity (assessed by CO_2 adsorption at 273 K), has been demonstrated. In previous studies of our research group, we have shown that this type of porosity can be obtained by chemical alkaline hydroxide activation of carbon precursors with careful control and thorough understanding of the variables affecting the carbon activation process.

Acknowledgements

Authors thank financial support from Ministerio de Fomento (70012/T-05), MEC-FEDER (ENE2005-23824-E/CON and CTQ2006-08958) and Generalitat Valenciana (ACOMP06/089).

References

1. R.C. Bansal, J. Donnet and F. Stoeckli, *Active Carbon* (Marcel Dekker, New York, 1988) pp. 1–26.
2. H. Jankowska, A. Swiatkowski and J. Choma, *Active Carbon* (Ellis Horwood, New York, 1991) pp. 29–38.
3. M.J. Muñoz-Guillena, M.J. Illán-Gómez, J.M. Martín-Martínez, A. Linares-Solano and C. Salinas-Martínez de Lecea, Activated carbons from Spanish coals. 1. Two-stage CO_2 activation, *Energy Fuels* 6(1), 9–15 (1992).
4. H. Marsh, E.A. Heintz and F. Rodríguez-Reinoso. *Introduction to Carbon Technologies*. (Servicio de Publicaciones de la Universidad de Alicante, Alicante, 1997).
5. D. Lozano-Castelló, M.A. Lillo-Ródenas, D. Cazorla-Amorós and A. Linares-Solano, Preparation of activated carbons from Spanish anthracite I. Activation by KOH. *Carbon* 39(5), 741–749 (2001).
6. M.A. Lillo-Ródenas, D. Lozano-Castelló, D. Cazorla-Amorós and A. Linares-Solano, Preparation of activated carbons from Spanish anthracite II. Activation by NaOH. *Carbon* 39(5), 751–759 (2001).
7. J.A. Maciá-Agulló, B.C. Moore, D. Cazorla-Amorós and A. Linares-Solano, Activation of coal tar pitch carbon fibres: physical activation vs chemical activation, *Carbon* 42(7), 1361–1364 (2004).
8. A. Linares-Solano, D. Lozano-Castelló, M.A. Lillo-Ródenas and D. Cazorla-Amorós, Carbon activation by alkaline hydroxides: preparation and reactions, porosity and performances, In: L.R. Radovic (Ed.), *Chem. Phys. Carbon* 30, Dekker, New York (2006).
9. D.F. Quinn and J.A. MacDonald, Natural gas storage. *Carbon* 30(7), 1097–1103 (1992).
10. D. Lozano-Castelló, D. Cazorla-Amorós, A. Linares-Solano and D.F. Quinn, Activated carbon monoliths for methane storage: Influence of binder, *Carbon* 40(15), 2817–2825 (2002).
11. F. Rouquerol, J. Rouquerol and K.S.W. Sing, *Adsorption by Powders and Porous Solids. Principles, Methodology and Applications* (Academic Press, London, 1999).
12. F. Rodriguez-Reinoso and A. Linares-Solano, in: *Chemistry and Physics of Carbon*, edited by P.A. Thrower (Marcel Dekker, New York, 1988), pp. 1–146.
13. D. Cazorla-Amorós, J. Alcañiz-Monge and A. Linares-Solano, Characterization of activated carbon fibers by CO_2 adsorption, *Langmuir* 12, 2820–2824 (1996).
14. D. Cazorla-Amorós, J. Alcañiz-Monge, M.A. de la Casa-Lillo and A. Linares-Solano, CO_2 as an adsorptive to characterize carbon molecular sieves and activated carbons, *Langmuir* 14, 4589–4596 (1998).
15. D. Lozano-Castelló, D. Cazorla-Amorós and A. Linares-Solano, Usefulness of CO_2 adsorption at 273 K for the characterization of porous carbons, *Carbon* 42(7), 1231–1236 (2004).
16. F. Derbyshire, M. Jagtoyen, R. Andrews, A. Rao, I. Martin-Gullon and E.A. Grulke in: *Chemistry and Physics of Carbon*, edited by L.R. Radovic (Marcel Dekker, New York, 2001), pp. 1–66.
17. K.L. Foster, R.G. Fuerman, J. Economy, S.M. Larson and M.J. Rood, Adsorption characteristics of trace volatile organic compounds in gas streams onto activated carbon fibers, *Chem. Mater.* 4(5), 1068–1073 (1992).
18. M.P. Cal, M.J. Rood and S.M. Larson, Removal of VOCs from humidified gas streams using activated carbon cloth, *Gas. Sep. Purif.* 10(2), 117–121 (1996).
19. Z.H. Huang, F.Y. Kang, Y.P. Zheng, J.B. Yang and K.M. Liang. Adsorption characteristics of trace volatile organic compounds on activated carbon fibres at room temperature, *Adsorp. Sci. Technol.* 20(5), 495–500 (2002).

20. M.A. Lillo-Ródenas, J. Carratalá-Abril, D. Cazorla-Amorós and A. Linares-Solano. Usefulness of chemically activated anthracite for the abatement of VOC at low concentrations, *Fuel Process. Technol.* 77–78, 331–336 (2002).
21. M.A. Lillo-Ródenas, D. Cazorla-Amorós and A. Linares-Solano, Behaviour of activated carbons with different pore size distributions and surface oxygen groups for benzene and toluene adsorption at low concentrations, *Carbon* 43(8), 1758–1767 (2005).
22. M.A. Lillo-Ródenas, A.J. Fletcher, K.M. Thomas, D. Cazorla-Amorós and A. Linares-Solano, Competitive adsorption of a benzene-toluene mixture on activated carbons at low concentration, *Carbon* 44(8), 1455–1463 (2006).
23. N.D. Parkyns and D.F. Quinn, in: *Porosity in Carbons*, edited by J.W. Patrick (Edward Arnold, 1995) pp. 293–325.
24. V.C. Menon and S. Komarneni, Porous adsorbents for vehicular natural gas storage: a review, *J. Porous. Mater.* 5(1), 43–58 (1998).
25. T.L. Cook, C. Komodromos, D.F. Quinn and S. Ragan. in: *Carbon Materials for Advanced Technologies*, edited by T.D. Burchell (Pergamon/Elsevier Science, New York, 1999) pp. 269–302.
26. D. Lozano-Castelló, J. Alcañiz-Monge, M.A. de la Casa-Lillo, D. Cazorla-Amorós and A. Linares-Solano, Advances in the study of methane storage in porous carbonaceous materials, *Fuel* 81(14), 1777–1803 (2002).
27. J. Burger, H. Holland, M. Ter Brake, G. Venhorst, E. Hondebrin, R.J. Meier, H. Rogalla, R. Coesel, W. Dierssen, R. Grim, D. Lozano-Castelló and A. Sirbi, Vibration-free 5 K sorption cooler for ESA's Darwin mission, *European Space Agency (Special Publication) ESA* SP (539), 379–384 (2003).

LIQUID-PHASE ADSORPTION/OXIDATION OF SULFUR-CONTAINING SPECIES BY ACTIVATED CARBON

R.V.R.A. RIOS, J. SILVESTRE-ALBERO,
A. SEPULVEDA-ESCRIBANO,
F. RODRIGUEZ-REINOSO*
Laboratorio de Materiales Avanzados, Departamento de Química Inorgánica, Universidad de Alicante, E-03080 Alicante, Spain

Abstract. Liquid phase (*n*-hexene) adsorption of propanethiol on activated carbons is commonly accompanied by surface assisted oxidation processes of propanethiol to dipropyl disulfide (DPDS). In fact, both the porous structure and surface chemistry influence the adsorption/oxidation process. Whereas the porous structure is the main parameter defining the removal kinetics, the surface chemistry affects the extent of propanethiol oxidation and, consequently, the total removal capacity.

Keywords: activated carbon; propanethiol; sulfur removal; porous structure; surface chemistry

1. Introduction

Mercaptan molecules are undesired compounds present in crude petroleum and also produced as a decay of animal and vegetable matter. Worldwide regulations for environmental protection are forcing the petroleum refining industry to drastically decrease the sulfur content in transportation fuels.[1,2] Deep desulfurization using conventional hydrotreating technology (HDS) exhibits important limitations when dealing with larger molecules such as benzothiophene and di-benzothiophene (refractory molecules). In fact, an

*To whom correspondence should be addressed. E-mail: reinoso@ua.es

J.P. Mota and S. Lyubchik (eds.), Recent Advances in Adsorption Processes for Environmental Protection and Security, 107–118.

improved catalyst or increased reactor volume and/or more severe reaction conditions, especially higher temperatures and higher H_2 pressures, would be required.[3] Consequently, removal under mild conditions of organic sulfur compounds, both in gas and liquid streams, is becoming actually a challenging task in environmental chemistry.

One of the most promising "non-HDS" based technologies for sulfur removal is desulfurization by physical adsorption on a solid adsorbent. More specifically, recent studies have proposed activated carbon as sorbent for methyl mercaptan (MM) removal from air streams.[4–7] Activated carbons are well known as versatile adsorbents for many different applications.[8,9] The main advantages of activated carbon compared to conventional oxide-based adsorbents are their high surface area, the presence of a well-developed microporous structure, the high adsorption capacity and the possibility to tailor their surface chemistry and porous structure during the manufacture or by post-treatment.

Gas-phase removal experiments have shown that methyl mercaptan (MM) adsorption on activated carbon is highly dependent on both the porous structure and surface chemistry. Additionally, these studies have shown that the adsorption process is accompanied by surface assisted oxidation reactions of MM to dimethyl disulfide (DMDS) and even to sulfonic acid.[4–6] Similar studies also report some carbon dioxide formation under excess oxygen at higher temperatures (473 K).[5] Katoh et al. proposed an oxidation mechanism through hydroxyl and oxygen radicals created on the surface of wet activated carbon fibers, a process that was assisted by trace amounts of ferrous cations present on the carbon surface.[4] Similar studies using activated carbons from different origins proposed the presence of two reaction mechanisms for the oxidation of methyl mercaptan depending on the presence or absence of moisture.[6] In dry conditions, the authors proposed an oxidation process with MM and oxygen adsorbed from the gas phase on the carbon surface, with water and DMDS as final reaction products. However, an "island" mechanism was proposed for wet conditions, with MM and oxygen firstly being dissolved in water cluster followed by surface reaction between thiolate ions (CH_3S^-) and dissociatively adsorbed oxygen in water, a surface pH dependent process.

The scenario in liquid phase adsorption becomes more complex due to the presence of the solvent and many other compounds such as aromatics, olefins, etc. which will modify the adsorption/oxidation behavior. Preliminary results obtained by our group in liquid-phase removal of propanethiol using different activated carbons have shown that the process is highly dependent on the porous structure and surface chemistry of the sorbent.[10] Interestingly, even in the absence of an external oxygen supply (only the mercaptan

molecule and the solvent are present together with the activated carbon), the results show the presence of parallel oxidation reactions of propanethiol to dipropyl disulfide. Unfortunately, to our knowledge no studies have been reported in the literature concerning this oxidation reaction on liquid-phase experiments using activated carbon.

With this, the aim of the present work is to give more insight into the liquid-phase removal of mercaptan molecules using activated carbons. The effect of the porous structure and surface chemistry of different activated carbons on the adsorption/oxidation of a simple mercaptan molecule such as propanethiol will be overviewed. Additionally, the oxidation of propanethiol to dipropyl disulfide will be studied in more detail by performing fixed-bed adsorption/breakthrough experiments. The effect of dissolved and chemisorbed oxygen in the oxidation process will be discussed.

2. Experimental

Three different commercial activated carbons were used in this study: CNR (CNR 115, phosphoric acid activated carbon, from Norit), 208 (208C, steam activated carbon, from Chemviron) and R2 (R2030, steam activated carbon, from Norit).

Activated carbons were characterized by nitrogen adsorption at 77 K and temperature-programmed decomposition (TPD) experiments, as described elsewhere.[10] N_2 adsorption experiments were used to determine the porous structure while TPD experiments were used to characterize the surface chemistry (oxygen surface groups).

Propanethiol removal kinetic experiments were carried out at room temperature and atmospheric pressure.[10] The propanethiol solution (10 mL; $[C_o]$:168 ppmw S in *n*-hexene) containing the activated carbon sorbent (200 mg) was periodically analyzed using a gas chromatograph (Varian GC 3800) equipped with flame ionization (FID) and pulsed flame photometric (PFPD) detectors.

Fixed-bed adsorption/breakthrough tests were performed in a continuous flow packed glass bed reactor (1 cm i.d., 17 cm length). Initially, 2 g of the corresponding activated carbon (particle size $0.5 < \times < 0.7$ mm) were packed into the glass column and heated in a He flow (50 mL min^{-1}) at 473 K during 4 h, in order to remove surface impurities. After cooling down to room temperature, the He gas was switched to a sulfur free hydrocarbon effluent (*n*-pentane) until the activated carbon was completely wet. After wetting the carbon for 30 min, the feed was switch to the *n*-hexene/propanethiol mixture (420 ppmw S) at 0.5 mL min^{-1}. Once *n*-hexene starts to leave the column, effluent samples were collected at regular intervals following the reaction products by GC, as described above.

3. Results and Discussion

Activated carbons CNR, 208 and R2 have been already characterized in a previous work.[10] Briefly, these three activated carbons posses a well-develop microporous structure, as deduced from N_2 isotherms at 77 K. However, while carbon CNR exhibits a wide pore size distribution with a BET surface area of 1,834 $m^2\ g^{-1}$ and a total pore volume of 0.95 $cm^3\ g^{-1}$, samples 208 and R2 have a similar porous structure with a narrow pore size distribution, BET surface area of 1,274 $m^2\ g^{-1}$ and 1,183 $m^2\ g^{-1}$ and total pore volume of 0.56 $cm^3\ g^{-1}$ and 0.60 $cm^3\ g^{-1}$, respectively. Surface chemistry analysis of these carbons using temperature-programmed decomposition experiments denotes important differences in the amount and nature of oxygen surface groups depending on characteristics of the sample. In this sense, carbon CNR exhibits by far the highest amount of oxygen surface groups, these groups being mainly evolved as CO and attributed to decomposition of phenol, ether and carbonyl/quinone groups.[11,12] The total amount of oxygen evolved as CO_2 and CO was 872 and 4,326 μmol g^{-1}, respectively. TPD profile for carbon 208 exhibits also low and high temperature decomposition peaks although with a lower contribution (422 μmol g^{-1}, as CO_2 and 681 μmol g^{-1}, as CO) as compared to carbon CNR. Finally, carbon R2 exhibits a poor surface chemistry with only 64 μmol g^{-1}, evolved as CO_2 and 160 μmol g^{-1}, evolved as CO.

In summary, activated carbon CNR exhibits by far the highest surface area and the highest amount of oxygen surface groups evolved both as CO and CO_2. On the contrary, carbons 208 and R2, although having a similar porous structure, exhibit important differences in the surface chemistry. Consequently, an appropriate comparison and inter-correlation of these three samples will help in defining the effect of porous structure and surface chemistry for the liquid phase removal of propanethiol.

3.1. LIQUID PHASE REMOVAL OF PROPANETHIOL

The kinetics of propanethiol removal from a liquid solution containing 168 ppm S in *n*-hexene has been studied for the three activated carbons. Figure 1 shows the removal kinetics together with the analysis of the amount of propanethiol oxidized and released to the solution, and that retained on the carbon surface (as propanethiol and/or dipropyl disulfide).

As it can be observed in Figure 1, the kinetics of propanethiol removal differs considerably depending on the nature of the activated carbon. In this sense, while carbons CNR and 208 show faster removal kinetics with mainly 100% efficiency after 25 h, carbon R2 achieves only 60% removal with a slower kinetic behavior. The kinetics and total removal capacity can

not be exclusively explained by the porous structure (compare carbon 208 and R2 with similar porous structure) because of the presence of associated oxidation processes of propanethiol to dipropyl disulfide (DPDS). Interestingly, in all samples the DPDS formed is immediately released to the solution, thus, providing free surface sites able to adsorb more propanethiol and, finally favoring the removal kinetics. Taking a closer look to the amount of DPDS formed, it can be observed that the oxidation ability decreases in the order 208 > CNR > R2. The lower oxidation ability of carbon R2 can be explained by its poor surface chemistry (considering that the oxygen surface groups are responsible for the oxidation reaction); however, the comparison becomes more difficult for samples 208 and CNR (carbon CNR exhibits by far the highest amount of oxygen surface groups). Thus, from these results it is clear that not the amount but mainly the nature of the oxygen surface groups seems to be responsible for the oxidation reaction.

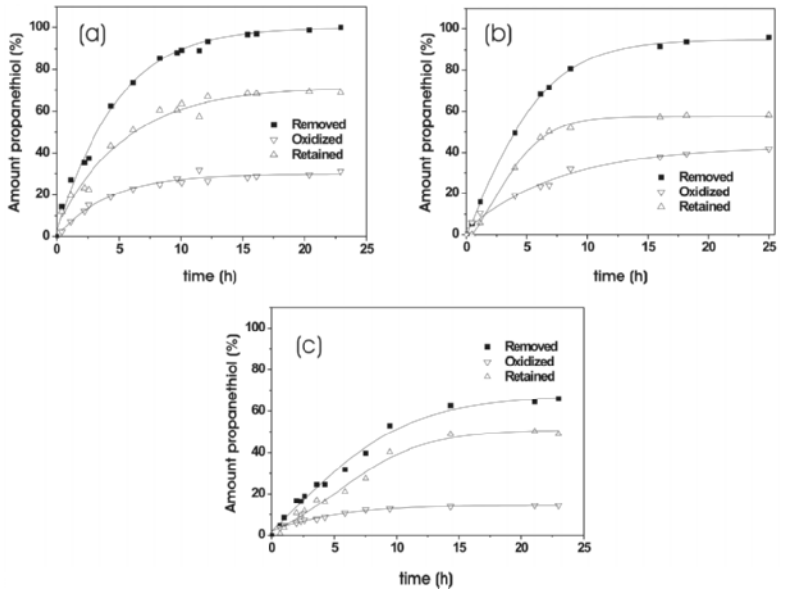

Figure 1. Kinetics of propanethiol removal for activated carbons (a) CNR, (b) 208, and (c) R2 at 303 K. Additionally, the amounts of propanethiol oxidized and retained in the carbon are also included. $[S]_o$: 168 ppm.

The high facility of the activated carbons to release DPDS to the solution almost from the beginning is somehow in contradiction with gas-phase experiments where some authors proposed a higher adsorption strength for the oxidized product (DMDS) due to its larger size and higher boiling

point.[6] This result confirms that the presence of spectators (solvent) provides a different scenario for liquid phase removal experiments.

3.1.1. *Effect of the porous structure*

To further explore the effect of the porous structure in the removal of propanethiol, activated carbon R2, which exhibits a lower oxidation capacity, has been submitted to a re-activation treatment in CO_2 (100 mL/min) at 973 K for 8h, in order to enlarge its microporous structure. N_2 adsorption analysis at 77 K shows that the re-activation treatment produces the development of wider micro and mesopores.[10] The re-activated sample R2 (R2/CO_2) exhibits a higher surface area (1,497 m^2/g), as well as a higher micropore (0.53 cm^3/g) and total (0.87 cm^3/g) pore volume. Figure 2 compares the propanethiol removal kinetic at room temperature for samples R2 and R2/CO_2.

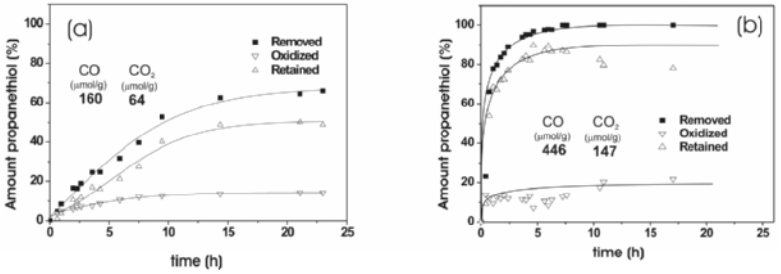

Figure 2. Kinetics of propanethiol removal for activated carbons (a) R2 and (b) R2/CO_2 at 303 K. Additionally, the amount of propanethiol oxidized and that retained in the carbon is also included. $[S]_o$: 168 ppm.

The re-activation treatment of carbon R2 produces an important increase in the kinetics of propanethiol removal as inferred from Figure 2. These results clearly show that on activated carbons with a low oxidation capacity, the propanethiol removal kinetics and the total removal capacity are basically defined by the porous structure. Thus, the kinetics and total amount of propanethiol removed from the liquid phase and retained on the carbon surface will depend on the total adsorption capacity of the carbon sorbent.

3.1.2. *Effect of oxygen surface groups*

Previous studies on gas-phase removal of organic sulfur compounds have shown that carbon materials are able not only to adsorb but also to oxidize mercaptan molecules to disulfides.[4–6,13] Furthermore, several studies described an important promoting effect of the surface chemistry (oxygen and nitrogen

surface groups), the presence of water and of metal ions constituent of the ash in the oxidation process. [4,5,14–16] In order to get more insight into the effect of the surface chemistry on the oxidation ability of activated carbons, samples R2 and R2/CO_2, both exhibiting a low oxidation capacity, have been submitted to an oxidation treatment with HNO_3 followed by a thermal treatment in He at 973 K. As expected, the oxidation treatment produces an important increase in the amount of oxygen surface groups evolved both as CO and CO_2 (see inset in Figure 3). A subsequent thermal treatment in He at 973 K produces the partial removal of the oxygen surface groups, this effect being more detrimental for the less stable (more acidic) groups. After characterization, the modified carbons have been tested in the removal of propanethiol (see Figure 3).

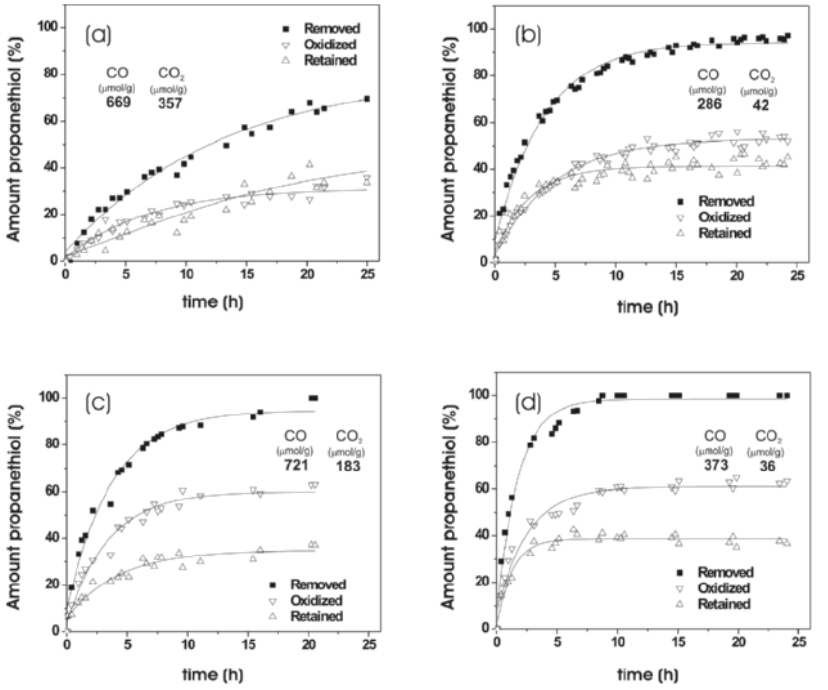

Figure 3. Kinetics of propanethiol removal on carbons (a–b) R2 and (c–d) R2/CO_2 at 303 K after an oxidation treatment with HNO_3 (a–c) and after a subsequent thermal treatment in He at 973 K (b–d).[10] Additionally, the amount of propanethiol oxidized and that retained in the carbon is also included. $[S]_o$: 168 ppm.

The oxidation treatment of carbon R2 produces mainly no effect in the removal kinetics and total removal capacity. On the contrary, carbon R2/CO_2 exhibits a slight decrease in the removal kinetics, most probably attributed

to the presence of steric hindrance in the pore mouth by newly created oxygen surface groups. This treatment also produces an important increase (two- or threefold increase) in the oxidation capacity of both samples, a clear indication of the critical role of surface oxygen in the formation of DPDS. Interestingly, a subsequent thermal treatment in He at high temperature (973 K) produces in both samples an increase in the propanethiol removal kinetics, probably due to the expected carbon gasification and, contrary to the expectations, it has no effect or even a slight increase in the oxidation ability. In summary, these results confirm that: (i) the oxidation of propanethiol to DPDS requires the presence of specific oxygen surface groups, (ii) these groups are located in the inner porous structure, i.e. the decomposition of groups produced by He favors the accessibility of propanethiol and, thus, increase the amount of DPDS formed and (iii) the high stability of these groups to a high temperature treatment indicate that the less acidic groups (most probably quinone groups) seem to be responsible for the oxidation reaction.

3.2. OXIDATION OF PROPANETHIOL TO DIPROPYL DISULFIDE (FIXED BED ADSORPTION/BREAKTROUGH EXPERIMENTS)

The oxidation of mercaptan to disulfide at room temperature on carbon materials has been widely described in the literature for gas-phase experiments.[4,6,13] It is clearly stablished that the oxidation reaction proceeds via oxygen adsorbed from the gas phase,[5,6] with water and disulfide as final products. However, the absence of an external oxygen supply for liquid-phase experiments enhances the critical role of dissolved and/or chemisorbed oxygen in the oxidation reaction. The role of dissolved oxygen in the oxidation process has been ruled out in this work by performing kinetic experiments on propanethiol/*n*-hexene solutions previously saturated with O_2 or N_2 (after bubbling oxygen or nitrogen through the solution for 20 min). In all cases, the oxidation capacity of the carbon sorbent was independent of the saturation pre-treatment.

For the second hypothesis, as chemisorbed oxygen is a limiting factor, i.e. there is a limited amount of oxygen in the reaction system, one would predict a limit in the extent of the oxidation for liquid-phase adsorption experiments. In order to check this effect of chemisorbed oxygen, activated carbon 208, which exhibits the highest oxidation ability, has been used in fixed-bed adsorption/breaktrough experiments. Figure 4a shows the breaktrough curve for propanethiol adsorption and oxidation on activated carbon 208 at room temperature.

As it can be observed, almost from the beginning of the experiment 80% of the propanethiol leaves the reactor without being adsorbed and/or

oxidized. Taking a closer look to the oxidation profile, after an initial maximum of 21%, the amount of propanethiol oxidized to DPDS stabilizes in a plateau around 15%, independently of time on stream. As expected, at longer adsorption times the oxidation profile falls down to a value close to 4%. This deactivation in the oxidation reaction with time on stream has been already described in the literature for gas-phase adsorption experiments of H_2S[13,17] and methyl mercaptan.[5]

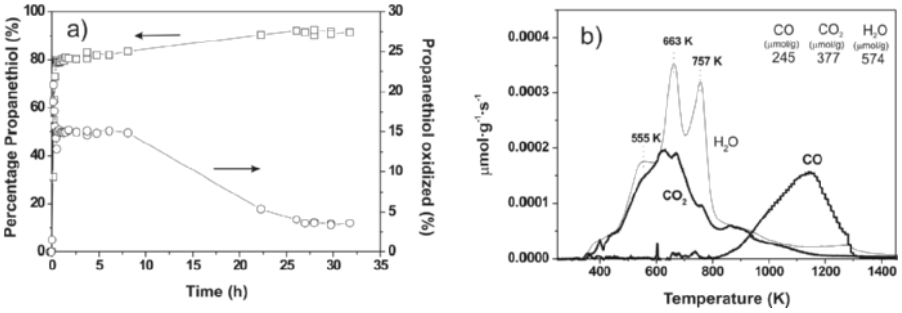

Figure 4. (a) Fixed-bed adsorption/breakthrough experiment on activated carbon 208 at 298 K. The amount of propanethiol removed and oxidized is reported versus time on stream ($[S]_o$: 467 ppm). (b) Temperature-programmed decomposition (TPD) spectra of activated carbon 208 after the breakthrough test (after 35 h time on stream).

In the case of H_2S, the deactivation was attributed to the deposition of elemental sulfur on the surface of wood ash and activated carbon, as deduced from XRD. In the oxidation of methyl mercaptan, the deposition of dimethyl disulfide on the activated carbon surface, which is more strongly adsorbed than MM due to its larger size and higher boiling point, was proposed as responsible for the deactivation observed. However, contrary to the behavior on activated carbon, Kastner et al. observed no decline in the oxidation activity of methyl mercaptan to disulfide when using wood ash.[13] For liquid-phase adsorption experiments, no data can be found in the literature about this deactivation process. However, the deactivation in the oxidation of propanethiol to dipropyl disulfide must be due either to the deposition of DPDS or to the consumption and exhaustion of chemisorbed oxygen (as surface groups) due to the absence of an external oxygen supply. The first hypothesis can be ruled out from the results reported in previous sections. Contrary to the behavior in gas-phase experiments, in liquid-phase studies DPDS is released to the solution already in the first minutes of the analysis. Thus, for liquid-phase experiments, the presence of other species, i.e. the solvent, must be responsible for the desorption of the disulfide from

the carbon surface. Consequently, chemisorbed oxygen consumption must be the reason for the deactivation observed in the oxidation process. In order to confirm this point, activated carbon 208 was submitted to a temperature programmed decomposition experiment (TPD) after being used for 35 h in fixed-bed adsorption experiment. Figure 4b shows the H_2O (m/s 28), CO (m/s 28) and CO_2 (m/s 44) profiles as a function of temperature (fragmentations coming from *n*-hexene, propanethiol and DPDS have been appropriately subtracted from the m/s 28 and m/s 44 signals). The TPD shows the evolution of CO_2 (at low temperature) and CO (at high temperature) typical profiles of an activated carbon.[9] Interestingly, the TPD exhibits three water desorption peaks. Comparing the amount of CO, CO_2 and H_2O evolved in Figure 4b with those of the original 208 activated carbon (CO: 681 μmol/g; CO_2: 422 μmol/g and H_2O: 56 μmol/g), there are important differences. While the amount of CO exhibits a nearly threefold decrease, the amount of CO_2 remains mainly unaffected. Additionally, this decrease in the amount of oxygen evolved as CO is accompanied by a tenfold increase in the amount of water. Considering the reaction mechanisms proposed in the literature, water and DPDS would be the expected reaction products. In the same way, oxygen surface groups would be expected to be consumed in the oxidation reaction from propanethiol to DPDS.

From a quantitative point of view, the TPD data show that only those oxygen surface groups evolved as CO are consumed in the breakthrough column experiment. The consumption of a specific type of oxygen surface groups (436 μmol CO/g) would confirm experimentally the hypothesis proposed above, i.e. only the more stable oxygen groups participate in the oxidation reaction (quinone groups). Additionally, the formation of water (518 μmol H_2O/g of activated carbon) after the breakthrough column experiment would also confirm that (i) water is also a final product in the oxidation reaction and (ii) water is preferentially adsorbed on the carbon surface (maybe the more strongly adsorbed water is responsible for the progressive desorption of the dipropyl disulfide formed). Interestingly, the amount of CO consumed and H_2O formed on carbon 208 during the breakthrough column experiment are very close to the total amount of dipropyl disulfide formed (367 μmol DPDS/g) in the same experiment (after the 35 h time on stream), as detected by gas-chromatography. Thus, from these results a stechiometry for the oxidation reaction of (2:1:1) for propanethiol, dipropyl disulfide and H_2O is proposed for liquid-phase adsorption/oxidation experiments. Additionally, the TPD profile exhibits desorption peaks (not shown) for *n*-hexene, with a single contribution centered at 419 K, and for propanethiol,

with two maxima centered at 671 and 733 K. No peaks corresponding to dipropyl disulfide were observed. These results confirm that, contrary to the behavior in gas-phase adsorption experiments, DPDS is weakly adsorbed on the carbon surface in liquid-phase experiments and thus, it is released to the solution almost from the beginning.

It is noteworthy to mention the high temperature observed for the desorption of water from activated carbon 208 after the column test, as compared to the original sample (single H_2O desorption peak at 398 K). These differences in the desorption temperature for water denote a difference in the nature of adsorption, i.e. while the water in the original 208 activated carbon is weakly adsorbed (physisorbed), on the already used activated carbon the water, coming from the oxidation reaction, must be strongly adsorbed (chemisorbed) as it corresponds to a reaction (formation) mechanism between chemisorbed oxygen and H^+ coming from the initial dissociation of propanethiol.

4. Conclusions

From the results described above, activated carbon can be envisaged as alternative adsorbents for the removal of propanethiol from liquid-phase effluents. Both, the porous structure and the surface chemistry of the activated carbons affect the removal process. Interestingly, the adsorption of propanethiol is accompanied by surface assisted oxidation processes of propanethiol to dipropyl disulfide. In fact, whereas the porous structure is the main parameter in defining the removal kinetics, the surface chemistry has a strong influence in the oxidation reaction and consequently, in the total removal capacity. Selective modifications of the surface chemistry show that the oxidation reaction is mainly promoted by the more stable oxygen surface groups, i.e. those evolved as CO, most probably quinone groups. The limited amount of these oxygen groups on the carbon surface constitutes a limiting factor in defining the extent of the oxidation reaction, as observed on fix-bed adsorption/breakthrough experiments.

Acknowledgements

Authors acknowledge the support from MEC (NAN2004-09267-C03-03 and MAT2004-03480-C02-02), European Network of Excellence “InsidePores” and Generalitat Valenciana (GRUPOS03/212).

References

1. EU Directive 2003/17/CE.
2. EPA 420-R-99-023.
3. R. T. Yang, *Adsorbents: Fundamental and Applications* (Wiley-Insterscience, Hoboken, NJ, 2003).
4. H. Katoh, I. Kuniyoshi, M. Hirai and M. Shoda, Studies of the oxidation mechanism of sulfur-containing gases on wet activated carbon-fiber, *Appl. Catal. B* 6, 255–262 (1995).
5. A. K. Dalai, E. L. Tollefson, A. Yang and E. Sasaoka, Oxidation of methyl mercaptan over an activated carbon in a fixed-bed reactor, *Ind. Eng. Chem. Res.* 36, 4726–4733 (1997).
6. A. Bagreev, S. Bashkova and T. J. Bandosz, Dual role of water in the process of methyl mercaptan adsorption on activated carbons, *Langmuir* 18, 8553–8559 (2002).
7. T. J. Bandosz, *Activated Carbon Surfaces in Environmental Remediation* (Elsevier, Amsterdam, 2006).
8. F. Rodríguez-Reinoso, The role of carbon materials in heterogeneous catalysis, *Carbon* 36, 159–175 (1998).
9. H. Marsh and F. Rodríguez-Reinoso, *Activated Carbon* (Elsevier, London, 2006).
10. R. V. R. A. Rios, J. Silvestre-Albero, A. Sepúlveda-Escribano and F. Rodríguez-Reinoso, *Colloids Surf. A* 300, 180–190 (2007).
11. J. L. Figueiredo, M. F. R. Pereira, M. M. A. Freitas and J. J. M. Órfao, Modification of the surface chemistry of activated carbons, *Carbon* 37, 1379–1389 (1999).
12. F. Rodríguez-Reinoso and M. Molina-Sabio, Textural and chemical characterization of microporous carbons, *Adv. Colloids Interf. Sci.* 77, 271–294 (1998).
13. J. R. Kastner, K. C. Das, Q. Buquoi and N. D. Melear, Low temperature catalytic oxidation of hydrogen sulfide and methanethiol using wood and coal fly ash, *Environ. Sci. Technol.* 37, 2568–2574 (2003).
14. S. Bashkova, A. Bagreev and T. J. Bandosz, Adsorption/oxidation of CH3SH on activated carbons containing nitrogen, *Langmuir* 19, 6115–6121 (2003).
15. A. Bagreev, J. Angel Menendez, I. Dukhno, Y. Tarasenko and T. J. Bandosz, Oxidative adsorption of methyl mercaptan on nitrogen-enriched bituminous coal-based activated carbon, *Carbon* 43, 208–210 (2005).
16. A. Turk, E. Sakalis, J. Lessuck, H. Karamitsos and O. Rago, Ammonia injection enhaces capacity of activated carbon for hydrogen-sulfide and methyl mercaptan, *Environ. Sci. Technol.* 23, 1242–1245 (1989).
17. A. Primavera, A. Trovarelli, P. Andreussi and G. Dolcetti, The effect of water in the low-temperature catalytic oxidation of hydrogen sulfide to sulfur over activated carbon, *Appl. Catal. A: Gen.* 173, 185–192 (1998).

ADSORPTION PROPERTIES OF FUNCTIONAL SILICAS TOWARDS SOME TOXIC METAL IONS IN WATER SOLUTIONS

VALENTIN TERTYKH, LILYA POLISHCHUK, VICTOR YANISHPOLSKII
Institute of Surface Chemistry of National Academy of Sciences of Ukraine, Gen. Naumov Street 17, 03164 Kyiv, Ukraine

ELINA YANOVSKA, ARSENTIJ DADASHEV, VALERII KARMANOV
Chemistry Department of Kyiv National Taras Shevchenko University, Ukraine

OLYA KICHKIRUK
Franko State University, Zhitomir, Ukraine

Abstract. Processes of preconcentration of heavy toxic metal ions, such as Pb(II), Cd(II), Zn(II), Hg(II), and Mo(VI) on the silica with covalently bound complexing phenolic-type analytical reagents 8-hydroxyquinoline, 1-(2-pyridylazo)-2-naphthol, 4-(2-pyridylazo)resorcinol have been studied. Structures of the surface complexes of toxic metals with grafted analytical reagents were determined using IR, ESR and electronic diffuse reflectance spectroscopies. Possibility of simultaneous determination of micro amounts of heavy metals was demonstrated using the x-ray fluorescence analysis of modified adsorbents after absorption of metal ions from their multicomponent mixtures in natural and artificial water solutions. Silica gel with adsorbed polyionene (1,4-MePh) was shown to have high adsorption properties towards some metal-containing anions, in particular MoO_4^{2-}, WO_4^{2-} and $Cr_2O_7^{2-}$ in water solutions. Adsorption isotherms of these metal-containing anions on initial silica gel and silica-supported polyionene were investigated.

Keywords: modified silica; immobilized 8-hydroxyquinoline; 1-(2-pyridylazo)-2-naphthol; 4-(2-pyridylazo)resorcinol; polyionene; preconcentration; heavy metal ions; x-ray fluorescence analysis

J.P. Mota and S. Lyubchik (eds.), Recent Advances in Adsorption Processes for Environmental Protection and Security, 119–132.

1. Introduction

Low concentrations of toxic metals in natural and waste waters can be efficiently determined after their extraction and concentrating using modified silica adsorbents functionalized with complexing ligands. As such complexing ligands it is possible to apply 8-hydroxyquinoline and some heterocyclic azo compounds 1-(2-pyridylazo)-2-naphthol (PAN), 4-(2-pyridylazo)resorcinol (PAR) forming stable complexes with heavy metal ions in solutions.[1, 2]

Silica carriers with supported oxine or physically adsorbed azo reagents are usually used for metal ions preconcentration.[3–5] These adsorbents are characterized by a different level of washing out of the adsorbed complexing reagents under different conditions of application. On the contrary, adsorbents with covalently bound ligands, having hydrolytically stable chemical bonds with the carrier surface sites, are more stable to washing out and they have more reproducible properties. Method of the multi-step surface assembly reaction involving grafting of benzene rings, their nitration with following reduction, diazotization and azo coupling had been usually applied for synthesis of adsorbents with covalently bound oxine, PAR and PAN.[6,7] Such synthetic pathway results in non-uniform chemical composition of the modifying surface layer and low content of the grafted complexing groups. Recently the single-stage aminomethylation reaction with simultaneous use of amino-containing alkoxysilane and paraformaldehyde was successfully realized for covalent anchorage of the phenolic-type analytical reagents on the silica surface.[8]

Chemical attachment of phenolic-type analytical reagents (8-hydroxyquinoline, PAN, PAR) was carried out in accordance with the following scheme:

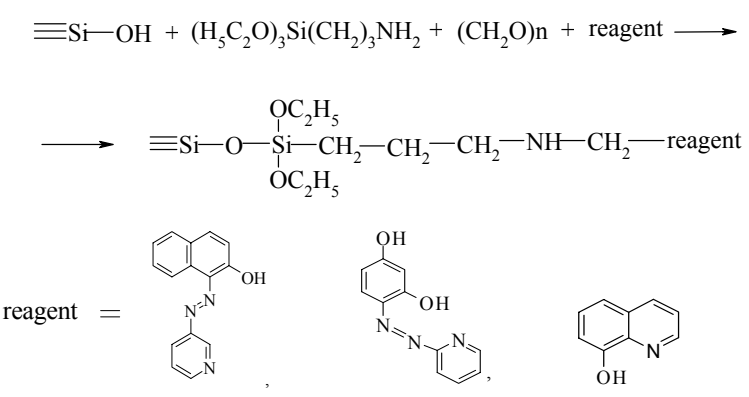

Introducing polymers with the quaternary nitrogen atom into the surface layer of silica carrierss permits one to obtain inorganic adsorbents with pronounced anion-exchange properties. In this respect the application of water-soluble polyionens with the quaternary nitrogen atoms in the main chain is of obvious interest.

2. Results and Discussion

Adsorption characteristics of silicas with covalently bound phenolic-type analytical reagents (8-hydroxyquinoline, PAN, PAR). Silicas with covalently anchored (via the one-step Mannich reaction) phenolic-type analytical reagents were applied for separation of toxic metals ions (Table 1). In accordance with the obtained data, in the pH range 6–8 silica with grafted 8-hydroxyquinoline extracts toxic metal ions, such as Pb(II), Zn(II), Mo(VI) (full removal), Cu(II), Fe(III) (90–98% removal) and Cd(II) and Al(III) (partial removal, from 60 to 80%). In the neutral and low-alkaline media silica with covalently bound PAR quantitatively removes ions of such high-toxic metals as Pb(II), Cd(II), Hg(II), Ni(II) and partially adsorbs Zn(II), Co(II), Cu(II), and Fe(III). In the acidic media (at pH = 1–4) this adsorbent did not extract quantitatively any metals studied. At pH = 6–9 silica with grafted PAN removes 92–95% of Zn(II), Pb(II), Cu(II) ions and adsorbs partly Cd(II), Ni(II), Fe(III) ions. Obtained results correlate well with the stability constants of complexes of the studied metals with 8-hydroxyquinoline, PAR and PAN in solutions.[1,9]

TABLE 1. Adsorption properties of silica gels with covalently bound analytical reagents towards toxic metal ions.

Adsorbent	pH of solutions	Toxic metals adsorbed with a separation degree of 95 ± 5%
Silica with bound oxine	4–9	Zn^{2+}, Pb^{2+}, Al^{3+}, Mo^{6+}, Cu^{2+}
Silica with bound PAR	6–9	Zn^{2+}, Pb^{2+}, Cd^{2+}, Hg^{2+}, Ni^{2+}, Cu^{2+}
Silica with bound PAN	7–9	Zn^{2+}, Pb^{2+}, Cd^{2+}, Ni^{2+}, Cu^{2+}

Sorption capacities of the synthesized modified silicas for toxic metals studied are sufficiently high (about 4 mmol/g), and such adsorbents can be applied for extraction of micro amounts of these metals from water solutions within a concentration interval of 0.1–100 ng/mL. This circumstance can be applied for development of the adsorption water-purification process.[10]

All synthesized adsorbents are characterized by a high rate of extraction of heavy metals: the maximum degree of adsorption can be achieved for 2–5 min of contact (Figure 1 and Table 2). Therefore, the obtained materials

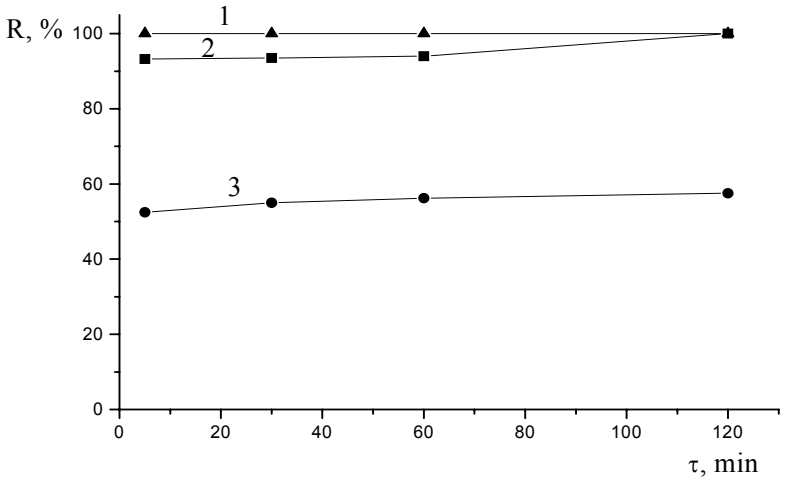

Figure 1. Dependence of degree of extraction (*R*) of Pb^{2+} (1), Zn^{2+} (2) and Cd^{2+} (3) ions by silica with covalently bound 8-hydroxyquinoline on adsorption time at pH = 6.8–7.

TABLE 2. Kinetics of adsorption of toxic metals ions by silica gel with covalently bound PAR.

Metal ion	pH of solutions	Sorption time (min)			
		5	10	20	60
		Adsorption degree (%)			
Zn^{2+}	6.8	88.8	89.3	89.3	89.3
Cd^{2+}	7.0	99.9	99.9	99.9	99.9
Pb^{2+}	6.8–7.0	99.9	99.9	99.9	99.9
Cu^{2+}	6.8	83.7	75.0	83.0	80.0
Fe^{3+}	6.8	94.2	95.1	95.4	95.8
Co^{2+}	6.8	98.8	99.9	99.9	99.9
Ni^{2+}	6.8	51.3	73.4	79.8	99.9

can be employed to remove heavy metal ions from water solutions in the dynamic adsorption mode.

Data about structure of the surface complexes of toxic metals with grafted phenolic-type analytical reagents (8-hydroxyquinoline, PAN, PAR). Structures of the complexes of toxic metal with phenolic-type analytical reagents anchored on the silica surface were studied by IR, ESR and electronic diffuse reflectance spectroscopies.

ESR spectra of the complexes of copper with 8-hydroxyquinoline, PAN and PAR, covalently bound with silica surface are characterized by

anisotropy and hyperfine structure of the g_{II} signal (Tables 3 and 4). These data testify about divalent state of copper on the surface of the chemically modified silicas.

TABLE 3. Characteristics of ESR spectra of Cu(II) complexes with PAN chemically bound with silica surface.

Sample	$[Cu^{2+}]_{ads}$ (mmol/g)	g_{II}	$g_{\perp}$	$A_{II}\cdot10^{-4}$ (cm^{-1})	Structure of the coordination unit
1	0.01	2.254	2.030	147	Cu $[2N_2O]$
2	0.05	2.276	2.025	149	Cu $[2N_2O]$ with deformation
3	0.20	–	2.047	–	planar structure

TABLE 4. Parameters of ESR spectra of Cu(II) complexes with PAR chemically bound with silica surface.

Sample	$[Cu^{2+}]_{ads}$ (mmol/g)	g_{II}	$g_{\perp}$	$A_{II}\cdot10^{-4}$ (cm^{-1})	Structure of the coordination unit
1	0.013	2.38	2.039	179	Cu $[2N_2O]$
2	0.062	2.31	2.028	173	Cu $[4O_2O]$ similar to $CuSO_4\cdot5H_2O$

In electronic diffuse reflectance spectra the absorption bands of grafted PAN molecules and bands *d–d* transitions for complexes with Zn(II) – at 580 nm, with Pb(II) – at 620 nm, with Cu(II) and Cd(II) – at 550 nm were observed. These bands correlate well with values of absorption bands for *d-d* transitions these metals in complexes with PAN in solutions.[1,9] It shows that coordination of these metal ions with PAN molecules bound with silica surface is similar to their interactions in solutions.

According to calculations based on ESR spectra of complexes of copper(II) ions with bound 8-hydroxyquinoline, the value of the $g_{\|}$-factor is 2.372, $g_{\perp} = 2.064$, constant of hyperfine coupling $A = 201 \times 10^{-4}$ cm^{-1}. This allows one to assume the nearest coordination surrounding of Cu^{2+} ions in the surface complex. Most probable, 4[O] and 2[N] distorted octahedron structures are formed with O-atoms of hydroxyl groups in the equatorial position and N-atoms in the axial position, or with N-atom and two O-atoms in the equatorial position and two O-atoms in the axial position.[11,12]

Form and calculated parameters of ESR spectra of the complexes of copper(II) ions with covalently bound PAN (Table 3) allow to conclude that:

– At copper(II) concentrations on the adsorbent surface ($[Cu^{2+}]_{ads}$) less than concentration of grafted PAN molecules (sample 1), environment of copper(II) in complex corresponds to four-coordinated Cu(II) with $[2N_2O]$ coordination[12,13]

– At an increase of $[Cu^{2+}]_{ads}$ value (sample 2) signals from some types of complexes with similar parameters were observed, it can be connected with distortion of the planar structure of complexes[14]
– At $[Cu^{2+}]_{ads}$ more than concentration of grafted PAN molecules (sample 3), signal of hyperfine splitting is indistinct, but asymmetry and anisotropy of the spectrum are retained

The *g*-factor and A_{II} values calculated from ESR spectra of complexes of copper(II) ions with bound PAR for sample 1 (Table 4), where concentration of adsorbed copper is less in some times than concentration of grafted PAR molecules, are characteristic for the octahedron oxygen-containing complexes such as $Cu[4O_2O]$-adducts of bischelates of copper with strong axial coordination into 5 and 6 place or octahedron complexes such as realized in $CuSO_4 \cdot 5H_2O$.[13,14] Such complexes may be formed at coordination copper(II) with atoms of oxygen of two hydroxyl groups of two PAR molecules and two water molecules or two hydroxyl groups of one PAR molecule and four water molecules. As a result of this unusual coordination (different from pathway of coordination in solutions) of Cu(II) with PAR molecules, covalently bound with silica surface, incomplete adsorption of Cu(II) ions (82–85% at pH = 6–9) can take place, though in water solutions the stability constant of the complex of Cu(II) with PAR has the highest value among metals studied.[1,2]

ESR spectrum of sample 2 (a quantity of adsorbed copper is compare with concentration of grafted PAR molecules) showed that g_{II} and A_{II} values are decreasing (Table 4). Calculated parameters of spectrum of sample 2 (concentration of coordinated metal was 0.062 mmol/g) are close to complexes of four-coordinated copper(II) with coordination unit $[2N_2O]$[11,12] as it takes place at coordination PAR molecules with Cu(II) ions in the solutions.

Electronic diffuse reflectance spectra of metal complexes with chemically bound PAR are characterized by following absorption bands in the visible region of spectrum: for Cu(II) – at λ_{max} = 525 nm; for Cd(II) – at λ_{max} = 510 nm; for Fe(III) – at λ_{max} = 700 nm; for Pb(II) – at λ_{max} = 520 and 700 nm; for Zn(II) – at λ_{max} = 500 nm. These dates testify that pathway of coordination of PAR molecules chemically bound with silica surface for Cd(II) and Pb(II) is the same as in solutions. Absorption band at 500 nm for Zn(II) correlates well with data of paper,[15] where Zn(II) complexes with PAR-containing adsorbent obtained by sol-gel method are also characterized by absorption at 500 nm.

Peculiarities of adsorption-x-ray fluorescence determination of toxic metals after their preconcentration on the silica with covalently bound

8-hydroxyquinoline and PAR. For ascertainment of a possibility of simultaneous x-ray fluorescence determination of heavy toxic metals, which quantitatively adsorbed onto synthesized chemically modified silica (Table 1), model water solutions (25–1,000 ml) contained mixtures of metal ions of different concentrations were prepared. These solutions were transmitted through a cone-shaped plastic column filled with 0.2 g adsorbent. The samples of modified silica with adsorbed metals were dried in air, then were ground in an agate mortar and studied by x-ray fluorescence spectroscopy. The content of every metal in the adsorbent phase has been calculated by a comparison of the absolute characteristic x-ray intensities of metals adsorbed on silica from the model solution with the calibration curves for the individual metals.

According to the obtained data, micro amounts of lead and cadmium ions can be quantitatively detected by x-ray fluorescence method after preconcentration these metals upon silica with covalently bound 8-hydroxyquinoline. At the same time zinc and molybdenum can be detected in these conditions only at 50–60%, it is caused their non-complete extraction in the lead(II) presence. Therefore adsorption-x-ray fluorescence analysis with application of the silica with covalently bound 8-hydroxyquinoline can be used only for the qualitative detection of these elements.

Micro amounts of lead, cadmium and mercury adsorbed upon silica with covalently bound PAR from neutral water solutions (pH = 6.8–7) can be quantitatively detected by x-ray fluorescence method using intensity of the characteristic L_α-line of lead, K_α-line of cadmium and L_α-line of mercury. Influence of the other metals presence on an intensity of characteristic x-ray lines of the detecting element was studied at simultaneous adsorption-x-ray fluorescence analysis of samples after preconcentration of metal ions by the silicas with covalently bound 8-hydroxyquinoline and PAR. A decrease of intensity of the L_α Pb-line was shown to take place at the presence of micro amounts of cadmium and zinc in the adsorbent phase (Figure 2). An increase of intensities of the K_α-line of cadmium and L_α-line of zinc was detected in the presence of lead, mercury and other more heavy metals on the silica surface (Figure 3). Effect of intensity decrease for L_α Pb-line in the presence of micro amounts of cadmium and zinc in the adsorbent phase can be explained by higher absorption coefficients (μ) of L_α-line of lead in the presence of zinc and cadmium in comparison with adsorbent containing only lead (μ of Pb L_α-line is 111 cm^2/g). Introducing zinc and cadmium into samples results in decrease of the lead signal.[16,17]

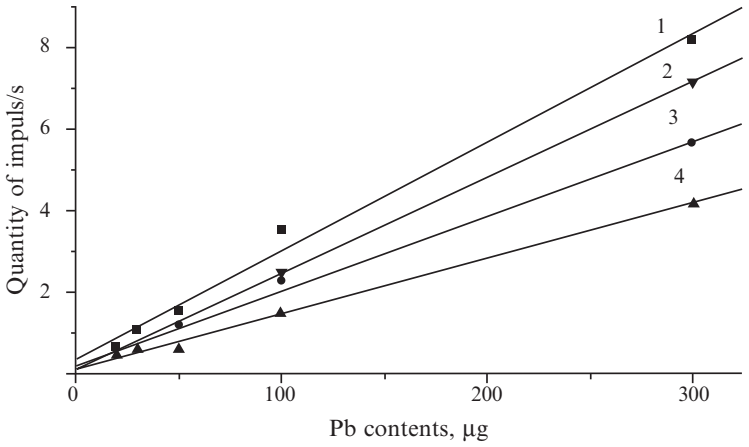

Figure 2. Dependence of intensity of characteristic x-ray fluorescence Pb *Lα*-line on surface lead contents without (1) and in the presence of cadmium (3), zinc (4), cadmium and zinc simultaneously (2) in the adsorbent phase.

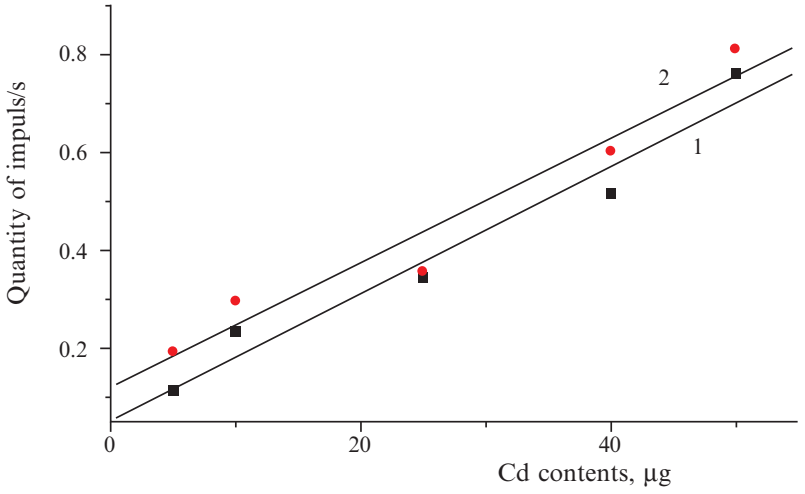

Figure 3. Comparison of calibration curves for adsorption-x-ray fluorescence determination Cd after solid-phase extraction by silica chemically modified with PAR: 1 – only Cd, 2 – Cd with the same amount Pb and Hg.

Elaborated adsorption-x-ray fluorescence method was applied for determination of micro amounts of Pb(II), Cd(II) and Hg(II) in the Kyiv's rivers Dnipro and Lybid during the winter period after metals preconcentration upon the silica with chemically bound PAR. The column adsorption method was used for the preconcentration studies. With this aim 1 L of water from the river was flowed through a column with the adsorbent and intensities of the characteristic Pb, Cd and Hg lines were measured in the adsorbent. Results of these measurements were confronted with the calibration curves of the appropriate metals mixtures. As it follows from the data of Table 5, results of adsorption-x-ray fluorescence determination of micro amounts of Pb(II), Cd(II) and Hg(II) after their preconcentration upon silica with chemically bound PAR correlate well with values of concentration of these metals, obtained by flame atomic absorption analysis after an evaporation of the solution volume up to 20 times smaller.

TABLE 5. Pb(II), Cd(II) and Hg(II) contents in water from river Lybid (samples I and II) and river Dnipro detected by atomic absorption analysis and x-ray fluorescence method (after extraction by silica modified with PAR).

River Dnipro		River Lybid sample I		River Lybid sample II	
Atomic absorption analysis	Adsorption-x-ray fluorescence analysis	Atomic absorption analysis	Adsorption-x-ray fluorescence analysis	Atomic absorption analysis	Adsorption-x-ray fluorescence analysis
		Pb(II) concentration (μg/L)			
100	125 ± 5	<5	20 ± 2	5	30 ± 2
		Cd(II) concentration, μg/L			
<10	8 ± 2	<10	<2	2	<2
		Hg(II) concentration (μg/L)			
–	5 ± 2	–	4 ± 2	–	<2

It is necessary to take into consideration that the adsorption-x-ray fluorescence method is faster, more accurate and simpler than usual atomic absorption analysis. Moreover, apparently quantities of lead in the river Lybid (samples I and II) obtained by flame atomic absorption method were incorrect. Really, the amounts of lead, determined by adsorption-x-ray fluorescence method, manifest a gradual increase of the metal concentration from the sample I to the sample II. It seems more probable, because water probe of the sample I was taken up-stream and probe of the sample II was drawn down-stream from urban area.

Hereby, the developed adsorption-x-ray fluorescence method of determination of micro amounts of Pb(II), Cd(II) and Hg(II) after their preconcentration upon silica with chemically bound PAR can be effectively applied for analysis of natural and artificial multicomponent water solutions.

Adsorption characteristics of silicas with immobilized polyionene towards metal-containing anions. Adsorption of 1,4-MePh polyionene, synthesized in the laboratory of Prof. M. Burmistr[18] and having the following structure ($n \leq 6$):

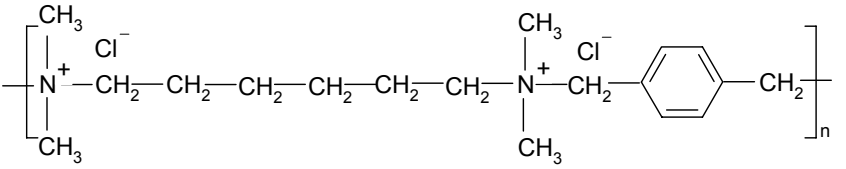

was carried out on silica gel with specific surface area about 256 m^2/g (Merck, fraction with a diameter of particles of 0.06–0.16 mm). In water solutions because of partial dissociation of silanol groups the silica surface has negative charge. Adsorption of polyionene on silica surface would thus be expected to result in formation of adsorption complexes due to electrostatic interactions:

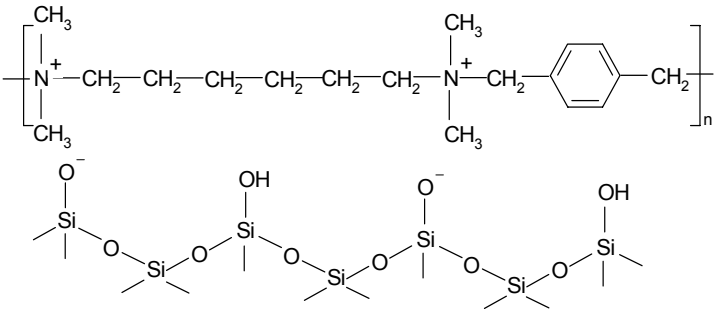

The concentrations of polymer were determined by spectrophotometric analysis using bromphenol blue (λ = 600 nm). Silica with adsorbed polymer was applied for preconcentration of molybdenum-, chromium- and tungsten-containing anions from water solutions. Photometric determination of MoO_4^{2-}, WO_4^{2-}, $Cr_2O_7^{2-}$ ions concentrations based on their ability to form color complexes. Mo-containing anions form a red complex in the presence of SCN-anions (λ = 470 nm).[19] In water solutions W(VI) can be identified in the form of blue heteropolyacid (λ = 610 nm)[20] formed after reaction with molybdate ions. Cr-containing anions were detected as a violet complex with 1,5-diphenylcarbazide (λ = 540 nm).[19]

Adsorption properties of the silica-supported polyionene in respect to metal-containing anions, in particular dependence of separation degree (%) on the medium pH are represented in Table 6.

TABLE 6. Dependence of separation degree (%) of metal-containing anions by silica-supported polyionene on pH medium at the static adsorption mode.

Anions	Separation degree (%)						
	pH = 1.0	pH = 1.7	pH = 4.0	pH = 6.8	pH = 7.0	pH = 8.0	pH = 9.2
Mo(VI)	88.0	95.2	92.7	88.0	88.0	67.8	67.0
W(VI)	67.0	74.0	94.0	0	0	0	55.6
Cr(VI)	8.9	64.9	35.3	11.2	10.2	25.0	0

As it follows from these data, amounts of W(VI) and Cr(VI) adsorbed upon silica gel with immobilized polyionene were rather larger (up to 94% and 65% accordingly) in the acidic media at pH = 1.7–4, when polytungstate- and polychromate-ions are usually formed.[21] The molybdate-ions are preferably extracted in the acidic medium (up to 95%), where they present as anions of the isopolyacid. At the same time, a separation degree is 67% for adsorption from the basic medium, where Mo(VI) prevails as MoO_4^{2-} ions.[21]

Data on kinetics of adsorption of metal-containing anions on silica gel with immobilized polyionene at the optimum for each metal value of the medium pH are presented in Figure 4. It was established that all studied anions could be mostly extracted from solutions for several minutes. Thus, silica gels with anchored in the surface layer polyionene conserve kinetic properties of silica matrices and are characterized by a high rate of an establishment of the adsorption equilibrium. Such type adsorbents can be used for extraction of metal-containing anions from water solutions in the dynamic adsorption mode.

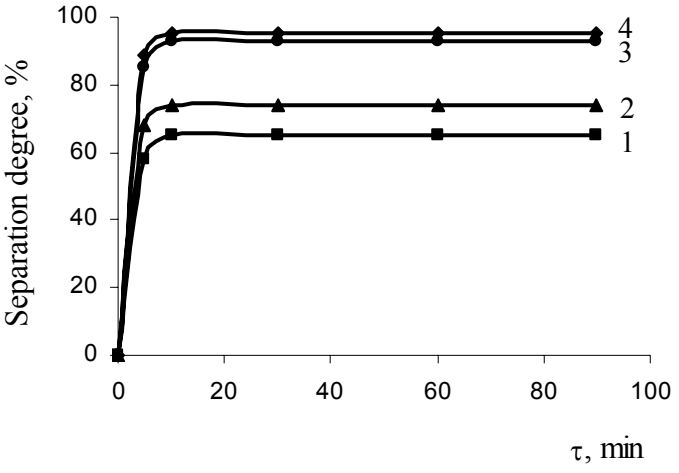

Figure 4. Kinetics of adsorption of metal-containing anions on silica-supported polyionene: 1 – Cr(VI), pH 2; 2 – W(VI), pH 4; 3 – Mo(VI), pH 2.

Comparison of isotherms of adsorption for anions of molybdenum (Figure 5), tungsten (Figure 6) and chromium (Figure 7) upon nonmodified silica gels (curves 1) and silica gels with immobilized polyionene (curves 2) testifies that modified adsorbents exhibit expressed specificity towards the studied anions.

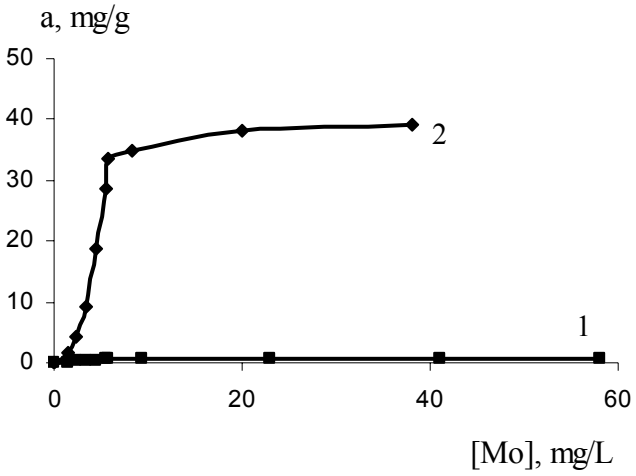

Figure 5. Adsorption isotherms of MoO_4^{2-} ions on initial silica gel (1) and silica-supported polyionene (2).

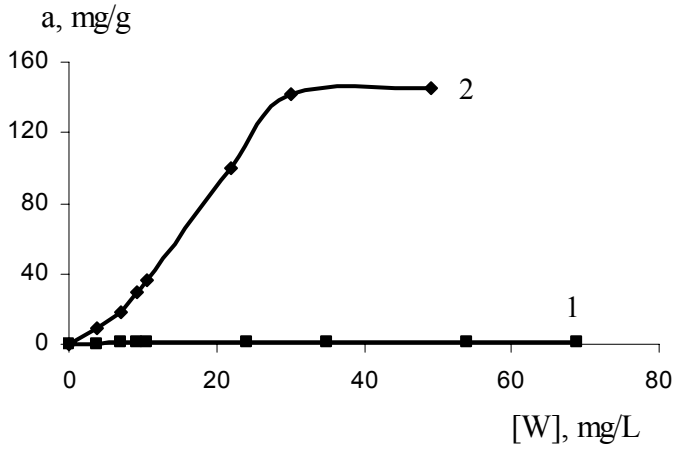

Figure 6. Adsorption isotherms of WO_4^{2-} ions on initial silica gel (1) and silica-supported polyionene (2).

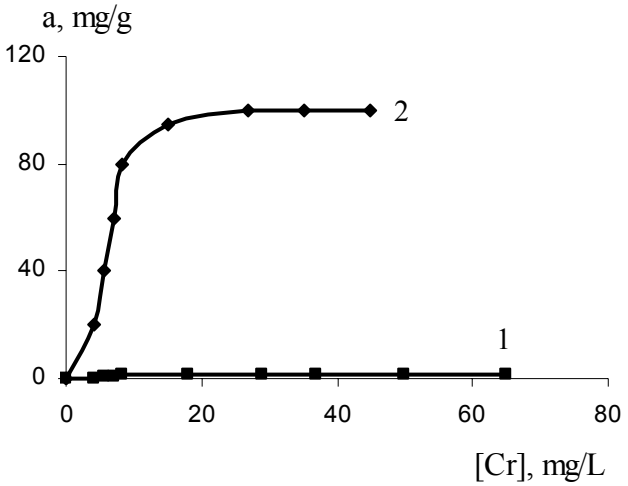

Figure 7. Adsorption isotherms of $Cr_2O_7^{2-}$ ions on initial silica gel (1) and silica-supported polyionene (2).

From obtained isotherms it is possible to estimate limiting adsorption values for the anions studied. In particular, modified adsorbent adsorbs (estimation on pure metal): molybdenum up to 38 mg/g, chromium up to 110 mg/g and tungsten up to 158 mg/g. All studied anions was shown are adsorbed upon the silica gel with immobilized polyionene in 60–100 times better in comparison with their adsorption on the initial nonmodified silica gel.

3. Conclusion

Micro amounts of Pb(II), Zn(II), Cd(II) and Hg(II) ions in aqueous solutions can be quantitatively measured using the x-ray fluorescence spectroscopy after preconcentration by silica with grafted 8-hydroxyquinoline and 4-(2-pyridylazo)resorcinol. Mutual influence of other toxic metal on characteristic line intensities of determined ion should be taken into consideration when analyzing multicomponent systems.

Silica gels with supported polyionene was shown to have satisfactory adsorption properties in respect to such metal-containing anions as Mo(VI), W(VI) and Cr(VI). The adsorbent practically quantitatively extracts Mo(VI) and Cr(VI) ions at pH from 2 to 4 and W(VI) at pH > 4 in the static adsorption mode. Obtained non-swelling adsorbent possesses good kinetic characteristics (all studied anions were extracted for 10 min) and has high adsorption capacity towards metal-containing anions.

References

1. A. Pilipenko, L. Pilipenko, A. Zubenko, *Organic Reagents in Inorganic Analysis* (Naukova Dumka, Kiev, 1994) [in Russian].
2. P. Janoš, Reversed-phase liquid chromatography of metal chelates of 4-(2-pyridylazo)-resorcinol: retention model and its verification, *Anal. Chim. Acta* 414, 113–122 (2000).
3. I. Narina, M. Soylak, The uses of 1-(2-pyridylazo)-2-naphtol (PAN) impregnated Ambersorb 563 resin on the solid phase extraction of traces heavy metal ions and their determinations by atomic absorption spectrometry, *Talanta* 60(1), 215–221 (2003).
4. O. Shvoeva, V. Dedkova, S. Savvin, Sensitivity and selectivity of the reaction of vanadium(V) with 4-(2-pyridylazo)resorcinol on a solid support containing anion-exchange groups and modified with 8-hydroxyquinoline or 8-hydroxyquinoline-5-sulfonic acid, *J. Anal. Chem.* 55, 21–24 (2000).
5. O. Shvoeva, V. Dedkova, S. Savvin, Determination of lead with 4-(2-pyridylazo)-resorcinol after the sorption of lead as its thiosulfate complex on a fibrous sorbent filled with AV-17, *J. Anal. Chem.* 56, 1080–1083 (2001).
6. O. Zaporozhets, O. Gaver, V. Sukhan, Immobilized analytical reagents, *Uspekhi Khimii* 66, 702–712 (1997).
7. V. Zaitsev, *Complexing Silica: Synthesis, Structure of Bound Layer and Chemistry of Surface* (Pholio, Kharkiv, 1997) [in Russian].
8. V. Tertykh, V. Yanishpolskii, O. Panova, Covalent attachment of some phenol derivatives to the silica surface by use of single-stage aminomethylation, *J. Therm. Anal. Cal.* 62, 545–549 (2000).
9. K. Burger, *Organic Reagents in Inorganic Analysis* (Mir, Moscow, 1975) [in Russian].
10. O. Glushchenko, E. Yanovska, O. Kichkiruk, V. Tertykh, Adsorption properties of silica gel with covalently bound 8-hydroxyquinoline towards toxic metal ions, *Funct. Mater.* 13(2), 265–269 (2006).
11. I. Marov, N. Kostromina, *ESR and NMR in Chemistry of Coordination Compounds.* (Nauka, Moscow, 1979) [in Russian].
12. T. Lipatova, Yu. Nizelskii, *Progress in Chemistry of Polyurethanes* (Naukova Dumka, Kiev, 1972) [in Russian].
13. A. Shklyaev, Yu. Nizelskii, *Catalytic Properties of Metal β-diketonates* (Naukova Dumka, Kiev, 1983) [in Russian].
14. S. Altshuler, B. Kozyrev, *Electronic Paramagnetic Resonance* (Nauka, Moscow, 1972) [in Russian].
15. P. Jeronimo, A. Araujo, M. Conceicao, B. Montenegro, Development of a sol–gel optical sensor for analysis of zinc in pharmaceuticals. *Sens. Actuat. B: Chem.* 103, 169–177 (2004).
16. M. Blohin, I. Shveitser, *X-ray Spectral Reference-Book* (Znanie, Moscow, 1982) [in Russian].
17. V. Zagorodnii, V. Karmanov, Influence of filling particle size on X-ray fluorescence analysis of multicomponent materials, *Zavodskaya laboratoriya* 12, 22–25 (1985).
18. V. Kravtsov, M. Burmistr, T. Tyurina, Study of polymeric quaternary ammonium salts preparation in water-acetone mixtures, *Ukr. Khim. Zh.* 46(4), 397–399 (1980).
19. Z. Marchenko, *Photometric Determination of Elements* (Mir, Moscow, 1971) [in Russian].
20. A. Busev, V. Ivanov, T. Sokolova, *Analytical Chemistry of Tungsten* (Nauka, Moscow, 1976) [in Russian].
21. M. Karapetyanc, S. Drakin, *General and Inorganic Chemistry* (Khimiya, Moscow, 1981) [in Russian].

WASTE CONVERSION INTO ACTIVATED CARBON FOR HEAVY METAL REMOVAL FROM WASTE WATER

S. LYUBCHIK,[1*] M. KHODORKOVSKIJ,[2]
T. MAKAROVA,[3] LILIYA TIKHONOVA,[4]
JOSÉ P.B. MOTA,[5] ISABEL FONSECA[5*]

[1]*Institute of Physical Organic and Coal Chemistry, National Academy of Science of Ukraine, R. Luxemburg Street 70, 83114 Donetsk, Ukraine*

[2]*Russian Scientific Centre of Applied Chemistry, Dobrolubova pt. 14, 197198 St. Petersburg, Russia*

[3]*Ioffe Physico-Technical Institute, 26 Politechnicheskaya, 194021 St. Petersburg, Russia*

[4]*Institute for Sorption & Endoecology, National Academy of Science of Ukraine, Gen. Naumova Street 13, 03680 Kiev, Ukraine*

[5]*REQUIMTE/CQFB, Departamento de Química, Faculdade de Ciências e Tecnologia, Universidade Nova de Lisboa, 2829-516 Caparica, Portugal*

Abstract. Activated carbons were prepared from co-mingled natural organic waste, comprising 25% sunflower husks, 50% petroleum waste and 25% low-grade bituminous coal. The porous carbon materials were obtained either by direct activation with steam at 1,123 K, or through pre-oxidation stages with binary eutectic Na/K carbonates, followed by carbonization at 623 K in an inert atmosphere, and then steam activation at 1,123 K. The activated carbons prepared from the co-mingled natural organic wastes were used as adsorbents to remove copper (II), cobalt (III), nickel (II), iron (II), and manganese (II) from real multi-component solutions. Batch experiments were carried out to study the kinetics of multi-component, competitive adsorption. The mechanisms of heavy-metal adsorption on activated carbon are discussed.

[*]To whom correspondence should be addressed. E-mail: sve_lubchik@yahoo.com; iss@dq.fct.unl.pt

J.P. Mota and S. Lyubchik (eds.), Recent Advances in Adsorption Processes for Environmental Protection and Security, 133–146.

Keywords: waste recovery; activated carbon; polluted water; heavy metals; adsorption

1. Introduction

Presently, due to the accumulation of waste materials, environmental problems are getting acute worldwide. The conditions for waste materials storage and disposal frequently do not meet current health requirements and cause pollution of the surface and ground water, soils, and air. There is clearly an awareness of how serious the situation is becoming, with respect to the protection of our natural resources, and the necessity for dealing with environmental problems.

In the last decade, several commercial waste recovery projects have been implemented for waste conversion into secondary gaseous, liquid, or solid products. The interest for developing and using those processes is increasing due to economic and environmental reasons. Within this context, the conversion of natural organic wastes into environmentally-friendly porous materials is a technological alternative to their disposal.

Low-cost adsorbents for air/water purification have recently been reviewed by Pollard et al. [1]. Activated carbons from coconut husk, grain husk, domestic wastes, and tires have been used for phenols removal [2]. Several low-cost activated materials from rice husk [3], coconut [4, 5], bituminous coal [6], sphagnum moss peat [7], sawdust [8], and industrial solid wastes [9] have been reported as adsorbents for heavy metals removal. Activated carbons from soybean hull, sugarcane bagasse, peanut shell, and rice straw were found to be suitable for air purification from toxic gases [10].

Recently, a novel approach to the wastes recovery via their co-processing has been proposed. The existence of synergistic effects between the blend components during their conversion into solid products is still an open issue. Some authors have observed the absence of synergistic effects [11–16], whereas evidence of their presence has been reported for co-gasification [17–19] and co-pyrolysis [20].

We have observed a synergistic effect during the co-activation of co-mingled wastes [21]. The adsorption capacity of the activated carbons produced was found to be higher than those of commercial Norit and Merck activated carbons for Cr (III) removal [21]. Therefore, there is a strong interest in developing innovative processes, for producing secondary environmental friendly adsorbent materials from co-mingled wastes, and to optimize their properties in order to selectively remove heavy metals from waste water.

The main purpose of this study is to produce an activated carbon from co-mingled waste, and to use it as an adsorbent to remove 3-d transition

metals, such as Cu (II), Co (II), Ni (II), Fe (II), and Mn (II), from real waste-water solutions.

2. Experimental

2.1. PREPARATION AND CHARACTERIZATION OF ACTIVATED CARBON FROM CO-MINGLED WASTES

The activated carbons were prepared from the mixture of co-mingled natural organic liquid and solid wastes. For the blending process, the components were combined in the proportion of 25% biomass, 25% low-grade coal, and 50% petroleum wastes (either aliphatic petroleum stock or aromatic tar stock).

All of the blend components were obtained from local sources in the Ukrainian Donbass region. Bituminous coal h_8^b was obtained from Lidievka mine, located in Donetsk (Eastern Ukraine).

The selected biomass was sunflower husks. Sunflower husks were graciously provided by the Oil Process Plan "Cargil" of Joint Ukrainian–USA Oil Corporation in Donetsk.

Petroleum feedstock components were courtesy of Coke Process Plan "Avdeevka", located in Donetsk, and of Odessa Harbor's Unloading Petroleum Station. The aliphatic/aromatic nature of the petroleum components was evaluated by ^{1}H-NMR aromaticy monitoring.

The feedstock from Coke Process Plan "Avdeevka" had 40.2% of aromatic fraction; in the present study it is referred to as "aromatic tar stock". The petroleum feedstock from Odessa Port's Unloading Petroleum Station is referred to as "aliphatic petroleum stock", due to the high content (up to 89.2%) of branched hydrocarbons.

In order to gain some insight into the reactions which may occur between the components of the co-mingled waste during the activation process, the pyrolytic behaviour of the single components and of their blends was investigated by thermogravimetric analysis (TG/DTG) using a Perkin-Elmer TGA 7 thermal analyser. The heating rates varied between 5°C/min and 20°C/min, and the samples were heated up to 1,273 K under inert atmosphere. The thermogravimetric parameters, such as the temperature of initial weight loss (T_{init}), the temperature of final weight loss (T_{final}), the temperature of maximum rate of weight loss (T_{max}), the rate of weight loss (mg/min) and the carbon yield at 1,223 K (%), were determined from the TG and DTG data.

For the activated carbon synthesis, either direct high-temperature activation with steam at 1,123 K or activation via a step of low-temperature carbonization at 623 K under inert atmosphere, were adopted. The soaking time of both processes was varied between 1 and 3 h. In order to avoid coke

formation during the activation process, 5% (from weight of the blends) of additives of binary eutectic of Na/K carbonates was used.

The structural parameters of the produced carbons were evaluated by nitrogen adsorption at 77 K and temperature-programmed desorption. The experiments were carried out using Micromeritics ASAP 2010 and Micromeritics TPD/TPR 2900 equipments. The degree of heterogeneity of the samples was visually assessed by Scanning Electron Microscopy (SEM); the topography of the surface was also studied by high-resolution Auger Depth Profiling with PHI SAM–660 equipment.

2.2. ANALYSIS OF THE HEAVY METALS ADSORPTION FROM TECHNOLOGICAL SOLUTIONS

Real multi-component aqueous solutions, proceeding from "Pridneprovskij Plan of Color Metals" State Enterprise (Power Ministry of Ukraine), were used as a source for copper (II), cobalt (III), nickel (II), iron (II), and manganese (II) chlorides.

The adsorption process was analyzed in batch mode using as adsorbent the parent activated carbon from the co-mingled wastes and also its oxidized form, which was obtained by treating the parent carbon with 1M HNO_3 (reflux) during 6 h at 90°C.

Sorption-kinetics experiments were carried out to evaluate the specific rate constants of the simultaneous adsorption of the 3-d transition metals on the activated carbons with different surface oxygen functionalities.

Kinetics studies were carried out at fixed initial pH of 3.6 of the wastewater source, without adding any buffer to control the pH to avoid an additional electrolyte in the system.

The carbon loading was fixed at 5 g/L and the metal concentrations in the real solution were 11.4 mg/L of copper (II), 9.4 mg/L of cobalt (III), 9.8 mg/L of nickel (II), 11.07 mg/l of iron (II) and 9.5 mg/L of manganese (II). The process was carried out at constant temperature (297 ± 1 K).

To enhance the adsorption rate, the carbon/metal solutions were stirred on a shaker at 160–180 rpm. The adsorption time was varied between 1 and 72 h.

At the end of the experiments, the adsorbent was removed by filtration through membrane filters with a pore size of 0.45 μm. The metal equilibrium concentration in the aqueous solution was measured by atomic adsorption spectroscopy with AA-6300 Flame Emission equipment, according to standard procedures [22].

The equilibrium amount of adsorbed metal on the activated carbon was quantified by mass balance. The following parameters were used: adsorption capacity expressed as amount of metal adsorbed per unit mass of adsorbent, i.e. Me uptake (mg/g); and sorption efficiency of the system, determined as

the percentage of metal ions removed relative to their initial amount, i.e. Me_{rem} (%). The specific rate constants for the heavy metal adsorption were found from the Lagergren equation [23]:

$$\log(q_{eql} - q_t) = \log q_{eql} - \frac{k_{ads} t}{2.303} , \quad (1)$$

where q_t is the amount of metal (mmol/g) adsorbed at time t and q_{eql} is equilibrium amount ($t \to \infty$). The rate constants (k_{ads}) were calculated from the slope of the $\log(q_{eql} - q_t)$ vs time plot.

3. Results and Discussion

3.1. ACTIVATED CARBON FROM CO-MINGLED WASTES

In order to gain some insight into the reactions which may occur between the components of the co-mingled wastes, the thermal decomposition of the individual components, as well as of their blends, was studied by thermal analysis (DTG/TG). The emphasis is given here to the correlation between the experimental data and the theoretically predicted curves under the assumption of no interaction between components, in order to evaluate possible synergetic effects.

The thermal decomposition of the blend gives rise to simultaneous cracking reactions generating volatile products, and to polycondensation reactions favoring the formation of solid-state products.

The TG/DTG data reveal that the blend components interact during pyrolysis, changing the temperatures of initial weight loss, maximum rate of weight loss, yield of the volatile products, and char (Table 1).

According to the obtained data, there are three main zones of temperature decomposition of the single components and of the blends (Figure 1, Table 2): water decomposition in the temperature range 383–443 K, the first thermal decomposition at 463–623 K, and a second one over the temperature interval 643–773 K.

The first thermal decomposition step shows two overlapping peaks with maximum at *ca.* 523–548 K and 568–583 K; the process starts at 453–463 K, then gradually increases and ends at 608–623 K (Figure 1). Therefore, this initial thermal decomposition step occurs over the temperature range for the decomposition of hemicellulose, cellulose, aromatic tar stock, and maltenes fraction of the aliphatic petroleum stock.

However, in contrast to the theoretical predicton, the maximum rate of weigh loss for the blends starts at a lower temperature, and the overall process for the first thermal decomposition step is found to be stronger. The yield of volatiles (12–24%) is higher than the calculated ones based on the

additive behavior of the blend components. Thus, there is evidence for some interaction between the blend components (Figure 1).

The second thermal decomposition step is observed in the temperature range of T_{init} = 633 K – T_{max} = 668–688 K – T_{final} = 773 K, which corresponds to the temperature range for decomposition of lignin, coal, and aliphatic (asphaltenes) petroleum stock. Synergetic effects are observed for the decomposition of the blend component: a negative trend (19% wt. loss) for aliphatic petroleum stock, and a positive trend (12% wt. loss) for aromatic tar stock.

The interaction between the blend components is more apparent when the total product yield (char, volatiles) is compared to the theoretical calculated one (Table 1). The deviation of 7–10% in the char yield is more pronounced for the blends with aliphatic petroleum stock and is related to repolymerisation (cross-linking) reactions.

Despite of the different decomposition character of individual petroleum and tar stocks, the degradation of their co-mingled blends with coal and biomass was found to be nearly similar (Figure 1). Differences between the aromatic tar and aliphatic petroleum wastes were found only for volatiles/ char yield (Table 1), and char properties.

From the DTG/TG analysis, the temperature ranges for the synergetic effects were evaluated. The data obtained were used for the optimization of the carbonisation/activation processes of the co-mingled liquid and solid organic wastes. Emphasis is done to the polycondensation and repolymerisation reactions via secondary vapour-solid blend components interaction.

According to the laboratory tests, the best conditions for the synthesis were found to be direct high-temperature (1,123 K for 1.5 h) activation with steam, or two-step activation via low temperature (at 623 K for 2 h) carbonisation under inert atmosphere. The optimum blend composition was found to be 25% of biomass, 25% of low-grade coal, 50% of petroleum wastes (either aliphatic petroleum stock or aromatic tar stock), and 5% wt of blends of binary eutectic Na/K carbonates.

The activated carbons produced under optimal conditions exhibited a high surface area and a well-balanced pore size distribution (Table 2). It can be concluded that direct activation seems to be more efficient for the surface and porous structure development (Table 2).

The surface roughness and homogeneity of the materials were studied by Scanning Electron Microscopy (SEM). It was observed that the surface topography drastically changes depending on the conditions of the activation process. Activation via carbonization stage completely eliminates the carbon heterogeneity, and the porous carbon obtained exhibits uniform particle and

TABLE 1. Thermogravimetric analysis of the decomposition of the single components and of their blends.

Samples	Decomposition temperature range (T_{init}–T_{max}–T_{final})	Average rate of weight loss (min^{-1})	Total weight loss at 1,223 K (%)
Bituminous coal	398–673–968	0.27	38.7
Sunflower husks	543–578–628	2.04	83.4
	628–783	0.35	
Aliphatic petroleum stock	488–608–623	0.33	85.4
	623–688–748	0.83	
Aromatic tar stock	438–553–668	0.63	44.7
	668–1223	0.13	
Coal/biomass/aliphatic petroleum stock 1:1:1	313–408–453	0.36	47.3 (Experimental) 53.9 (Theoretical)
	453–548–608	0.74	
	608–688–888	0.46	
Coal/biomass/aromatic tar stock 1:1:1	448–543	0.51	41.9 (Experimental) 38.1 (Theoretical)
	543–583–623	0.70	
	623–763	0.26	

TABLE 2. Textural parameters of the activated carbons from co-mingled wastes. Influence of blends composition and conditions of the activation process.

Activated carbon Precursors	S_{BET} (m^2/g)	V_{total} (cm^3/g)	V_{micro} (cm^3/g)	V_{meso}/V_{micro}
	Direct activation			
Coal/biomass/aliphatic petroleum stock	1,038	0.47	0.39	0.20
Coal/biomass/aromatic tar stock	638	0.32	0.23	0.39
	Activation via carbonisation			
Coal/biomass/aliphatic petroleum stock	979	0.46	0.38	0.21
Coal/biomass/aromatic tar stock	111	0.11	0.05	1.2

pore size distribution. On the other hand, samples obtained by direct activation, despite exhibiting a high surface area, contain both charcoal and some husk residue with wide pores of few microns.

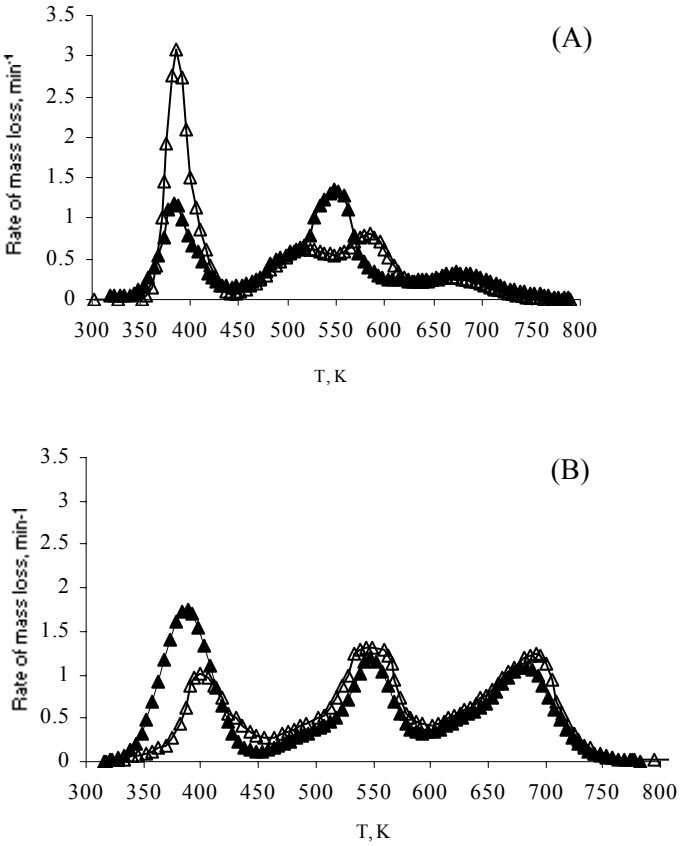

Figure 1. Differential thermogravimetry (DTG) profiles of the co-mingled wastes decomposition: (A) blend on the base of Aliphatic petroleum stock; (B) blend on the base of Aromatic tar stock. ▲ – Theoretical calculation; △ – DTG experimental data.

The topography study and the elemental analysis of the surface were also studied by the Auger method. Auger Depth Profiling provides quantitative information on composition as a function of depth below the surface (near-surface characteristics). The presence of some elements, such as Si, Ba, and Fe, was detected due to initial mineral content of the components in the blend. The distribution of these elements was found to be non-uniform. Under the optimal conditions used, the porous materials synthesized consisted mainly of carbon (up to 86%). Furthermore, measurements of the depth profile concentration by Auger technique did not reveal the presence of any other elements besides of carbon.

3.2. KINETIC DATA FOR SIMULTANEOUS METALS ADSORPTION FROM MULTI-COMPONENT TECHNOLOGICAL SOLUTION

The kinetic data for the simultaneous adsorption of Fe (II), Cu (II), Ni (II), Co (II) and Mn (II) on the parent and post-oxidized carbons from co-mingled wastes (25% sunflower husk, 25% bituminous coal, 50% aromatic petroleum stock; direct activation at 1,123 K with steam) are presented in Figure 2.

The Lagergren equation, Eq. (1), was applied to the kinetic data in order to evaluate the rate constants for simultaneous metal adsorption on activated carbons with different surface oxygen functionalities.

The linear plots of log ($q_{eql} - q_t$) vs t [an example is provided in Figure 3 for the case of Fe (II)] for all of the studied metals corroborates the applicability of Lagergren equation, thus providing evidence for first-order adsorption kinetics. The specific rate constants, k_{ads}, were calculated from the slopes of the linear plots and are listed in Table 3.

Simultaneous adsorption of the 3-d transition metals on the parent activated carbons from co-mingled waste shows that Cu (II) and Fe (II) ions adsorb faster (specific rate constants in the range $0.41–0.48 \times 10^{-4}$ min^{-1}) and more efficiently (Me_{rem} of 21–26%) than Mn (II) and Co (II) (k_{ads} of $0.12–0.24 \times 10^{-4}$ min^{-1} and Me_{rem} of 15–20%). There was almost no removal of Ni (II).

However, the situation is drastically changed when the post-oxidized activated carbon from co-mingled wastes is used as adsorbent. There is an increase of the specific adsorption-rate constants for Fe (II) and Cu (II) ions and also an increase of the percentage of removal (89% and 54%). Also, for Mn (II), Ni (II) and Co (II) a slightly increase is observed for the specific rate constant and percentage of removal (Figure 2).

From the TPD experiments it is seen that the oxidized carbon is enriched with carboxylic (hydrous and anhydrous) and quinones groups, which are, probably, responsible for the adsorption of the metals. Furthermore, post-oxidation by nitric acid essentially modifies the structure of the parent activated carbon. The specific surface area decreases due to partial destruction of the initial micropores, along with the formation of a mesoporous structure. As a result, the post-oxidized carbon adsorbs heavy solvated metal ions from liquid phase better than the parent carbon (Figure 2).

Based on the obtained kinetics results, on previous work on adsorption equilibrium of Cu (II) and Cr (III) on synthetic and natural activated carbons [21, 24], and on data reported in the literature [25–31], we propose a mechanism for the adsorption of 3-d transition metals in real aqueous solutions.

TABLE 3. Adsorption capacity and adsorption efficiency of parent and post-oxidized activated carbons from wastes for 3-d transition metals.[a] The specific rate constants of the simultaneous adsorption of 3-d transition metals from multi-component technological solutions.

Metal	Me uptake (mg/g)	Me removal (%)	Specific rate constants $\times 10^{-4}$ (min^{-1})
Adsorption on parent[b] activated carbon from wastes			
Cu (II)	0.41	20.6	0.48
Fe (III)	0.57	25.9	0.41
Co (II)	0.28	14.9	0.12
Ni (II)	0.08	4.2	0.04
Mn (II)	0.38	20.0	0.16
Adsorption on post-oxidized activated carbon from wastes			
Cu (II)	1.17	54.0	1.05
Fe (II)	1.94	89.1	7.41
Co (II)	0.44	23.4	0.23
Ni (II)	0.56	28.5	0.28
Mn (II)	0.43	22.5	0.37

[a]Data are given for 72 h of contact time

[b]Activated carbon from co-mingled 25% sunflower husk, 25% bituminous coal, 50% aromatic petroleum stock; direct activation at 850°C with steam

In previous work on Cu (II) adsorption over activated carbon in the absence of oxygen surface groups we observed the formation of a metallic film on the carbon surface (similar to the galvanic covering process) [24]. However, copper adsorption on carbons enriched with oxygen surface groups originated a decolorized solution with no metallic film formation [24]. The obtained results suggest that there are different mechanisms for copper adsorption on oxidized and non-oxidized carbons.

According to the theory of reductive adsorption [31], the spontaneous process of reduction of electrochemical ions is thermodynamically favored when the equilibrium potentials of metal ions reduction are more positive than the carbon surface potential:

$$\varphi\ Me^{m+}/\ Me^{0} > \varphi\ \text{Carbon} \qquad (2)$$

The standard potential of Cu^{2+}/Cu^{0} pair is 340 mV (for the diluted metal solution this value is slightly lower), whereas the potential of gaseous oxygen electrode on carbon surface is 770 mV, which is significantly higher than the potential of reduction of copper cations. According to thermodynamics, the reductive adsorption of metals on the carbon surface in the presence of oxygen is not allowed. Thus, carbons enriched with oxygen groups exhibit an oxidation-reduction potential higher than the parent ones and the oxidized carbon surface can not reduce the metal cations to the metallic state.

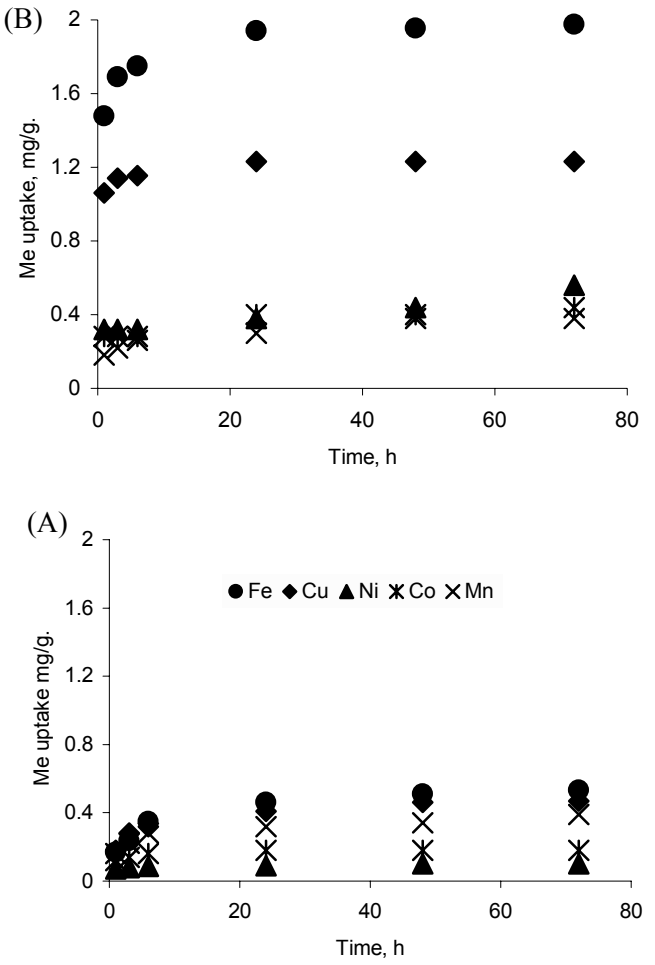

Figure 2. Adsorption kinetics on parent (A) and post-oxidized (B) activated carbons from multi-components technological solution containing $\Sigma_{[Ni, Co, Cu, Fe, Mn]} = 0.05$ g/L.

In the case of the activated carbon from co-mingled wastes, the carbon/ metal ions interaction via electron transfer or redox–reactions accompanied by metal ions reduction to a lower oxidation state is not favorable.

The pH_{PZC} of the parent carbon is 5.8, and if electrostatic interactions take place then the net carbon surface will be positive charged at pH = 3.6, and the repulsion forces will inhibit the adsorption of cations, which seems to explain the low carbon adsorption capacity.

According to the pH_{PZC} of the oxidized carbon from co-mingled waste ($pH_{PZC} = 3.4$), and taking in account that the initial pH of the real solution is 3.6, the carbon surface charge is almost neutral. Thus, the electrostatic

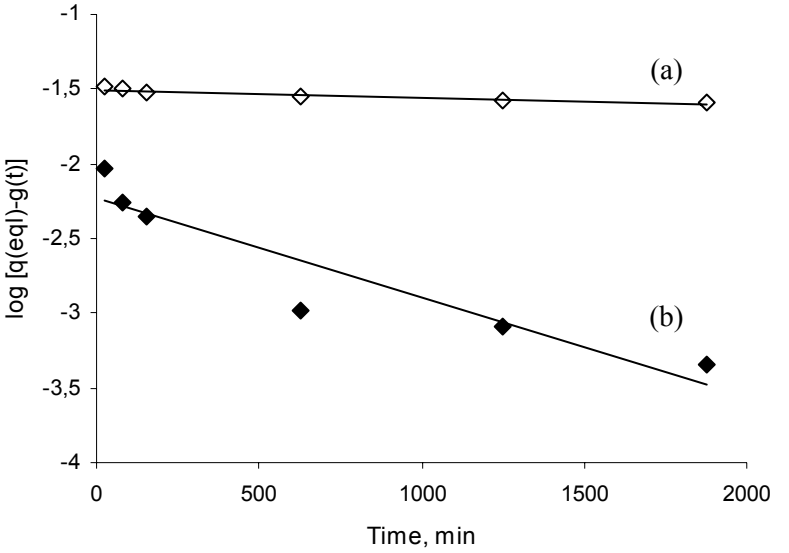

Figure 3. Typical Lagergren plot for heavy metals adsorption on parent (a) and post-oxidized (b) activated carbons from co-mingled wastes [example is given for Fe (II) adsorption].

interactions (attraction or repulsion) do not seem to have an important role on the adsorption mechanism of the metal.

It is plausible that the adsorption mechanism be a fast ion-exchange, Eqs. (3) and (4), of the aqueous metals ions, followed by their surface hydrolysis and slower chemisorption, Eq. (5), or/and an outer-sphere complexation (most probably with the first hydrolyzed hydrolytic species) that converts to inner-sphere complexation with time, Eq. (6):

$$2(-R_xOOH) + Me^{2+} = 2(-R_xOO)Me + 2H^+ \quad (3)$$

$$-R_xOOH + Me(OH)^{1+} = (-R_xOO)MeOH + H^+ \quad (4)$$

$$2[R_xOO]^- + Me^{2+} \rightarrow [2R_xOO^-Me^{2+}] \quad (5)$$

$$R_xOOH + Me(OH)^{2+} = R_xOOH\ldots\ Me(OH)^{2+} \longrightarrow R_xOO\text{-}MeOH^+ + H^+ \quad (6)$$

It was observed that the oxidation with nitric acid modified the structure of the parent carbon increasing the pore size. Considering purely a physisorption process an increase of the pore size may explain the increase of the uptake.

4. Conclusions

An approach to recycled waste *re-use* for environmental applications was developed under the framework of a NATO Science for Peace project (SfP

977984). Using this approach, inexpensive and high-quality activated carbons from co-mingled liquid/solid organic waste can be obtained. The properties of the novel materials are comparable to those of the best commercially available activated carbons (surface area of 600–900 m^2/g, total pore volume of 0.32–0.56 cm^3/g).

The use of the activated carbon from co-mingled waste as an adsorbent for heavy metals offers an attractive approach to simultaneous heavy metal removal from multicomponent aqueous solutions under practical conditions. Within this context, natural organic waste conversion into porous materials with environmentally-friendly applications is a technological alternative to their disposal.

Acknowledgements

Financial support of the NATO Science for Peace Programme SfP project No 977984 is gratefully acknowledged.

References

1. Pollard SJT, Fowler GD, Sollars CJ, Perry R. *Sci Total Environ* 1992; 116(1–2):31–52.
2. Nakamoto S, Machida N. *Water Res* 1992; 26(1):49–54.
3. Srinivasan K, Balasubramanian N, Ramakrishnan TV. *Ind J Environ Health* 1998; 30(40):376–87.
4. Alaerts GJ, Jitjaturant V, Kelderman P. *Water Sci Technol* 1989; 21:1701–1704.
5. Chand S, Agarwal VK, Pavankumar C. *Ind J Environ Health* 1994; 36(3):151–158.
6. Rawat NS, Singh D. *Asian Environ* 1992; 14:30–41.
7. Sharma DC, Forster CF. *Water Res* 1993; 27(7):1201–1208.
8. Raji C, Anirudhan TS. *Ind J Chem Technol* 1996; 3:345–350.
9. Bhatnagar, Jain AK. *J Coll Interface Sci* 2005; 281(1):49–55.
10. Paruya SK, Sarkar SC, Bose A. *J Mines Met. Fuels* 1996; 44(3):117–124.
11. Maxa D. *Pet Coal* 1998; 40(4):224–227.
12. Ndaji FE, Ellyatt WAT, Malik AA, Thomas KM. *Fuel* 1999; 78(3):301–307.
13. Mastral M, Murillo R, Callén MS, García T. *Fuel Process Technol* 2001; 69(2):127–140.
14. Luo M, Curtis ChW. *Fuel Process Technol* 1999; 59(2–3):163–187.
15. Ramdoss PK, Tarrer AR. *Fuel Process Technol* 1997; 51(1–2):83–100.
16. Pinto F, Franco C, Neto André R, Tavares C, Dias M, Gulyurtlu I, Cabrita I. *Fuel* 2003; 82(15–17):1967–1976.
17. Chmielniak T, Sciazko M. *Appl Energy* 2003; 74(3–4):393–403.
18. Sjöström K, Chen G, Yu Q, Brage C, Rosé C. *Fuel* 1999; 78(10):1189–1194.
19. Kurkela E. Recent results and plans concerning co-gasification of biomass and coal – an overview, In: Chartier P. (ed.). Biomass Energy Environ Proc Eur Bioenergy 9th Conf. Elsevier, Oxford, 1996.
20. Collot G, Zhuo Y, Dugwell DR, Kandiyoti R. *Fuel* 1999; 78(6):667–679.
21. Lyubchik SI, Lyubchik AI, Galushko OL, Tikhonova LP, Vital J, Fonseca IM, Lyubchik SB. *Colloids Surf A: Physicochem Eng Aspects* 2004; 242(1–3):151–158.

22. Standard Methods for the Examination of Water and Wastewater, 18th ed. American Public Health Association, Washington, DC, 1992.
23. Namasivayam C, Ranganathan K. *Ind J Chem Technol* 1995; 1:351–355.
24. Kopyl S, Lapko V, Lysenko A, Tarasenko Yu, Tomizuka I. *J Ion Exchange* 2003; 14:157–160.
25. Carrott PJM, Ribeiro Carrott MML, Nabais JMV, Prates Ramalho JP. *Carbon* 1997; 35(3):403–410.
26. Raji C, Anirudhan TS. *Water Res* 1998; 32:3772–3780.
27. Lakatos J, Brown SD, Snape CE. *Fuel* 2002; 81:691–698.
28. Fendorf SE. *Geoderma* 1995; 67(1–2):55–71.
29. Chong KH, Volesky B. *Biotechnol Bioeng* 1995; 47:451–460.
30. Rhee I.H, Dzombak DA. *Langmuir* 1998; 14:935–943.
31. Csobán K, Joó P. *Colloids Surf A: Physicochem Eng Aspects* 1999; 151:97–112.

MODELING CARBON MASK ADSORPTIVE FILTERS

JOSÉ MIGUEL LOUREIRO,* ANA MAFALDA RIBEIRO
Laboratory of Separation and Reaction Engineering (LSRE), Department of Chemical Engineering, University of Porto, Rua Dr. Roberto Frias, 4200-465 Porto, Portugal

Abstract. The mathematical modeling of beds employed in individual protection is reviewed. The first models presented in the literature considered that the removal of the toxic compounds was done only by physical adsorption. However for some compounds an efficient protection cannot be attained if only adsorption is present. Consequently adsorbents which eliminate the toxic compounds by physical adsorption coupled with chemical reaction are used in the filters. Thus, several models that take into account these two phenomena were proposed.

Keywords: carbon filters; process modeling

1. Introduction

Individual and collective protection equipment prevents its user from contacting toxic compounds present in the surrounding atmosphere and thus avoid severe injury. The primary item of protection is the personal respirator which is frequently employed both in industrial and military environments. The background of expertise on respiratory protection is its military application which dates back to the First World War, conflict in which chemical agents/weapons were used for the first time. The individual defense technology evolved very quickly since the defenders in Ypres used any available tissue as an instinctive protective mean, until pre-wetted masks produced to cover the entire face, and finally fully sealed mask with eye lenses and filters were carefully designed and produced.

*To whom correspondence should be addressed. E-mail: loureiro@fe.up.pt

J.P. Mota and S. Lyubchik (eds.), Recent Advances in Adsorption Processes for Environmental Protection and Security, 147–153.

The introduction of a protective barrier between the individual and the hazard compounds allows for a temporary reduction to its exposure. However, it must be remembered that sooner or later all chemical will end up penetrating through the protective barriers. Depending on diverse factors, this protection time can range from a few seconds to days, but no equipment is capable of protecting its wearer against anything indefinitely. As the incorrect use of the gas masks can cause serious risks to human health it is very important to be able to predict the dynamic behavior of these filters, and consequently its useful time, under different operating conditions.

The objective of this paper is to give an historical overview of the mathematical modeling employed in the field of individual protection.

2. State of the Art

The first predictive equation of the dynamic behavior of the filters was proposed by Bohart and Adams in 1920 [1]. In their work, Bohart and Adams [2] developed an equation based on a "chemical kinetic" model type, that is, assuming that the adsorption kinetic was the controlling step of the process (instantaneous diffusion), for the case of irreversible isotherm and neglecting the accumulation on the fluid phase. The obtained equation can be expressed as [3]:

$$\frac{C}{C_E} = \frac{exp\left(k_1 C_E t\right)}{exp\left(k_1 C_E t\right) + exp\left(\frac{k_1 W_e \rho_b z}{u_0}\right) - 1} \tag{1}$$

where C is the solute concentration at the axial position z, C_E is the solute concentration at the bed inlet, k_1 is the adsorption kinetic constant, t is the time, W_e is the adsorbent capacity, ρ_b is the bed density and u_0 is the superficial velocity.

Since then several authors have developed equations for the prediction of the breakthrough time (t_b) of the filters [1], namely the Danby equation [4], the Klotz equation [5], the Wheeler-Jonas equation [6, 7] and the Yoon-Nelson equation [8, 9] given respectively by:

$$t_b = \frac{W_e \rho_b L}{u_0 C_E} - \frac{1}{k_D C_E} ln\left(\frac{C_E - C_b}{C_b}\right) \tag{2}$$

$$t_b = \frac{W_e A}{Q C_E}\left[L \rho_b - \frac{1}{a} Re^{0.41} Sc^{0.67} ln\left(\frac{C_E}{C_b}\right)\right] \tag{3}$$

$$t_b = \frac{W_e W}{Q C_E} - \frac{W_e \rho_b}{k_{WJ} C_E} ln\left(\frac{C_E - C_b}{C_b}\right) \tag{4}$$

$$t_b = \frac{W_e W}{Q C_E} - \frac{W_e W}{k_{YN} C_E Q} ln\left(\frac{C_E - C_b}{C_b}\right) \tag{5}$$

In these equations L and A represent the bed length and cross section area, C_b is the breakthrough concentration, Q is the volumetric flowrate, a and W are the adsorbent superficial area and weight. Re and Sc are respectively the Reynolds and Schmidt numbers.

The Danby, Wheeler-Jonas and Yoon-Nelson equations are equivalent and can be obtained directly from the Bohart and Adams equation assuming that

$$exp\left(\frac{k_1 W_e \rho_b z}{u_0}\right) >> 1$$

and merely modifying the definition of each respective adsorption kinetic constant.

The equation known as the Klotz equation is empirical and is based on the work of Mecklenburg. This author developed an equation assuming that until the breakthrough time, the solute accumulation on the fluid phase is negligible, that is, that all the solute entering the bed is retained on the adsorbent. Through this hypothesis he defined a new variable designated critical bed depth [1]. Klotz [5] reintroduced the Mecklenburg equation using the Gamson, Thodos and Hougen correlation for the calculation of the critical bed depth [10].

From all these equations, the most frequently employed in the correlation of filter breakthrough times obtained experimentally is the Wheeler-Jonas equation [11–18].

In the derivation of the above mentioned equations it was always considered that the toxic compound is removed only by physical adsorption. However, it is known that for the case of some compounds with low molecular weight, such as those with military interest (HCN, CNCl, etc.), an efficient elimination can not be achieved with only physical adsorption. The adsorbent (activated carbon) is then normally impregnated with metals such as copper, chromium and silver that react with the toxic compounds after adsorption [19] enhancing the filter protective capacity.

The first models that consider systems where adsorption is coupled with reaction were developed in the scope of chromatograph reactors [20–22]. Afterwards, Schweich et al. [23] studied these systems through an equilibrium model with linear adsorption and instantaneous reversible equation.

Loureiro et al. [24, 25], using also an equilibrium model analyzed a system with Langmuir adsorption and irreversible reaction of several orders.

Friday [26] developed the first model with coupled adsorption and reaction for application on individual protection filters, and more specific for the system ASC activated carbon/cyanogen chloride. This author considered isothermal operation, plug flow, external (film) and internal (LDF) resistances and Langmuir adsorption followed by irreversible second-order reaction between the adsorbed CNCl and the impregnated metals.

A similar study was performed by Graceffo et al. [27] but, contrarily to Friday, these authors consider that the impregnated metals do not react with the adsorbate but act as a catalyst that deactivates with time. The reaction rate is expressed as function of the fluid phase CNCl concentration and the Freundlich isotherm is used to represent the adsorption equilibrium.

Chatterjee and Tien [28, 29] proposed a model in which they assume that the reaction between CNCl and the impregnated metals is instantaneous and only after the metals are totally consumed is the solute adsorbed. As the toxic compound is being removed, the adsorbent particle is seen as being composed of two distinct zones. In the first one, the metal has already been fully used-up and adsorption is taking place while the second zone is completely free from adsorbate which is reacting at the frontier. The radial position of this frontier decreases with time (shrinking core model).

Friday's model was later modified by Soares et al. [30] in order to include the effect of axial dispersion. The authors concluded that axial dispersion affects significantly the breakthrough time of the filters and should not be neglected. The effect of axial dispersion is important not only due to the shallow bed length, but also because the threshold toxic concentration is very low. The simulation results showed that this parameter should be carefully evaluated.

The models were then further extended by Ribeiro and Loureiro [31] that considered different filter geometries, that is, the fixed bed operating in either axial or radial (inner and outer) flow. Mathematical models of increasing complexity were solved for each geometry and the influence of the dimensionless parameters on the breakthrough time assessed. It was shown that the filter breakthrough time is significantly dependent on the model considered and on the different parameters values. Comparing the results between geometries they concluded that the one with axial flow was better, as it was with this one that longer breakthrough times were attained in the simulations with the models that best represent reality. The same authors validated the model results with experimental results [32]. Due to the high risks associated with the compounds that are eliminated by the impregnated activated carbons by physical adsorption followed by chemical reaction no experimental data was obtained for such systems. Instead, the validation

was done using results taken from the literature. They observed that, using an optimized value for the reaction kinetic constant, the prediction of the experimental breakthrough times was globally reasonable. Experimental data was then obtained for systems where only adsorption occurs and used to validate the mathematical models. They chose as adsorbents three activated carbons (BPL, ASC and ASC-Teda) and as adsorbates a volatile organic compound, methyl tert-butyl ether (MTBE), and water vapor. This last adsorbate was also studied as it is usually present in common use of individual protection filters either pre-adsorbed and/or as humidity in the in flow stream. The results obtained with MTBE in the BPL were reasonably simulated by the more complex model. The breakthrough curves determined in the impregnated carbons suggested the presence of a higher internal resistance in this kind of carbons. The simulations that took into account this effect reproduced better these experimental results. The water vapor adsorption tests point to the presence of an increasing internal resistance at larger concentrations, even higher than that considered with the inclusion of the adsorption isotherm derivative in the calculation of the homogeneous effective diffusivity. It was verified that simulations which consider a lower value for the effective diffusivity reproduce satisfactorily all the experimental results of sequential saturation at higher concentrations and even the 0–80% tests.

3. Conclusions

The different mathematical models employed in the scope of individuals' protection by carbon mask adsorptive filters were reviewed. Several models with increasing complexity have been proposed in the literature along the time. Each discussed model intends to simulate the dynamic behavior of the filters and to predict their useful time according to toxic limits. Taking into account that these filters are used in the protection of human lives, it is essential to accurately predict their behavior, making the use of the more complex models necessary and also the knowledge of the different parameters values as rigorously as possible very important.

References

1. E. Balieu, Fundamental aspects in air filtration and purification by means of activated carbon filters, *Gas Separation Technology*, 90–136 (1990).
2. G.S. Bohart and E.Q. Adams, Some aspects of the behavior of charcoal with respect to chlorine, *Journal of American Chemical Society*, 42, 523–544 (1920).

3. A.E. Rodrigues, *Elementos sobre a teoria da percolação* (Departamento de Engenharia Química, Universidade de Luanda, Luanda, 1974).
4. C.J. Danby, J.G. Davoud, D.H. Everett, C.N. Hinshelwood and R.M. Lodge, The kinetics of absorption of gases from an air stream by granular reagents, *Journal of Chemical Society*, 115, 918–934 (1946).
5. I.M. Klotz, The adsorption wave, *Chemical Reviews*, 39, 241–268 (1946).
6. L.A. Jonas and J.A. Rehrmann, The kinetics of adsorption of organo-phosphorus vapors from air mixtures by activated carbons, *Carbon*, 10, 657–663 (1972).
7. L.A. Jonas and J.A. Rehrmann, Predictive equations in gas adsorption kinetics, *Carbon*, 11, 59–64 (1973).
8. Y.H. Yoon and J.H. Nelson, Application of gas adsorption kinetics. I. A theoretical model for respirator cartridge service life, *American Industrial Hygiene Association Journal*, 45, 509–516 (1984).
9. Y.H. Yoon and J.H. Nelson, Application of gas adsorption kinetics. II. A theoretical model for respirator cartridge service life and its practical applications, *American Industrial Hygiene Association Journal*, 45, 517–524 (1984).
10. B.W. Gamson, G. Thodos and O.A. Hougen, Heat, mass and momentum transfer in the flow of gases through granular solids, *AIChE Journal*, 39, 1–35 (1943).
11. G.O. Wood, and P. Lodewyckx, An extended equation for the rate coefficients for the adsorption of organic vapors and gases on activated carbons in air-purifying respirator canisters, *American Industrial Hygiene Association Journal*, 64, 646–650 (2003).
12. G.O. Wood and J.F. Stampfer, Adsorption rate coefficients for gases and vapors on activated carbons, *Carbon*, 31, 195–200 (1993).
13. O. Busmundrud, Vapour breakthrough in activated carbon beds, *Carbon*, 31, 279–286 (1993).
14. I. Nir, D. Kaplan and Y. Suzin, Extension of the Wheeler-Jonas model (WJM) for dynamic adsorption to pulsating flow, in *Fundamentals of Adsorption 7*, edited by K. Kaneko, H. Kanoh, and Y. Hanzawa (IK International, Chiba, 2001), pp. 833–840.
15. P. Lodewyckx and E.F. Vansant, The influence of humidity on the overall mass transfer coefficient of the Wheeler-Jonas equation, *American Industrial Hygiene Association Journal*, 61, 461–468 (2000).
16. P. Lodewyckx and E.F. Vansant, Estimating the overall mass transfer coefficient k_v of the Wheeler-Jonas equation: a new and simple model, *American Industrial Hygiene Association Journal*, 61, 501–505 (2000).
17. P. Lodewyckx and L. Verhoeven, Using the modified Wheeler-Jones equation to describe the adsorption of inorganic molecules: chlorine, *Carbon*, 41, 1212–1219 (2003).
18. E.B. Sansone and L.A. Jonas, Prediction of activated carbon performance for carcinogenic vapors, *American Industrial Hygiene Association Journal*, 42, 688–691 (1981).
19. M. Molina-Sabio, V. Pérez and F. Rodríguez-Reinoso, Impregnation of activated carbon with chromium and copper salts: effects of porosity and metal content, *Carbon*, 32, 1259–1265 (1994).
20. E.M. Magee, The course of a reaction in a chromatographic column, *Industrial and Engineering Chemistry Fundamentals*, 2, 31–36 (1963).
21. F.E. Gore, Performance of chromatographic reactors in cyclic operation, *Industrial and Engineering Chemistry Process Design and Development*, 6, 10–16 (1967).
22. C. Chu and L.C. Tsang, Behavior of a chromatographic reactor, *Industrial and Engineering Chemistry Process Design and Development*, 10, 47–53 (1971).
23. D. Schweich, J. Villermaux and M. Sardin, An introduction to the nonlinear theory of adsorptive reactors, *AIChE Journal*, 26, 477–486 (1980).
24. J.M. Loureiro, C. Costa and A. Rodrigues, Dynamics of adsorptive reactors. I – Instantaneous nonlinear adsorption and finite zero order irreversible reaction, *The Canadian Journal of Chemical Engineering*, 68, 127–138 (1990).

25. J.M. Loureiro, C.A. Costa and A.E. Rodrigues, Propagation of Concentration Waves in Fixed-bed Adsorptive Reactors, *The Chemical Engineering Journal*, 27, 135–148 (1983).
26. D.K. Friday, The breakthrough behavior of a light gas in a fixed-bed adsorptive reactor, *AIChE Journal Symposium Series*, 84, 89–93 (1988).
27. L.A. Graceffo, S.G. Chatterjee, H. Moon and C. Tien, A model for the retention of toxic gases by impregnated carbon, *Carbon*, 27, 441–456 (1989).
28. S.G. Chatterjee and C. Tien, Retention of toxic gases by modified carbon fixed beds, *Carbon*, 28, 839–848 (1990).
29. S.G. Chatterjee and C. Tien, Adsorption with chemical reaction in a single modified-carbon pellet, *Chemical Engineering Science*, 44, 2283–2294 (1989).
30. R.C. Soares, J.M. Loureiro, C. Sereno and A.E. Rodrigues, Modeling and simulation of carbon mask adsorptive reactors, *Industrial and Engineering Chemistry Research*, 34, 2762–2768 (1995).
31. A.M. Ribeiro and J.M. Loureiro, Simulation of toxic gases and vapours removal by activated carbon filters, *Chemical Engineering Science*, 57, 1621–1626 (2002).
32. A.M. Ribeiro, Filtros de carvão activado impregnado. Sua aplicação da remoção de gases e vapores tóxicos por adsorção e reacção química simultâneas., Ph.D. thesis, FEUP, Universidade do Porto, Portugal, 2006.

ADSORPTION PROCESSES IN GAS MASK FILTER CANISTERS: PRACTICAL ASPECTS, NEW MATERIALS AND MODELING

MARCO J.G. LINDERS*
TNO Defence, Security and Safety, Lange Kleiweg 137, 2288 GJ Rijswijk, The Netherlands

Abstract. Three topics are addressed related to adsorption processes in gas mask filter canisters. In the first section "practical aspects" two items are addressed: (a) the influence of the flow pattern, i.e. a breathing or pulsating flow versus continuous flow, on the breakthrough behavior; and (b) the risk of desorption: the possibility that adsorbed contaminants are released from the filter. The second section "new materials" deals with the use of carbon monoliths. The third section "modeling" discusses a gas mask model that has been implemented in a software tool that simulates chemical and biological incidents.

Keywords: Adsorption, gas mask, carbon monoliths, modeling, incidents.

1. Practical Aspects

During actual use of a gas mask canister the flow through the activated carbon bed is pulsating, i.e. during inhalation air is drawn through the canister, while during exhalation there is a stand-still of air in the canister. In approval tests for filters mostly a constant flow pattern is applied. The time-averaged gas velocity has to be equal when applying a constant continuous flow or a pulsating flow for a fair comparison of the breakthrough behavior for both cases. Figure 1 shows the respiration pattern with a breathing cycle time of 4 s, that is, during 2 s air is flowing through the canister and the next 2 s the air is still.

*To whom correspondence should be addressed. E-mail: marco.linders@tno.nl

J.P. Mota and S. Lyubchik (eds.), Recent Advances in Adsorption Processes for Environmental Protection and Security, 155–164.

Breakthrough measurements applying continuous and pulsating flows were performed using toluene on shallow activated carbon beds (Norit R1). Toluene is a good representative for the type of vapors for which activated carbon forms a suitable adsorbent. Pulsating flow was studied by using the positive halves of a sinusoidal flow pattern, which closely resembles the actual breathing pattern. Figure 2 shows breakthrough profiles of toluene for constant and pulsating flow, where a bed length was applied of 1.5 cm, a toluene concentration of 7.5 g/m^3, and the time averaged superficial gas velocity was 0.127 m/s. The observed difference between the two breakthrough profiles is very typical: pulsating (breather) flows are found to be less favorable for the breakthrough behavior compared to a constant flow pattern.[1] Furthermore, the difference between the two becomes larger for low concentrations. Since in gas masks the low concentration range is of extreme importance in case of high toxic compounds, this difference becomes even more important. The influence of flow rate on the mass transfer from the bulk gas phase to the surface of the adsorbent particles is ultimately responsible for the difference in breakthrough times.[1] Clearly, pulsating flow is a factor to take into account if one requires a reliable assessment of the performance of an activated carbon canister in practice.

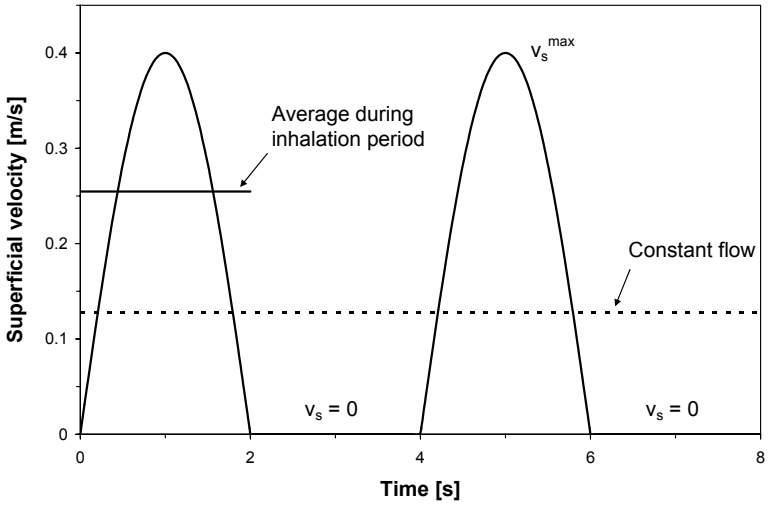

Figure 1. The respiration pattern is represented by a sine wave pattern (solid line), which closely resembles the actual breathing pattern. The dashed line is the corresponding constant flow.

A second practical aspect that is discussed is the risk of desorption.[2] There exists a tendency in industry to equip respiratory protective devices (RPD) with a blower device, which turns them into power assisted devices. The function of the blower is to continuously draw air through the canister

and to blow the air into the protective part around the head of the user. The reason for this approach is obvious: in RPD it is important to have as low a pressure drop as possible. This ensures both a better protection and a higher comfort for the user. This development of equipping RPD with a blower device entails the hazard of desorption. Because air is continuously drawn through the canister, also during exhalation, the possibility increases that adsorbed contaminants are desorbed from the activated carbon. The occurence of desorption was examined under various conditions in order to explore whether or not significant risks exist.

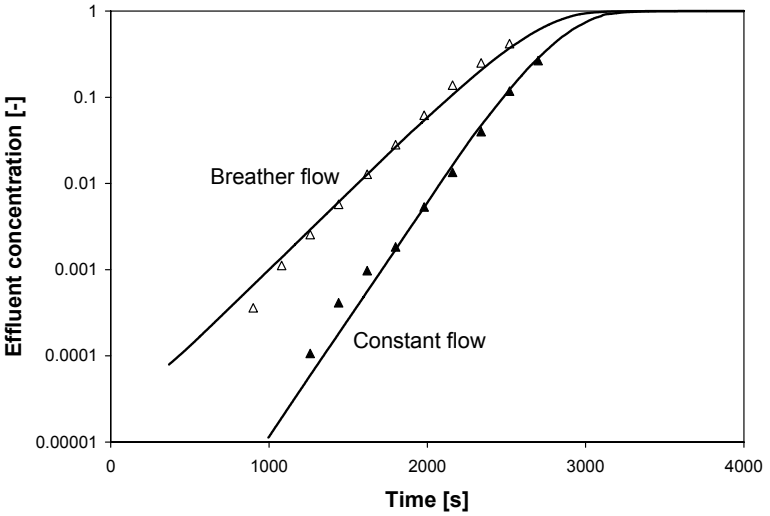

Figure 2. Breakthrough profiles of toluene on Norit R1; comparison between pulsating (breather) and constant flow. The symbols represent the experimental data, the solid lines represent the simulation results.

The existence of a desorption risk was examined by means of a series of sorption experiments in which the same procedure was followed. During a certain period of time a bed of activated carbon was exposed to an air flow containing a contaminant. After this period the supply of the contaminant was stopped while a flow of clean air was continued. The effluent contaminant concentration was monitored during the entire experiment. From the viewpoint of a possible occurrence of a desorption risk it is especially interesting what happens after the supply of contaminant has been stopped. The sorption experiments were carried out with cyclohexane and Norit R1 carbon. The bed height was 2 cm and the total flow rate was 7.5 L/min, which corresponds to a superficial gas velocity of 6.4 cm/s. The entire carbon bed was divided into two separate beds, in series, of 1 cm each. The cyclohexane concentration was monitored gas chromato-graphically after

each bed, providing extra information about the progress of the concentration front.

Figure 3 shows the results of experiments where challenge times for cyclohexane were applied of 10, 20, and 30 min. In all three cases cyclohexane was positively detected after the first part of the bed. The point at which the feed of cyclohexane was stopped, is visible as well: the concentration rises less fast or decreases even at that moment. The system is flushed with clean air that causes the concentration to rise less fast or even to decrease initially. Subsequently, previously adsorbed cyclohexane starts to release: desorption occurs and the concentration shows a further increase. A longer challenge time results in a higher concentration. Although at 20 and 30 min challenge time the concentration rises above the breakthrough criterion of 5 mg/m^3, this is measured halfway through the carbon bed (1 cm). The concentration at the end of the bed is of more importance, as filter canisters are equipped with carbon beds that typically have a bed length of 2 cm. Only in case of a challenge time of 30 min cyclohexane was detected at the end of the bed. This occurred, though, only after more than 200 min; nevertheless, the concentration did rise above the breakthrough criterion of 5 mg/m^3. For 10 and 20 min challenge time no cyclohexane was detected at the end of the bed even after 10–12 h of clean air flow, i.e. the concentration is below the detection limit of 0.01 mg/m^3.

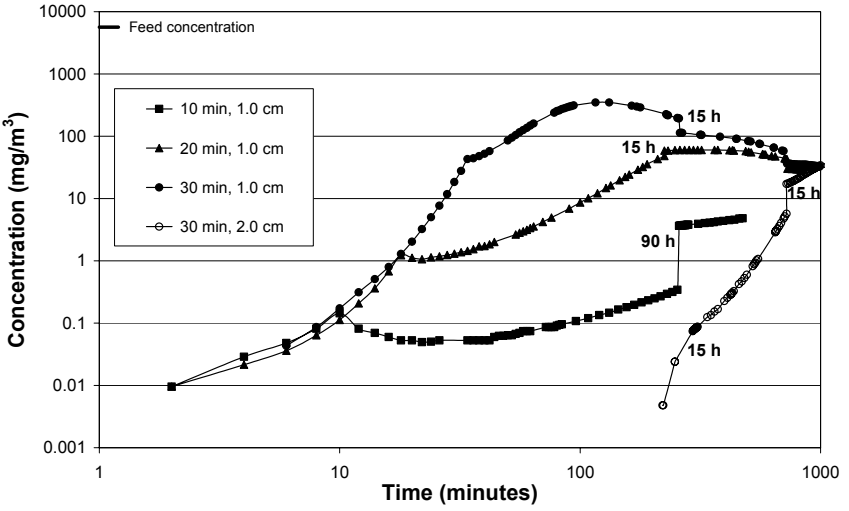

Figure 3. Breakthrough profiles of cyclohexane on Norit R1. The feed concentration was 5.63 g/m^3, supplied during 10, 20, and 30 min; the carbon was dried and the feed humidity was ≤10%. The concentration jumps are a consequence of a period of air standstill.

For a more detailed discussion of the results of this study (including experimental results at different conditions) is referred to the recent publication by Linders et al.[2] It is concluded that physisorbed contaminants

may be released from activated carbon filters in significant concentrations once the influent concentration of the contaminant has been reduced to zero. A redistribution of physisorbed contaminants over the activated carbon bed occurs in a period of rest (e.g. one night or more), which may lead to augmented release of contaminant when the filter is re-used. Under humid conditions the desorption of physisorbed contaminants occurs more rapidly than under dry conditions. Because desorption phenomena pose a risk for the users of RPD, it is advisable to address this somehow in all approval tests for vapor filters.

2. New Materials: Monoliths

The protection against chemical warfare agents is based on sorption on activated carbon, both in gas mask canisters as well as in protective clothing. The carbon applied are granulates (mask) or small spheres (clothing). A new development in adsorption processes is the use of monoliths,[3] either carbon monoliths or carbon-coated ceramic monoliths. Figure 4 shows a carbon monolith. Monoliths consist of many parallel channels separated by thin walls. The main advantages are low-pressure drop and short diffusion distances.

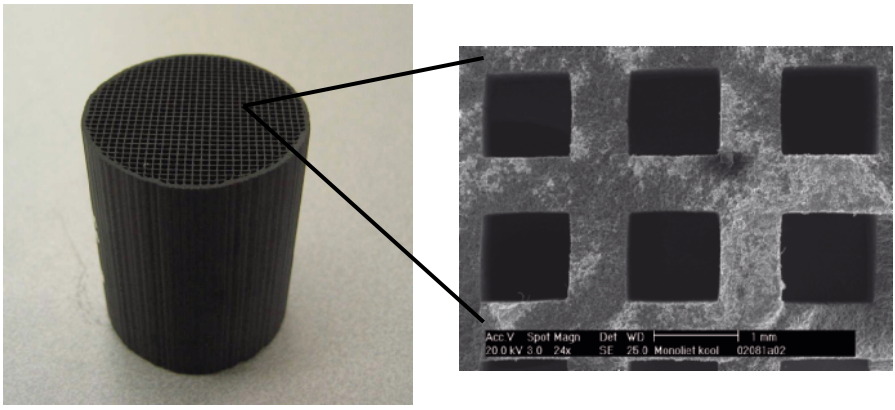

Figure 4. Carbon monolith and detail of the channels on the right.

Carbon and carbon-coated ceramic monoliths have been studied for the dynamic adsorption of low-concentration *n*-butane.[4] Figure 5 shows breakthrough profiles of carbon coated ceramic monoliths and of Norit R1 carbon extrudates. The experiments with Norit carbon were performed with an equivalent amount of carbon as the corresponding monoliths, under similar conditions. Experimental conditions were as follows. The total flow rate was 1.5 L/min, which corresponds to a superficial gas velocity of 0.017 m/s, and the *n*-butane concentration was 7.2 g/m^3 (3,100 ppm). Bed lengths of 5

and 10 cm monolith (made from individual pieces of 5 cm length) were applied at a cell density of 400 cells per square inch (cpsi). Figure 5 clearly shows that breakthrough profiles are much steeper for the coated monoliths compared to carbon extrudates, especially in the low concentration regime. This makes monoliths an attractive option for gas mask canister applications, which is even more so taking into account the low pressure drop (low breathing resistance).

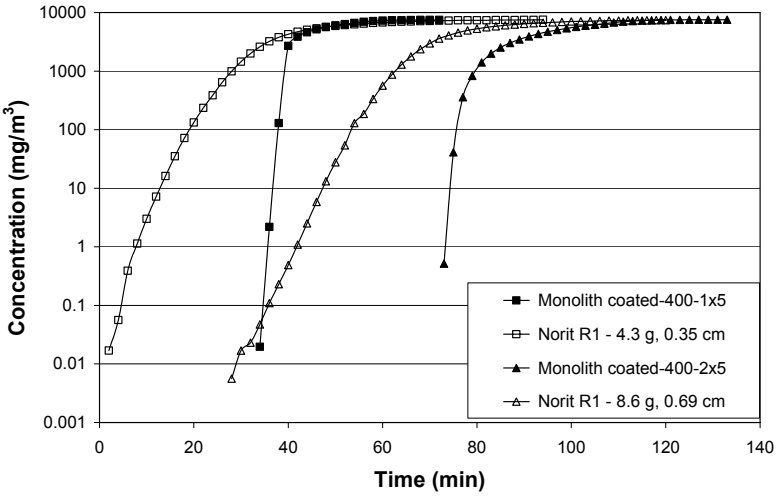

Figure 5. Breakthrough profiles of *n*-butane on carbon coated ceramic monolith and Norit R1 carbon.

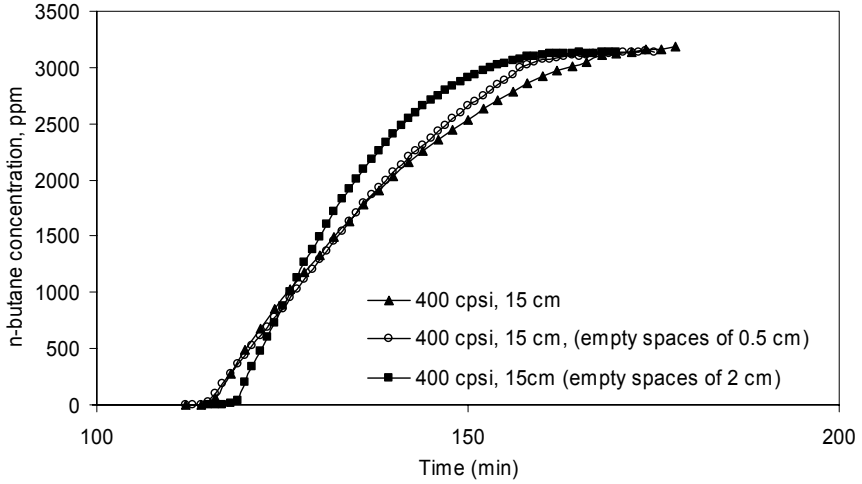

Figure 6. Breakthrough profiles of *n*-butane on carbon coated ceramic monoliths, total length 15 cm; the 5 cm pieces are stacked without empty space and with 0.5 and 2 cm empty space between the pieces.

Another interesting feature is presented in Figure 6. Breakthrough profiles are shown of *n*-butane on carbon coated ceramic monoliths with a total length of 15 cm. The individual 5 cm pieces are stacked without empty space between the pieces and with 0.5 and 2 cm empty space between the pieces. Clearly, empty spaces between the monoliths result in a positive effect on the breakthrough profiles, which become steeper when the empty space is increased. This effect can be related to redistribution of flow between the monolith pieces.

3. Modeling

The gas filter of the presently used gasmasks consists of an activated carbon bed. A two-dimensional mathematical model for physically adsorbed gases was used to describe the dynamic behavior of the activated carbon bed. This model is valid for the adsorption behavior of a vast number of organic contaminants and includes convection, dispersion, external film resistance, macropore diffusion in the sorbent particles, and the Dubinin–Radushkevich model to describe adsorption equilibrium.

A gasmask never fits perfectly, meaning that a certain contribution of leakage is always present. Therefore, apart from the activated carbon filter model a leakage model completes the model of a gasmask. This gas mask model has been implemented in a software tool that simulates chemical and biological incidents.[5] This "Chemical and Biological Incident Simulator" (CABIS) – a chain of linked simulation models (see Figure 7) – simulates the dispersion of chemical and biological warfare agents, detector responses, the effects of protective equipment such as masks and suits, and the human toxicological responses for large numbers of scenarios considered realistic given a certain threat. The ultimate result is an estimation of casualties, varying from mildly affected, severely affected, to the worse category being dead. Next the CABIS model is discussed in somewhat more detail, keeping in mind that the gas mask model is one of its constituent models.

The calculations start by simulating "the agent release and transport" in an incident scenario which results in concentration-time profiles at the locations of detectors and personnel. Figure 8 shows a typical plot of the liquid deposition density on a target area after an attack with a multiple rocket launcher. The detector module generates an alarm-time profile when a chemical or biological agent is detected, an example of which is shown in Figure 9. Based on the concentration-time and alarm-time profiles the skin and respiratory protection models calculate exposure profiles, using given protective equipment characteristics. In this respect Figure 10 shows the influence of wearing respiratory protection on the exposure to sarin.

Finally, the toxic effects module translates the exposure profiles into casualty probabilities for the personnel. Operational behavior, like changes in "Dress State" and typical reaction times are taken into account in the simulations.

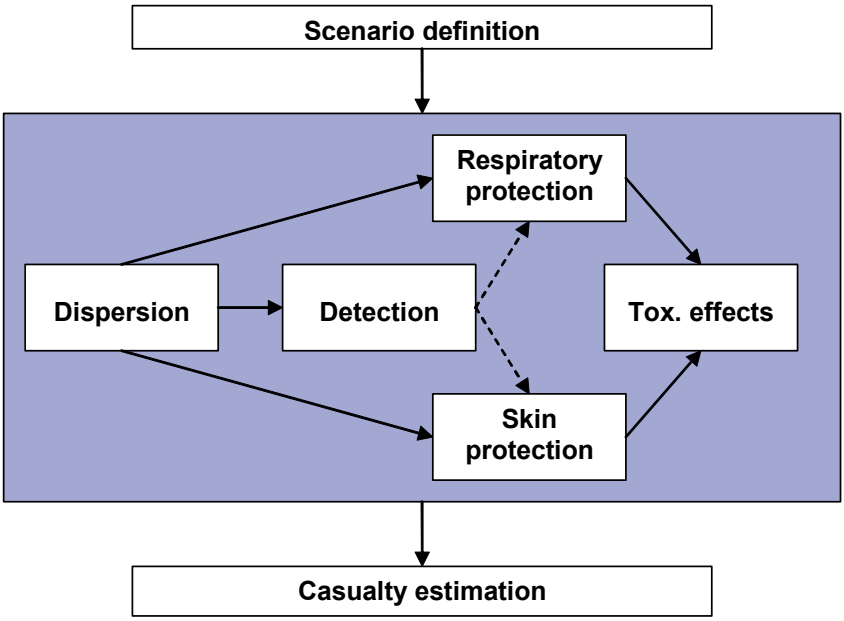

Figure 7. Scheme of the CABIS model chain.

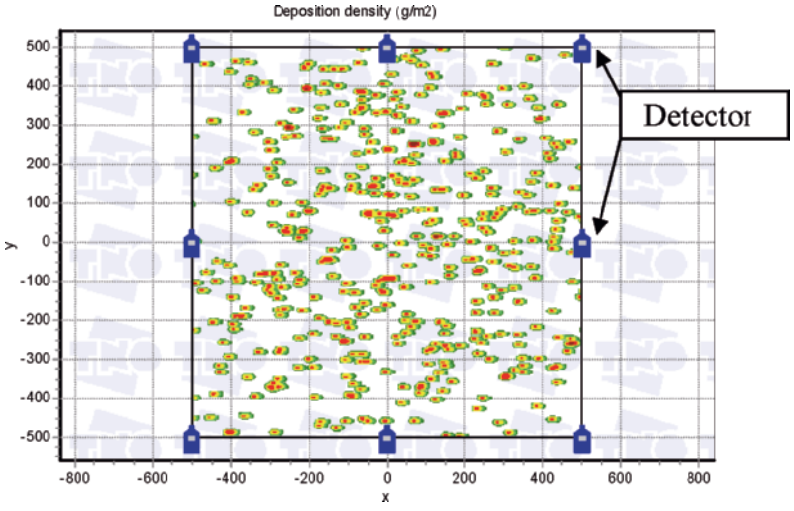

Figure 8. Liquid deposition density of sarin on a target area 500 × 500 m.

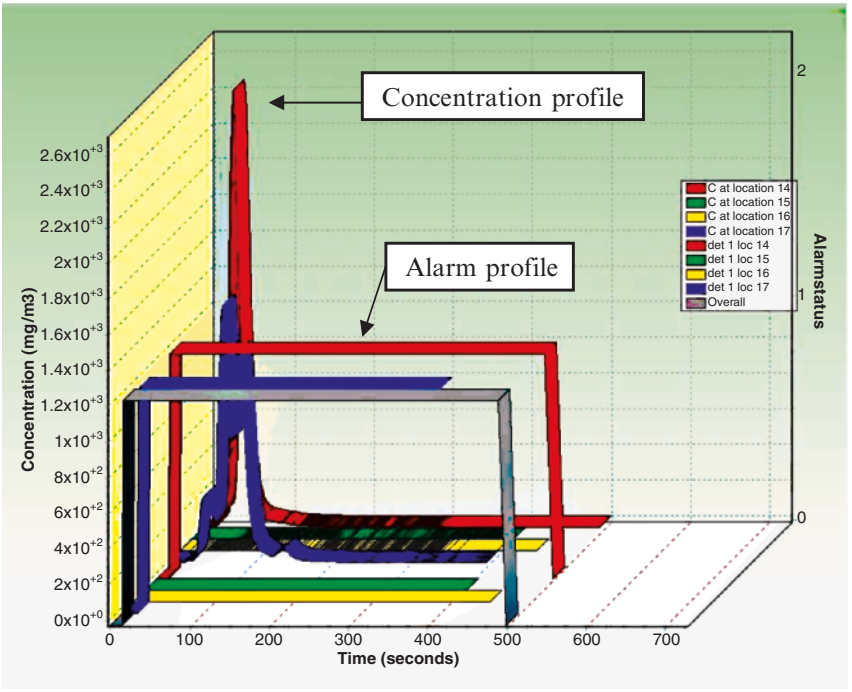

Figure 9. Concentration-time and alarm-time profiles of the individual detectors and the composed overall alarm profile.

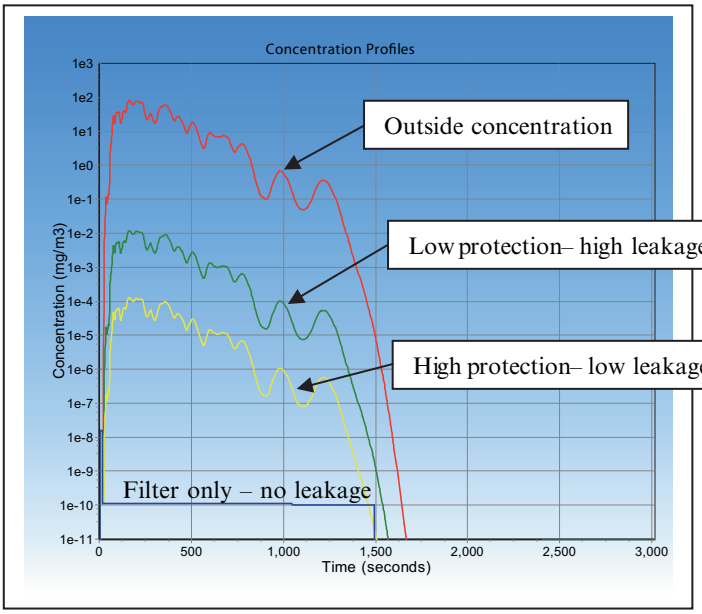

Figure 10. Influence of wearing respiratory protection on the exposure to sarin.

All input parameters, scenario definitions and results are stored in a database for easy access and retrieval. Analysis of individual scenario results and statistical analysis over all scenarios (or any subset) is possible. Typical individual scenario results are the deposition and the dosage on the attacked target, the number of casualties, and the severity of injuries. Typical statistical analysis results are dosage and deposition threat spectra, and casualty spectra. The casualty spectra can be obtained for various health effect levels (eye effect, incapacitation, lethal) and protection levels (no protection, suit only, mask only, mask and suit, collective protection). The CABIS simulation tool thus largely eliminates the subjectivity involved in scenario studies, protective and detector equipment procurement.

Finally, an interesting feature of CABIS is the possibility of distributed computing. This enables many instances of CABIS (running on different computers) to operate simultaneously on scenarios from the same database. A locking mechanism inhibits the write access to one scenario by more than one CABIS instance at a time. In this way a great number of scenarios can be calculated in a short amount of time and multiple users can access scenarios from the same database simultaneously.

Summarizing, the CABIS simulation tool provides useful information on all of the above aspects – dispersion, detection, protection, casualty estimation – as well as on threat analysis, procurement, research policy, and planning operations in order to optimize passive BC defense.

References

1. M.J.G. Linders, E.P.J. Mallens, J.J.G.M. van Bokhoven, F. Kapteijn, and J.A. Moulijn, Breakthrough of shallow activated carbon beds under constant and pulsating flow, *AIHA Journal* 64(2), 173–180 (2003).
2. M.J.G. Linders, P.J. Baak, and J.J.G.M. van Bokhoven, Exploratory investigation of the risk of desorption from activated carbon filters in respiratory protective devices, *Ind. Eng. Chem. Res.* (2007) (accepted for publication).
3. Th. Vergunst, M.J.G. Linders, F. Kapteijn, and J.A. Moulijn, Carbon based monolithic structures, *Catal. Rev.-Sci. Eng.* 43, 291–314 (2001).
4. T. Valdés-Solís, M.J.G. Linders, F. Kapteijn, G. Marbán, and A.B. Fuertes, Adsorption and breakthrough performance of carbon-coated ceramic monoliths at low concentration of n-butane, *Chem. Engng. Sci.* 59(13), 2791–2800 (2004).
5. M.J.G. Linders, C.A. van Beest, P. Brasser, L.F.G. Geers, G. van ‘t Hof, R.A. Rumley-van Gurp, R.P. Sterkenburg, S.C. van Swieten, H.W. Zappey, A.R.T. Hin, Chapter 6: Chemical Incident Simulator: a new approach for deriving passive defence requirements, in: *Medical Treatment of Intoxications and Decontamination of Chemical Agents in the Area of Terrorist Attack*, edited by C. Dishovsky, A. Pivovarov, H. Benschop. NATO Security through Science Series – A: Chemistry and Biology; Proceedings of the NATO Advanced Research Workshop, Ukraine, 2005. Springer, The Netherlands (2006).

HYDROGEN ADSORPTION ON CARBON MATERIALS AT HIGH PRESSURES AND DIFFERENT TEMPERATURES

F. SUÁREZ-GARCÍA,* M. JORDÁ-BENEYTO,
D. LOZANO-CASTELLÓ, D. CAZORLA-AMORÓS,
A. LINARES-SOLANO
Departamento de Química Inorgánica. Universidad de Alicante. Ap. 99, E-03080, Alicante, Spain

Abstract. In this work, we present experimental results corresponding to H_2 adsorption at high pressures and different temperatures (77 and 298 K) for a wide variety of carbons materials in order to analyze the effect of the porosity on the H_2 adsorption capacities in gravimetric basis. Likewise, we point out the importance of the packing density of the materials in order to obtain high H_2 adsorption capacities in volumetric basis and high total storage capacities. At 298 K, the H_2 adsorption capacity depends on both the total micropore volume and the micropore size distribution. At 77 K, H_2 adsorption depends only on the total micropore volume of the carbon material. Packing density of the carbon materials decreases with increasing the porosity development. Therefore, a good balance between porosity and packing density is needed. The total H_2 storage on the best activated carbon at 298 K and 20 MPa is 16.7 g H_2/L and 38.8 g H_2/L at 77 K and 4 MPa.

Keywords: active carbon; hydrogen adsorption; hydrogen storage; packing density

1. Introduction

Development of hydrogen fueled vehicles can bring economical and environmental benefits through a decrease in using oil, and, consequently, a decrease in air pollution and other greenhouse gases. The Department of

*To whom correspondence should be addressed. E-mail: fabian.suarez@ua.es

J.P. Mota and S. Lyubchik (eds.), Recent Advances in Adsorption Processes for Environmental Protection and Security, 165–175.

Energy of the United States (DOE) has established different targets for on-board hydrogen storage systems, including the minimum "gravimetric" and "volumetric" capacity. For the 2010 year, the storage system should have a gravimetric capacity of 2 kWh/kg (6 wt.%) and a volumetric capacity of 1.5 kWh/L (0.045 kg H_2/L). These values are referred to the whole system, including the storage medium, the vessel, the refuelling infrastructure, any regulators, electronic controllers, sensors, and so on (for more information see: www.eere.energy.gov/hydrogenandfuelcells). Therefore, the targets for the storage medium are very high and difficult to achieve.

In this work, we present experimental results corresponding to hydrogen adsorption at high pressures and different temperatures (77 and 298 K) for a wide variety of carbons materials in order to analyze the effect of the porosity on the hydrogen adsorption capacities in gravimetric basis. Likewise, we point out the importance of the packing density of the materials in order to obtain high hydrogen adsorption capacities in volumetric basis and high total storage capacities.

2. Experimental

A wide variety of carbon materials has been used in the present work including: multi-wall carbon nanotubes (provided by Professor Hui-Ming Cheng, Institute of Metal Research Chinese Academy of Science, China); chemically activated multi-wall carbon nanotubes[1]; commercially available vapor grown carbon nanofibers (sample NF); sample NF after chemical activation with KOH; a series of activated carbons prepared from a Spanish anthracite and from Subituminous coal by chemical activation with KOH as described by D. Lozano-Castelló et al.[2,3]; commercially pitch-based carbon fiber (sample CF) from Kureha Company; commercially available activated carbons AX-21 from Anderson Carbon Co., Maxsorb3000 from Kansai Coke & Chemicals and commercial activated carbon fibers A20 from Osaka Gas Co.

Porous texture characterization of all the samples was performed by physical adsorption of N_2 at 77 K and CO_2 at 273 K, using an automatic adsorption system (Autosorb-6, Quantachrome). The micropore volume was determined by application of Dubinin–Radushkevich equation to the N_2 adsorption isotherm at 77 K up to $P/P_0 \leq 0.1$ ($V\mu p\ (N_2)$). The volume of narrow micropores (mean pore size lower than 0.7 nm) was calculated from CO_2 adsorption at 273 K ($V\mu p\ (CO_2)$).

The packing density of the materials was determined by pressing a given amount of activated carbon (0.5 g approximately) in a mould at a pressure of 550 kg/cm^2.[4] The measurements were repeated several times. The densities obtained have an error smaller than 3%.

Hydrogen adsorption measurements were carried out at 298 and 77 K both at high pressures. Hydrogen isotherms at 298 K were carried out in an automatic volumetric apparatus designed and built up in our laboratory to perform hydrogen isotherms up to 20 MPa following the experimental process described previously.[5] The bulk gas amounts have been calculated by the equation of state of Modified-Benedic-Webb-Rubin,[6] and the cell volume has been calculated taken into account the procedure described in the literature.[7]

Hydrogen isotherms at 77 K and up to 4 MPa were carried out in a DMT high-pressure microbalance following the experimental process described previously.[5] The experimental results were corrected for buoyancy effects related to the displacement of gas by the sample, sample holder and pan.[8]

3. Results and Discussion

3.1. POROUS TEXTURE CHARACTERIZATION

The selection of preparation variables during chemical activation with KOH of coals, has allowed obtaining activated carbons with apparent BET surface areas from 1,058 to 3,808 $m^2\ g^{-1}$. The synthesised materials and commercial ones cover a broad range of porosities; their microporore volume calculated from N_2 isotherms ($V\mu p\ (N_2)$) varies from 0 to 1.27 $cm^3\ g^{-1}$ and the microporore volume calculated from CO_2 isotherms ($V\mu p\ (CO_2)$) from 0.18 to 0.72 $cm^3\ g^{-1}$. Moreover, the selected samples present different micropore size distribution (MPSD). For example, the commercial carbon fibre CF presents CO_2 adsorption at 273 K (0.18 $cm^3\ g^{-1}$) but does not adsorb N_2 at 77 K. This is due to the existence of very narrow microporosity (mean pore size around 0.3–0.5 nm, approximately), where N_2 adsorption at 77 K has diffusional limitations.[9,10] On the other hand, there are other materials that present a similar micropore volume calculated from CO_2 and N_2 isotherms, indicating a narrow MPSD with a mean pore size around 0.6–0.7 nm.[9] Finally, there are other samples with $V\mu p\ (N_2) > V\mu p\ (CO_2)$, indicating a wider MPSD with larger mean pore size.[9,10]

Regarding carbon nanotubes (MWCNT) and nanofibers (NF), they have a much lower development of the porosity compared with activated carbons. MWCNT has a BET surface area of 74 $m^2\ g^{-1}$. Chemical activation with KOH increases its BET surface area up to 1,220 $m^2\ g^{-1}$. Also, activation increases the porosity of the NF from 150 to 255 $m^2\ g^{-1}$.

3.2. HYDROGEN ADSORPTION CAPACITIES IN GRAVIMETRIC BASIS

3.2.1. *Hydrogen adsorption at 298 K*

Figure 1 includes the adsorption excess of hydrogen (weight percent) at 20 MPa, versus the total micropore volume (*Vμp (N_2)*) (Figure 1a) and versus the narrow micropore volume (*Vμp (CO_2)*) (Figure 1b).

As a general trend, hydrogen adsorption capacity increases with total micropore volume. However, some deviations to this general trend exist. It can be seen that, at high micropore volume values, the sample with the highest porosity development does not present the highest hydrogen adsorption capacity. The highest hydrogen adsorption capacity value obtained in the present study is 1.2 wt.% and corresponds to the sample which has a very high micropore volume (*Vμp (N_2)* = 1.1 $cm^3\ g^{-1}$) and also a quite narrow MPSD, as it can be deduced for the relatively low value of the difference between *Vμp (N_2)* and *Vμp (CO_2)* (0.38 $cm^3\ g^{-1}$). If the hydrogen adsorption capacity values are plotted versus the narrow micropore volume (*Vμp (CO_2)*) (Figure 1b) a linear trend is also observed. In this case, the sample with higher hydrogen adsorption capacity is the sample with higher narrow micropore volume (*Vμp (CO_2)*). These results point out the importance of developing materials having both high micropore volume and narrow micropore size distribution for the adsorption of hydrogen at room temperature. This conclusion agrees with that obtained in previous papers, which showed that the optimum pore size for hydrogen adsorption on porous carbons is close to 0.6 nm.[11,12]

Carbon nanotubes and nanofibres follow the same trends that activated carbons (see, Figure 1a and b), indicating that hydrogen adsorption on these

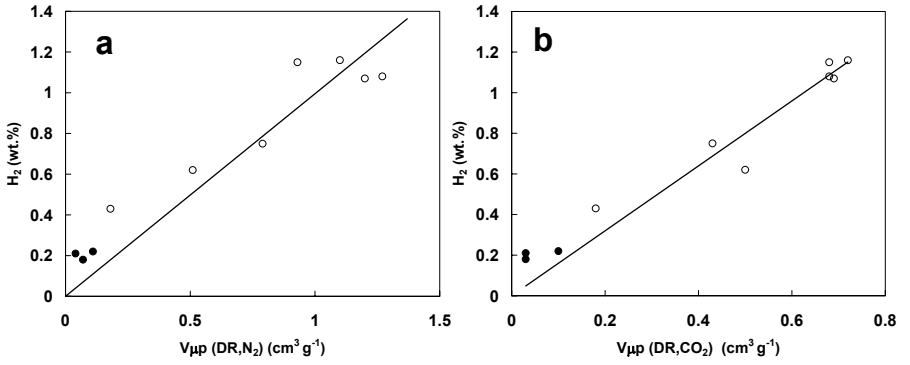

Figure 1. Adsorption excess of H_2 at 298 K and 20 MPa in activated carbons (open symbols) and in carbon nanotubes and nanofibers (closed symbols) versus (a) total micropore volume [*Vμp (N_2)*] or (b) narrow micropore volume [*Vμp (CO_2)*].

materials is also taking place by a physisorption process. Due to their low porosity, these materials present very low hydrogen adsorption capacities compared with activated carbons.

3.2.2. *Hydrogen adsorption at 77 K*

Figure 2 includes the adsorption excess of hydrogen (weight percent) at 77 K and 4 MPa, versus the total micropore volume (Figure 2a) and versus the narrow micropore volume (Figure 2b).

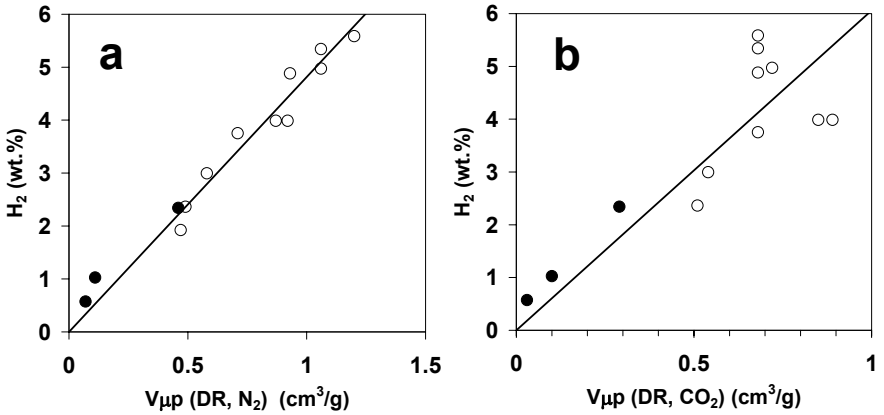

Figure 2. Adsorption excess of hydrogen at 77 K and 4 MPa by activated carbons (open symbols) and carbon nanotubes and nanofibres (closed symbols) versus (a) the total micropore volume and (b) the narrow micropore volume.

As in the case of hydrogen adsorption at room temperature, a linear relationship is obtained between the amount of hydrogen adsorbed at 77 K and the porosity of the samples. As it can be observed in Figure 2a, a good correlation is obtained between the amount of hydrogen adsorbed at 4 MPa and the total micropore volume. However, contrary to the results obtained at room temperature, in this case, the highest adsorption capacity corresponds to the activated carbon with the highest development of porosity. That means that, at 77 K and at the pressure range studied, no effect of the micropore size distribution (MPSD) on the hydrogen adsorption capacity has been observed.

When the hydrogen adsorption capacity at 77 K is plotted versus the narrow micropore volume ($V\mu p\ (CO_2)$) (Figure 2b), it can be seen that, the correlations are worse compared to those with the total micropore volume.

As observed in Figure 2, the results obtained for carbon nanofibers and carbon nanotubes (solid symbols) fit in the tendencies obtained for activated carbons, showing that hydrogen adsorption depends only on the porosity of the sample and does not depend on its morphology.

From these results, it can be concluded that hydrogen adsorption at 77 K and at pressures up to 4 MPa requires porous solids with a very high micropore volume. At these adsorption conditions, the micropore size distribution is not the controlling key point, what is an important difference to the results at room temperature.

These results, both at 298 and 77 K, can be interpreted from the fundamentals of supercritical adsorption. H_2 has a critical pressure (Pc) equal to 1.315 MPa and a critical temperature (Tc) of 33.19 K. That means that, hydrogen adsorption at both temperatures takes place under supercritical conditions and a saturation pressure for hydrogen does not exist. However, it is possible to estimate a "saturation pressure" under supercritical conditions by using different empirical equations,[8] for example, the equation proposed by Dubinin ($P_S = P_C\ (T/T_C)^2$),[8,13] what is useful for a qualitative interpretation of the experimental data. This equation gives a value of P_S = 106 MPa for hydrogen at 298 K and of 7 MPa at 77 K. Using these values of saturation pressure, hydrogen adsorption isotherms can be expressed as a function of relative pressures (P_r). Then, an estimated relative pressures of P_r = 0.19 are reached at 298 K and 20 MPa. Considering this value of relative pressures, it can be understood that, at 20 MPa, there is a correlation between hydrogen adsorption capacity and both total micropore volume and narrow micropore volume of the samples. On the other hand, at 77 K and 4 MPa the estimated relative pressure is of P_r = 0.57 and there is not a correlation between hydrogen adsorption capacity at 4 MPa and the narrow micropore volume ($V\mu p\ (CO_2)$) (see Figure 2b), because at this high relative pressures (P_r = 0.57), not only the narrow micropores, but also the wider microporosity has an important contribution to the hydrogen adsorption.

3.3. HYDROGEN ADSORPTION CAPACITIES IN VOLUMETRIC BASIS

As it was mentioned in the introduction, the hydrogen storage systems not only have to achieve the target in gravimetric basis but also in a volumetric one. From an application point of view it will be much more relevant to compare storage data on a volume-specific rather than on a weight-specific storage capacity basis, because hydrogen storage would be carried out in a material filled vessel. Thus, in addition to the micropore volume and surface area, another important parameter, which has to be taken into account, is the packing density of the materials.

Figure 3 shows the evolution of the packing density of porous carbon materials with their total micropore volume.

The values obtained for the porous carbon materials studied in this work vary between 0.4 and 0.75 cm^3/g. From these results, it can be said that, in

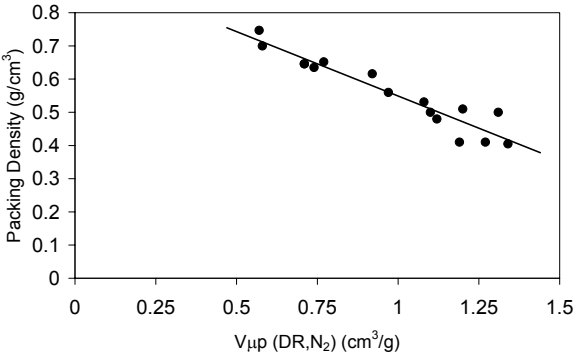

Figure 3. Packing density of the powder activated carbons versus the total micropore volume.

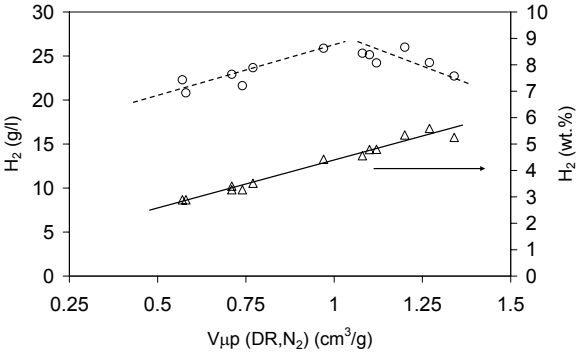

Figure 4. Amount of hydrogen adsorbed at 77 K and 4 MPa (in volumetric and gravimetric basis) versus the total micropore volume.

general, the higher the porosity development of the materials, the lower the packing density, following a linear trend.

Using the values of packing density presented in Figure 3, hydrogen adsorption capacities at 77 K and up to 4 MPa in volumetric, have been estimated and presented in Figure 4 versus the micropore volume.

For comparison purposes, this plot also contains the hydrogen adsorption capacities for these materials in gravimetric basis. As it was indicated in the previous section the hydrogen adsorption capacity in gravimetric basis (wt.%) at 77 K and at pressures up to 4 MPa follows a good correlation with the total micropore volume, obtaining the highest value for the sample with the highest micropore volume. On the other hand, for the data in volumetric basis (g/L) it can be seen that the maximum hydrogen adsorption does not correspond to the sample with the highest micropore volume. The maximum in volumetric basis corresponds to samples with a relatively high porosity

and packing density. Thus, according to these results, in order to get a maximum hydrogen adsorption capacity in volumetric basis we should choose an activated carbon with a good balance between porosity development and packing density or, in other words, an activated carbon with a high micropore volume in volumetric basis [$V\mu p$ *(DR,N$_2$)* (cm^3 g^{-1})] and [packing density (g cm^3)].

3.4. TOTAL HYDROGEN STORAGE AT 298 AND 77 K

The results presented so far, correspond to the adsorption excess of hydrogen on carbon materials at different temperatures and pressures. However, a more important parameter from an application point of view, which is rarely found in the literature, is the total storage capacity, the available H_2 stored in the tank that can be used in the car. The total storage capacity in a specified volume filled with an adsorbent is the sum of the capacity due to adsorption on the solid surface and the volumetric capacity due to compression in the void space.[14] The void space per unit volume can be assessed by: $V_s = 1 - \rho_p/\rho_s$,[4,14,15] where ρ_p is the packing density and ρ_s is the skeleton density of adsorbent, determined by the helium expansion method.

Figure 5 includes the total hydrogen storage capacity of the best activated carbon prepared in this work at 298 and 77 K on the basis of a 1 L container. This figure also includes the amount of hydrogen stored just by compression and the adsorption excess data on volumetric basis.

It can be seen that storage of hydrogen at 298 and 77 K achieves considerable enhancement due to both adsorption and compression. The total storage capacity of a 1 L container filled with this activated carbon is 16.7 g H_2 (3.2 wt.%) at 20 MPa and 298 K and 38.8 g H_2 (8 wt.%) at 4 MPa and 77 K. It is remarkable that the total storage capacity obtained at 77 K (38.8 g H_2/L or 8 wt.%), which is very close to the volumetric target proposed by the DOE (45 g H_2/L) and higher than ones of the European

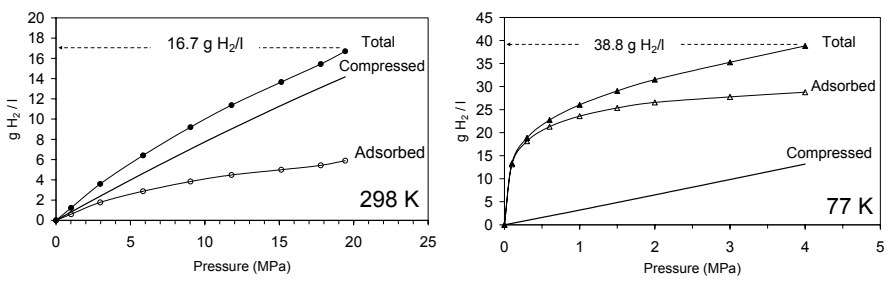

Figure 5. Total hydrogen storage capacity of the best activated carbon prepared in this work on the basis of a 1 L container at 298 and 77 K.

Hydrogen & Fuel Cell Technology Platform (about 33 g H_2/L).[16] This high value indicates that adsorption at 77 K in activated carbons is a promising method for hydrogen storage.

4. Conclusions

The results obtained at 298 K for carbon materials indicate that the hydrogen adsorption capacities in gravimetric basis up to 20 MPa depend on both micropore volume and micropore size distribution. The results obtained with carbon nanofibers and nanotubes fit into the tendencies obtained with the other type of carbon materials, indicating that hydrogen adsorption on these materials is also taking place by a physisorption process. At 298 K and 20 MPa, the sample with the best hydrogen adsorption capacity is an activated carbon, which has both high micropore volume and narrow micropore size distribution.

Hydrogen adsorption capacity in gravimetric basis at 77 K and at pressures up to 4 MPa follows a good correlation with the total micropore volume for all the samples, including carbon nanofibres and carbon nanotubes. These results indicate that hydrogen adsorption depends on the porosity of the sample and does not depend on its morphology. The results obtained for the series of carbon materials analyzed point out that, at these adsorption conditions, micropore size distribution does not play an important role, contrary to what happened at room temperature.

From an application point of view, not only the gravimetric target has to be achieved but also the volumetric one. For this reason it is necessary to know the packing density of the materials. The packing density of the carbon materials decreases with increasing the porosity development. Therefore, the hydrogen adsorption capacity, expressed per unit of volume, goes through a maximum. Thus, the samples with the highest porosity do not present the best volumetric performance, but the samples with a relatively high porosity and packing density give the best values. Therefore, a good balance between porosity development and packing density is needed.

The highest total hydrogen (adsorbed plus compressed) stored at room temperature and 20 MPa is 16.7 g H_2/L (3.2 wt.%). The best value of total hydrogen storage capacity obtained in the present work at 77 K and 4 MPa was 38.8 g H_2/L (8 wt.%). These high values obtained remark the importance of developing materials with suitable porosity and high packing density for this application.

It has been shown that highly activated carbons have a great potential as carriers of hydrogen. On the other hand, carbon nanotubes and carbon nanofibers are not promising storage media for hydrogen from an application

point of view, contrary to what is concluded from many results published in the literature.

Acknowledgements

Authors thank financial support from Ministerio de Fomento (70012/T-05), MEC (ENE2005-23824-E/CON and CTQ2006-08958) and Generalitat Valenciana (ACOMP06/089). F. Suárez-García thanks MCYT for his contract "Juan de la Cierva" and M. Jorda-Beneyto thanks MEC for her Ph.D. fellowship.

References

1. E. Raymundo-Pinero, P. Azais, T. Cacciaguerra, D. Cazorla-Amoros, A. Linares-Solano and F. Beguin, KOH and NaOH activation mechanisms of multiwalled carbon nanotubes with different structural organization, *Carbon* 43(4), 786–795 (2005).
2. D. Lozano-Castello, M.A. Lillo-Rodenas, D. Cazorla-Amoros and A. Linares-Solano, Preparation of activated carbons from Spanish anthracite I. Activation by KOH, *Carbon* 39(5), 741–749 (2001).
3. D. Lozano-Castelló, *Preparación y Caracterización de materiales carbonosos avanzados para la separación de gases y el almacenamiento de gases y energía*, Universidad de Alicante, Alicante, Spain, Ph.D. thesis (2001).
4. D. Lozano-Castello, D. Cazorla-Amoros, A. Linares-Solano and D.F. Quinn, Influence of pore size distribution on methane storage at relatively low pressure: preparation of activated carbon with optimum pore size, *Carbon* 40(7), 989–1002 (2002).
5. M. Jordá-Beneyto, F. Suárez-García, D. Lozano-Castelló, D. Cazorla-Amoros and A. Linares-Solano, *Carbon* 45(2), 293–303 (2007).
6. C. Zhang, X.S. Lu and A.Z. Gu, How to accurately determine the uptake of hydrogen in carbonaceous materials. *Int. J. Hydrogen Energy* 29(12), 1271–1276 (2004).
7. T. Kiyobayashi, H.T. Takeshita, H. Tanaka, N. Takeichi, A. Zuttel, L. Schlapbach and N. Kuriyama, Hydrogen adsorption in carbonaceous materials – How to determine the storage capacity accurately, *J. Alloy. Compd.* 330–332, 666–669 (2002).
8. R.K. Agarwal and J.A. Schwarz, Analysis of high-pressure adsorption of gases on activated carbon by potential-theory, *Carbon* 26(6), 873–887 (1988).
9. D. Cazorla-Amoros, J. Alcaniz-Monge, M.A. de la Casa-Lillo and A. Linares-Solano, CO_2 as an adsorptive to characterize carbon molecular sieves and activated carbons, *Langmuir* 14(16), 4589–4596 (1998).
10. F. Rodriguez-Reinoso and A. Linares-Solano, in: *Chemistry and Physics of Carbon*, vol. 21, edited by P.A. Thrower (Marcel Dekker, New York, 1989), pp. 1–146.
11. M. Rzepka, P. Lamp and M.A. Casa-Lillo, Physisorption of hydrogen on microporous carbon and carbon nanotubes, *J. Phys. Chem. B* 102(52), 10894–10898 (1998).
12. S. Patchkovskii, J.S. Tse, S.N. Yurchenko, L. Zhechkov, T. Heine and G. Seifert, Graphene nanostructures as tunable storage media for molecular hydrogen. *Proc. Natl. Acad. Sci. USA* 102, 10439–10444 (2005).

13. M.M. Dubinin, in: *Progress in Surface and Membrane Science*, vol. 9, edited by D.A. Cadenhead, J.F. Danielli and M.D. Rosemberg (Academic Press, New York, 1975), pp. 1–70.
14. L. Zhou, Y.P. Zhou and Y. Sun, Enhanced storage of hydrogen at the temperature of liquid nitrogen. *Int. J. Hydrogen Energy* 29(3), 319–322 (2004).
15. D. Lozano-Castello, J. Alcaniz-Monge, M.A. de la Casa-Lillo, D. Cazorla-Amoros and A. Linares-Solano, Advances in the study of methane storage in porous carbonaceous materials, *Fuel* 81(14), 1777–1803 (2002).
16. S. Barrett, Patent analysis identifies trends in fuel cell R&D. *Fuel Cells Bull.* 2005, 12–13 (2005).

ADSORBED NATURAL GAS TECHNOLOGY

JOSÉ P. B. MOTA*
Requimte/CQFB, Departamento de Química, Faculdade de Ciências e Tecnologia, Universidade Nova de Lisboa, 2829-516 Caparica, Portugal

Abstract. The current status of adsorbed natural gas technology for the vehicle fueling sector is reviewed. It is shown that there are solutions to the all of the problems associated to adsorption storage, and that it is possible to build a light, compact, and efficient system for storage, distribution, and dispensing of natural gas. The practical achievement of this objective is essential for the natural gas vehicle to create a strong and sustained interest of the automotive market.

Key words: Natural gas; adsorption storage; gaseous fuels; natural gas vehicles

1. Natural Gas as an Alternative Fuel

The use of alternative fuels in the transportation sector is the best short- and medium-term options to lower urban pollution and our current dependence on oil. From the currently available alternatives, natural gas (NG) is clearly the more advantageous one due to its environmental friendly behavior, and because it is a truly and effective alternative to oil-derived fuels [1].

- **A clean fuel**. NG provides a clean and efficient combustion, practically free of sulphur and lead oxides, benzene, and solid particles. The CO_2 emission level is 23% less than that of conventional vehicles and the CO emission level can be reduced by 85%.
- **Cheaper than gasoline and diesel fuels**. Although there is no uniform price list for natural gas in the transportation sector across Europe, the experience in countries where natural gas vehicles (NGV) are well spread has shown that the price of NG is, at least, half of the equivalent price of gasoline.

J.P. Mota and S. Lyubchik (eds.), Recent Advances in Adsorption Processes for Environmental Protection and Security, 177–192.

TABLE 1. Estimated number of natural gas vehicles and NG refueling stations in several countries. These numbers are continuously increasing, propelled by policies of energy savings and environmental protection.

Country	NGVs	Refueling stations	Country	NGVs	Refueling stations
Argentina	385,500	504	Brazil	14,000	39
Italy	290,000	280	Colombia	4,600	22
USSR	205,000	187	Indonesia	3,000	12
USA.	40,000	1102	India	2,500	6
New Zealand	25,000	245	Pakistan	2,500	12
Canada	17,220	120	Germany	2,415	55
Total in 48 countries: ±1,002,625 NGVs, ±2,789 refueling stations.					

- **Efficient**. Because the octane index of NG is much higher than that of gasoline, the performance of motors running 100% on NG can be increased by at least 15% through higher compression rates.
- **Safer and nontoxic**. As opposed to the other currently available fuels, natural gas is less dense than air, which makes it spread in the case of a leak. As a consequence, natural gas vehicles are not subject to any restrictions in underground parking. In countries where NG is used as a vehicle fuel, there has never been reported any disaster due to its use.

It is estimated that there exists currently over one million NG vehicles (Table 1). This amount still represents a small proportion of the total number of existing vehicles, but it is steadily increasing propelled by policies of energy savings and environmental protection. This fuel is widely spread in several countries, some of them having large fleets and governmental programs to stimulate the reconversion of traditional fleets.

Most NG vehicles have been converted to dual-consumption, in which they are able to run on both gas and gasoline [2]. This operating mode has the advantage of not reducing the driving range of the vehicle when the number of NG refueling stations is limited. The conversion has, nevertheless, the inconvenience of not taking full profit from the specific combustion characteristics and lower pollutant emissions of NG. Currently, technological developments are targeted towards building vehicles running exclusively on NG.

2. Advantages of Low-Pressure Storage

For the NG vehicle to stir up a strong and sustainable interest of the transportation market, it must compete with conventional vehicles in terms of economy, performance and ease of use, because the price of fuel is not the

only determining market factor. For this aim to be achievable, the system for storage, distribution, and utilization of NG must be economic, light, compact, and efficient.

Natural gas is a gaseous fuel because its main component – methane – cannot be liquified at ambient temperature. As a consequence, the energy content of natural gas on a volume basis is low. Currently, NG must be stored under compressed form at pressures in the range 180–240 atm, to be stored compactly and dispensed quickly.

The equipment employed in high-pressure compression storage systems is costly, bulky, heavy, and complex, compared to that of storage and distribution of liquid fuels from oil. The cost of the compression equipment, storage reservoirs and high-pressure metering equipment, corresponds to about 50% of the total investment required to convert a fleet of vehicles to NG operation.

The high cost of private refueling stations has discouraged fleet operators to opt for NG. On the other hand, the individual consumer is not interested in converting his vehicle to dual-fuel operation, and even less to NG only, unless there is a substantial network of NG refueling stations. Lastly, the private sector is apprehensive to invest on the construction of public NG refueling stations as long as the NGV market stays small.

The need to substantially reduce the maximum storage pressure, for safety reasons and the high-pressure compression cost, has led to the search for competitive storage alternatives for NG at pressures well below that employed in traditional compression. The maximum operating pressure value that has reached a large consensus is of the order 35–40 atm, although a few researchers suggest even lower values (21 atm). The maximum operating pressure in this range of values reduces considerably the cost of building and operating a NG refueling station. In places close to the NG residential network, the gas can be compressed to 35 atm by a single-stage compressor, which allows for the construction of small refueling stations at a reduced cost. In the outskirts of metropolitan areas, the servicing stations can refuel the vehicles directly from the high-pressure gas distribution network without the need for compression equipment.

3. Adsorption Storage

The most promising method for NG storage at low pressure is adsorption storage [3, 4], which consists of retaining the gas inside a porous adsorbent. Due to the strong attractive surface forces of the adsorbent, the distance between gas molecules inside the pores of the adsorbent is much shorter that of the molecules of the compressed gas at the same pressure. For this reason, the density of the gas contained inside the pores of the adsorbent is

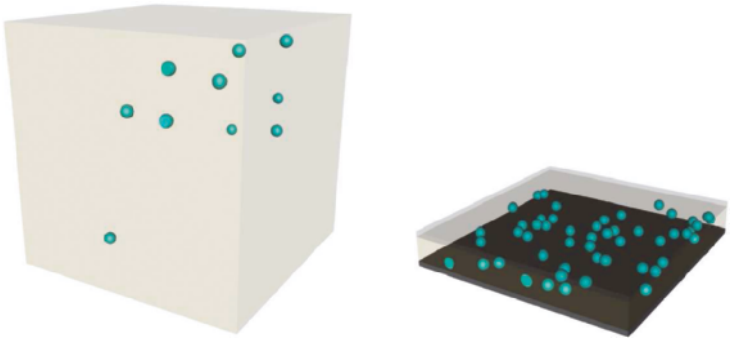

Figure 1. Molecular simulation of methane adsorption (P = 1 atm, T = 298 K) in a graphitic slit-shaped pore of width 10 Å: (a) gaseous phase (ρ_{CH4} = 0.67 kg/m^3); (b) adsorbed phase (ρ_{CH4} = 27.4 kg/m^3). The attractive forces exerted by the adsorbent reduce the distance between the gas molecules inside the pores, thereby increasing considerably the density of the adsorbed phase.

much higher than the density of the compressed gas. This way, the storage capacity can be increased.

Any porous solid whose average pore diameter is smaller than 2 nm (2×10^{-9} m) can adsorb gas in an amount which is proportional to its pore volume. Activated carbons, due to their large microporous volume, their ability to be efficiently compacted and their low production cost, are the adsorbents with the most favorable characteristics for NG storage [5]. These adsorbents are usually produced under the form of small particles by the carbonization of several precursors, such as coal, organic matter (wood, fruit shell, resin), and polymeric matter.

There are currently several commercial activated carbons that can store at a pressure of 35 atm the same amount of gas that is stored by compression at a pressure 2.5 times larger. With the advancement of materials sciences in the fields of adsorbent production and modification, is is expected that in the near future it will be possible to store an amount close to that obtained by standard compression of the gas at 130–150 atm.

Molecular simulation of methane adsorption in a model carbon adsorbent made of parallel graphite plates has enabled us to predict the optimum pore size that maximizes the density of the stored gas (Figure 1). Under these ideal conditions, a storage reservoir by adsorption at 35 atm has a storage capacity of 137 v/v, if the carbon is in granular form, and 195 v/v if the carbon is compacted to form a monolith [6] (Table 2; see Table 3 for comparison with other fuels). The actual production of such ideal carbon is a technological challenge that has not yet been attained.

TABLE 2. Comparison of the net capacity of various NG storage systems. The capacity is usually measured on a volume basis because the limiting factor is the available storage space in the vehicle. The more commonly employed quantifier is defined by the volume of NG, measured under normal pressure and temperature conditions, that is stored per unit volume of reservoir (v/v).

Storage method	Charge pressure (atm)	Net capacity (v/v)
Pure compression	207	216
A.C. granular	35	137 theoretical
A.C. monolith	35	195 limit
Target to achieve	35	150
A.C. granular	35	110 obtained in
A.C. monolith	35	140 laboratory

A.C. = activated carbon.

4. The Adsorbent

In a NG storage reservoir by adsorption there are four distinct zones where the gas density is substantially different (Figure 2):

- The void volume between adsorbent particles, where the gas is compressed at the pressure of the reservoir
- The macroporous and mesoporous volumes of the adsorbent, where the density of the gas is not significantly higher than that of the compressed gas in the void volume
- The volume taken by the solid matrix of the adsorbent, which does not contribute for storage
- The microporous volume of the adsorbent, where most of the stored gas is located. The density of the adsorbed gas in the micropores must compensate for the volume taken by the adsorbent and for the lower density of the gas in the void volume between particles and in the macropores and mesopores of the adsorbent.

There are several aspects that must be taken into account in the evaluation of an adsorptive storage reservoir. The more relevant ones are those related to the internal structure of the adsorbent. For example, it is clearly

TABLE 3. Energy density of various vehicular fuels.

Natural gas								
Liquid fuels						ANG		
Diesel	Gasoline	Methanol	LPG	LNG	CNG	Actual	Future	Cell
37	32	16	29	23	9.7	5.8	6.7	0.2–0.3

LPG: liquefied petroleum gas; LNG: liquefied natural gas at –160°C; CNG: compressed natural gas at 200 atm; ANG: adsorbed natural gas at 35 atm; Cell: Pb/acid and Ni/Cd.

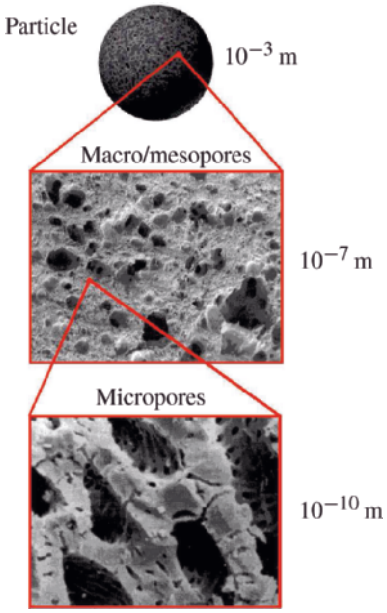

Figure 2. Characteristic dimension of the various existing volumes in an adsorptive storage reservoir.

advantageous that the existing microporous volume in the reservoir be as large as possible. The distribution of the porous volumes among the various spatial scales of the reservoir depends on the following characteristics of the adsorbent:

- The specific microporous volume, usually expressed in cubic centimeter per gram of adsorbent
- The packing density of the adsorbent bed, expressed in grams of adsorbent per cubic centimeter of storage volume.

There are other characteristics of the adsorbent which are related to the operation of the reservoir. For example, the adsorbent must not break nor produce fine particles easily if subjected to long-term vibration conditions, such as when the vehicle is running. Since the fine particles are easily dragged with the gas during the discharge of the reservoir, they can damage various component of the engine. These operating restrictions reduce the range of candidate precursors for the production of carbons with high storage capacity and of activating processes to increase the microporous volume.

The format and the compaction of carbons is extremely important in adsorptive storage. The two more widely employed methods of packing carbon beds are:

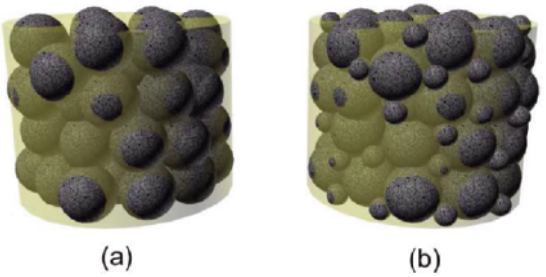

Figure 3. Virtual image that shows the effect of mixing to efficiently pack a carbon bed: (a) carbon packing with a uniform particle size distribution; (b) carbon packing with a bimodal particle size distribution. The smaller particles are usually obtained by breaking and sieving the larger ones under controlled conditions. This process can increase the bed density by about 30%.

- Mechanical stirring for the production of beds with adsorbents of multiple dimensions
- The compaction of fine carbon particles under the form of monoliths.

The first method, is easy to implement and is very effective in practice [3]. By packing particles with two different sizes, in the correct proportion, can increase the bed density by about 30% (Figure 3). The smaller particles are usually obtained by crushing and sieving in a controlled manner the larger ones. It is not advisable to employ multiple-size carbon beds because, although there is an additional increase of storage capacity, the smaller particles are too fine which may lead to operational problems.

The production of monoliths, although it is technically more complicated, leads to the most compacted carbon beds [5]. The procedure is basically that of mechanically pressing at high pressure (2,000 atm) a mixture of fine carbon particles with an aqueous solution of a binding polymer, and then removing moisture by heating. The monoliths are normally produced in the form of small disks with the same shape as that of the cross section of the reservoir. By superposing the discs it is possible to completely fill the reservoir.

5. Adsorption Isotherm

Despite the presence of the adsorbent inside the reservoir, its operation is identical to that of a regular compression tank. The pressure inside the reservoir decreases progressively with fuel consumption.

The operation of the reservoir under vacuum conditions is not easily and economically achievable onboard a vehicle. The impediment for this is that the gas can only flow to the combustion chamber if the tank pressure is higher than that of the engine. For this reason, the reservoir is considered depleted when its pressure attains a value which is slightly above atmospheric (1.2–1.4 atm).

Due to this operational constraint, adsorptive storage poses a challenge which is directly related to the shape of the adsorption curve. As opposed to compression storage, the amount of stored gas by adsorption does not vary linearly with pressure: the adsorption curve is concave, showing a steeper slope in the region of lower pressures (Figure 4). As a consequence, a significant amount of gas remains in storage when the pressure attains its minimum operating value [7]. Depending on the adsorbent, the amount of undelivered gas can total up to 30% of the amount stored at charge pressure (35 atm).

For this reason, a carbon which adsorbs a large amount of NG at charge pressure (35 atm), is not necessarily a good candidate for a storage reservoir. In fact, what defines the available (net) capacity of the reservoir is the difference between the amount of gas stored at charge pressure and that stored at depletion pressure (Figure 4).

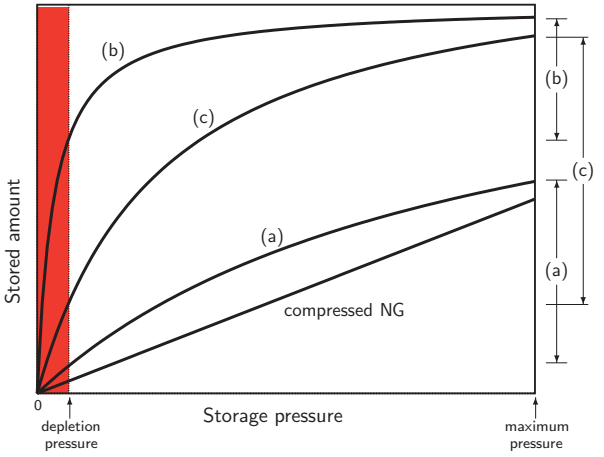

Figure 4. Adsorption storage curves for three different adsorbents. The reservoir represented by curve (a) has a total capacity which is not enough; the system characterized by curve (b) has an insufficient net deliverable capacity although its total capacity is large; the reservoir represented by curve (c) has more desirable characteristics.

A promising solution to reduce the effect of depletion pressure is to introduce a gaseous additive in the NG that can selectively compete with it for the available space in the micropores [8]. If the affinity of the carbon towards the additive over natural gas decreases with increasing pressure, then the net result is an increase of the deliverable capacity of the reservoir.

In practice, this method corresponds to artificially changing the shape of the adsorption curve by introducing a competitive species. The optimum operating conditions depend on the nature and concentration of the additive. An inherent difficulty associated to this method is that the additive is dragged by the discharge stream and has to be reintroduced into the reservoir during the subsequent charge.

6. Thermal Effects During Refueling of the Reservoir

The adsorption of a gas is highly temperature dependent: the amount of adsorbed gas decreases with increasing temperature. Therefore, the storage capacity of an adsorptive reservoir decreases with increasing temperature. On the other hand, physical adsorption is an exothermic process: the adsorption of a gas releases heat. In the specific case of NG adsorption on activated carbon, there is a significant amount of heat (17 kJ/mol) that is released.

If the reservoir is quickly charged, the bed temperature will increase considerably. Less gas will be stored, which has a negative impact on capacity. Computer simulations have shown that in a quick charge the temperature inside the carbon bed can increase by 55°C, reducing the capacity by about 25% with respect to an isothermal charge [9]. This prediction has been confirmed experimentally [10].

The ideal charge should be carried out with a sufficiently small feed flow rate in order to allow the heat of adsorption to dissipate to the environment. This way, one would prevent the undesirable heating of the reservoir and its consequent capacity loss. Unfortunately, this process cannot be widely applicable in practice because the duration of a refueling operation cannot be excessively long (below 10 min), otherwise NG would loose competitiveness against liquid fuels which require very short refueling times.

There are, however, a few transportation sectors where the above-mentioned procedure can be applied. These are fleets whose normal driving range is predefined, as is the case of public transportation. Usually, the dimension and consumption level of such type of fleets justifies the investment on the construction of small private refueling stations. In these cases, the reservoirs can be charged overnight which would provide enough time to dissipate the heat of adsorption.

A solution that can be applicable to a quick refueling consists of an external recirculation of the charged gas to remove the heat of adsorption. During the charge of the reservoir, the gas at 35 atm is continuously recirculated through the reservoir in a closed loop. The heat released by the adsorption process is removed from the reservoir by the circulating gas and released to the environment through a heat exchanger and a cooler (Figure 5).

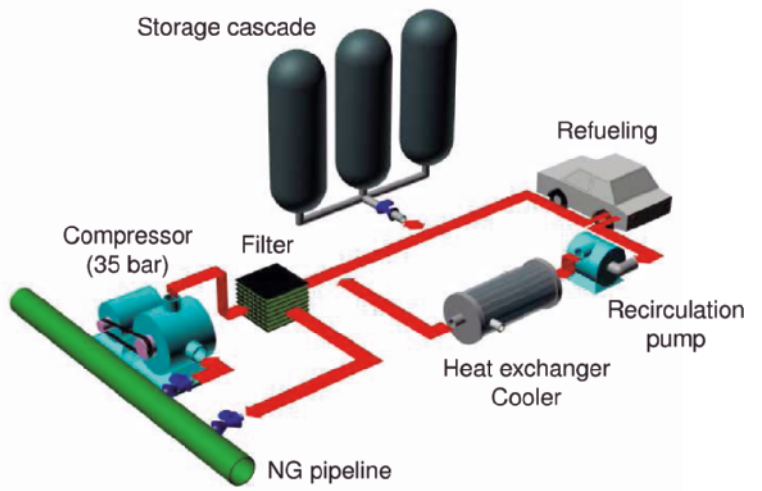

Figure 5. Schematic drawing of a natural gas refueling station. The gas supplied by the residential network flows across a filter, to retain the heavier components and prevent the poisoning of the carbon bed, and is charged into the reservoir. The heat released by the adsorption process is removed by the recirculating gas and dissipated to the environment.

An alternative method to control temperature is to introduce into the reservoir an encapsulated material (usually an inorganic salt) that changes phase at ambient temperature and that has a high heat of fusion. With the phase change form solid state to liquid, the material absorbs the heat of adsorption, acting like a surge for temperature changes [7].

The use of a phase-change material has, however, the disadvantage of reducing the available volume for the carbon bed. Consequently, there is an optimum amount of phase-change material that maximizes the storage capacity. This method has been studied both experimentally and computationally. Although it is appealing, it has some disadvantages such as the high cost of the phase-change material and its possible degradation when subject to a large number of cyclic phase-changes.

7. Thermal Effects During Discharge of the Reservoir

During discharge of the reservoir the desorption of the gas consumes energy. This consumption gives rise to a decrease in the temperature of the reservoir. If the gas discharge rate is not sufficiently slow, or if the heat of adsorption is not resupplied to the reservoir, the temperature drops (Figure 6), thereby increasing the residual amount of gas that remains in storage a depletion pressure [7]. The net deliverable capacity will decrease. It should be noted that this problem cannot be solved by manipulating the discharge flow rate, because this variable is controlled by the power requirements of the engine.

Probably the best way to solve this problem is to employ the energy content of the exhaust gas, which leaves the engine at high temperature, in order to compensate for the heat of adsorption consumed during discharge [11]. The usual course of the exhaust gas is altered, before it is expelled to the environment, by forcing it to flow along a jacket that raps the reservoir, along which the hot gas transfers heat to the carbon bed in contact with the internal wall of the reservoir (Figure 7). From the environmental point of view, this process has the added advantage of reducing the temperature of the expelled exhaust gas.

In traditional storage cylinders the gas flows axially. This means that radial heat transfer across the carbon bed takes place solely by conduction. In this case, the low thermal conductivity of the carbon bed acts as a heat

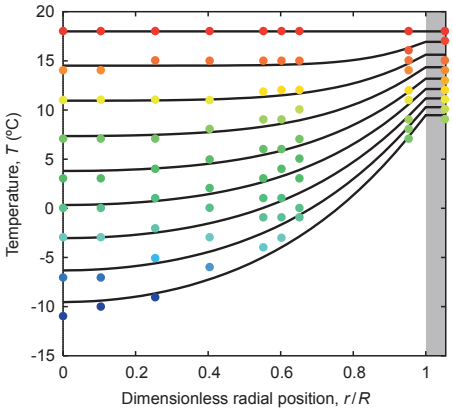

Figure 6. History of radial temperature profile during discharge of a methane adsorptive storage cylinder. Symbols represent experimental temperature measurements at radial locations in the reservoir, taken every 20 min; the curves are the prediction of a simulation model of the reservoir. Cylinder dimensions: L = 74 cm, D = 20 cm; amount of carbon = 15.78 kg; discharge flow rate = 6.7 L/min.

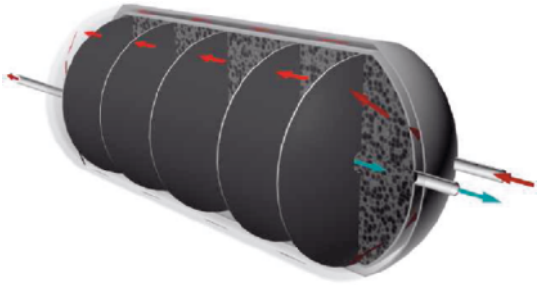

Figure 7. Virtual image of a natural gas storage reservoir with temperature control system. The heat of adsorption consumed during discharge is compensated by the energy of the exhaust gas. Heat transfer to the carbon be takes place whilst the gas is flowing along the jacket wrapping the cylinder. (•: natural gas; •: exhaust gas.)

transfer resistance, thereby limiting the usefulness of the thermal capacity of the cylinder wall and the energy of the exhaust gas. This problem can be somewhat reduced by introducing internal fins that increase the conductive heat transfer and change the flow direction from axial to radial (Figure 8). Convective heat transfer to the center of the reservoir is, thereby, enhanced.

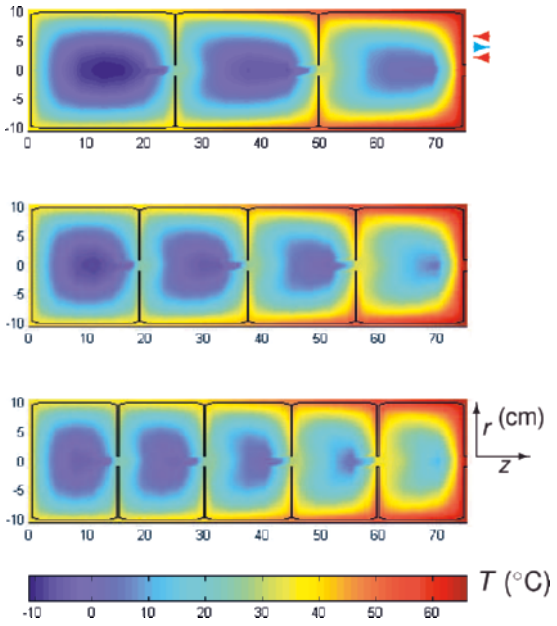

Figure 8. Temperature profiles inside a natural gas adsorptive storage cylinder with external recirculation of the exhaust gas and internal finning; the profiles refer to the end of the discharge. If the gas flows into the jacket at a temperature of 80°C, the net storage capacity of the system is identical to that of an isothermal system. L = 74 cm, D = 20 cm, thickness of annular space of the jacket = 5 mm, fin thickness = 2.5 mm.

8. Effect of Natural Gas Composition

Besides methane, which is the main component in a proportion usually above 90%, natural gas contains small amounts of nitrogen, carbon dioxide, and decreasing volumetric percentages of other hydrocarbons with an increasing number of carbon atoms: ethane, propane, butane, pentane, etc. (Table 4).

TABLE 4. Chemical composition (%-vol) of natural gas that Portugal imports from the Algerian Hassi R'Mel well. (Gás de Portugal.)

Methane	CH_4	83.7%	Propane	C_3H_8	1.9%
Ethane	C_2H_6	7.6%	Butane	C_4H_{10}	0.7%
Nitrogen	N_2	5.4%	Pentane	C_5H_{12}	0.2%

Like methane, the other hydrocarbons are also adsorbed in the micro-porous volume of the carbon during refueling of the reservoir. However, the higher hydrocarbons, due to their higher adsorption potential, are easily desorbed during discharge. As the number of refueling and discharge cycles increases, the higher hydrocarbons progressively occupy the available micro-porous volume of the carbon which should be filled with methane [12]. This gives rise to a decrease of the net storage capacity of the reservoir (Figure 9).

In order to solve this problem, it is necessary an efficient and economic means of controlling the contaminants that are introduced into the reservoir during charge. The most economical solution is to install a purification system for natural gas at the refueling station [13]. The filter is quite simply a carbon bed because, as has been referred, it preferentially retains the higher hydrocarbons over methane.

The net capacity of the *i*th component (1 = CH_4, 2 = C_2H_6, . . .) is defined as η_i

$$= \begin{pmatrix} \text{Amount of } i \\ \text{available in} \\ \text{practice} \end{pmatrix} \begin{pmatrix} \text{amount of} \\ \text{pure } CH_4 \\ \text{available} \\ \text{isothermallt} \end{pmatrix}^{-1} \cdot z_i^{-1},$$

where z_i is the mole fraction of species i in the source gas. η_{1-5} groups all hydrocarbons (HCs) and gives the total net capacity of the reservoir, because all HCs are combustibles. After many cycles the tank attains a cyclic steady state.

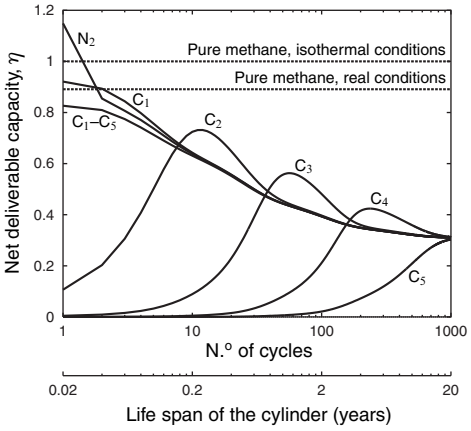

Figure 9. Decrease of storage capacity with the number of charge/discharge cycles, due to the effect of gas composition given in Table 4.

The carbon for this guard bed should, nevertheless, have slightly larger pores than those of the carbon employed in the storage tank. This way, kinetic effects that could degrade the selectivity of the guard bed are avoided. Regeneration is done by heating in an inert atmosphere.

9. The Adsorptive Storage Reservoir

In the design of an adsorptive storage reservoir, several factors should be taken into account. The more relevant ones are:

- Reduction of storage pressure
- Efficient use of the available storage space in the vehicle, a well as ease of installation

- Lightness in order not to penalize the energetic consumption
- Ease of construction
- Safety and certifiability as any commercial tank for compression storage.

The wall of a reservoir for compression storage must withstand the charge pressure during the expected operating life of the vehicle. As a safety precaution, the reservoir is always over-dimensioned to withstand a burst pressure of 2.5 times its normal charge pressure. In compressed gas storage, the high storage pressure forces the use of cylindrical reservoirs. But this geometry is not the most efficient one from the point of view of profiting from the available space in the vehicle.

Traditionally, steel has been the more commonly used material in the manufacture of pressurized tanks. With the emergence of composite materials, the weight of the reservoirs has substantially decreased. The most economic solution in terms of weight is a body with walls of reduced thickness made of aluminium reinforced by a fibrous composite high tensile strength, such as glass fiber. The use of these composite materials can reduce the weight of the tank by as much as 40%.

One advantage of adsorption storage is that its charge pressure is sufficiently low that does not restrict the shape of the reservoir to be cylindrical. This degree of freedom can be profitably used to maximize the storage space onboard the vehicle.

The proposed solution is the manufacture of small storage cells that can be easily packed to profit from the available space in the vehicle. The storage cell has a triangular cross section. This geometric shape is sufficiently flexible that it can efficiently fill any volume (Figure 10).

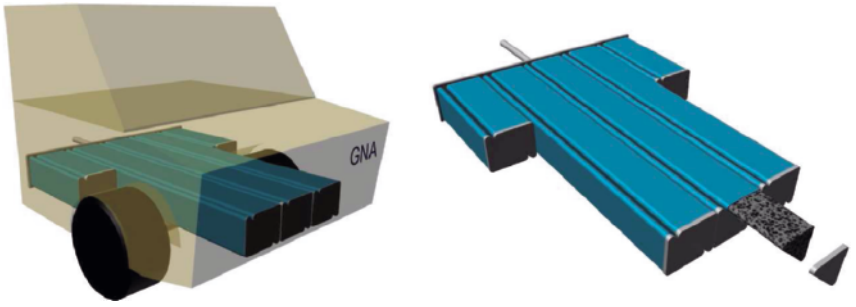

Figure 10. Multicellular reservoir for onboard NG storage by adsorption. The shape of the storage cell allows for an efficient filling of the available space inside the vehicle for fuel storage. The inlet/outlet fuel port which is common to all cells, is located at one of the extremes of the reservoir. Each cell is easily filled with contiguous carbon monolith disks with a geometrical shape identical to the cross section of the cell.

It should be noted that the design, manufacture and certification of a specific storage reservoir for a given vehicle model increases significantly the production costs of the vehicle. This will hardly be accepted by the automotive industry where the low-cost, automated manufacture is a determining factor of competitiveness. The manufacture of small storage cells with a fixed geometry that allows for a flexible design of the final storage tank eliminates that sort of difficulties.

10. Concluding Remarks

In this work, we have reviewed three main aspects of the utilization of natural gas as an automotive fuel in the transportation sector.

- The use of an alternative automotive fuel – **natural gas** – which is efficient and environmentally advantageous. This point of view is reinforced by the conclusions of the Task Force on "Car of the Future" of the *Green Book for innovation* of the European Commission, where it is considered an important and promising alternative fuel.
- A novel storage technology for natural gas – **adsorption storage** – that can overcome the economic obstacles that have impeded the large acceptance of natural gas as a competitive automotive fuel in the transportation sector.
- The research and technological efforts that have been developed to, on one hand, solve the problems of adsorption storage, and on the other hand, take maximum advantage from the low pressure required by this technology.

It has been demonstrated that there are solutions to the all of the problems associated to adsorption storage, and that it is possible to build, a light, compact, and efficient system for storage, distribution, and dispensing of NG. The practical achievement of this objective is essential for NGVs to create a strong and sustained interest of the automotive market.

The low cost of NG, together with governmental aids, compensates for the higher costs of the initial phase of implementation and dissemination of a new alternative fuel. The current state of knowledge is already sufficiently developed so that a solid European network of cooperation and technology transfer can be established, grouping industry and academia around such a strategic area for the economic and technologic development of the European market, the utilization of natural gas as an automotive fuel in the transportation sector.

References

1. R.N. Penillr J.M.O. Paez, G.A. Plata, The Use of Natural Gas. In *Proc. 14th World Petroleum Congress*, Stavenger, Wiley New York (1994).
2. J.G. Ingersoll, Natural Gas Vehicles. The Fairmont Press, Lilburn, GA (1996).
3. O. Talu, An Overview of Adsorptive Storage of Natural Gas. In *Proc. 4th Int. Conf. on Fundamentals of Adsorption*, Kyoto, International Adsorption Society, pp. 655–662 (1992).
4. T.L. Cook, C. Komodromos, D.F. Quinn, S. Ragan, Adsorbent Storage for Natural Gas Vehicles, In *Carbon Materials for Adsvanced Technologies*, T.D. Burchell (ed.), Elsevier, Amsterdam, 269–302 (1999).
5. D. Lozano, M.A. De la Casa, J. Alcañiz, D. Cazorla, A. Linares, Advances in the Study of Methane Storage in Porous Carbonaceous Materials. *Fuel* **81**, 1777–1803 (2002).
6. K.R. Matranga, A.L. Myers, E.D. Glandt, Storage of Natural Gas by Adsorption on Activated Carbon. *Chem. Eng. Sci*. **47**, 1569–1579 (1992).
7. J.P.B. Mota, A.E. Rodrigues, E. Saatdjian, D. Tondeur, Dynamics of Natural Gas Adsorption Storage Systems Employing Activated Carbon. *Carbon* **35**, 1259–1270 (1997).
8. O. Talu, Use of Additives to Increase Adsorptive Storage Capacity. In *Proc. Topical Conf. on Separations Technologies: New Developments and Opportunities*, Florida, AIChE, pp. 409–414 (1993).
9. J.P.B. Mota, E. Saatdjian, D. Tondeur, A.E. Rodrigues, A Simulation Model of a High-Capacity Methane Adsorptive Storage System. *Adsorption* **1**, 17–27 (1995).
10. K.J. Chang, O. Talu, Behavior and Performance of Adsorptive Natural Gas Storage Cylinders During Discharge. *Appl. Thermal Eng*. **16**, 359 (1996).
11. J.P.B. Mota, I.A.A.C. Esteves, M. Rostam-Abadi, Dynamic Modeling of an Adsorption Storage Tank Using a Hybrid Approach Combining Computational Fluid Dynamics and Process Simulation. *Comp. Chem. Eng*. **28**, 2421–2431 (2004).
12. J.P.B. Mota, Impact of Gas Composition on Natural Gas Storage by Adsorption. *AIChE J*. **45**, 986–996 (1999).
13. I.A.A.C. Esteves, M.S. Lopes, P.M. Nunes, M.F.J. Eusébio, J.P.B. Mota, Automatic Filtering and Reodorization of Adsorbed Natural Gas Storage Systems. *Adsorption* **11**, 905–910 (2005).